https://ntrs.nasa.gov/search.jsp?R=19900012493 2020-03-19T23:21:45+00:00Z

NASA Contractor Report 185224

Framework for a Space Shuttle Main Engine Health Monitoring System

(NASA-CR-185224) FRAMEWORK FOR A SPACE SHUTTLE MAIN ENGINE HEALTH MONITORING SYSTEM Final Report (United Technologies Research Center) 189 p CSCL 21H

N90-21809

Unclas
G3/20 0278779

Michael W. Hawman, William S. Galinaitis,
Sharayu Tulpule, and Anita K. Mattedi
United Technologies Research Center
East Hartford, Connecticut

Jeffrey Kamenetz
United Technologies Hamilton Standard
Windsor Locks, Connecticut

May 1990

Prepared for
Lewis Research Center
Under Contract NAS 3-25626

National Aeronautics and
Space Administration

Framework for a Space Shuttle Main Engine Health Monitoring System

TABLE OF CONTENTS

	Page
GLOSSARY	iii
PROGRAM SUMMARY	1
SECTION 1.0 - INTRODUCTION	3
SECTION 2.0 - IDENTIFICATION OF THE SSME FAILURE MODES	4
2.1 SSME Database	4
2.2 Major Component Classes of the SSME	12
2.3 SSME Failure Modes	13
2.4 Failure Mode Ranking	13
SECTION 3.0 - METHODS TO DETECT FAILURES AND MINIMIZE ENGINE DAMAGE	22
3.1 Failure Detection Algorithms	22
3.2 Advanced Technology Sensors	56
SECTION 4.0 - FRAMEWORK FOR THE HEALTH MANAGEMENT SYSTEM	69
4.1 HMS Functional Architecture	69
4.2 HMS Breadboard Hardware Architecture	73
4.3 Optimization Tool for Hardware/Software Integration	96
4.4 Summary	99
SECTION 5.0 - IMPLEMENTATION PLAN FOR THE HEALTH MANAGEMENT SYSTEM	100
5.1 Baseline System Discussion	101
5.2 Subsystem Description	106

TABLE OF CONTENTS (continued)

SECTION 6.0 – CONCLUSIONS 110

APPENDIX A – FAILURE DETECTION ALGORITHM RESULTS 111

REFERENCES 179

GLOSSARY

A/D	Analog-to-Digital
ADAS	Architecture Design and Simulation ADEC
AE	Acoustic Emission
AI	Artificial Intelligence
ALS	Advanced Launch System
AR	Auto-Regressive
ARMA	Auto-Regressive Moving Average
ASI	Augmented Spark Igniter
ATD	Alternate Turbopump Development
ATF	Advanced Tactical Fighter
BIT	Built-In-Test
CADS	Command and Data Simulator
CCV	Coolant Control Valve
CPU	Central Processing Unit
CSC	Computer Software Configuration
CSCI	Computer Software Configuration Item
DBD	Detailed Block Diagram
DoD-STD	Department of Defense Standard
DPFG	Data Processing Functional Group
DSP	Digital Signal Processing
DTM	Digital Transient Model

GLOSSARY (continued)

DTS	Development Test System
EMI	Electro–Magnetic Interference
FA	False Alarm
FASCOS	Flight Accelerometer Safety Cutoff System
FCR	Fault Containment Region
FDI	Fault Detection and Isolation
FFT	Fast Fourier Transform
FM	Frequency Modulated
FMEA	Failure Modes and Effects Analysis
FOLVS	Fiber Optic Laser Vibration Sensor
FPOV_ACT POS	Fuel Preburner Oxidizer Valve Actuator Position
FPB	Fuel Preburner
FPB_PC	Fuel Preburner Chamber Pressure
FPE	Final Prediction Error
FPOV	Fuel Preburner Oxidizer Valve
FRS	Facility Recording System
FU_FL	Fuel Flowrate
HCF	High Cycle Fatigue
HGM	Hot Gas Manifold
HM	Health Management
HMS	Health Management System

GLOSSARY (continued)

HPFP	High Pressure Fuel Pump
HPFP_IN_PR	High Pressure Fuel Pump Inlet Pressure
HPSP_SPD	High Pressure Pump Speed
HPFT	High Pressure Fuel Turbine
HPFTP	High Pressure Fuel Turbopump
HPFT_DS_PR	High Pressure Fuel Turbopump Discharge Pressure
HPOP_IN_PR	High Pressure Oxidizer Pump Inlet Pressure
HPOT_DS_T	High Pressure Oxidizer Turbine Discharge Temperature
HPOT_SPD	High Pressure Oxidizer Turbine Speed
HPOTP	High Pressure Oxidizer Turbopump
HS	Hamilton Standard
HSDB	High Speed Data Bus
I/F	Interface
IRD	Independent Research and Development
IRS	Interface Requirement Specification
JIAWG	Joint Avionics Working Group
LOX	Liquid Oxygen
LPFP	Low Pressure Fuel Pump
LPFTP	Low Pressure Fuel Turbopump
LPFT_DS_PR	Low Pressure Fuel Turbopump Discharge Pressure
LPOP_DS_PR	Low Pressure Oxidizer Pump Discharge Pressure

GLOSSARY (continued)

LPOTP	Low Pressure Oxidizer Turbopump
LRM	Line Replaceable Modules
LRU	Line Replaceable Unit
LVDT	Linear Variable Differential Transducer
MA	Moving Average
MCC	Main Combustion Chamber
MCC_CLNT-DS-PR	Main Combustion Chamber Coolant Discharge Pressure
MCC_PC	Main Combustion Chamber Pressure
MDF	Missed Detection of Fault
MFV	Main Fuel Valve
MIL_STD	Military Standard
MIPS	Million Instructions per Second
MOV	Main Oxidizer Valve
MTBF	Mean Time Between Failures
NASA-MFSC	NASA: Marshall Space Flight Center
NASP	National Aero-Space Plane
NPSH	Net Positive Suction Head
OPADS	Optical Plume Anomaly Detection System
OPB	Oxidizer Preburner
OPOV	Oxidizer Preburner Oxidizer Valve
OPOV_ACT-POS	Oxidizer Preburner Oxidizer Valve Actuator Position

GLOSSARY (continued)

P&W	Pratt & Whitney
PBM	Power Balance Model
PBP_DS_PR	Preburner Pump Discharge Pressure
PID	Parameter Identification
PR	Pattern Recognition
PVDF	Polyvinylidene Flouride
RAM	Random Access Memory
RECMS	Rocket Engine Condition Monitoring System
RESID	Recursive Structural Identification
RPL	Rated Power Level
SAFD	System for Anomaly and Failure Detection
SBD	System Block Diagram
SDD	Software Design Document
SMT	Surface Mount Technology
SRS	Software Requirement Specification
SSC	Stennis Space Center
SSME	Space Shuttle Main Engine
SSS	System Software Specification
T/A	Turn Around
TIP/88	Test Information Program, version 88
UCR	Unsatisfactory Condition Report

GLOSSARY (continued)

UTC	United Technologies Corporation
UTMC	United Technologies Microelectronics Center
UTRC	United Technologies Research Center
VHSIC	Very High Speed Integrated Circuit

PROGRAM SUMMARY

United Technologies Research Center (UTRC) has developed a framework to integrate state-of-the-art rocket engine technology with fault detection algorithms for a Health Management System (HMS) for the space shuttle main engine (SSME). UTRC has developed this HMS framework on the basis of an analysis of the SSME failure modes and the engine monitoring requirements. The UTRC HMS utilizes the existing SSME flight instrumentation and satisfies NASA requirements of using near-term technologies to enable ground testing of the HMS within five years. The UTRC HMS is initially targeted to support SSME ground tests, however, the system design provides for a clear migration path to a flight system. UTRC has also developed an implementation plan for the HMS. Which provides for phased implementation and integration of the HMS on the SSME teststand.

The HMS framework development process drew upon numerous resources such as SSME design and failure history, SSME operations and teststand procedures, and SSME teststand data. UTRC evaluated a broad range of fault detection algorithms, sensor technologies, and hardware architectures before selecting the most promising algorithms, sensors, and hardware architecture, consistent with the NASA program goals, to incorporate into the HMS framework.

To establish the requirements for the failure detection methods, UTRC first analyzed the SSME failure modes, available teststand data, SSME models, and SSME operations. The facts that the SSME analytical models are directed at performance analysis and that the teststand data are directed at performance measurements rather than diagnostics put constraints on the selection of failure detection methods. The SSME Power Balance and Digital Transient models are very complex, and can not be easily modified to simulate engine failures. Furthermore, the available SSME teststand data was primarily from the development phase of the SSME program, and thus, exhibited significant test-to-test variation due to hardware design and build changes. The complexity of the analytical models and the variability of the teststand data dictated that empirical/data-driven fault detection techniques be selected over techniques which require accurate analytical engine models for all conditions of interest.

A major objective of this program was to assess and evaluate candidate approaches to detect SSME failures earlier than redline cutoff. The approaches included a study of fault detection algorithms, along with an assessment of existing and near-term sensor technologies that could be used to augment the performance of the HMS. The fault detection approach developed by UTRC uses algorithms and a system hierarchy which exploits the interrelatedness of the SSME components and parameter measurements; provides a methodology which is robust to sensor loss and engine build variability, while covering all phases of engine operation.

A set of three algorithmic approaches was developed and implemented to detect faults which manifest themselves in engine parameter measurements as gradual long term trends, quick and high amplitude excursions, and oscillatory or nonsteady state behavior. Autoregressive Moving Average (ARMA) models, based on time series analysis, were developed to detect fast excursions in engine parameters and also changes from a stationary to a nonstationary condition. The UTRC Recursive Structural Identification (RESID) algorithm was used to develop a regression model between the SSME propellant flows and the thrust chamber pressure during open-loop start and shutdown sequences. This RESID model was then used to detect abnormal behavior during startup and shutdown. A sensor fusion technique, clustering, was developed to detect failures which manifest themselves as gradual trends in performance parameter measurements and to

distinguish this behavior from trends associated with normal engine operation. Because it exploits the interrelationships of the sensor measurements, the clustering technique is robust to sensor loss and build-to-build variations in the SSME. The three algorithmic approaches were tested on data from 15 SSME failures and provided fault detection times equal to or better than redline cutoff times for fourteen of the fifteen cases.

Recommendations for improving the quality of information available to the fault detection algorithms as well as for extracting more information from the existing sensor suite were presented. The addition of new nonintrusive sensors directed specifically at component health assessment were suggested for long-term incorporation within the SSME. Near-term enhancements could also be derived by exploiting the higher frequency bandwidths of the pressure transducers currently installed in the SSME. The computational requirements for each of these approaches were assessed for incorporation in the HMS architecture.

A design methodology was developed and demonstrated to map the HMS functionalities onto a hardware architecture. This design methodology provides a modular, flexible approach to architecture design, thereby delineating a clear migration path from the ground test HMS to a flight system. An implementation plan, developed for the groundtest breadboard HMS architecture, provides a phased implementation of HMS functionalities on the teststand, and includes the program schedules, manpower requirements, and materials cost.

To demonstrate the benefits of an HMS for the SSME, the program required the provision of a measure of HMS effectiveness. UTRC selected seven criteria which encompass nearly all performance, reliability, and implementability issues. The first criterion was the probability of a fault detection. The UTRC HMS demonstrated 100% detection for the data that was available. The second criterion was a low false alarm rate. For the data tested to date, the UTRC algorithms exhibited only three false alarms during power transitions which were caused by missing data from one or more highly weighted sensors. It is anticipated this small number of false alarms can be further reduced through slight adjustments in the algorithms. The third criterion, time of detection, was demonstrated by the UTRC HMS through fault detection times which were, in most cases, better than redlines. The fourth criterion selected was the probability of a hardware failure. UTRC chose a high reliability design to minimize the chance of hardware failures, and a modular architecture to minimize the impact of such a failure in the unlikely event that one occurred. The fifth criterion, complexity, was minimized through the development of algorithms which require minimal processing of the SSME data. Feasibility of implementation, the sixth criterion, was maximized through the development of a phased implementation plan which provides benefits from the HMS early in the implementation program. Cost, which was the seventh criterion, was minimized through the selection of commercially available, industry standard hardware.

The purpose of this study program was to demonstrate feasibility of and lay the foundation for a program to enhance the safety of SSME operation in both ground test and flight scenarios. The key issues of fault detection algorithms, hardware architectures, and implementation plans were successfully addressed. The results clearly indicate that it is feasible to use the existing flight SSME instrumentation as the basis for an HMS that can provide significant near-term improvements in operation safety. Furthermore, the flexibility of the approach developed in this program provides for ease of growth to incorporate and accommodate new advances in health monitoring technology, thus, providing long-term enhancements to safety.

SECTION 1.0
INTRODUCTION

The space shuttle main engine (SSME) is the first operational liquid rocket engine developed for reuse. NASA's space exploration objectives rely heavily on the performance of the SSME. The SSME is a man-rated, power dense engine with high thrust requirements which are met by a staged combustion cycle operation. The SSME development began in the 1970's, and since then it has performed reliably and safely for over 30 space shuttle missions, and for over 411,000 seconds of ground testing. However, four minor failures have occurred during launches or launch attempts, and, out of 40 premature shutdowns, there have been 27 major failures during ground testing which resulted in substantial teststand and engine hardware damage.

A major SSME failure has catastrophic consequences during flight, but it can also prove to be very expensive during ground test, not only in terms of the loss of hardware, but also the accumulated testing time on a given engine. The SSME undergoes a significant amount of testing before they are qualified for flight. Engine monitoring, therefore, can play a significant role in providing improved availability, reliability, safety, and reduced cost to meet NASA's space objectives.

The current technique of using parameter redlines for monitoring the SSME is a sensor-intensive, algorithmically simple approach that is incapable of detecting incipient failures. Rocketdyne has developed and is implementing the System for Anomaly and Failure Detection (SAFD) to provide improved gound test monitoring for the SSME[1]. The SAFD algorithms use statistical confidence intervals on sensed parameters to achieve fault detection. SAFD algorithms are suitable only for mainstage operation of the SSME. In recent years, considerable advances have been realized in the theory and practice of failure detection algorithms for many different mechanical and electronic systems. These techniques cover a wide range of approaches from matched filters and Bayesian detectors to adaptive learning networks and artificial intelligence. The computational complexities of these techniques vary widely, although, with the continuing advances in the computing power of digital processors, most of these techniques are within reach of a real-time health monitoring system. UTRC has developed a framework for such a Health Management System for the SSME that integrates near-term sensor technologies with a failure detection methodology for early detection of faults.

The framework developed by UTRC emphasizes an HMS focused to enhance safety. It uses existing instrumentation and near-term technology concepts to enable ground testing within five years. It is designed to initially support ground tests, with the clear capability to migrate to a flight system. The UTRC HMS framework incorporates fault detection algorithms, sensor technologies, and the SSME performance models, and maps these key components onto a hardware architecture consistent with the program goals.

A detailed discussion on the HMS Framework developed by UTRC is presented in this final report. Section 2 describes the SSME database used to identify the SSME failure modes. The information about these failure modes was used to identify the monitoring requirements for the HMS. Section 3 of this report presents the fault detection algorithms and an evaluation of the near-term sensor technology. Section 4 discusses the hardware architecture followed by an implementation plan for the HMS in Section 5. Finally, Section 6 discusses program conclusions, and is followed by Appendix A, in which a detailed discussion of HMS failure detection algorithm results are presented.

SECTION 2.0
IDENTIFICATION OF THE SSME FAILURE MODES

The SSME entered developmental testing in 1975 and has since accumulated over 411,000 seconds of operation in over 1500 hot-fire tests. Although the engine has exhibited high reliability, 27 major incidents have occurred during ground test. Many of these failures have resulted in significant repair costs to engine and facility hardware, program schedule delays, and loss of fleet leader components. Extensive documentation consisting of teststand data and failure analysis reports exist for many of the incidents. These data can be used to guide the development of an HMS by identifying those failures whose detection prior to catastrophic failure would produce the greatest increase in operational safety of the SSME. Thus, Task 1 of the HMS Framework Development Program deals with the identification of the SSME failure modes. This task prepares the groundwork for establishing the HMS Framework by identifying the monitoring requirements for the SSME. In order to establish a systematic procedure for developing the HMS Framework, Task 1 characterizes the failure modes in terms of a set of criticality criteria.

It was anticipated that certain fault-specific algorithms would be required to provide optimal detection. Characterization of the SSME failure modes was a necessary first step in the identification and the development of fault-specific algorithms. Although fault-specific detection algorithms were later deemed unnecessary, the information provided by the study of the SSME failure modes identified major SSME components whose operational health was required to be monitored by the HMS.

2.1 SSME Database

The successful design of an HMS for the SSME requires knowledge of the engine operation, engine failure modes, the existing sensor set, the parameters currently monitored, the ground test operations, and the processing capabilities. UTRC has assembled an SSME database which includes the SSME teststand data, SSME analytical models, and written SSME documents.

2.1.1 SSME Teststand Data.—UTRC has acquired SSME test firing data tapes which include 16 failure incidences, 2 nominal firings, and 1 nominal cluster firing. The failure data cover a test period from 1977 to 1989. The teststand data include CADS (Command and Data Simulator) data and Facility data. The CADS data represent data from the sensors mounted on the engine and sampled every 40 ms, while Facility data consists of data from facility and engine mounted sensors, sampled every 20 ms. Table 2.1 presents the test numbers, along with the power level settings at which failures occurred, run time duration, and failure information for each of the data files.

Each CADS data file contains 130 columns of data, with each column identified by a CADS parameter identification (PID) number. There are many redundant sensor measurements. For example, Main Combustion Chamber Pressure is measured on 8 different channels. Also, some data columns contain information regarding vehicle interface or pogo connections. Consequently, out of the 130 columns of data, approximately 50 contain nonredundant information about engine performance. The facility data files consist of about 250 columns of data. As in the case of CADS data, there are many redundant sensor measurements, and also those measurements such as air temperature, command words, purge system pressures, and bleed valve positions that are not directly relevant to monitoring engine performance or engine failures.

Each of the SSME test profiles can be divided into four operational phases: pre-startup, startup, mainstage, and shutdown. The pre-startup stage is not considered relevant for engine performance analysis.

Table 2.1 SSME TESTSTAND DATA

Test #	Power Level at Failure (%)	Run Time Duration (secs)	Failure Information Component	Failure Information Cause	Type of Data CADS	Type of Data Facility
902-249	109	450.58	HPFTP	Turbine Blades Cracked	X	
901-340	109	405.50	HPFTP	Discharge Turnaround Duct Rupture	X	
901-364	109	392.15	HPFTP	Kaiser Hat Nut Design Defect	X	
901-436	109	611.06	HPFTP	Coolant Liner Buckle	X	
901-110	75	74.07	HPOTP	LOX Seal Burning	X	
901-225	100	255.61	Valve	Main Oxidizer Valve Retaining Screw Failure	X	
901-284	Startup	9.88	Control	PC Sensor Failure	X	
901-173	92	201.17	Preburner & Main Burner	Main Injector Post Crack	X	
902-198	102	8.52	Preburner & Main Burner	Main Injector Post Crack	X	
901-222	Startup	4.33	Ducts	Heat Exchanger Weld Rupture	X	
750-259	100	101.50	Ducts	MCC Outlet Manifold Crack	X	
750-168	Shutdown	300.2	Valve	OPOV Failure	X	X
901-307	109	75.03	Fuel Preburner	Injector Failure	X	X
901-331	100	233.14	Main Burner	Injector Failure	X	X
SF10-01	102	104.80	Fuel Preburner	Injector Failure	X	
SF6-01	100	18.58	Valve	Main Fuel Valve Failure	X	
902-457	104-109	310.00		Nominal Operation	X	X
CF902	100	578.16		Nominal Operation	X	
902-463	109-111	535.00		Nominal Operation	X	X

During startup and shutdown, the SSME controller invokes open-loop, time sequenced regulation logic, while during mainstage operation, closed-loop feedback is provided. The SSME controller regulates engine thrust and oxidizer/fuel mixture ratio during mainstage operation by sensing the main combustion chamber pressure (MCC_PC) and the volumetric fuel flow rate (FU_FL). Control of these parameters is achieved by modulating the oxidizer and fuel preburner oxidizer valves (OPOV_ACT_POS and FPOV_ACT_POS).

The parameter MCC_PC is proportional to the engine thrust, and hence, a plot of MCC_PC represents a thrust profile for a complete test. Figure 2.1 shows a sample test profile. Available test data show a wide variation in the test profiles in terms of power levels achieved, throttling and venting procedures, and sensors that were recorded during the tests. During normal operation, all CADS sensors show a strong correlation with MCC_PC. Most of the CADS data show stationary behavior during mainstage operation at a given power level. The significant changes in data values, during normal operation, are due to power level changes (Figure 2.2), or (based upon the conclusions in Rocketdyne Accident/Incident Reports) venting of the propellant tanks (Figure 2.3). Figure 2.4, however, shows that some sensor data, such as valve actuator positions or turbine discharge temperatures, do show fluctuating behavior during normal operations.

During failure incidences, most of the CADS data remain stationary until a few seconds before the redline induced shutdown, at which time there is a sudden increase in data values for almost all the sensors. Only in a very few cases is there an early indication (about hundred seconds before redline cutoff) of failure in terms of a large change in sensor value (Figure 2.5). Some of the sensor data, as shown in Figure 2.6, show gradual trends during failure incidences.

2.1.2 SSME Analytical Models.—To understand the SSME behavior during normal or abnormal operation, UTRC has utilized analytical models of the SSME. Two SSME simulation models, the Power Balance Model (PBM) and the Digital Transient Model (DTM), and the SSME controller model run at UTRC. A third simulation model, Test Information Program (TIP88), runs at the UTC Pratt & Whitney (P&W) facility.

The PBM models a "typical" SSME with a set of nonlinear equations and calculates the engine steady-state power balance through iterative techniques. The governing equations are focused upon a conservation of energy approach. The model progresses step by step through SSME sections and iterates parameters until pressures, temperatures, and flowrates for the section/assembly are continuous: the energy available, based upon these parameters, is equal to the energy required by the assembly. The PBM provides steady-state "design point" values for SSME operation from minimum power level of 50% rated thrust to full power level of 109% rated thrust, and at mixture ratios from 5.8 to 6.2.

The DTM simulates the SSME through startup, mainstage, and shutdown operations. The model partitions the engine into a set of subsystems of component processes. These process elements are modeled with collections of equations which describe both the static and dynamic physical processes which occur in the engine subsystems. The DTM does not, however, model low frequency effects at a steady power level.

The SSME controller model is based upon state-space and transfer function equations, and models the OPOV and FPOV commands and actuators. Actual test data for MCC_PC and calculated mixture ratio were used as inputs to the model which was implemented in an interactive data analysis package called MATLAB. Predicted OPOV and FPOV commands and positions were compared to measured commands and positions to establish whether trends in the data were due to controller actions. The slight variations about equilibrium

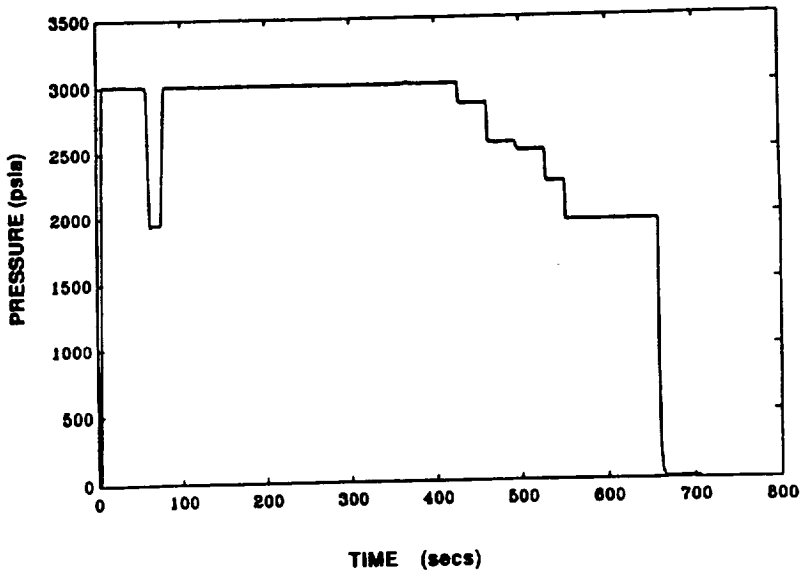

Fig. 2.1 MCC PRESSURE DATA REPRESENTS TEST PROFILE FOR A NOMINAL TEST (TEST CF-902).

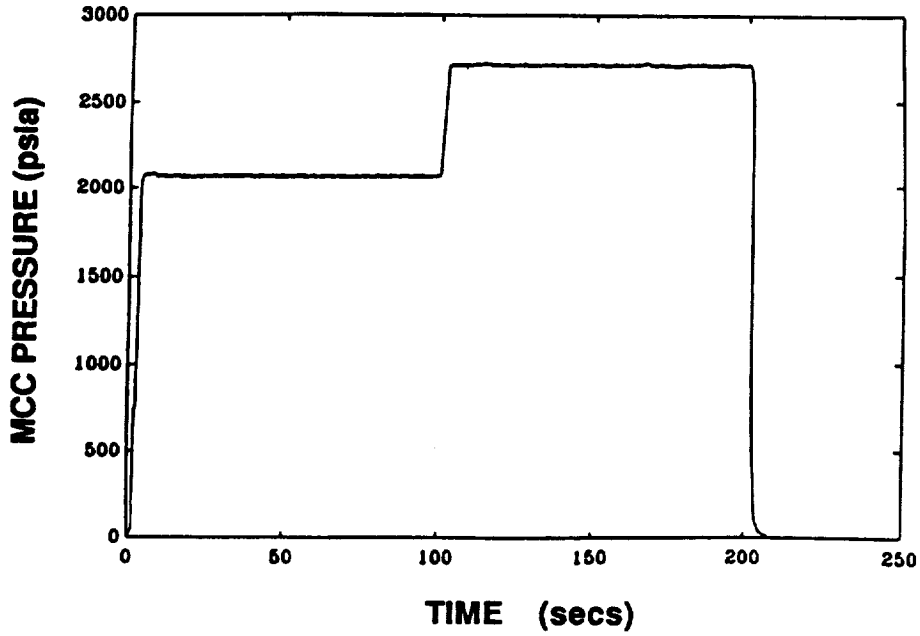

Fig. 2.2a MCC PRESSURE REPRESENTS TEST PROFILE (TEST 901-173).

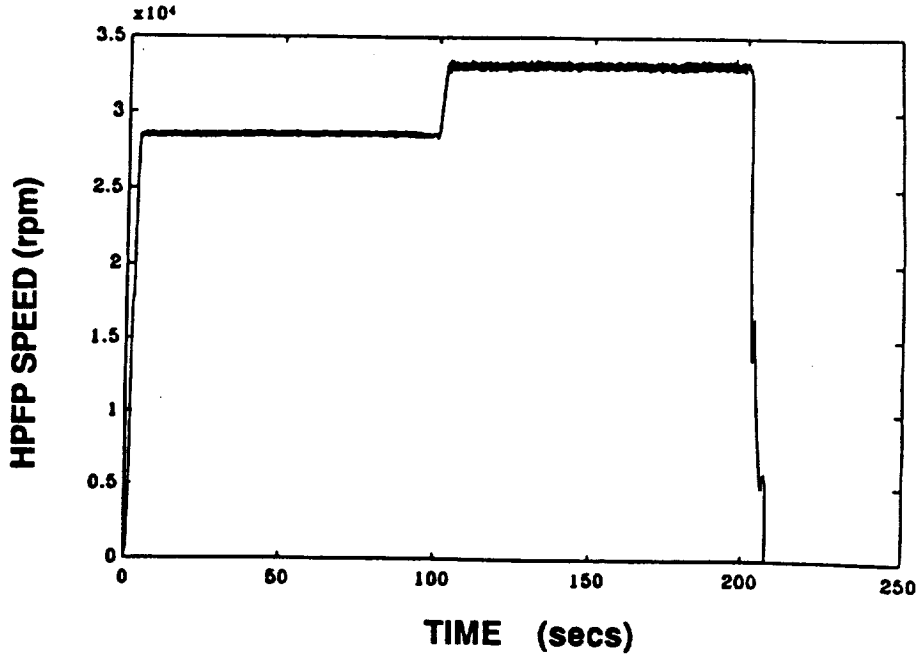

Fig. 2.2b MAJOR VARIATIONS IN HPFP SPEED ARE DUE TO POWER LEVEL CHANGES (TEST 901-173).

MWH FR
11/17/89-2.2

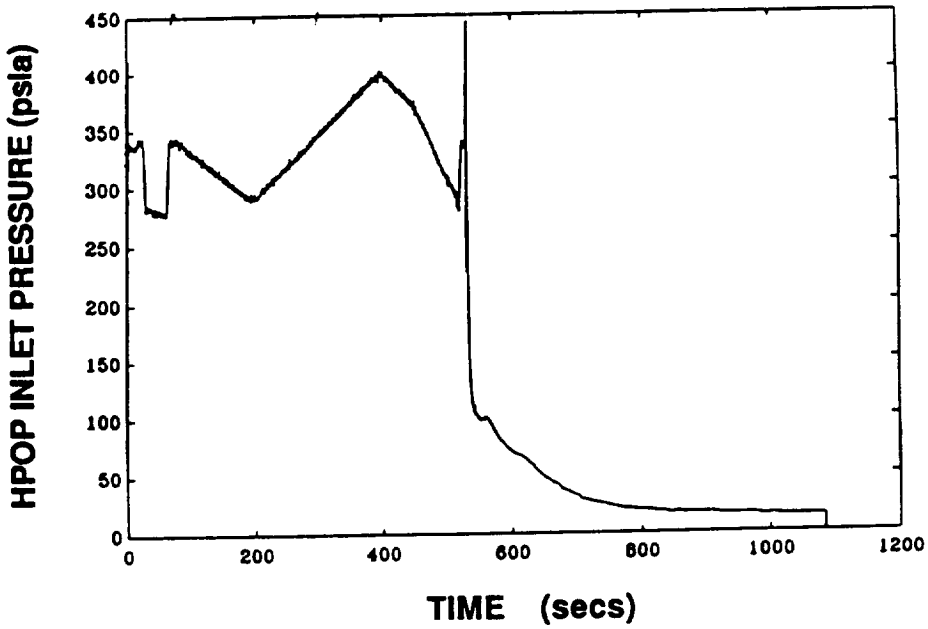

Fig. 2.3a VENTING OF OXYGEN TANKS AFFECTS HPOP INLET PRESSURE (TEST 902-463).

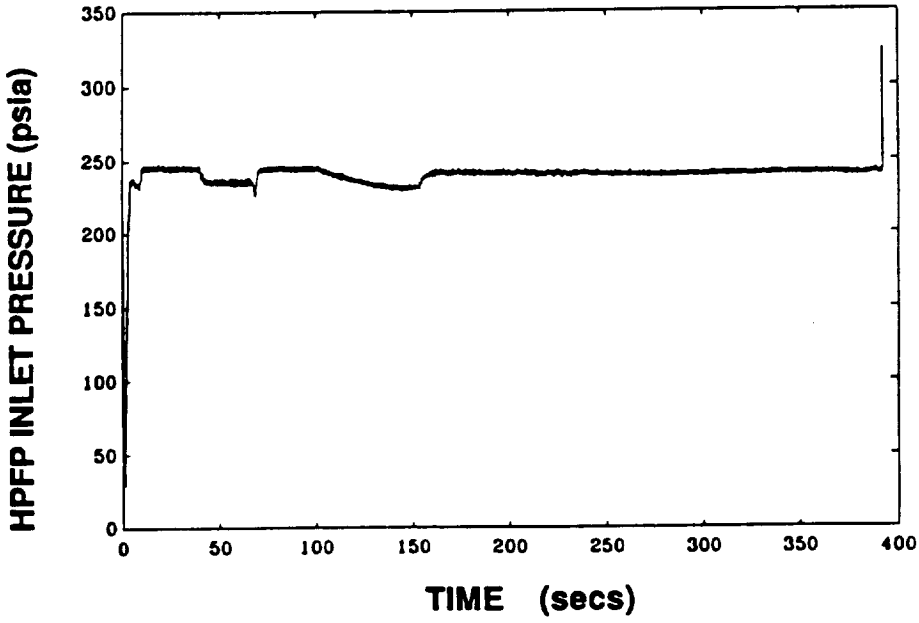

Fig. 2.3b VENTING OF FUEL TANKS AFFECTS THE HPFP INLET PRESSURE (TEST 902-463).

MWH FR
11/17/89-2.3

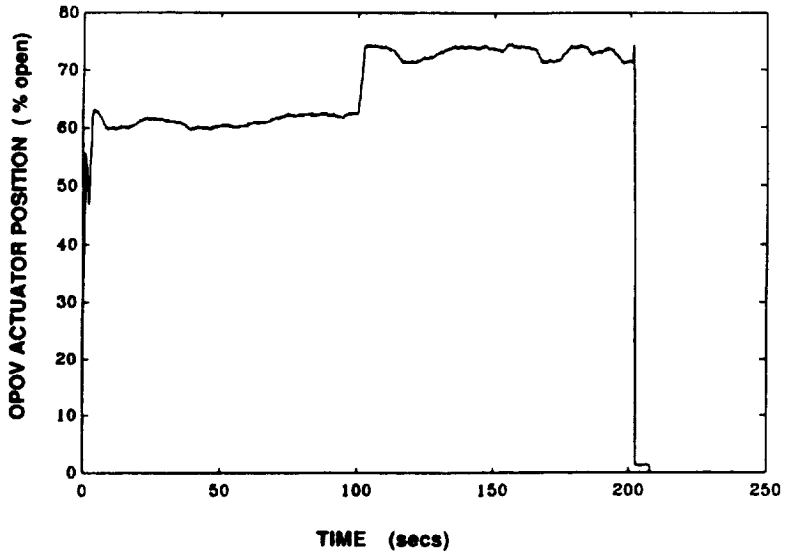

FIG. 2.4 TYPICAL ACTUATOR POSITION DATA SHOW VARIABILITY (TEST 901-173).

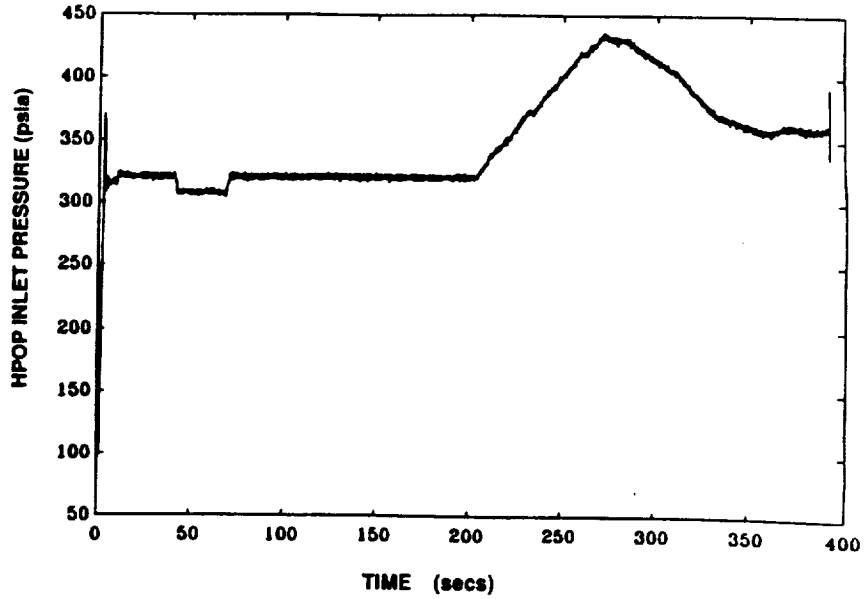

Fig. 2.5 QUICK TRANSITION IN SENSOR DATA CAUSED BY A FAILURE (TEST 901-364).

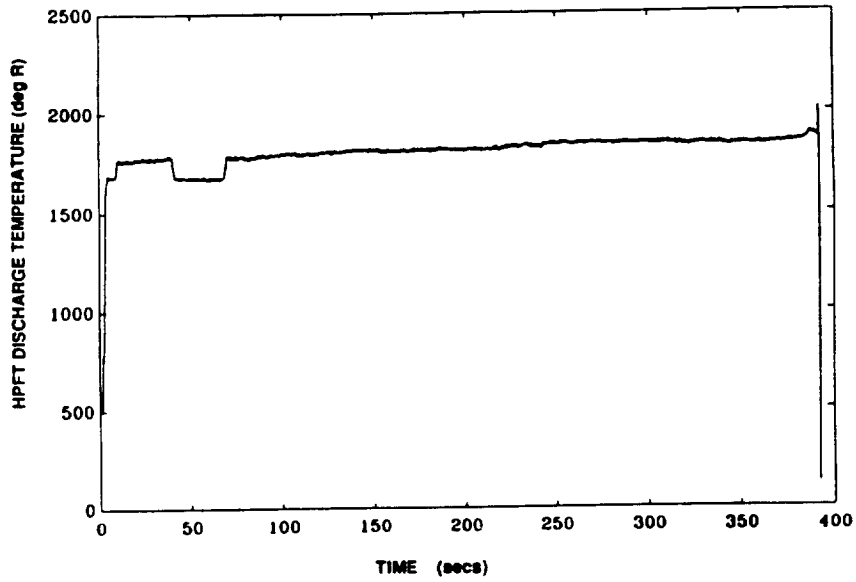

FIG. 2.6 TYPICAL TEMPERATURE DATA EXHIBITING A SLIGHT TREND (TEST 901-364).

or nominal valve positions were shown to be caused by controller actions, however, the model simulation was not conclusive in determining the cause of the long-term trends.

The Test Information Program (TIP88) is an SSME steady-state model consisting of three separate sections: Data Reduction, Base Balance, and Rated Programs. The Data Reduction Program examines measured test data (CADS and FRS) to define the operating characteristics specific to that particular engine. The Base Balance Program calibrates the engine model by adjusting performance variables based upon the data reduction results. The Rated Program essentially serves as an engine specific PBM; the calibrated model provides steady-state simulation of the specific engine at different power levels.

The process of seeding the analytical models with faults to examine fault propagation or verify algorithms was not accomplished due to the complexity of the models. The models, which are directed at modeling and evaluating engine performance, were used to provide design point inputs to the failure detection algorithms.

2.1.3 SSME Documents.—In the process of building a knowledge base for the SSME, UTRC has accumulated a large number of documents including accident/incident reports, unsatisfactory condition reports (UCRs), controller specifications, operational descriptions, and numerous reports from industry and academia on health monitoring of SSME and liquid rocket engines in general. These references were essential for understanding the SSME, its failures, and the current state-of-the-art in diagnostics and sensor technologies. The database of information provided a base from which the design of the UTRC HMS stemmed.

2.2 Major Component Classes of the SSME

UTRC divided the numerous components that make up the SSME into "Major Component Classes" as opposed to Line Replaceable Units (LRUs) or structural components. Each major component class, listed in Table 2.2, is a grouping of components with similar functionality, such as valves or turbopumps. This approach was used because the line replaceability of a component is not significant in terms of the criticality of its failure or its effect on safety. Although line replaceability is important from the maintenance standpoint, maintenance issues were not addressed in this program.

TABLE 2.2 - MAJOR SSME COMPONENT CLASSES

• Turbopumps
• Hot Gas Manifold
• Main Combustion Chamber
• Nozzle
• Controller
• Propellant Valves
• Interconnects (Lines and Ducts)
• Actuators
• Sensors
• Pogo Accumulator
• Structural Connectors
• Harnesses
• Flight Accelerometer Safety Cutoff System
• Pneumatic Controls

Each major component class is comprised of "components" which were further divided into "subcomponents". For example, the major component class of turbopumps has HPFTP, HPOTP, LPFTP, and LPOTP as components, and turbine blades, seals, and bearings as subcomponents. Table 2.3 lists the components of the major classes which have failed during the SSME ground testing.

2.3 SSME Failure Modes

The current Rocketdyne FMEA divides the numerous SSME failure modes into two categories: 1) Criticality 1 - Loss of life/vehicle, and 2) Criticality 3 - Other. Wide variations in the manifestation of each failure during the initial and intermediate stages exist. The detection of a failure by an HMS is determined by the physical phenomenon that gives rise to this failure, the speed and complexity of damage propagation, and the number and location of sensors that are able to detect the failure.

Based upon the Rocketdyne FMEA, P&W-ATD FMEA, and the UCR CALSPAN database, the total number of SSME failure modes identified (about 900 failure modes with Rocketdyne defined (criticality 1) is very high. The near-term implementation of the HMS for the SSME ground tests eliminated some of the complex failure modes as being too difficult to manage given the state-of-the art in sensors, signal processing, and the limitations of the Block I/II controller design. The scope of this HMS program called for establishing the viability of a health management system by analyzing a small number of failure modes that have a direct impact on the engine safety and are manageable, i.e. failure modes which can be detected rapidly by a HMS so that the engine damage can be minimized. Thus, failure modes associated with design problems or material defects have been eliminated, so also, the failure modes associated with fatigue cycles and remaining life, even though they may be important from a maintenance point of view.

There have been 27 ground test firings classified as major failure incidences. Each failure incidence represents the occurrence of one or more failure modes of the SSME. The most common engine failure modes are associated with seals, valves, bearings, turbine blades, and ducts. High cycle fatigue in the injector LOX posts initiated the most failures, while the high pressure fuel turbopump was the initiator of the most major incidences. Figure 2.7 shows the major SSME components and their associated failure modes.

2.4 Failure Mode Ranking

The purpose behind the ranking of failure modes is twofold: 1) to characterize the failure modes in terms of engine safety and impact on the mission; and 2) to use the rankings to select a set of failure modes for further analysis in Task 2. In order to proceed with the analysis in Task 2, the selected set of failure modes needed to be correlated with the SSME test firing data (the failure incidences data). Although there can be several failure modes associated with each incidence, the mode that was the initiator was considered to be the most significant from the perspective of this study. Therefore, the ranking of the failure incidences is also the ranking of the primary failure mode associated with that incidence. In cases where more than one failure incidence for a given failure mode exists, the ranking score for the worst case failure incidence was used for the failure mode score.

2.4.1 Ranking Criteria.—The following set of criteria was established to rank the major SSME failures. For each criterion, the higher the score, the more severe the failure. These criteria are consistent with the program goals to improve safety and minimize engine and teststand damage.

Table 2.3 MAJOR INCIDENCE FAILURES

SSME MAJOR COMPONENT CLASS	COMPONENT	SUBCOMPONENT	MECHANISM	TEST NO.
Turbopump	High pressure oxidizer turbopump HPOTP	Seal	rubbing	901-110
		Bearings	improper coolant flow	901-136
		Sensor	rubbing	902-120
		Turbine Blade	unknown	901-362
	High pressure fuel turbopump HPFTP	Turn-around duct	fracture	901-340 901-363
		Coolant Liner	buckle	902-118
		Seal	fracture	901-436
		Kaiser helmet	leak	901-364
		Kaiser hat nut	loss of	902-209
		Turbine blades	unknown	902-249 902-095 901-346
		Damper	loss of	901-410
		Bull nose nut	lost saverlesen	901-362
		Turbine	seizure	901-147
HGM	Main injector	LOX post	fracture	901-173 901-331 750-148 901-183 901-198
	HPFTP/Fuel preburner (FPB)	Injector - LOX post	fracture	901-307
		Injector	erosion	SF10-01
		Injector	blockage	750-160
	Heat exchanger	Coil leak	fracture	901-222
Sensors	Lee jet	Purge orifice	dislodge	901-284
Interconnects	High pressure oxidizer duct		fracture	750-175
	Fuel inlet line		blockage	902-112
	Coolant outlet neck		fracture	750-259
Nozzles	Stacked nozzle	Nozzle coolant tube	rupture	901-485
Valves	Main fuel valve	Housing	fracture	SF6-01
	Main oxidizer valve	Inlet joint	fretting	901-225
			misindexing	902-132
	Oxidixzer preburner valve	Seal	hot gas degradations	750-168

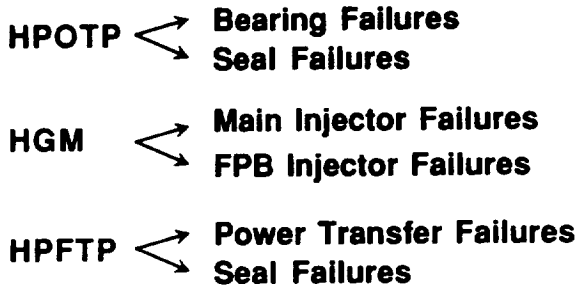

Fig. 2.7 FIVE GENERIC FAILURE MODES OF THE SSME

2.4.1.1 Definition of Ranking Criteria

I. Severity of Damage – determined from the descriptions of the overall damage that resulted from the incident.

3 - Loss of Engine
2 - Loss of One or More Components
1 - Minimal Damage

II. Time to Failure – determined from the data excursion intervals defined by the Rocketdyne System for Anomaly and Failure Detection (SAFD).

3 - Long (10 secs or greater)
2 - Medium (1-10 secs)
1 - Short (less than 1 sec.)

Failure incidences with a very short time to failure were considered "unmanageable" from the point of view of near-term detection methodologies.

III. Frequency of Occurrence – derived from the number of occurrences of "generic" failures or failures of a similar type.

3 - Chronic Problem
2 - Several Failures
1 - One Time Occurrence or Designed Out

IV. Power Level

3 - Failure Occurred during Mission Profile Power Level (start transient, 0-104% RPL, shutdown transient)
2 - Failure Occurred between Power Level of > 104% RPL and < = 109% RPL
1 - Failure Occurred at Power Level > 109% RPL

A higher score was given to failures which occurred during operation at normal mission profile power levels of the SSME. Failures at other power levels were assumed to be aggravated, at least in part, by the extended power operation. The extent of the influence of power level on the failure incidence is not easily determined. Since many failures are initiated by high-cycle-fatigue mechanisms, the same population of failures may occur during extended power operation, but at a lower number of cycles than that observed for mission power levels.

*2.4.2 **Results of Failure Mode Rankings.***—Table 2.4 presents the results of failure modes rankings with scores for the individual criterion and the composite scores. The failure incidences are indicated by the test firing numbers. The final ranking is the sum of all individual scores with a possible maximum value of 12, and a minimum value of 4. The highest score of 10 was achieved by the four failures listed in Table 2.5. The UCRs for each of these tests were used to further compare these failures to achieve the rankings shown in Table 2.5. Table 2.6 further summarizes the ranking of all of the failure modes along with information pertaining to the

Table 2.4 RANKING MATRIX FOR THE SSME FAILURE MODES

Failure Mode \ Ranking Criterion	I	II	III	IV	Total High = 12 Low = 4
COMPONENT: HPFTP					
T/A Duct Rupture					
902-118	1	2	1	3	7
901-340	1	3	1	2	7
901-363	1	3	1	3	8
Coolant Liner Buckle					
901-436	3	3	2	2	10
Kaiser Hat Failure					
901-364	3	3	1	2	9
Hot Gas Leak					
902-209	1	3	1	3	8
Turbine Blade Fracture					
902-249	2	3	2	2	9
901-346	1	3	2	3	9
Power Transfer Failure					
901-147	2	2	2	3	9
901-410	1	3	2	3	9
901-362	1	3	2	3	9
902-095	1	3	2	3	9
COMPONENT: VALVES					
Crack					
SF6-01	1	1	2	3	7
Fretting					
901-225	2	1	2	3	8
Seal Failure					
750-168	2	1	2	3	8
Valve Mis-Indexing					
902-132	2	1	1	3	8
COMPONENT: SENSORS					
Lee Jet Sensor Failure					
901-284	2	2	1	3	8
COMPONENT: NOZZLE					
Tube Rupture					
901-485	1	2	2	2	7

SHAR FR
2/22/90 TBL 2.4-4

Table 2.4 RANKING MATRIX FOR THE SSME FAILURE MODES (CONT.)

Failure Mode \ Ranking Criterion	I	II	III	IV	Total High = 12 Low = 4
COMPONENT: HPOTP					
Lox Seal Burning 901-110	2	3	2	3	10
Bearing Seal Failure 901-136	2	3	2	3	10
Experimental Speed Probe 902-120	1	1	1	3	6
COMPONENT: INTERCONNECTS					
Crack/Leak					
750-259	3	1	2	2	8
750-175	2	1	1	1	5
Blockage 902-112	2	1	1	3	7
COMPONENT: HGM					
FPB LOX Post Fracture 901-307	1	3	3	2	9
FPB Injector Errosion SF10-01	1	2	3	3	9
FPB Injector Blockage 750-160	2	2	1	3	8
Main Ejector LOX Post Fracture					
901-173	1	1	3	3	8
901-331	1	1	3	3	8
750-148	1	1	3	2	7
901-183	1	3	3	3	10
902-198	1	2	3	3	9
Heat Exchanger Tube Leak 901-222	1	2	2	3	8

Table 2.5 FOUR MOST CRITICAL SSME FAILURE MODES

Rank	Failure Mode	Component	Test #	Score	Comments
1	Coolant Liner Buckle	HPFTP	901-436	10	Engine Loss
2	Bearing Failure	HPOTP	901-136	10	Extensive Damage
3	LOX Seal Burn	HPOTP	901-110	10	Extensive Damage
4	Main Injector LOX Post Fracture	HGM	901-183	10	Several Failures

Table 2.6 FAILURE MODE RANKING AND DATA AVAILABILITY SUMMARY

Score	Description	Test	Data	SAFD	Test Date
10	Main inj. lox post fracture	901-183	—		06/05/78
10	HPOTP LOX seal burn	901-110	CADS		03/24/77
10	HPOTP bearing failure	901-136	—		09/08/77
10	HPFTP coolant liner buckle (interstage seal failure)	901-436	CADS		02/14/84
9	HPFTP kaiser nut failure	901-364	CADS	X	04/07/82
9	FPB LOX post fracture	901-307	CADS & facility		01/28/81
9	FPB injector erosion	SF10-01	CADS		07/12/80
9	Main inj. LOX post fracture	902-198	CADS		07/23/80
9	HPFTP turbine blade	901-349	CADS		09/21/81
9	HPFTP turbine blade	901-346	—		11/19/81
9	Power transfer failure	901-147	—		12/01/77
9	Power transfer failure	901-410	—		04/23/83
9	Power transfer failure	901-352	—		03/27/82
9	Power transfer failure	901-095	—		01/07/77
8	HPFTP T/A duct rupture	901-363	—		04/07/82
8	HPFTP gas leak	902-208	—		11/14/80
8	MOV fretting	901-225	CADS	X	12/27/78
8	Valve seal failure	750-168	CADS & facility		05/15/82
8	MOV mis-indexed	902-132	—		10/03/78
8	Lee jet sensor failure	901-284	CADS	X	07/30/80
8	MCC outlet duct fracture	750-259	CADS		03/27/85
8	FPB injector blockage	750-160	—		02/12/82
8	Main injector fracture	901-173	CADS	X	03/31/78
8	Main injector fracture	901-331	CADS & facility		07/15/81
8	Heat exchanger tube leak	901-222	CADS		12/06/78
7	T/A duct rupture	902-118	—		07/10/78
7	T/A duct rupture	901-340	CADS	X	10/15/81
7	MFV crack	SF6-01	CADS		07/02/79
7	Nozzle tube rupture	901-485	—		07/24/85
7	Inlet duct blockage	902-112	—		06/10/78
7	Main inj. fracture	750-148	—		09/02/81
6	HPOTP speed sensor	902-120	—		07/18/78
5	H.P. oxidizer duct	750-175	—		08/27/82
	Nominal - 1 second average	902-457	CADS		
	Nominal - noise spikes CF	CF902(?)	CADS		
	Nominal - 40 msec	902-457	Facility/CADS		
	Nominal	902-463	Facility/CADS		

CF = Cluster Firing

availability of test data. No attempt was made to rank the failures that received identical scores other than the highest ranked failures shown in Table 2.5.

2.4.3 Summary of Failure Mode Rankings.—The 14 failures receiving a score of 9 or 10 make up five generic types of failure modes occurring within 3 major LRUs. The HPOTP has experienced problems due to seal and bearing failures. The HGM has experienced a significant number of injector problems in both the main injector and the fuel preburner injector. The third LRU, the HPFTP, has experienced problems with power transfer components (including turbine blades) and with seals. One isolated incident of the HPFTP involved the failure of the Kaiser Nut which resulted in extensive engine damage. Thus, the failure detection methods in Phase I, Task 2 addressed these five failure modes of the three LRUs. In the case where data did not exist for a highly ranked failure mode, such as the main injector failure (901-183), data from a lower ranked, but similar failure was substituted (such as main injector failure 901-331 or 902-198).

SECTION 3.0
METHODS TO DETECT FAILURES AND MINIMIZE ENGINE DAMAGE

The primary goal of the SSME HMS is to detect engine failures as early as possible, and then direct the engine controller to shut down the engine to minimize damage. Program requirements dictate that the HMS must use existing instrumentation and near-term technology concepts to enable ground testing within five years. In the HMS framework development process, UTRC has emphasized new diagnostic sensors and failure detection algorithms as key ingredients to enhance engine health monitoring.

3.1 Failure Detection Algorithms

Most failures are preceded by growing intolerances or imbalances in the engine which initially manifest themselves through subtle deviations in engine parameters. The process of failure detection is concerned with observing these deviations from nominal operation in the sensor measurements. A component malfunction usually results from a number of distinct failure modes, and each of these failure modes may affect the sensor measurements in a different manner. The failure classification process is concerned with observing the different ways in which the various failure modes affect the sensor measurements.

The success of failure detection algorithms is directly related to the information content of the sensor signal. The current SSME sensor set is primarily used to monitor engine performance and provide input to the controller. Thus, the scope of the failure detection algorithms is limited to only those faults that produce changes in the engine operation which the sensors can detect.

Based on the preliminary analysis of the SSME sensor data, a failure can be identified as a deviation from the normal or the design envelope of the engine operation. It has not been possible, however, to identify a characteristic pattern of deviations in the sensor data associated with a particular type of failure mode. Given an extensive database of failure incidence documentation and data, it may be possible to perform fault identification and isolation. The scope of this program, however, and the limited failure documentation dictated that a methodology for failure detection, but not for failure identification and isolation, would be designed.

3.1.1 Candidate Failure Detection Algorithms.—There is not a single optimal failure detection algorithm. A range of techniques, from basic signal conditioning to pattern recognition and artificial intelligence, requires examination to determine the best approach.

3.1.1.1 Pattern Recognition (PR) Methods.—Pattern recognition techniques are data-driven, empirical methods, well suited for the SSME because it has undergone extensive testing and has produced a large experimental database of normal operations and failure modes. PR techniques can involve signal processing, feature extraction, and classification. These techniques are trained to discriminate between the normal and abnormal system behavior by means of a training data set, and then use that capability to classify test data into normal and failure classes.

3.1.1.2 Model-based Fault Detection and Isolation (FDI) Methods.—In the absence of experimental data, an engine simulation model is required. The SSME PBM and DTM models have been developed to predict the SSME performance during steady-state and transient operations. However, many sensor measurements show drifts and biases during normal operations that can not be accurately accounted for by the SSME models.

Model-based fault detection and isolation methods require an accurate mathematical model of the engine. Most of these methods work well with linear and time-invariant systems. However, modeling errors and system nonlinearities tend to affect FDI algorithm performance in terms of robustness and detection sensitivity.

FDI algorithms track the normal operations of the engine by processing the sensor measurements and utilizing an accurate mathematical model of the engine which links the engine inputs and control parameters with the output measurements. When the engine is operating in a normal mode, the sensor outputs follow certain predictable trajectories within specified limits of accuracy. A failure is indicated when the sensor measurements deviate from the model prediction.

3.1.1.3 Artificial Intelligence (AI) Methods.—In the absence of accurate mathematical models and experimental data, AI techniques make use of expert knowledge to develop qualitative models and perform qualitative reasoning about failure conditions. AI techniques use automated decision making processes based on a qualitative model of a system to deal with system performance or system failures. The automated decision making processes rely on knowledge-based rules or qualitative expressions derived from traditional physics concepts, and perform detailed analysis of the system to provide intelligent advice. These methods were not employed in the HMS due to the lack of adequately defined fault characteristics which could be used to develop the models of failure modes.

3.1.2 UTRC Failure Detection Methodology.—The availability of the SSME teststand data and the complexity of the SSME analytical models helped define the rationale for choosing the data-driven approaches for evaluation and testing. The SSME analytical models are performance driven, and do not generate failure related information. The models are also not capable of real-time operation on minicomputer. To compensate for the lack of sufficient nominal teststand data, the SSME models were mainly utilized to generate 'design point' parameter values for nominal engine operation. The data-driven approaches were thus utilized to characterize engine operation during nominal or failure modes.

The UTRC failure detection methodology is a two step process. The first step involves characterizing the nominal operation of the engine parameters. Analytical models and data from nominal tests are utilized to build empirical models for normal engine operations. The second step compares the teststand data with the model output, and declares a failure if the measured data diverge from the model values. Figure 3.1 shows the overall failure detection scheme.

3.1.3 Algorithms for UTRC Failure Detection Methodology.—The SSME operates in three phases: startup, mainstage, and shutdown. The startup and shutdown are open-loop operations commanded by time sequenced opening or closing of the SSME fuel and LOX valves, while during mainstage, the main combustion chamber pressure and the oxidizer/fuel mixture ratio are regulated by the controller. The algorithms used for failure detection grew out of an evolutionary process that systematically studied the information content of the SSME sensor data. Most of the data show stationary behavior during mainstage; significant changes in the data values during nominal operation are due to power level changes. Thus, algorithms (such as time series) that require stationary behavior of the data will work well during the mainstage operation. During startup and shutdown, the sensor data show nonstationary, transient behavior, and nonlinear regression algorithms are more suitable. The time series, linear/nonlinear regression, and clustering algorithms described below are the most promising of various approaches for failure detection.

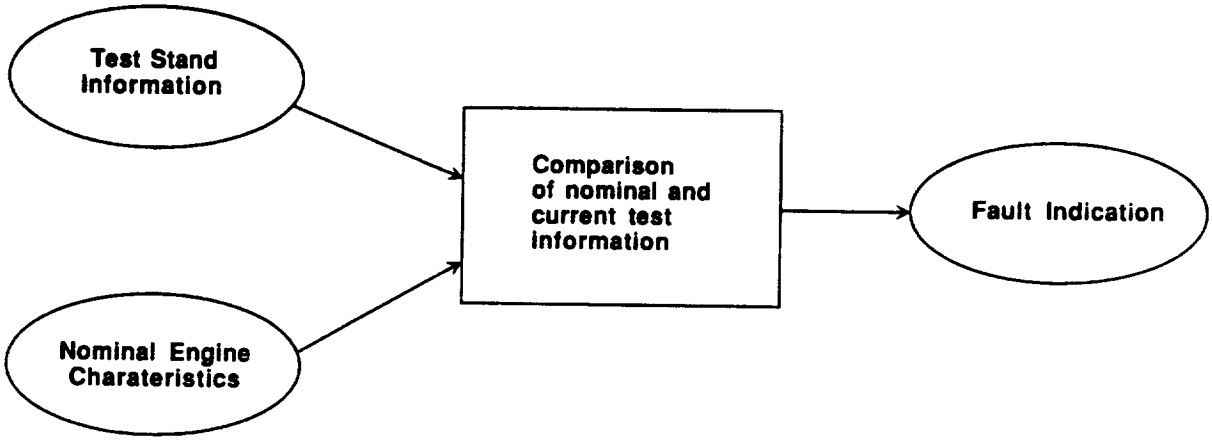

Fig. 3.1 HIGH LEVEL FAULT DETECTION SYSTEM STRUCTURE

3.1.3.1 Time Series Algorithms.—A time series represents a chronological sequence of observations of a particular variable. The SSME teststand data consist of time sequenced measurements of temperature, pressure, speed, and flowrates at various locations on the engine. The time series analysis techniques involve developing models based on the measured data to explain the behavior of the past data and to predict the behavior of the future data. It is important to note that the actual sensor values are not of interest to the time series model, but rather that the structure of the recent past data resembles that of the near future data.

The first step in the analysis involves developing univariate models. Univariate models explain the behavior of a single parameter based on the past data values of that parameter. The underlying assumption in a univariate model is that the system is in a steady state. For example, univariate models can be developed to characterize engine measurements when the engine is operating at a given power level. A time series algorithm will only work for stationary data, as it detects a fault by indicating the presence of a nonstationarity in the sensor data; anomalous behavior is indicated when the measured value of the parameter starts to diverge from the model predicted values. A time series algorithm will adapt to gradual trends evident in the data and thus will not detect those faults which are indicated by such behavior.

The general form of a time series model is given by:

$$z_k = \sum_{i=1}^{p} b_i \, z_{k-i} + r_k - \sum_{i=1}^{q} c_i \, r_{k-i} \qquad (1)$$

Here, z_k is the observation at time t_k, and r_k, called the residual at time t_k, is an uncorrelated gaussian random variable. The summation limits p and q, and the parameters b_i and c_i are adjusted to fit the data. This general time series model is called the mixed Autoregressive Moving Average (ARMA) Process.

An observed time series ($z_1, z_2, z_3, \ldots\ldots, z_n$) can be thought of as a particular realization of a stochastic process. Stochastic processes in general can be described by an n–dimensional probability distribution. To infer such a general probability structure from just one realization of a stochastic process will be impossible unless some simplifying assumptions are made. One such assumption is the stationarity of stochastic processes. The stationarity condition implies that the mean, μ, and the variance, V(z), of the process are constant and that the autocovariance

$$\mathrm{Cov}\,(z_t, z_{t-k}) = E[(z_t - \mu)\,(z_{t-k} - \mu)] \qquad (2)$$

and the autocorrelation

$$\varrho_k = \frac{\mathrm{Cov}(z_t, z_{t-k})}{[V(z_t) * V(z_{t-k})]^{1/2}} \qquad (3)$$

depend only on the time difference, or lag, k, between the two observations.

For a nonstationary stochastic process, a changing mean can often be described by low order polynomials in time. The coefficients in these polynomials are not constant, but vary randomly with time. Such nonstationary sequences can be transformed into stationary sequences by taking successive differences of the series. In case of nonstationary variance, the time series is subjected to logarithmic or power transformations.

Another approach to simplifying the time series models is to specialize the general ARMA models to either Autoregressive or Moving Average models as described below:

Autoregressive (AR) Process.—If it is assumed that the present observation is a linear combination of past observations plus a gaussian random variable, then

$$z_k = \sum_{i=1}^{p} b_i \, z_{k-i} + r_k \tag{4}$$

In this case, the residual, r_k, is the only portion of the measurement, z_k, which can not be predicted from previous measurements.

Moving Average (MA) Process.—If the time series is assumed to be generated by a finite linear combination of past and present inputs in the form of uncorrelated random variables, then the difference equation becomes

$$z_k = r_k - \sum_{i=1}^{q} c_i \, r_{k-i} \tag{5}$$

The model always produces a stationary process.

Time Series Algorithms for SSME Data.—The first step in time series analysis involves developing univariate models. The univariate models explain the behavior of a single parameter based upon the structure of its past values. For the SSME, the univariate models are well suited to characterize parameter behavior at a given power level. Parameters such as main combustion chamber pressure, fuel preburner cavity pressure, turbopump inlet and discharge pressures and temperatures most often show stationary behavior during nominal operation at a given power level.

Univariate ARMA models have been developed for the set of parameters listed inTable 3.1 by selecting training data sets of 100 points (4 secs duration). The structure of the ARMA models for different parameters is selected based upon five criteria: 1) a loss function based on the mean square error, 2) a prediction error based on Akaike's Final Prediction Error, 3) residual analysis, 4) frequency response, and 5) pole-zero plots.

TABLE 3.1. - SET OF PARAMETERS USED IN ARMA MODEL DEVELOPMENT.

1.	LPFT_DS_PR	10.	FPB_PC
2.	LPOP_DS_PR	11.	PBP_DS_PR
3.	HPFP_IN_PR	12.	MCC-CLNT_DS_PR
4.	HPFP_DS_PR	13.	MCC_FU_INJ_PR
5.	HPOP_DS_PR	14.	MCC_PC
6.	HPOT_IN_T	15.	HPFT_DS_T
7.	HPFP_IN_T	16.	OPOV_ACT_POS
8.	LPFP_SPD	17.	LPOP_SPD
9.	HPFP_SPD	18.	HPOT_SPD

The simplest criterion for selecting the ARMA model structure is to compute the sum of squared error (the Loss Function), and pick the structure with the smallest Loss Function. But if the model is validated on

the same data set that it was trained on, the loss function will always decrease as the model order increases. To compensate for the automatic decrease in the loss function, other selection criteria need to be considered simultaneously. The second criterion that is considered is Akaike's Final Prediction Error (FPE) which is formed as

$$\text{FPE} = \frac{1 + n/N}{1 - n/N} * (\text{The Loss Function}) \tag{6}$$

where n is the total number of estimated parameters, and N is the length of the data record.

Another criterion in the model order selection is residue analysis. The residuals associated with the data and a given model ideally should be white (uncorrelated for all lags) for the model to be a correct description of the system. If the residual correlation functions are substantially outside the 99% confidence intervals established for the training data set, then the corresponding model is not a good representation of the data. The last two criteria compare the model properties in terms of pole-zero plots and the frequency response. A pole-zero cancellation or near cancellation, and high frequency artifacts in the frequency response usually indicate that lower order models may be more appropriate. Figures 3.2, 3.3 and 3.4 illustrate the model order selection process using the different criteria.

As previously stated, for the model to be a correct description of the system, the residuals associated with it and the data should ideally be white; the correlation function of the residuals should remain within the confidence interval for lags greater than zero. Figure 3.5 shows the correlation function of residuals with 99% confidence intervals for low pressure fuel turbopump discharge pressure (LPFT_DS_PR) of test 901-110 at 75% of rated power level. The univariate ARMA models have been developed by selecting training data sets of 100 points (4 secs duration). The confidence intervals associated with the residuals widen as the number of data points for estimating a model is decreased. The design of a detection system would have to consider the trade-offs between a smaller training set and a wider confidence interval.

At the onset of a failure, the model output and the measured data diverge, and the residual correlation function lies outside the confidence intervals, as shown in Figure 3.6. Figure 3.7 shows the residual correlation function for an entire test duration (test 901-110); the peak in the correlation coefficient indicates an abnormal event.

The univariate time series models have the potential for rapid detection of changes in the parameter values, assuming that the parameter shows a stationary behavior before the change takes place. A fault is indicated by the evidence of nonstationarities in the parameter values. Oscillatory behavior, for example, is nonstationary. Defects which manifest themselves as oscillatory behavior in a sensor that is normally constant will be detected by the time series algorithm, regardless of whether or not the actual value of the sensor is within its nominal operating range.

For those, parameters for example OPOV_ACT_POS and HPOT_DS_T, in test 901-364 (shown in Figures 3.8 and 3.9), that exhibit nonstationary behavior the data needs to be subjected to a differencing operation to remove the nonstationarity before an ARMA model can be developed. It was observed that for both the OPOV_ACT_POS and HPOT_DS_T, the differencing operation removed the effects on the

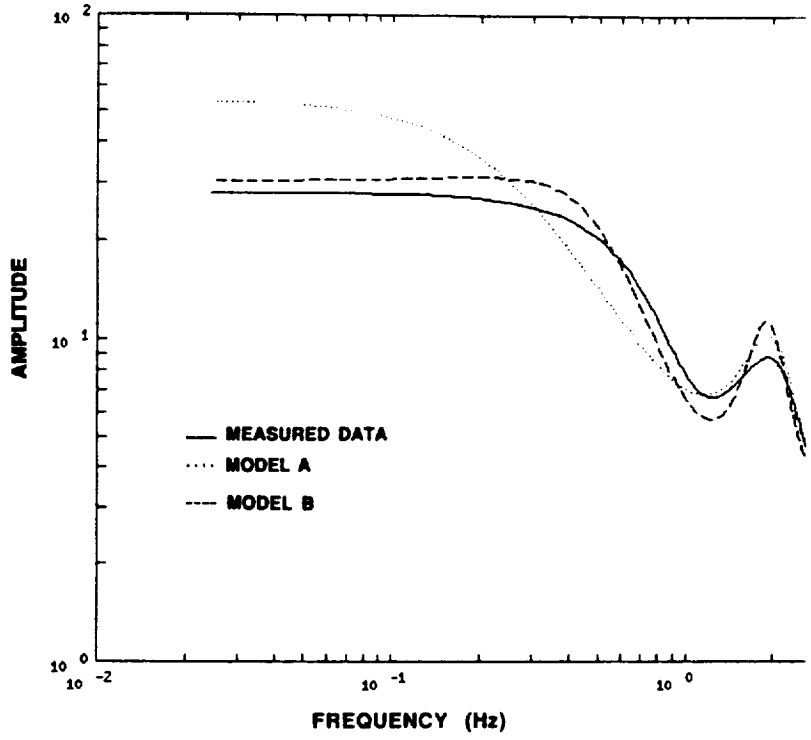

Fig. 3.2 ARMA MODEL ORDER DETERMINATION USING FREQUENCY RESPONSE

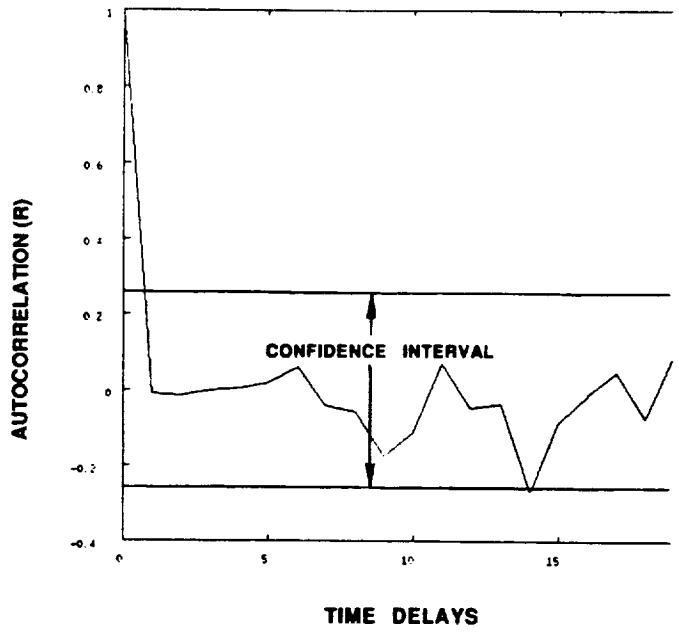

Fig. 3.3 ARMA MODEL ORDER DETERMINATION USING RESIDUAL ANALYSIS

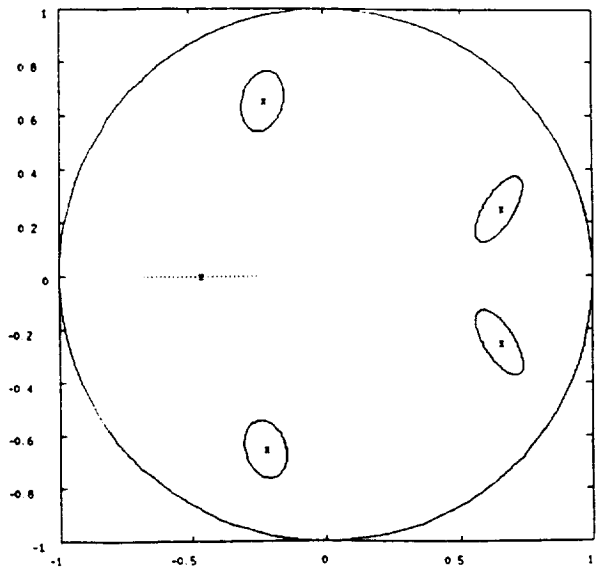

Fig. 3.4 ARMA MODEL ORDER DETERMINATION POLES AND ZEROS PLOT
Poles and zeros of model with confidence regions.

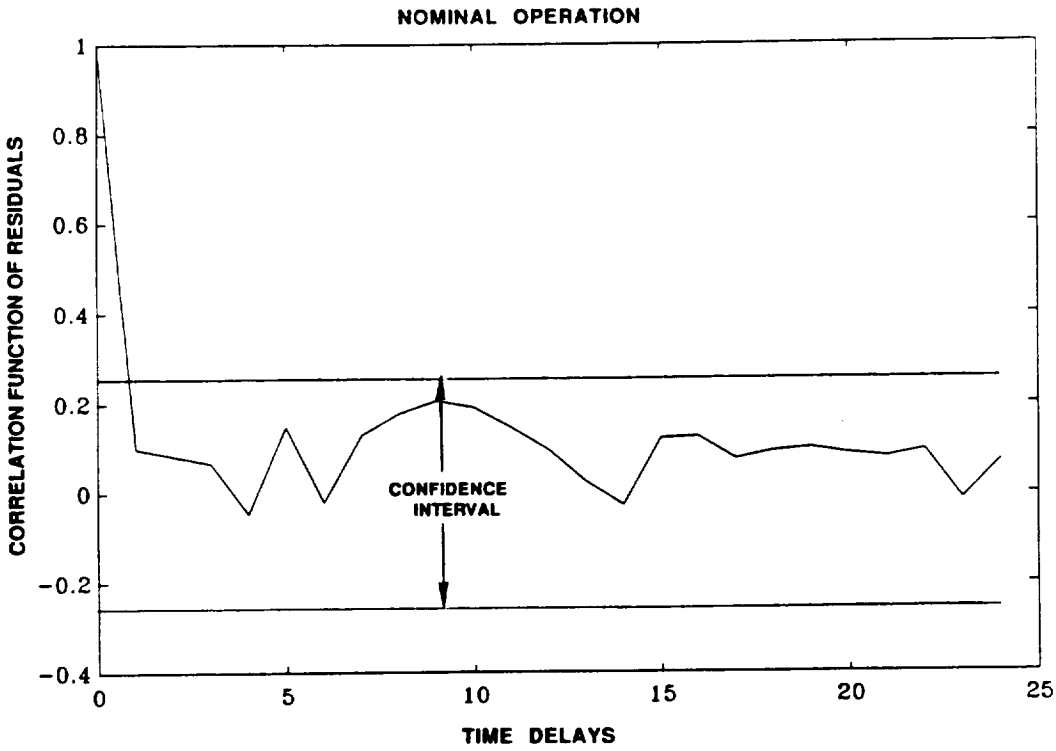

Fig. 3.5 RESIDUAL CORRELATION FUNCTION FOR LPFT DISCHARGE PRESSURE WHEN THE ARMA MODEL AND THE DATA ARE IN GOOD AGREEMENT (TEST 901-110).

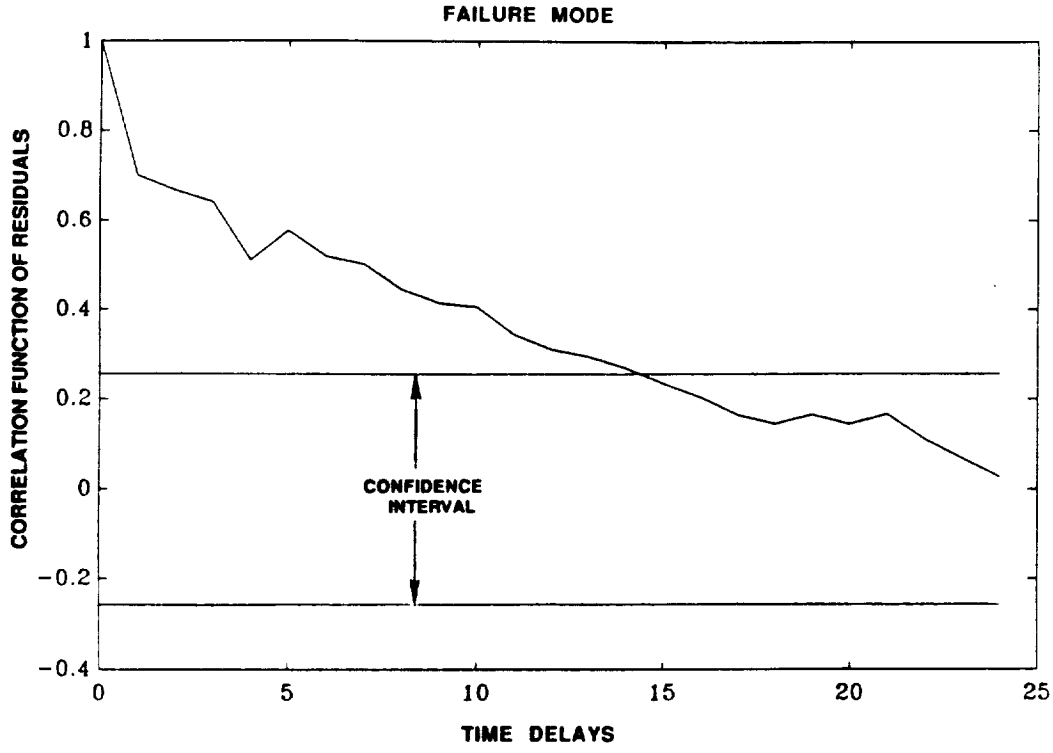

Fig. 3.6 RESIDUAL CORRELATION FUNCTION FOR LPFT DISCHARGE PRESSURE WHEN THE MEASURED DATA DIVERGED FROM THE ARMA MODEL PREDICTION (TEST 901-110).

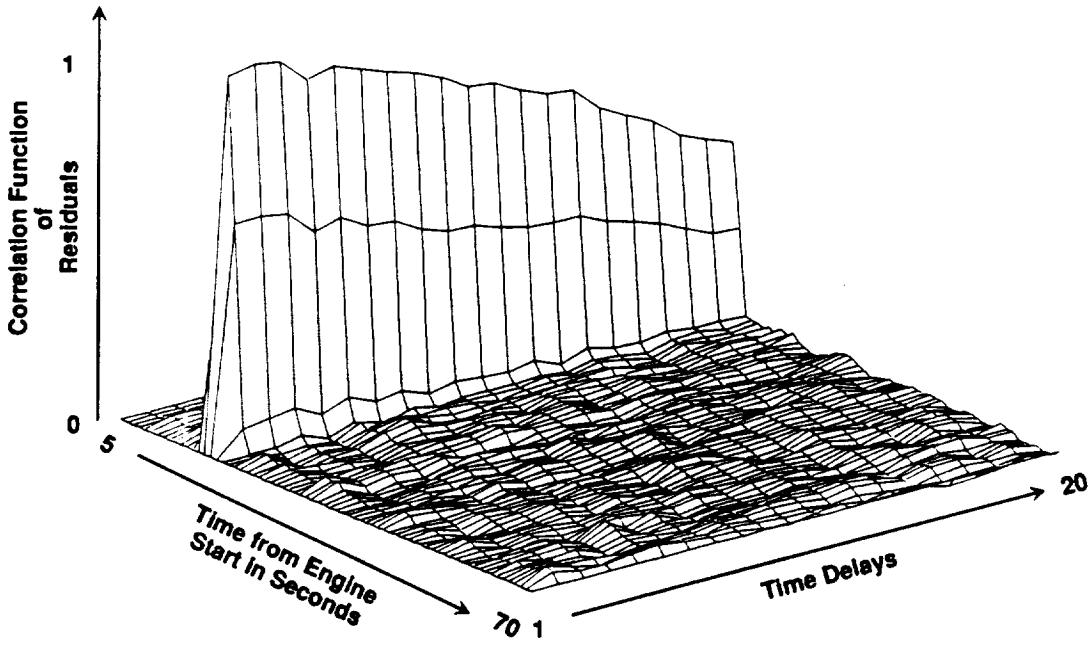

Fig. 3.7 FAILURE DETECTION USING ARMA MODELS FOR TEST 901-110

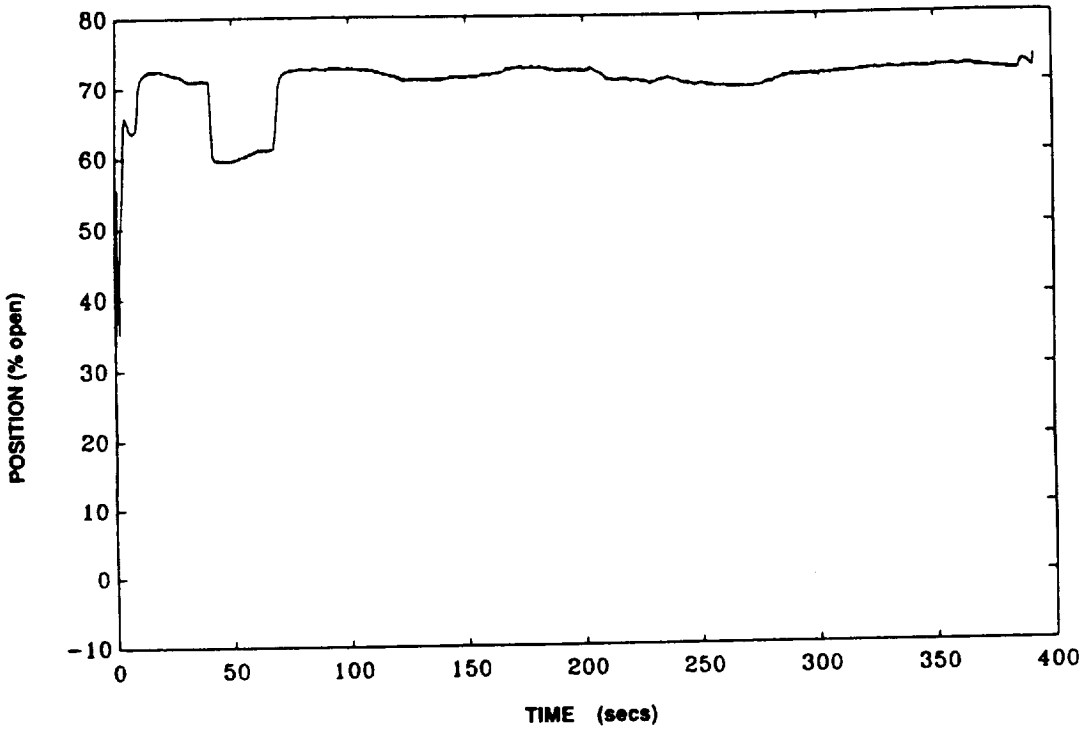

Fig. 3.8 OPOV ACTUATOR POSITION DATA SHOWING NONSTATIONARY BEHAVIOR (TEST 901-364).

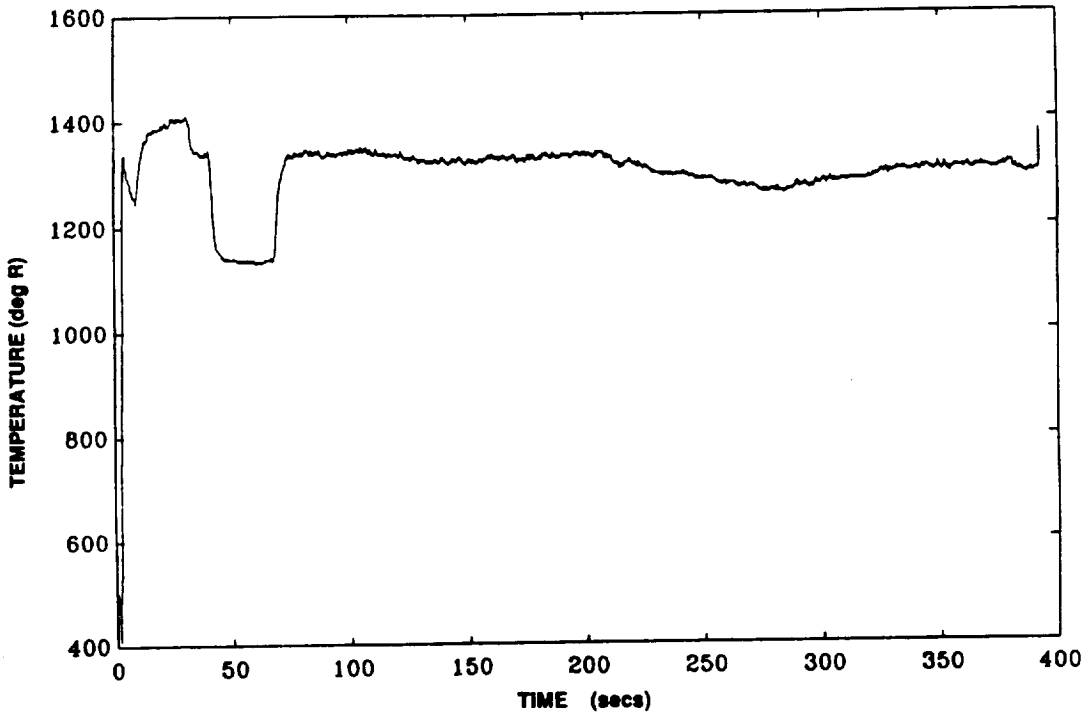

Fig. 3.9 HPOTP DISCHARGE TEMPERATURE DATA SHOWING NONSTATIONARY BEHAVIOR (TEST 901-364).

parameter values due to actual failures. For such parameters, univariate ARMA models are clearly not suitable for failure detection.

3.1.3.2 Regression Analysis.—Regression analysis can be used to detect faults in a system which are indicated by significant deviations of a sensor measured value from its expected nominal value. Regression analysis exploits sensor-to-sensor relationships to establish a set of equations (models) to predict the expected value of the sensor output during system operation. Deviation of the actual measured value from the model estimate indicates a fault. Figure 3.10 depicts the methodology for fault detection using regression analysis: models are developed in a training phase; an error signal is formed by subtracting the measured value from the linear estimate; the detection scheme determines if the error signal indicates a fault condition.

3.1.3.2.1 Linear Regression Analysis.—Linear regression analysis leads to the development of equations of the form:

$$Y = a_1 X(1) + a_2 X(2) + \ldots a_n X(n) \qquad (7)$$

The dependent variable, Y, is estimated with a weighted linear combination of the independent variables, X(i). Thus, the value of one sensor, Y, is estimated by using data obtained from other sensors, X(i). If the estimate of a sensor value differs significantly from its measured value, a change in engine performance has occurred such that the initial relationship between the sensor measurements is no longer valid. In such a case, the engine would be considered to be operating in an abnormal manner, which could indicate the presence of a fault.

The degree of association between two variables is quantified in terms of the correlation coefficient, R, and can be used to select the valid relationships for which the estimation equations can be formulated. Note, however, that the correlation coefficient should not be the sole criteria for selecting the dependent and independent variables, as the value of this statistical parameter contains no information regarding the physical operation of the system under study.

It was observed that the CADS sensors were highly correlated (see Figures 3.11 and 3.12). These large correlation values could be incorrectly interpreted to mean that significant, direct physical relationships exist between the majority of the engine parameters monitored by the CADS sensors. Furthermore, it could be incorrectly interpreted to mean that these sensors should be included as independent variables in estimating the dependent variable to which they are correlated. Detailed analysis of the SSME test data revealed that the high degree of sensor-to-sensor correlation could be attributed solely to the change in power levels that the SSME experiences in typical ground test or flight profiles.

The engine thrust level is proportional to the MCC_PC. Using the MCC_PC as the independent variable, X, the power dependency

$$Y = m X + b \qquad (8)$$

represents the resulting estimate for each of the sensors. The detrended time sequence for each sensor was produced by subtracting the estimate from the corresponding sensor data. An example of this process is shown in Figures 3.13 - 3.15. The MCC_PC (Figure 3.14) was used to estimate the Fuel Preburner Oxidizer Valve Position (FPOV POS). The estimate was subtracted from the actual measured FPOV POS (Figure 3.13) to produce the difference between the measured data and its estimated value (Figure 3.15).

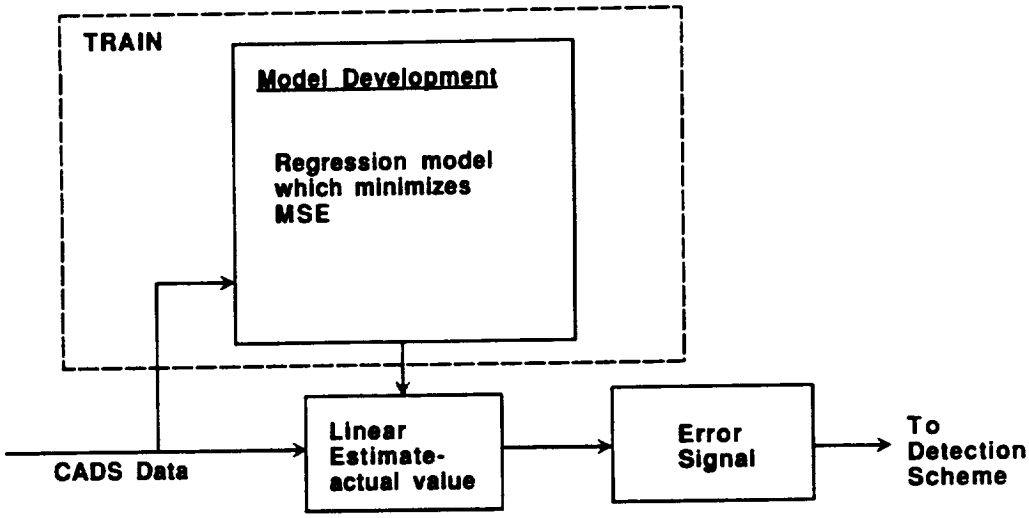

Fig. 3.10 METHODOLOGY FOR FAULT DETECTION USING LINEAR REGRESSION ANALYSIS

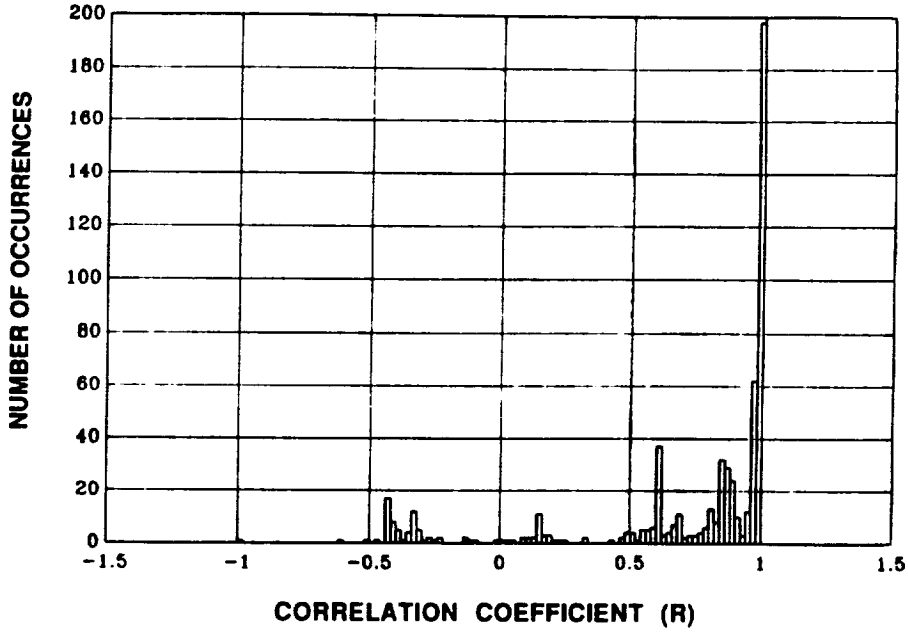

Fig. 3.11 HISTOGRAM OF CADS SENSOR CORRELATION

The CADS sensors were highly correlated.

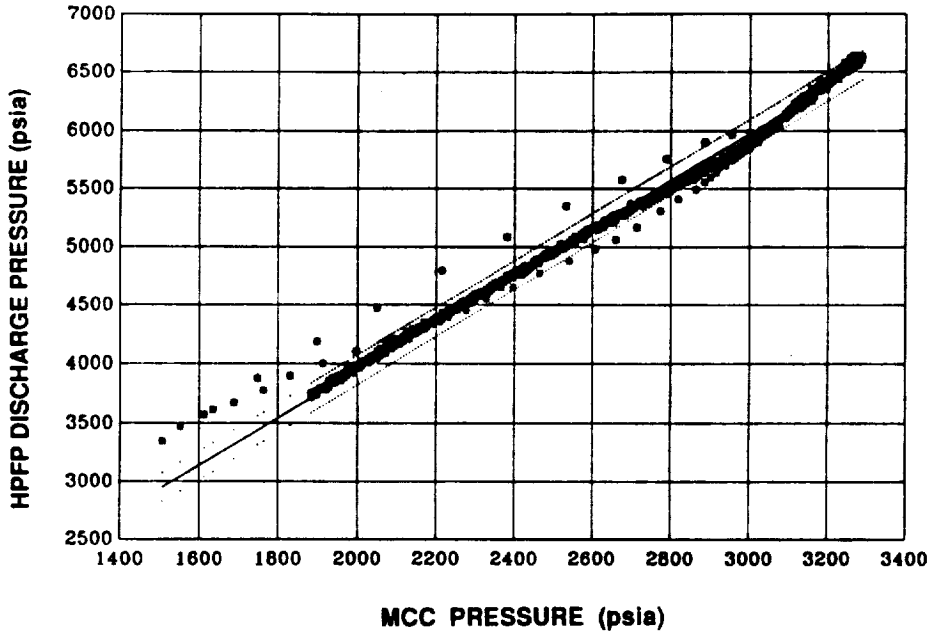

Fig. 3.12 SENSOR CORRELATION:
The CADS sensor HPFP discharge pressure data was highly correlated with the MCC pressure.

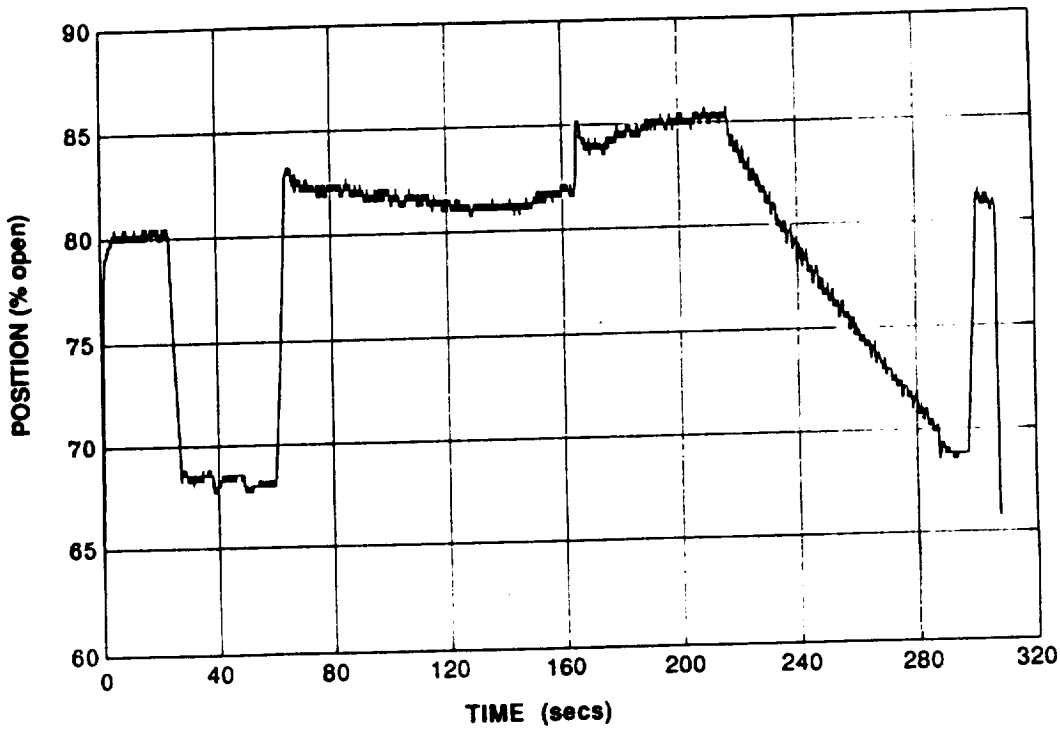

Fig. 3.13 MEASURED FPOV POSITION

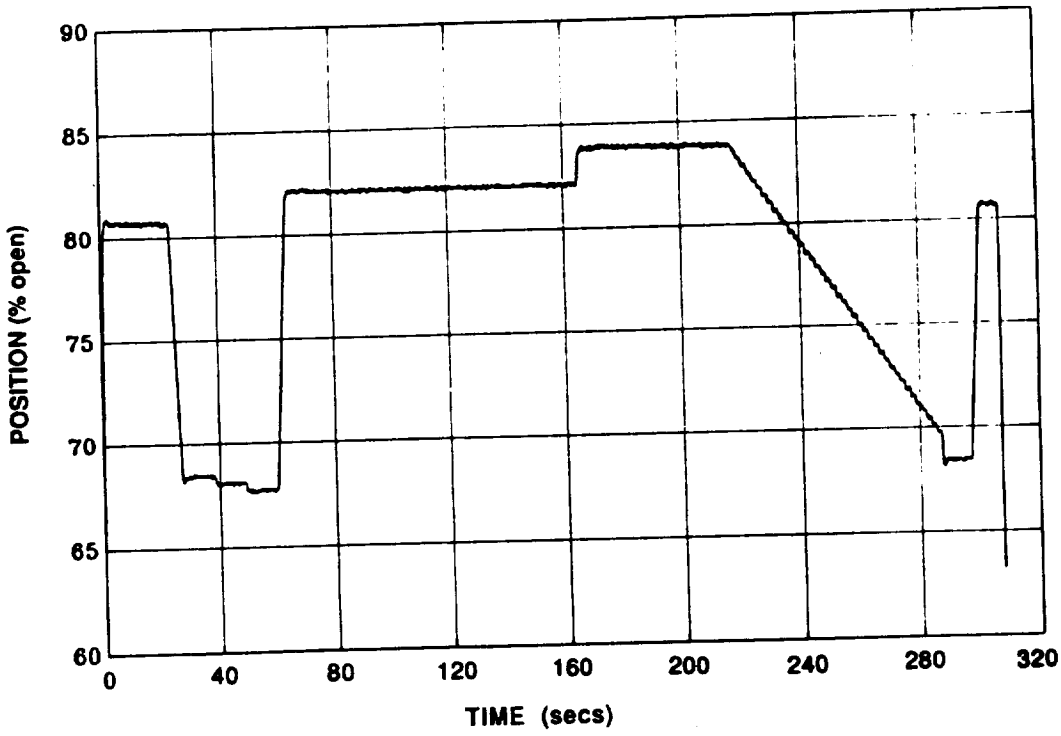

Fig. 3.14 ESTIMATE OF FPOV POSITION USING MCC PRESSURE

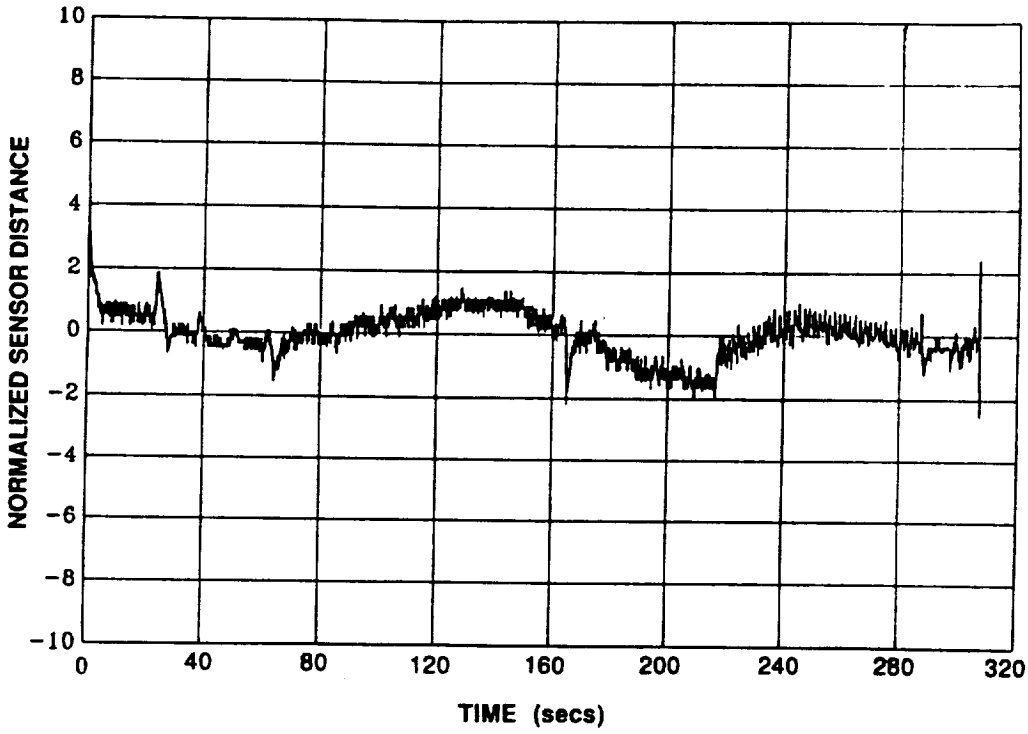

Fig. 3.15 DIFFERENCE BETWEEN THE MEASURED FPOV POSTION AND ESTIMATE OF FPOV POSITION

Once the MCC_PC trend was removed from the data, the sensor-to-sensor correlation decreased significantly (Figure 3.16), indicating that most of the sensor interdependency was associated with their dependency on the MCC_PC. Thus, using the MCC_PC as the independent variable, linear regressive equations (also known as models) for the other engine parameters were derived for estimating individual sensor values, and thereby identifying off-nominal SSME operation at steady-state power levels.

Linear models were developed for each sensor using data from the nominal data set 902-457. Evaluation of the linear regression approach by using the failure data indicated that the uncertainty of the condition of the engine components and build variations translated into fault indications, even though none were apparent. The single sensor model did not account for the variability, and thus, the deviation limits selected for the model resulted in either high false alarm (FA) rates or high missed detection of fault (MDF) rates. A model with higher limits treats all of the parameter variability as acceptable, regardless of whether the variation indicates a fault, and thus yields a high MDF rate.

Thus, the linear model approach was not sufficiently robust to accommodate normal engine variations. Consequently, linear models were not selected as viable for fault detection. The knowledge gained in exploring the linear models pointed to more robust, multivariate linear models that provide insight into the deviation from nominal operation. This technique is discussed in Section 3.1.3.3.

3.1.3.2.2 Nonlinear Regression Analysis.—During the startup and shutdown phases, the SSME operates in an open-loop mode with time sequenced commands for the opening and closing of the propellant and oxidizer valves. The MCC_PC is a function of the valve positions or the propellant flow rates. An algorithm based on nonlinear regression analysis was used to define the relationships between the MCC_PC and the valve positions or the flow rates during the startup and shutdown phases.

Description of Nonlinear Regression Algorithm (RESID).—The Recursive Structure Identification (RESID) algorithm is a nonlinear regression method based on the adaptive learning network concept. It approximates a complex nonlinear relationship between pattern features with a network of simple binary quadratic functions. It builds up the interconnections between different features recursively. The algorithm examines all pairwise quadratic combinations of features from the given feature set and builds a higher order nonlinear regression equation. The regression equation acts as the discriminant function and contains only those features that minimize, in the least-square sense, the total misclassification error.

In order to build the network, the algorithm provides a training and selection step. The input feature set is partitioned into training, selection, and evaluation subsets. During the training phase, the coefficients of the quadratic fit are determined for all pairwise combinations of the input variables. In the selection process, elements with poor performance in terms of the least-square-error criterion are rejected. The remaining elements become inputs to the next level of training, and selection steps. These training and selection steps are repeated until the performance measure does not show any further improvement. The final phase, the evaluation phase, is where the overall performance of the network is determined.

Let $X = (x_1, x_2,....,x_N)$ be the N-dimensional feature vector and $w_1, w_2,..$ be the coefficients or the weights of the decision function, D(X,w). Generally, D(X,w) is a nonlinear decision function. If two classes C_1, C_2 are separable, then the coefficients of the decision function are determined in RESID by minimizing a loss function based on the mean square error. A mean square error loss function can be written as:

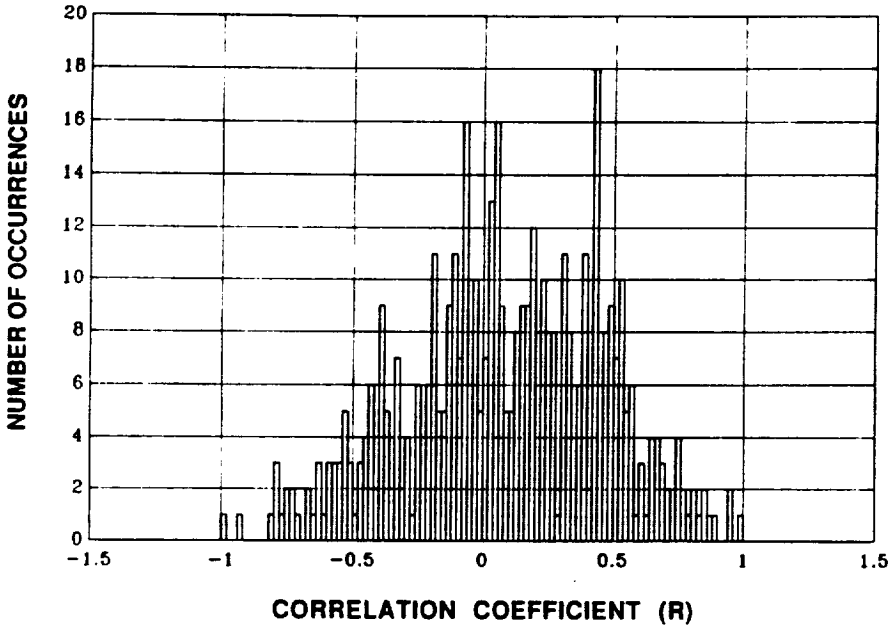

Fig. 3.16 HISTOGRAM OF CADS SENSOR CORRELATION

The correlation decreased when the variations in the FPOV associated with the engine power variation were removed.

$$J(w) = E(e^2/w),$$

where e denotes an error measure and is given by:

$$e = D(X,w) - g(X).$$

The function g(X) is some function with a desired classification property. For a two–class problem, g(X) can be defined as:

$$g(X) = \begin{cases} 1, \text{ for X element of class } C_1, \\ -1, \text{ for X element of class } C_2. \end{cases}$$

Figure 3.17 shows a two–layered RESID network. The three input variables are x_1, x_2, and x_3; and the decision function is given by D(X,w). An individual network element, E, is shown in Figure 3.18. The network element, E, combines the two inputs x_1 and x_2 by a quadratic equation to give an output, y_1:

$$y_1 = w_0 + w_1x_1 + w_2x_2 + w_3x_1x_2 + w_4x_1^2 + w_5x_2^2, \tag{9}$$

where w_0 etc. are the coefficients of the quadratic fit.

The decision function D(X,w) is given by

$$D(X,w) = az_1 + bz_2 + cz_3, \tag{10}$$

where $z_1 = f(y_1, y_2)$, etc., and a,b,c are functions of the weights, w_0, w_1, etc.

Application of RESID to the SSME Data.—During the startup and shutdown phases of the SSME operation, the controller operates in an open–loop mode with time sequenced commands to the five SSME valves (MFV, MOV, CCV, FPOV, and OPOV). Thus, during startup and shutdown, the MCC_PC is a function of the five valve positions. Since these valves control the flow of propellants, MCC_PC is also a function of the fuel and LOX flow rates.

The RESID algorithm was used to predict the MCC_PC as a function of propellant valve positions as well as propellant flow rates. Figure 3.19 shows the measured MCC_PC during startup along with its prediction calculated from propellant volumetric flow rates. Similarly, Figure 3.20 shows the measured MCC_PC during startup along with the predicted MCC_PC calculated from the propellant valve positions. Figures 3.21 and 3.22 show the ability to obtain similar MCC_PC predictions during shutdown.

The process of failure detection using RESID involves running the algorithm on nominal data first to generate the difference between the measured and predicted values of MCC_PC during startup (the nominal error signal) as shown in Figure 3.23, and then to compute the error signal. A failure is detected during startup or shutdown in other tests if the error signal crosses a threshold established at 3 times the standard deviation for the nominal error signal (see Figures 3.24 and 3.25).

Failures occurred during startup or shutdown in three instances (startup failures: 901–284 and 901–222; shutdown failure: 750–168). The RESID failure detection algorithm incorporating a model of MCC_PC as a

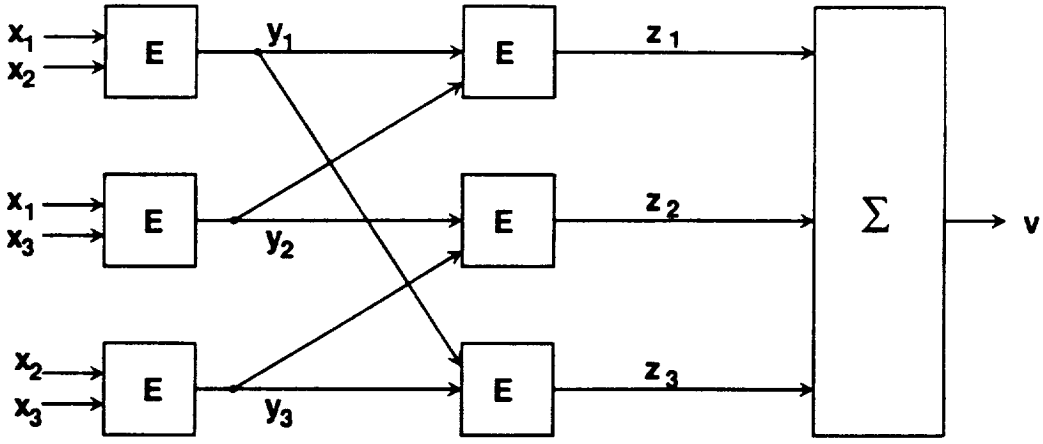

Fig. 3.17 TWO-LAYERED NETWORK OF ELEMENTS

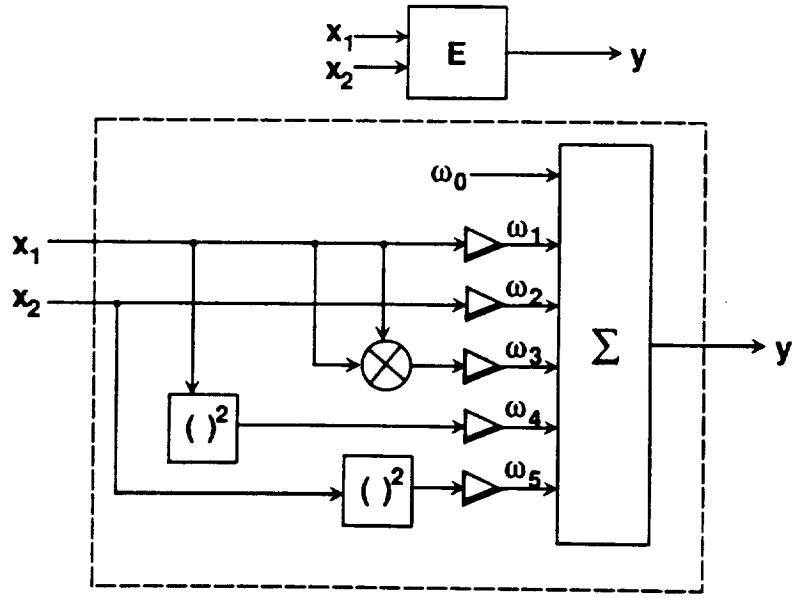

Fig. 3.18 NETWORK ELEMENTS

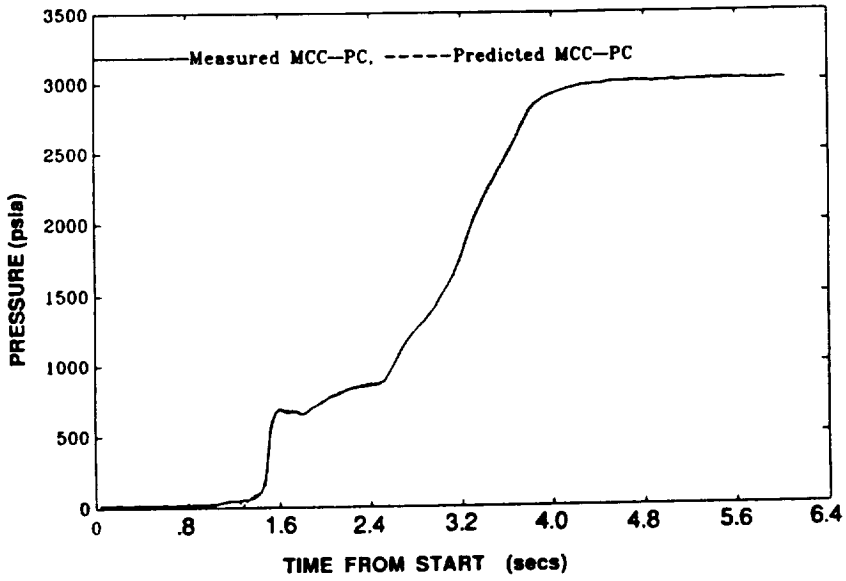

Fig. 3.19 PREDICTED MCC PRESSURE AS A FUNCTION OF PROPELLANT FLOW RATES DURING STARTUP (TEST 902-463).

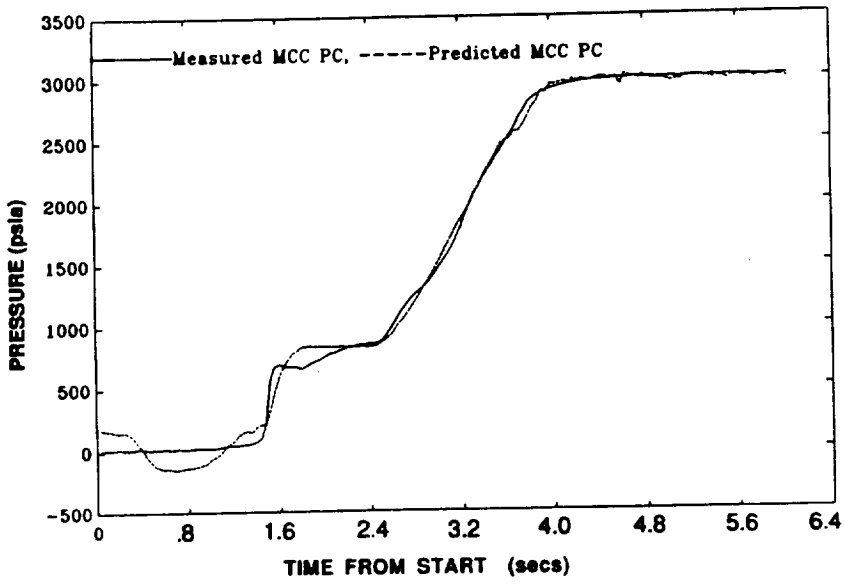

Fig. 3.20 PREDICTED MCC PRESSURE AS A FUNCTION OF PROPELLANT VALVE POSITIONS DURING STARTUP (TEST 902-463).

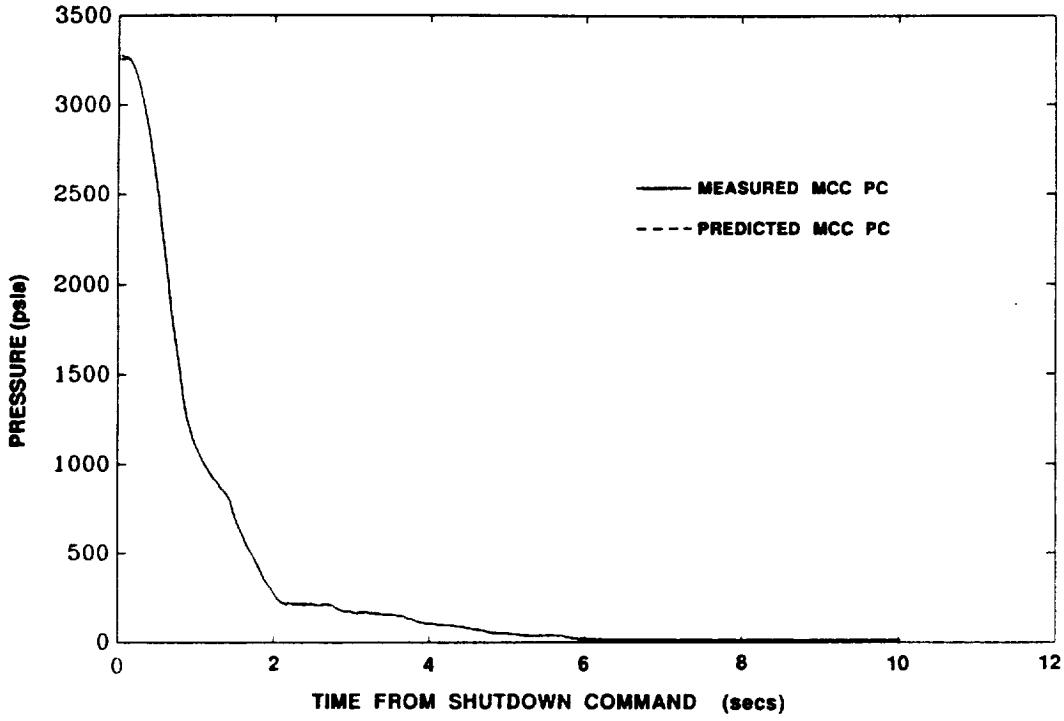

Fig. 3.21 PREDICTED MCC PRESSURE AS A FUNCTION OF PROPELLANT FLOW RATES DURING SHUTDOWN (TEST 902-463).

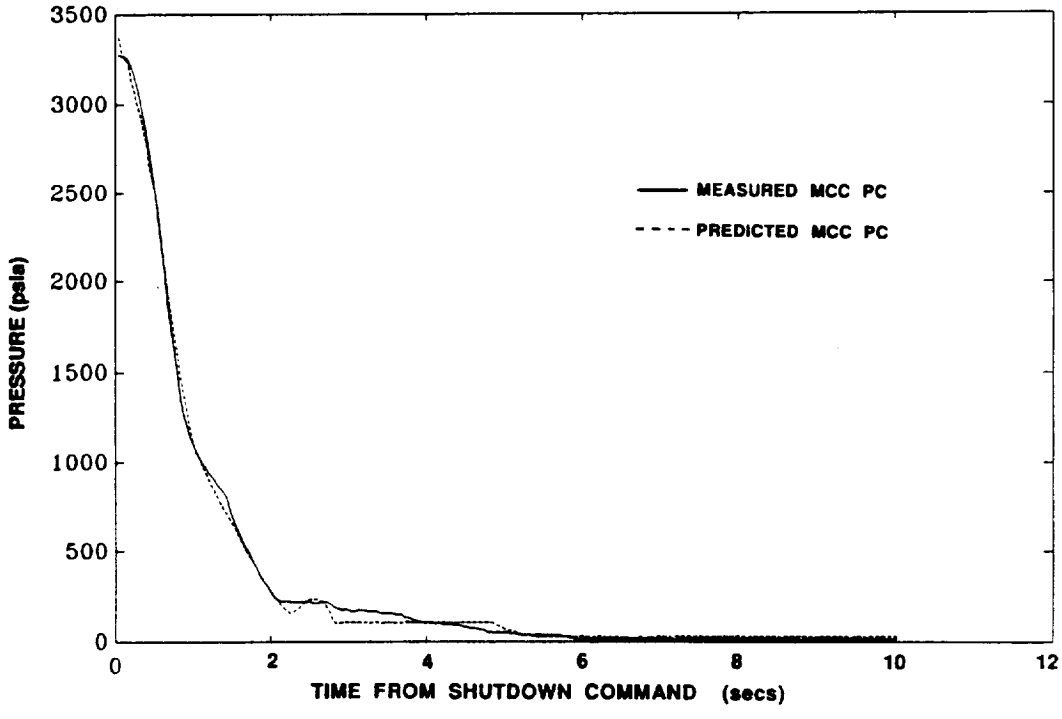

Fig. 3.22 PREDICTED MCC PRESSURE AS A FUNCTION OF PROPELLANT VALVE POSITIONS DURING SHUTDOWN (TEST 902-463).

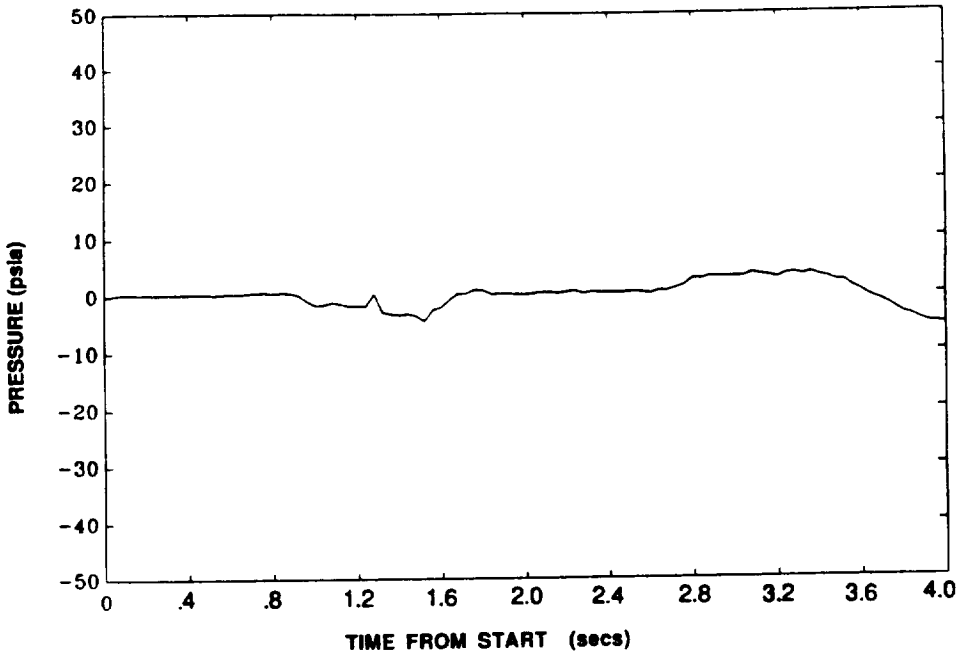

Fig. 3.23 DIFFERENCE BETWEEN PREDICTED AND MEASURED MCC PRESSURE DURING STARTUP USING NONLINEAR REGRESSION METHOD (TEST 902-463).

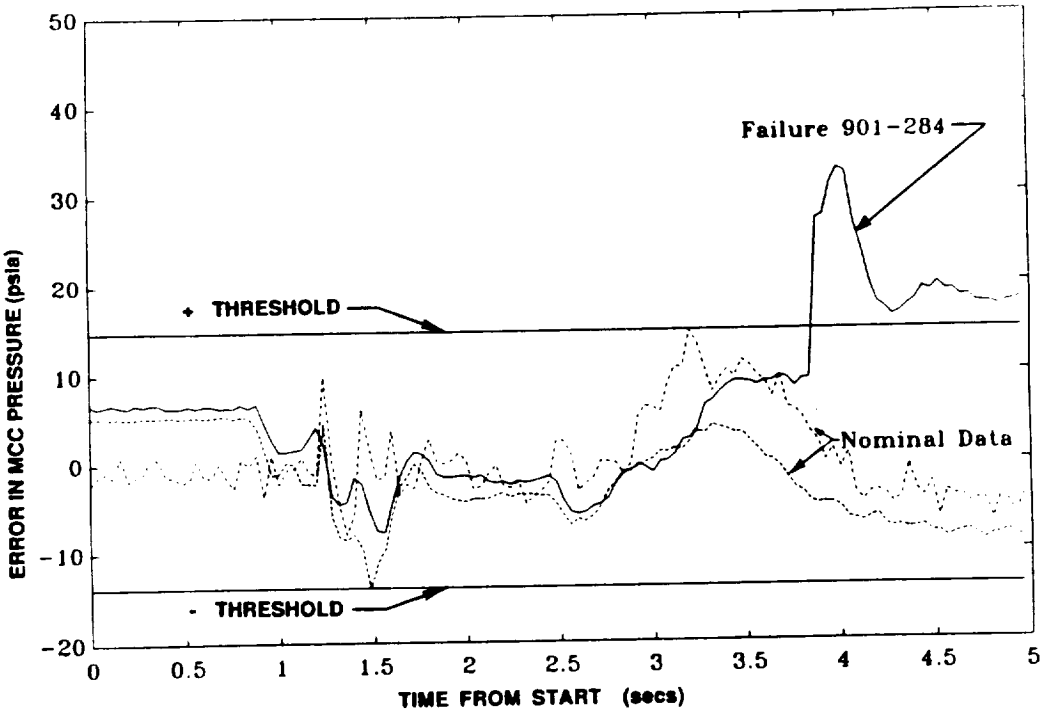

Fig. 3.24 NONLINEAR REGRESSION METHOD: DETECTION OF FAILURE DURING STARTUP

Error in predicted MCC pressure crossing threshold indicates failure.

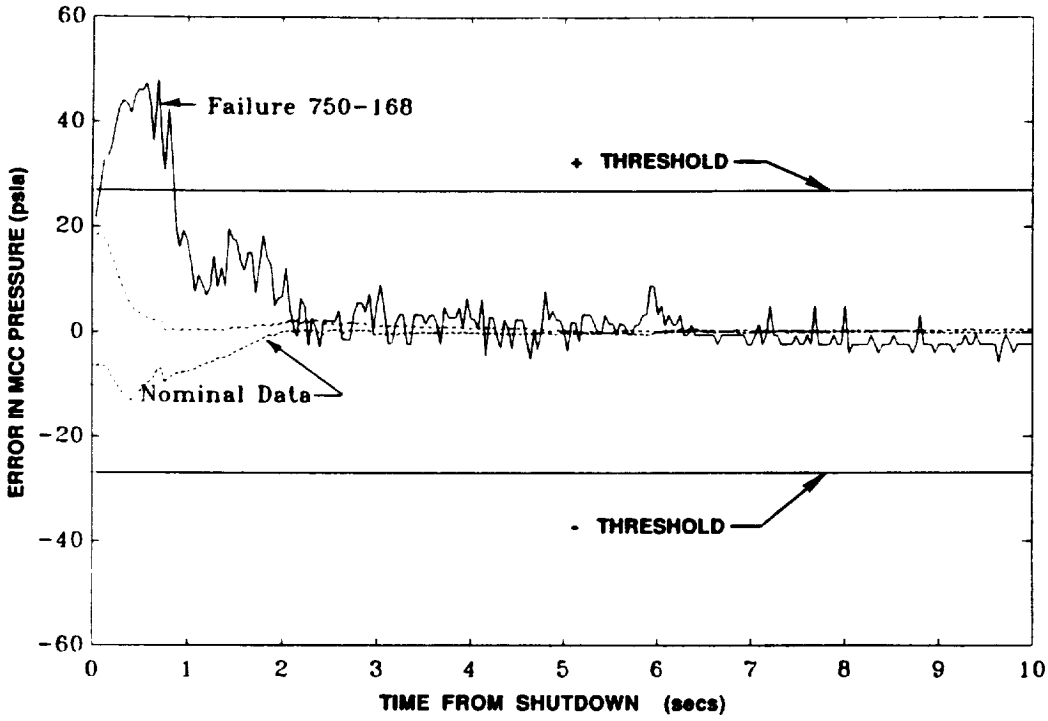

Fig. 3.25 NONLINEAR REGRESSION METHOD DETECTION OF FAILURE DURING SHUTDOWN

Error in MCC pressure crossing threshold indicates failure.

function of propellant flows was implemented. The algorithm successfully detected the startup and shutdown failures, and no false alarms were indicated with respect to the two nominal tests. Also with respect to those tests in which the failure incidence occurred during mainstage operation, there were no false alarms indicated (during startup) by this algorithm.

3.1.3.3 Cluster Analysis.—The detection of faults in the SSME can be viewed as a Pattern Recognition problem: failure detection consists of distinguishing patterns in the SSME test data which are associated with abnormal engine operation from those associated with nominal operation.

Pattern Recognition techniques encompass a variety of methods for recognizing patterns within a data sample which are associated with some phenomena (objects or processes measurable with a sensor suite). The majority of these pattern recognition algorithms are based on two fundamental procedures: a generic characterization of data patterns generated by each phenomenon to be recognized; and a recognition process in which a data pattern is compared to the generic characterization, and specific phenomena are declared to be present. How the characterization is defined and how the comparison is performed depend upon the technique used. In the following sections, these issues are discussed for the pattern recognition technique called clustering, first in general terms, and then with respect to fault detection in the SSME.

3.1.3.3.1 Clustering.—The clustering technique uses groups of multivariate data vectors to develop the generic patterns. Empirical data sources, with features derived from observations such as temperature and pressure, provide samples for these data vectors. The vectors are grouped in clusters according to their similarity. These clusters, in turn, are associated with the phenomena to be recognized.

In general, not all of the information in the cluster data vectors is required to characterize a generic pattern. Therefore, a template, or composite vector, which exhibits maximum similarity with the cluster's data vectors, should be developed for the individual clusters. One commonly used template is the mean data vector; it contains the mean value of the each variable defined by the sample data vectors. These templates represent, in a statistical sense, the significant information in the cluster samples.

Once the patterns of interest have been characterized with a set of templates, the recognition process consists of comparing a test sample to each of the templates and deciding which template matches the unknown. The best match identifies the unknown as belonging to the phenomena associated with that template; a match between an observation and a template implies the presence of specific phenomena.

3.1.3.3.2 Application to SSME.—UTRC applied clustering to the problem of fault detection by assuming the engine operates in two states: a nominal state, where the engine exhibits no performance degradation associated with a fault; and an off-nominal state, where the engine operates in any state not considered nominal. A fault detection algorithm, based on the clustering technique which detects a fault by mapping the CADS data into fault/no fault classes. This algorithm has three major components: a detection system database, a function for training and retraining the detection system, and a function for performing fault detection (see Figure 3.26).

Detection System Database.—The algorithm database contains the data required for training and detection processing. The parameters associated with training include: nominal data sets for establishing detection thresholds, the master nominal template, and a list of the active sensors. The parameters associated with detection include the test detection thresholds and the modified nominal template . Each of these parameters will be discussed more fully in the following sections.

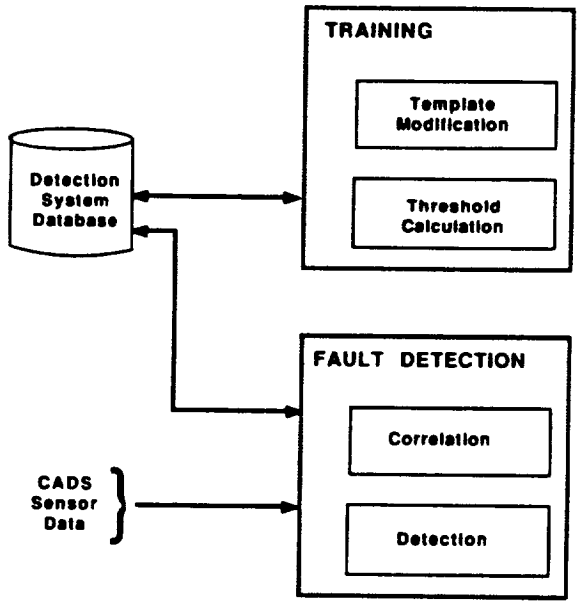

FIG. 3.26 CLUSTERING TECHNIQUE FAULT DETECTION ALGORITHM

Detection System Training.—Training the detection system involves developing the cluster templates and establishing the detection thresholds. Both will be discussed in the following paragraphs.

Template Development.—Templates represent the nominal characteristics of a cluster and are the patterns to which current test data is compared for fault detection. The cluster templates are established through the training process. Initial training for the clustering algorithm is performed off line using data taken from previous SSME firings. The three principal steps in the training process are: the selection of nominal data sets for a training database; the definition, extraction, and clustering of the multivariate data vectors from the database; and the creation of a template for each cluster.

Nominal Database.—The first step in training is the development of the sample population from which the templates are derived. Since the detection problem requires only nominal templates, the sample population consisted of the two nominal firings: tests 902–457 and 902–463. As explained in Section 2.1.1, the two nominal tests contain both CADS and Facility data. However, since facility data was not available on-site for many of the failures, only the CADS data was retained in the database and used for template development.

The CADS data provides parametric information on multiple SSME LRU's. Initially, the development of the templates was restricted to the problem of detecting faults in the HPFTP. Algorithm coverage for the other LRU's would follow in a similar manner. Hence, a subset of the CADS data which provided coverage of the HPFTP and its inputs and outputs has been selected. The list of sensors and their PID numbers is shown in Table 3.2a.

TABLE 3.2a - CLUSTER ANALYSIS SELECTED SENSORS

Order	PID No.	CADS Label
1.	32	LPFP Speed A
2.	225	LPFP Discharge Temperature A
3.	226	LPFP Discharge Temperature B
4.	52	HPFP Discharge Pressure A
5.	58	FUEL Preburner Pressure A
6.	260	HPFP Speed A
7.	261	HPFP Speed B
8.	231	HPFT Discharge Temperature A
9.	232	HPFT Discharge Temperature A
10.	24	MCC Hot Gas Injector Pressure A
11.	17	MCC Coolant Discharge Pressure A
12.	18	MCC Coolant Discharge Temperature B
13.	59	FUEL Preburner Pump Discharge Pressure

Data Normalization.—Clustering is based on a measure of similarity between multiple variables. Thus it is necessary to normalize the data in some manner to allow equal sensitivity to each of the sensors, whether they measure temperature, speed, or pressure. Data normalization is typically achieved by using population parameters, such as the mean and variance of a sensor signal. For this application, data normalization was complicated by the fact that the data did not appear to be distributed in a manner characterized by a typical distribution function and, further, because the nominal data sample was insufficient to characterize the population.

It was found, however, that normalization of the sensors could be achieved by using the PBM estimates of each CADS sensor in conjunction with the CADS data. A data vector, d(i,t), composed of the multiple sensors listed in Table 3.2a, was normalized at each time sample, t, using the following equation:

$$d(i,t) = \frac{\text{PBM ParameterEstimate (i, Power level (t)) - sensor value (i, t)}}{\text{PBM Parameter Estimate (i, Power level (t))}} \quad . \quad (11)$$

i - sensor index
t - sample was collected at time t

This equation can be restated in the form:

$$d(i,t) = 1 - \frac{\text{sensor value (i, t)}}{\text{PBM Parameter Estimate (i, Power level (t))}} \quad . \quad (12)$$

The PBM Parameter Estimates for each selected sensor were determined by extracting values at seven rated SSME power levels (65%, 70%, 80%, 90%, 100%, and 104% RPL) from the PBM output, and fitting a polynomial to these values. The polynomial coefficients for the parameters are listed in Table 3.2b, and were utilized in the cluster algorithm as follows:

$$\text{PBM Parameter Estimate (i, PL (t))} = c_1\, PL^3(t) + c_2\, PL^2(t) + c_3\, PL(t) + c_4$$

where i = sensor index
PL (t) = power level (%RPL) at time t.

TABLE 3.2b - COEFFICIENTS FOR PBM PARAMETER ESTIMATE POLYNOMIALS

POLYNOMIAL COEFFICIENTS				
PID No.	**C_1**	**C_2**	**C_3**	**C_4**
32	0	6.2331e-01	-4.0070e+01	1.3357e+04
225	1.1072e-05	-2.5400e-03	1.9834e-01	3.7197e+01
226	1.1072e-05	1.9834e-01	1.9834e-01	3.7197e+01
52	1.0601e-02	-2.4529e+00	2.4773e+02	-4.7743e+03
58	2.2294e-03	-4.0778e-01	7.9094e+01	-1.1197e+03
260	0	0	2.1157e+02	1.3126e+04
261	0	0	2.1157e+02	1.3126e+04
231	3.8781e-03	-9.33863-01	7.8306e+01	-7.2104e+02
232	3.8781e-03	-9.3386e-01	7.8306e+01	-7.2104e+02
24	0	0	3.3214e+01	-9.8566e+01
17	6.3262e-03	-1.4614e+00	1.5783e+02	-2.8293e+03
18	0	0	-1.2553e-01	4.7722e+02
59	0	0	8.3784e+01	-1.3382e+03

An example of a normalized data vector is shown in Figure 3.27. This is a bar plot of the d(i,t) vector for all thirteen sensors at one sample point in time. The x-axis is the PID number for a CADS sensor from Table 3.2a, and the y axis is the value of d(i,t) for each PID.

Nominal Template Development.—The normalized data vectors, d(i,t), were used to define a template for nominal operation of the SSME. The d(i,t) vectors were computed for mainstage operation of the nominal test 902–463. The data was then clustered by calculating the correlation coefficient between each sample vector, and grouping those with a correlation value greater than 0.95 into a cluster. A template was created from the cluster by averaging the d(i,t) vectors of the cluster over the time index. The resultant template is shown in Figure 3.28.

The nominal template shown in Figure 3.28 was tested to determine its degree of similarity to the two nominal data sets. The similarity was quantitatively measured by the correlation between the template and the sample data vectors. Figure 3.29 shows the correlation between each d(i,t) vector of nominal test 902–463 and the nominal template. As seen in the plot, the correlation is approximately 1 for most of the run. The exceptions are during rapid power transients and during operation at 65% RPL, where the correlation falls to 0.95.

Similarly for nominal test 902–457, the correlation between each sample vector and the nominal template was computed. The results are plotted in Figure 3.30. The correlation remained greater than 0.95 for the majority of the data except, again, during the rapid power transients. The template was thus considered to be an adequate characterization of nominal engine operation based on this limited data set.

Detection Thresholds.—Two detection thresholds must be established prior to a test: an event detection threshold, and a fault detection threshold. The event detection threshold is required by the algorithm to decide whether an observation, d(i,t), matches the nominal template, while the fault detection threshold is required to determine if a significant number of event detections have occurred for a fault indication.

The event detection threshold is calculated by the steps shown in Figure 3.31. First, the list of valid PIDs for the test is read from the Detection System Database and used to create a modified nominal template. The modified template is derived from the original template by removing those PIDs not contained in the list of valid PIDs for the specific test. Next, the correlation coefficients are calculated between the modified template and the 902–463 nominal test data. A histogram of the correlation coefficients is then computed and the correlation value for the 1st percentile is determined. This correlation value is multiplied by a scale factor of 0.95 and saved as the event threshold. The scaling by 0.95 was used to adjust the threshold, thereby, reducing the chance of a false alarm.

The event threshold is used to make the initial decision that a potential fault exists. The final decision is made using the fault detection threshold. The fault detection threshold is set to minimize the probability of a false alarm. Since the data populations are unknown, the fault detection threshold was selected using a false alarm probability derived from the 902–463 nominal data. An m out of n detector was used for fault detection. Based on the false alarm probability of test 902–463, m was set to 5 and n was set to 5. These values remained fixed for all further clustering algorithm tests.

Fault Detection.—Prior to the initiation of an engine test, the training module defines the template and the detection thresholds for the fault detection system. At runtime, the detection module processes the CADS data to detect engine faults. The fault detection module, shown in Figure 3.32, is composed of the functions for template/data correlation, event detection, and fault detection.

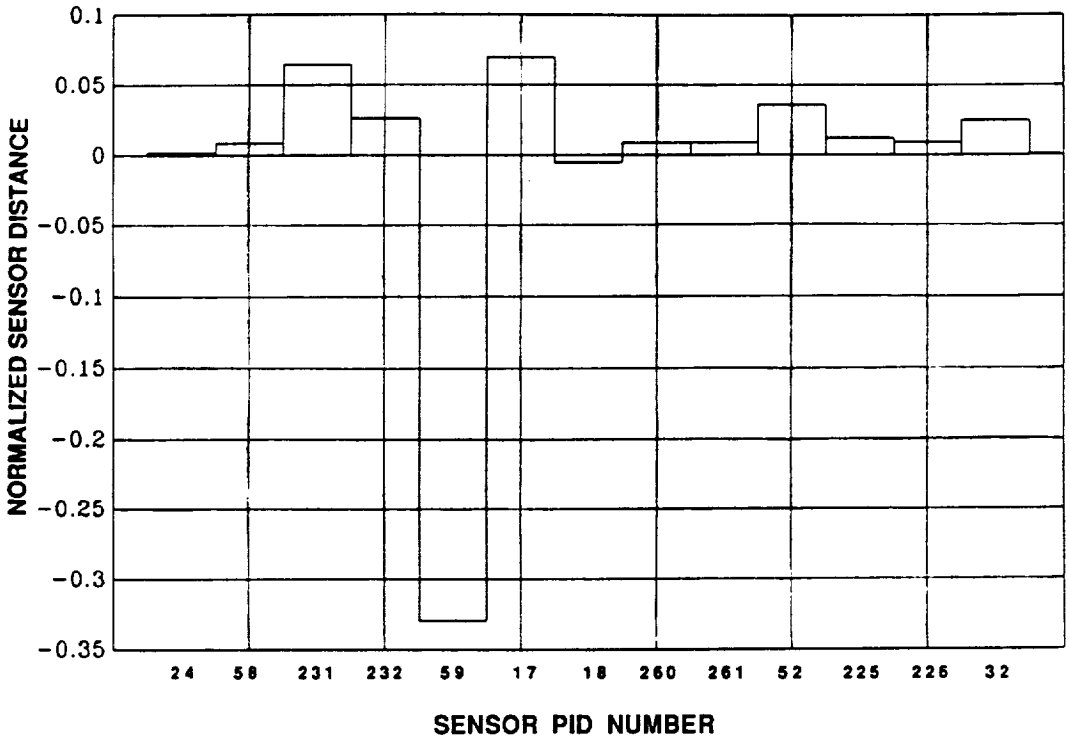

Fig. 3.27 EXAMPLE OF NORMALIZED SENSOR VALUES (d(i,t))

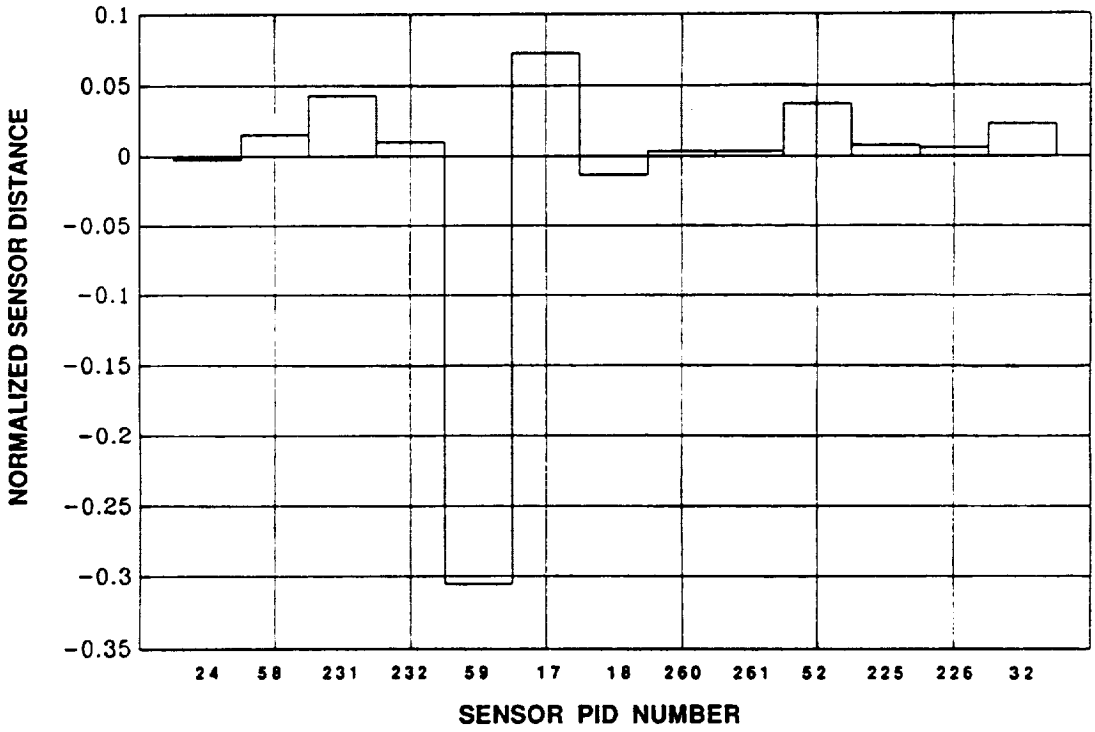

Fig. 3.28 NOMINAL TEMPLATE COMPRISED OF NORMALIZED SENSOR VALUES FROM TEST 902-463

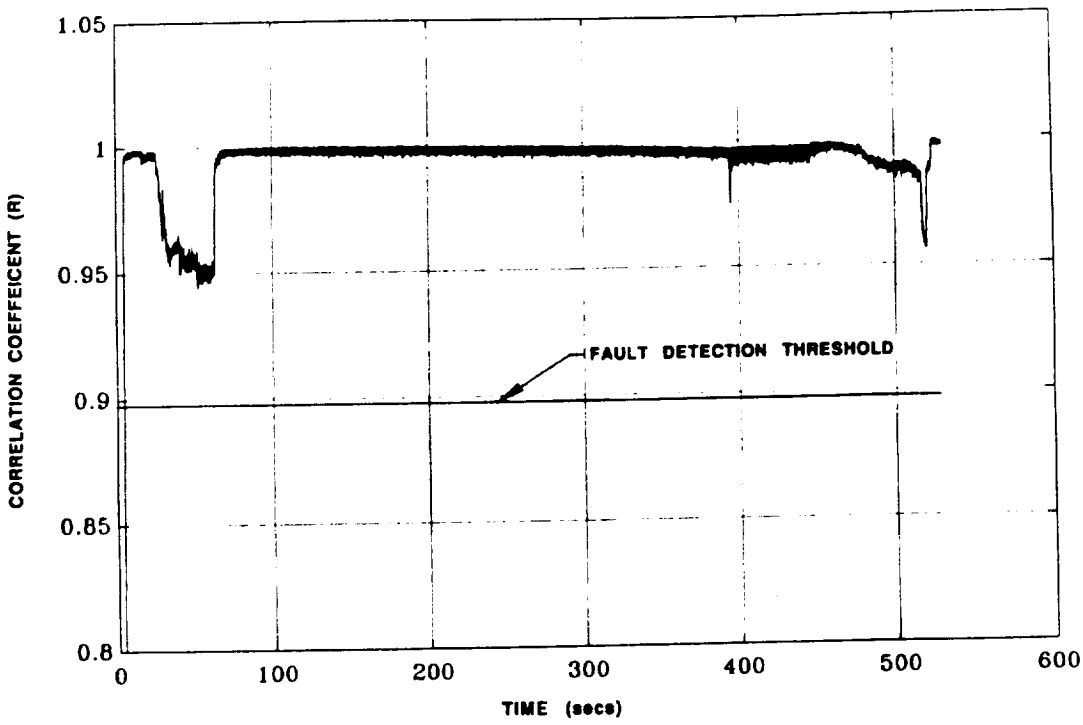

Fig. 3.29 CORRELATION BETWEEN NOMINAL TEMPLATE AND TEST 902-463 NOMINAL DATA SET.

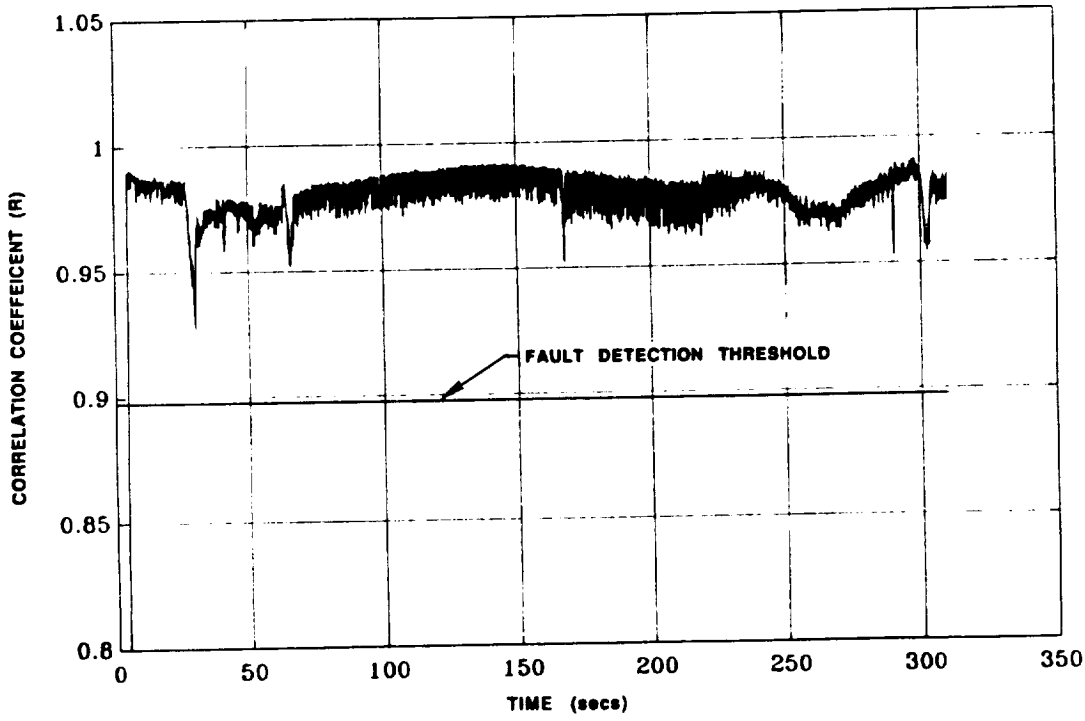

Fig. 3.30 CORRELATION BETWEEN NOMINAL TEMPLATE AND TEST 902-457 NOMINAL DATA.

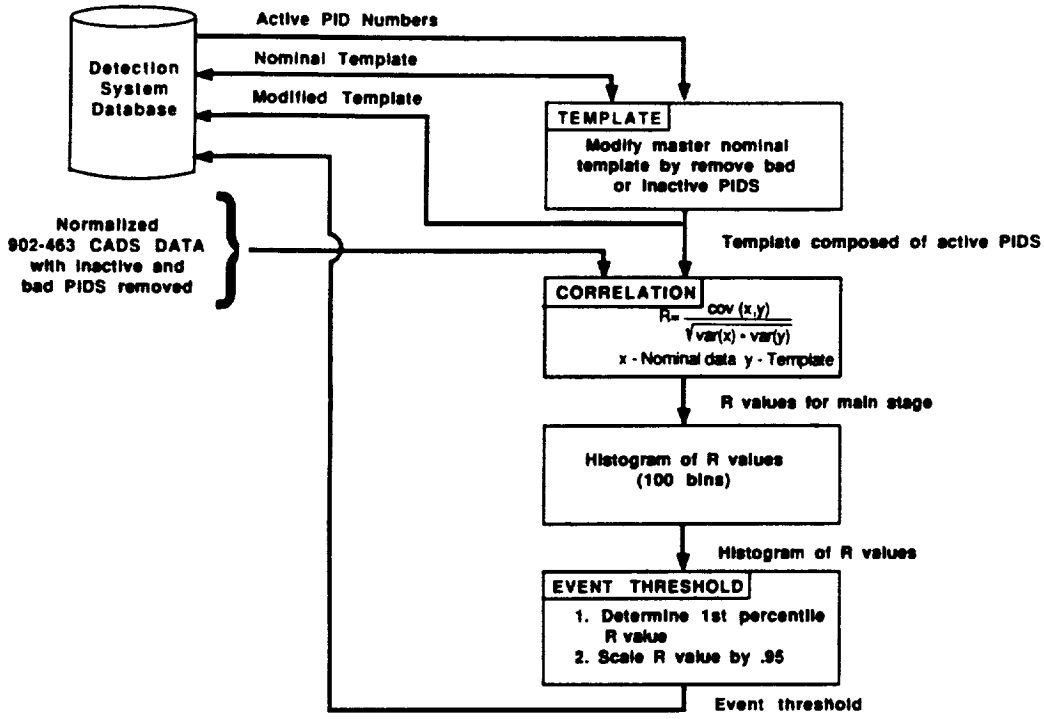

FIG. 3.31 CALCULATION OF EVENT DETECTION THRESHOLD

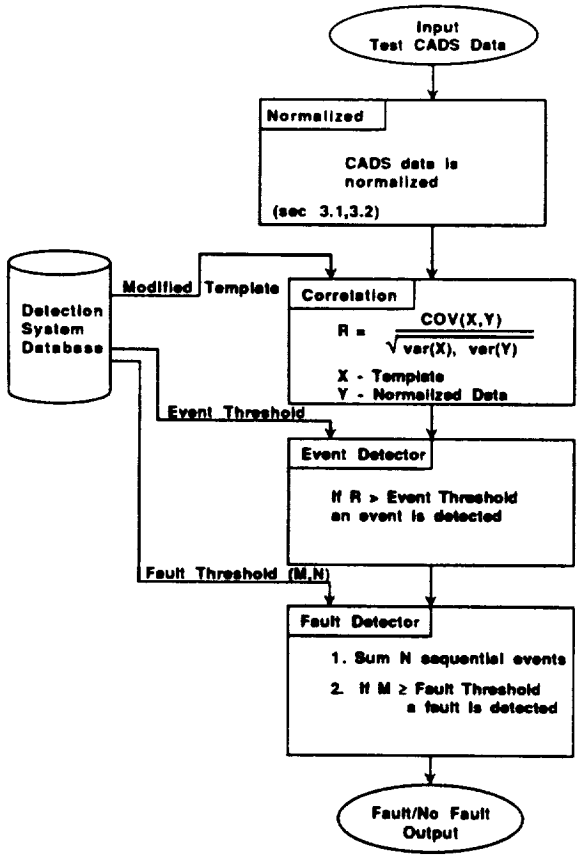

Fig. 3.32 FAULT DETECTION PROCESSING

The CADS data was first normalized by the procedure described above, then the correlation function performed a correlation between the CADS data and the current template for each time sample. The function output was a correlation value between 1 and -1 for each time sample.

The correlation values and the event detection threshold were input to the event detection function which compared the correlation value at each time sample to the event threshold. If the correlation value for the current sample exceeded the threshold values, an event is declared by outputting a 1. If the correlation value is within the thresholds, the detector outputs a 0.

The event detections were counted in the fault detector as they were outputted from the event detector. The fault detector counted the events sequentially for 5 samples. A fault was declared if the sum of the event counts exceeded the fault detection threshold of 5 events. The output of the fault detector was a 1 when the threshold was exceeded, and a 0 otherwise.

Factors Affecting Algorithm Performance — Empirically derived algorithms, such as clustering, achieve their optimal performance when operated within the constraints used to develop them. For the clustering algorithm, these constraints include the sensor set selected for input, the PBM estimators, and the use of the correlation value as a measure of the pattern similarity. Changes in any of these constraints may affect the fault detection performance of the algorithm. Three major factors which affect the clustering performance are currently under study by UTRC and NASA-LeRC.

The first factor affecting the clustering performance is the makeup of the sensor set selected for input to the algorithm. The sensor set shown in Table 3.2a was selected to provide the maximum physical coverage of the HPFTP with the sensors available for the nominal tests. The loss of certain individual sensors affects the performance of the algorithm more than other sensors, as observed in the test results given in in Appendix A. Efforts are underway to establish the sensitivity of each individual sensor to the fault detection performance of the algorithm.

The second factor affecting the algorithm performance is the equations used to estimate the PBM values and the normalization of the data based on those PBM values. The ratio of the measured sensor value to its PBM estimated value (Eq. 12) determines the magnitude of the deviations for a given template. As this ratio approaches one, small components of the sensor signal, which otherwise would not affect the algorithm, begin to dominate. A better estimator of nominal engine operation or a change in the engine such that it operates closer to its predicted state are two examples of conditions which will cause the normalization ratio to approach unity. Once this condition exists, factors such as sensor signal noise and errors in the PBM estimator due to engine power level changes tend to dominate the resultant of Eq. 12, and thus, produce erratic results for the fault detection. Furthermore, it can be shown that the PBM estimator in Eq. 12 acts as a weighting function which emphasizes each parameter according to its accuracy of estimation. In this manner, certain parameters may be unintentionally weighted to have more of an effect on the clustering algorithm (see Sections A-10 and A-13). Therefore, it is important that the PBM estimation coefficients listed in Table 3.2b be used for the clustering algorithm to achieve successful results. UTRC and NASA-LeRC are studying the weighting function of the PBM estimator to improve algorithm performance and robustness. One potential improvement is the selection of a weighting value for each parameter based on an engineering judgement rather than an arbitrary value.

The third factor which affects the clustering algorithm performance is the use of correlation to compare the test template with the nominal template. As stated previously, this technique may produce erratic results

when the normalization ratio approaches one. UTRC and NASA-LeRC are investigating other similarity measures which may be more appropriate.

3.1.4 Summary of Failure Detection Algorithms.—The objective of this task was to identify and evaluate fault detection algorithms that meet the HMS program goals for incorporation into the HMS framework architecture. According to program requirements, an algorithm performance evaluation criterion was established: failure detection algorithm performance was evaluated based upon its probability of failure detection; probability of false alarms; and time of detection.

A data-driven approach to the algorithm development process was taken because of inadequately defined fault characteristics which precluded the definition of precise analytical models of failure modes. The lack of analytical programs for fault modeling, and the availability of a large SSME database of nominal and failure data also contributed to the decision to use empirical methods. Furthermore, empirical methods are more suitable for fault detection in the HMS real-time environment. Analysis showed that faults manifest themselves in the SSME data as long duration trends, quick transitions, or oscillatory variations; each must be detected by the failure detection scheme. Finally, in lieu of sufficient nominal data, information from the SSME analytical models (PBM and DTM) was incorporated into the fault detection algorithms.

The HMS failure detection algorithms developed by UTRC successfully cover all modes of SSME operation. A nonlinear regression algorithm (RESID), which exploits the nonlinear relationships between engine parameters, was used to detect failures during the open-loop startup and shutdown modes. Fault detection during SSME mainstage operation was covered by both time series analysis and cluster analysis. The time series ARMA models use the behavior of past data to predict the behavior of future data and are capable of detecting rapid or oscillatory failures during mainstage. Cluster analysis utilizes the pattern of differences between measured and design point data to detect gradual, slow trend failures, as well as rapid failures.

The UTRC failure detection algorithms were run on test data from a total of 16 failure incidences and 2 nominal tests. The individual algorithms, when used with a complete sensor set, had no false alarms when tested on nominal data. Although the algorithms are generally robust to sensor loss, the results in Appendix A show that the clustering algorithm, in three cases, was sensitive during power transitions to the loss of certain sensors. Further study of this sensitivity is currently proceeding. Table 3.3 presents the failure detection times for the time series ARMA, RESID, and clustering algorithms. For each test, the UTRC HMS algorithm detection times are compared to those from SAFD and redline cutoff. The number of sensors missing for each test are also indicated.

The failure detection times were earlier than the redline cutoff times and the SAFD detection times except in cases of structural failures, where there were no prior indications. In most cases, the failures were detected early enough to allow for a normal engine shutdown. The UTRC HMS failure detection scheme is effective because it does not rely on a single algorithm or a single sensor measurement. The ARMA and clustering algorithms provide double coverage during mainstage operation, and have proven to be robust to sensor loss. Furthermore, the fact that the algorithms detected failures on data which covered an engine development and test period from 1977 to 1989, demonstrates that they are capable of handling engine build-to-build variations.

3.1.5 Failure Detection System.—The algorithms described above have shown their individual capabilities to detect failures within the engine. A simplistic failure detection system such as the one shown in Figure 3.33

Table 3.3 ALGORITHM PERFORMANCE - DETECTION TIMES

Test No.	SENSORS MISSING	UTRC HMS			SAFD	RED-LINE
		Non-Linear	Cluster	ARMA		
901-110	4	N/A	Missing PC Data	16.0	N/A	74.1
901-436	0	N/A	302.4	70.0	N/A	611.0
901-364	1	N/A	42.7	210.0	216.7	392.2
901-307	3	N/A	8.6	9.0	55.5	75.0
902-198	0	N/A	5.8	8.5	5.4	8.5
902-249	1	N/A	5.2	160.0	388.2	450.6
901-225	2	N/A	255.6	16.0	255.6	255.6
750-168	1	300.2	300.2	N/A	N/A	300.2
901-284	5	3.9	5.2	9.0	5.2	9.9
750-259	1	N/A	101.5	101.5	N/A	101.5
901-173	6	N/A	102.1	188.0	188.9	201.2
901-331	4	N/A	50.2	233.0	N/A	233.1
901-222	2	4.3	N/A	N/A	N/A	4.3
901-340	4	N/A	405.5	12.2	12.2	405.5
SF10-01	9	N/A	N/A	104.8	N/A	104.8
SF6-01	------- Corrupted Data -------				N/A	18.6

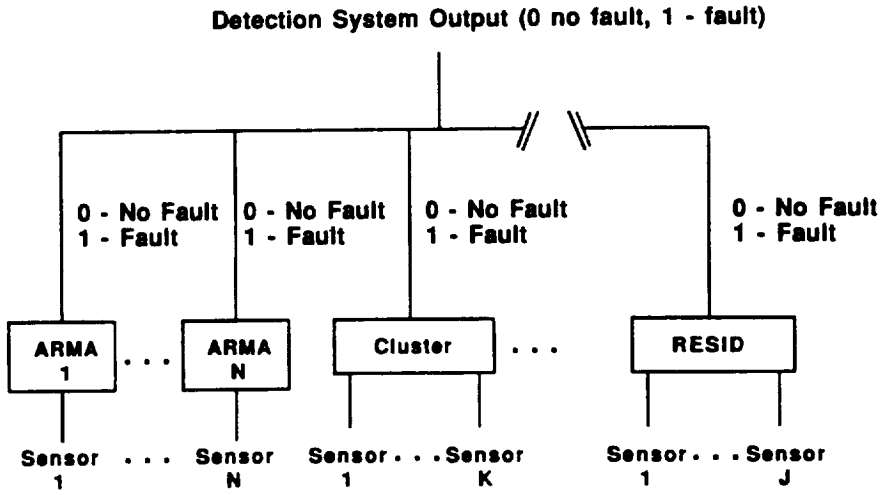

Fig. 3.33 SINGLE LEVEL FAULT DETECTION SYSTEM

could be designed to provide detection of the engine failures. The system would consist of parallel detection algorithms whose inputs are single or multiple CADS sensors, and whose output would be binary fault/no fault decisions. Each output would have equal opportunity to shutdown the engine. Such a system is simple and fast due to its parallel decision making and lack of vertical integration. However, the system is prone to a higher false alarm probability and a lower detection probability. Introduction of some vertical integration to the design will reduce these two fallacies, and only slightly degrade the system speed.

The detection system shown in Figure 3.34 is a hierarchical design which will provide fast and accurate detection of engine failures. The hierarchical design inputs the data as previously described in the single level scheme, but the outputs of the detection modules (ARMA, RESID, CLUSTER) are now integrated in the next higher level of the system to assess the health of the individual LRUs. This level then outputs its results to the next level for integration and an assessment of the overall engine status. At any point in the vertical direction, the output could be used to make a fault/no fault decision. However, a more robust detection methodology is achieved by using further integration. Further details of this design are given in Section 4.1.

3.2 Advanced Technology Sensors

The fault detection performance of an HMS for virtually any mechanical system is directly related to the quality of the information provided by sensors which monitor the system. A limitation common to retrofit installations of HM systems is that the existing set of sensors is typically directed at control functions, rather than health monitoring. The main purpose of the SSME sensor suite is to provide the ability to assess the performance of the engine, while providing information to the controller so that the thrust and mixture ratio can be controlled. Gas turbine and rocket engine controllers typically have a frequency response of a few hertz, and therefore, require the sensor signal to be conditioned with low pass filters so that the high frequency signal components are removed. Fault precursor information which is indicated by high frequency fluctuations in the sensor signal is therefore lost due to this conditioning. The ability of the HMS to access the raw, unfiltered sensor signal before it is processed by the controller may provide improved fault detection capability.

The performance of an HMS can also be dramatically improved through the use of sensors specifically directed at component health monitoring. This is illustrated in Figure 3.35 as a graph of detected flaw size versus fault detection time. Sensors which are directed at health assessment rather than performance can detect smaller flaws, which translates into an earlier time of detection. The decrease in time to detection provides more flexibility in the actions that the HMS can take in response to the presence of the flaw. The penalty paid for this improved performance is that the component health assessment sensors are usually not easily retrofitted to the engine.

The fault detection algorithms presented in the previous section have demonstrated excellent performance in nearly all cases tested using the existing CADS sensor information. These fault detection methodologies form the core of the HMS. Further improvements and enhancements can be achieved through the incorporation of new sensor information derived from both existing and new sensors on the SSME. As part of this program, UTRC evaluated the existing set of SSME sensors to assess the potential for extracting more information from the sensor signal if that signal was available unconditioned by the controller. Additionally, new advanced technology sensors were evaluated for potential incorporation in the HMS provided that they were nonintrusive and would be available for ground testing within 5 years.

3.2.1 Existing SSME CADS Sensors.—As previously discussed, the existing SSME CADS sensor suite consists of pressure, temperature, flow, and position sensors directed at monitoring engine performance and

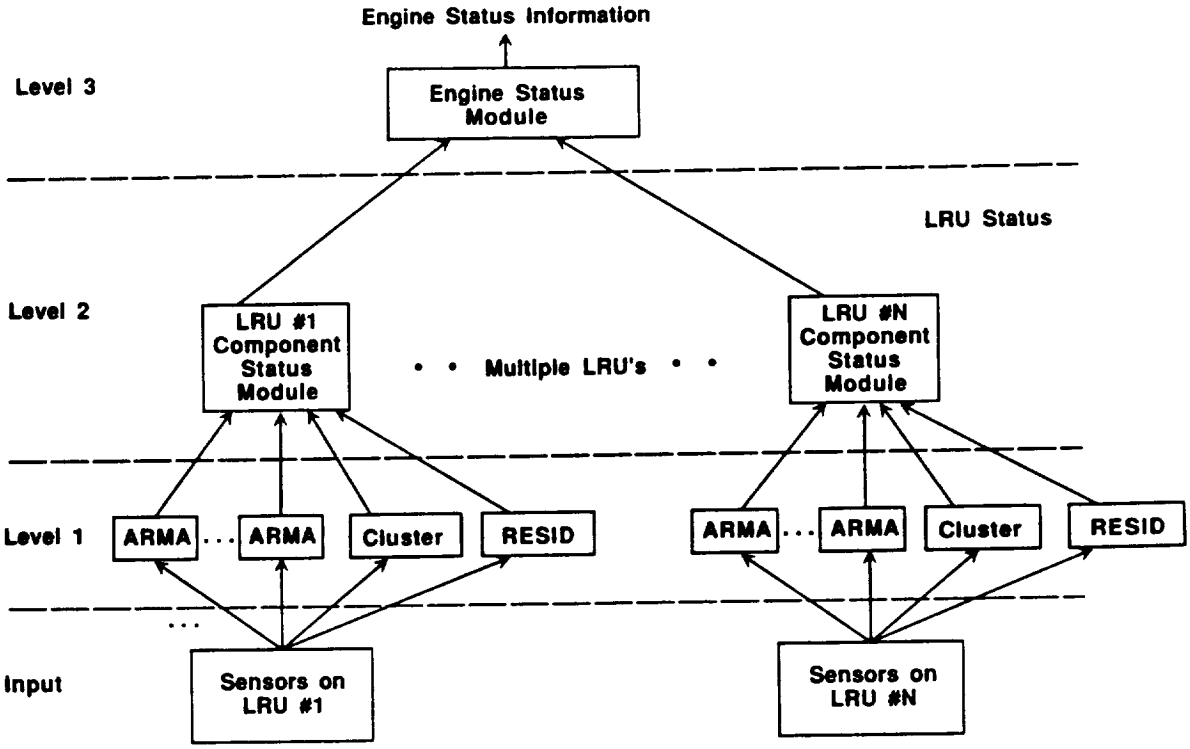

Fig. 3.34 HIERARCHICAL MULTILEVEL DETECTION SYSTEM

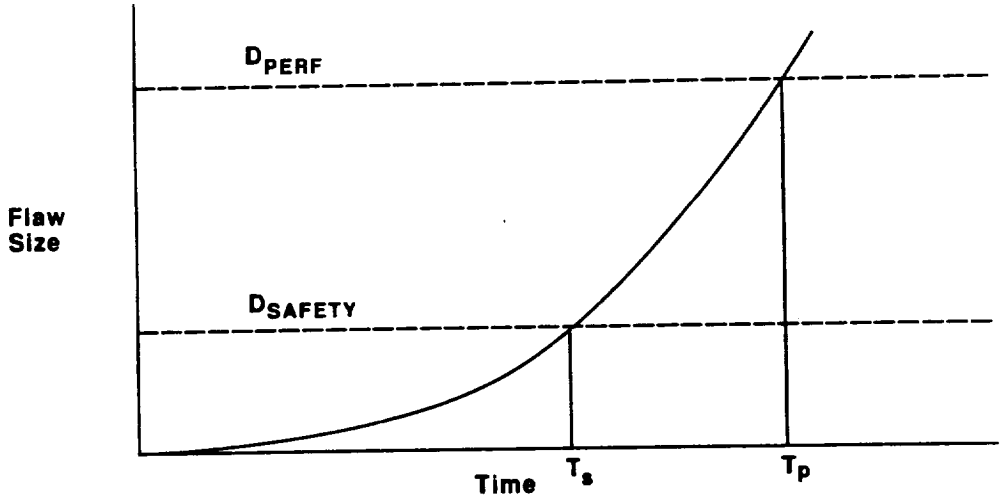

D_{PERF} - Flaw size at which performance sensors will detect faults

D_{SAFETY} - Flaw size at which safety (diagnostic) sensors will detect faults

Fig. 3.35 SENSORS DIRECTED AT COMPONENT DIAGNOSTICS CAN PROVIDE IMPROVED DETECTION TIMES

providing control information. The temperature sensors have an installed frequency response of 1 to 10 Hz, as stated in the Block II controller specification. The pressure sensors have a 100 Hz minimum frequency response. The accelerometers for the Flight Accelerometer Safety Cutoff System (FASCOS) system have minimum responses which range from 10 to 100 kHz. The controller conditions all pressure and temperature signals with a 21 ± 9 Hz low pass filter before the analog-to-digital conversion occurs at 25 Hz. The accelerometer signals are bandpass filtered between 50 and 800 Hz before energy computations are made. Thus, the filtering by the controller removes any potential high frequency information from the sensor signals that may indicate the onset of a fault within the SSME. This is especially true for the pressure sensors and accelerometers, which have frequency responses well above 21 Hz.

Although no documented study has been done to date for liquid rocket engines, an example of high frequency pressure fluctuations providing fault precursor information can be found in gas turbine engines. A phenomenon known as rotating stall can occur in gas turbine engines at certain points in the aircraft flight envelope. This condition causes the individual compressor blades to stall or lose their lift resulting in a loss of airflow through the engine. Rotating stall, as indicated by its name, is not a static condition. The stall is exhibited by a pressure wave that rotates around the compressor. UTRC and P&W are investigating methods to detect the onset of this phenomena through analysis of the signals from pressure sensors located in the compressor section. Efforts to date have revealed that significant precursor information is exhibited in pressure signals with a 1 kHz bandwidth. Filtering the pressure signal with a 21 Hz lowpass filter prevented the onset of the stall to be detected with the pressure information. Similarly, faults in the SSME which are indicated by high frequency pressure fluctuations may be detected through analysis of the unprocessed pressure transducer signals.

The UTRC HMS framework will thus include the capability for collecting and analyzing raw, unprocessed sensor information. Obtaining the raw CADS sensor signals will require interface electronics that tap into the sensor-to-controller signal lines. There are several techniques to accomplish this. The major issue will be maintaining the integrity of the sensor signals to the controller. The potential that a failure in either the interface electronics or any other part of the HMS could interrupt the information to the SSME controller must be eliminated. As will be shown in the implementation plan, the utility of the high frequency information as a diagnostic tool will be first demonstrated on facility sensors which have a less strict data integrity requirement. Once the technique has been demonstrated on the facility sensors as reliable, a similar approach can be taken with the CADS sensors.

The processing algorithms that will be required to extract the fault precursor information will not be known in specific detail until such data is available for study. It is anticipated that time series analyses (such as the ARMA technique previously discussed) will be appropriate for detecting the change in the signal structure which indicates an anomaly. Spectral estimation techniques such as the Fast Fourier Transform (FFT) may also be used to identify characteristic frequency patterns which may identify the fluctuations in the sensor signal. The HMS breadboard design will include the capability to perform time series and spectral estimation on the raw sensor signals from selected CADS and Facility sensors.

3.2.2 Near-Term Advanced Technology Sensors.—Numerous sensing technologies directed at developing dedicated diagnostic sensors for certain rocket engine components are being developed in government, university, and commercially sponsored programs. The goal of this portion of the program was to recommend advanced technology sensors for incorporation in the HMS framework to improve its fault detection performance. As part of the SSME-ATD program, the ALS Rocket Engine Condition Monitoring program,

and UTC sponsored internal research programs, UTRC and P&W have been assessing numerous sensor technologies for incorporation in rocket engine and gas turbine systems. A list of these technologies which encompasses many industry, government and university programs for potential rocket engine applications is shown in Table 3.4. A number of these programs are directed at combustion diagnostics which extract information from the exhaust plume of the engine. Others are directed at providing diagnostic information about specific rocket engine components or subcomponents, such as turbopumps and bearings. The sensor technologies include optical methods as well as advanced pressure, temperature, and leak detection transducers which, when coupled with signal processing techniques, provide unique information for rocket engine component health monitoring.

Each of the sensors listed in Table 3.4 is at a different level of maturity, has different requirements for signal processing, and differs in the extent of modification to the SSME required for its installation. Following the program guidelines to assess nonintrusive, near-term technologies along with those technologies being demonstrated under the SSME-ATD program, UTRC narrowed the list of potential candidates for inclusion in the HMS to those listed in Table 3.5 based on the following four additional criteria:

1. Nonintrusive in SSME application (except if part of SSME-ATD program)

2. Capable of ground testing within 5 years

3. Capable of real time operation during engine operation

4. Provides specific diagnostic information or health assessment of a component or components

The inclusion of intrusive SSME-ATD sensors was based on the possibility that these sensors, once qualified, may be placed on the production SSME-ATD turbopumps. This sensor information would be utilized by the HMS only when an SSME with a P&W turbopump was being operated. The fourth requirement was included so that the recommended sensors would provide a direct assessment of the health of specific components of the SSME, as opposed to simply a performance measurement made by a better, new-technology sensor. The following sections provide a brief description of these sensing technologies.

3.2.2.1 Plume Spectroscopy.—Plume spectroscopy is a comprehensive sensing technology being used to identify and quantify the spectral features observed in the SSME exhaust plume. Both normal and anomalous component wear will be evidenced by combusting particles and vapors in the engine plume. The plume spectrometer detects ultraviolet, visible, and infrared (0.2-1.5 microns) emission and absorption of ionized species within the SSME plume. The spectral lines of these species can be correlated to internal engine erosion and degradation. This technology has been demonstrated by NASA and Rocketdyne to be useful for detecting SSME bearing cage failure and injector erosion.

An Optical Plume Anomaly Detection System (OPADS), developed by Sverdrup under the direction of NASA-MSFC, is currently available for ground test use at SSC [2]. This nonintrusive optical detection system will greatly enhance detection of failures due to engine and component wear. The spectra of normal plumes and those peculiar to verified engine anomalies are being analyzed and characterized. A database will be developed through testing to identify those intensity patterns which correlate with faults. The intensity of the spectral lines apparent in the SSME plume will show the presence of species indicative of engine wear and erosion. Figure 3.36a depicts Sodium (Na) and Potassium (K) emission in a LOX/Methane plume spectra,

Table 3.4 CANDIDATE SENSOR TECHNOLOGIES FOR SSME HMS

1. Acoustic Emission
2. Optical Pyrometer
3. Surface Layer Activation
4. Plume Spectroscopy
5. Raman Temperature Profiling
6. CARS
7. Fiber Optic Deflectometer
8. Laser Vibration Sensor
9. Mass Spectrometer Leak Detection
10. Infrared Absorption Leak Detection
11. Solid State Leak Sensors
12. Microwave Turbine Blade Clearance Sensor
13. Cryogenic Mass Flowmeter (Vortex Shedding)
14. Microelectronic Pressure Sensor
15. Thin film Thermocouples and Strain Gauges
16. IR Gas Pyrometer
17. Ultrasonic Flowmeter
18. Plume Electrical Diagnostics
19. Plume Specie Concentration, Velocity, and Temperature Mapping
20. Laser Anemometry
21. Twin Core Fiber Optic Strain and Temperature Measurement
22. High Temperature Heat Flux Sensor
23. Nonintrusive Turbopump Speed Sensor
24. Flame Ionization Detector
25. Holographic Leak Detection
26. Emission Intensity Distribution Spectroscopy
27. Inductive Debris Monitor
28. Integrated Optic Pressure Sensor
29. Capacitive Turbine Blade Temperature Sensor
30. Laser Turbine Blade Tip Clearance Sensor
31. Polyvinylidene Flouride Sensor

Table 3.5 CANDIDATE ADVANCED TECHNOLOGY SENSORS THAT CAN SIGNIFICANTLY IMPROVE THE PERFORMANCE OF A NEAR TERM HMS

Sensor	Faults	Relative Computational Req'mts
Plume Spectroscopy	Erosion/Wear	Low
Acoustic Emission (ATD)	Bearing Faults	High
Optical Pyrometer (ATD)	Turbine Blade Faults	Medium
Polyvinylidene Flouride Sensor	Leaks, Burn Through	Low
Solid State Leak Sensors	Leaks	Low
Plume Electrical Diagnostics	Erosion/Wear	High
Fiber Optic Deflectometer	Bearing Faults	High
Laser Vibration Sensor (ATD)	Bearing Faults	High

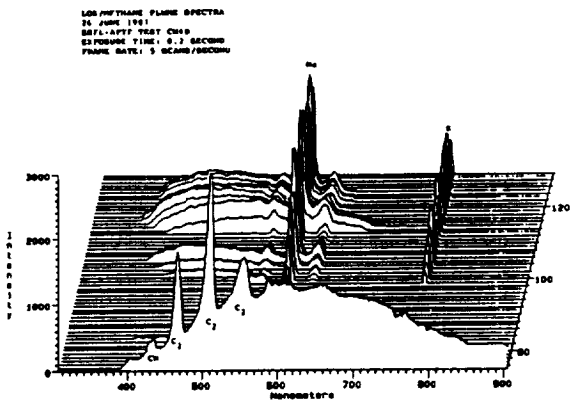

Fig. 36a LOX/Methane Plume Spectra

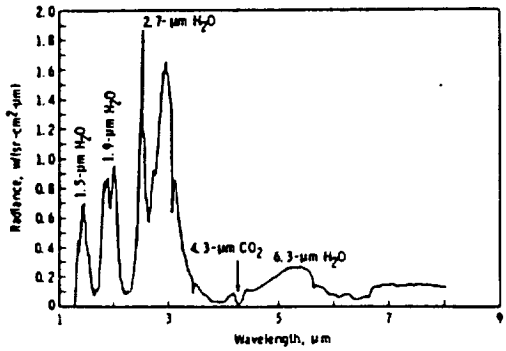

Fig. 36b Typical Mid IR Spectrum from SSME Plume

while Figure 3.36b shows a typical mid-IR Spectrum for the SSME plume. It is anticipated that the technology for maturing this technique to a useful real-time diagnostic monitor will be supported by existing NASA programs.

The relative computational requirements for the HMS will be low, as the output of the plume spectrometer 'sensor' will be the intensity of preselected spectral lines which correspond to species of interest. Fault detection signal processing will consist of individual specie redlines in combination with more complex pattern recognition and correlation analyses very similar to the clustering analyses presented in Section 3.1.3.3.

3.2.2.2 Acoustic Emission Bearing Diagnostics.—Acoustic Emission (AE) sensors monitor high frequency stress waves which result from the interaction of bearing components. As the frequency range (100 kHz - 1 MHz) monitored is well above the low frequency noise generated by gears, seals, and fluid flows, the AE monitoring has demonstrated earlier and more quantitative detection of bearing degradation and faults than that obtained from analysis of accelerometer data.

AE monitoring of bearings is under development at UTRC, and is being demonstrated as part of the SSME-ATD program as a health assessment technique for the turbopump ball and roller bearings[3]. The patented UTC Point Contact Transducer (PCT) was modified to withstand the cryogenic temperatures, high pressures, and LOX environment encountered in the turbopumps. Currently, this technique is nearing the end of the bearing rig demonstration phase of the program, and will be incorporated into several of the design verification SSME-ATD turbopumps. The sensor requires contact with the component to be monitored and is therefore intrusive. However, efforts are underway to develop the technique for sensors which are mounted external to the bearing race, either within the turbopump housing or on the exterior of the housing.

Bearing rig tests which simulate the load, speed, and cryogenic environment of the turbopumps have demonstrated the outstanding capability of this device to provide bearing health information. Subtle defects such as roller element instability and cage rubbing have been detected prior to any indication in the signals from internal accelerometers mounted on the bearing support. Figures 3.37 and 3.38 illustrate the acoustic emission signatures for stable and unstable roller elements.

Bearing health features are extracted from the AE signal time and frequency domains and analyzed by correlation and pattern recognition techniques to identify the state of operation of the bearing. The high frequency AE signal requires more complex hardware and signal processing software than what is typically used for vibration monitoring. Efforts are being made to reduce these requirements by implementing specialized analog preprocessing of the AE signal, and thus facilitate real-time operation.

3.2.2.3 Optical Pyrometer.—An optical pyrometer is an advanced technology sensor which will be used to monitor turbine blade health. Fiberoptic probes with indium-gallium-arsenide (InGaAs) detectors measure the radiant energy from turbine blades during engine operation to provide a linear map of blade temperature from root to tip.

An Optical Pyrometer is being developed as part of the SSME-ATD program for the HPFTP[4]. The pyrometer probe takes five radial measurements from the turbine blade root to tip as the blade passes. The probe is designed to collect a fixed percentage of the radiant energy emitted from the surface of the blade. The radiant energy emitted from the blade surface is transmitted through the fiber optic cable and converted by the external detector to a temperature measurement to provide a temperature profile of the turbine blades

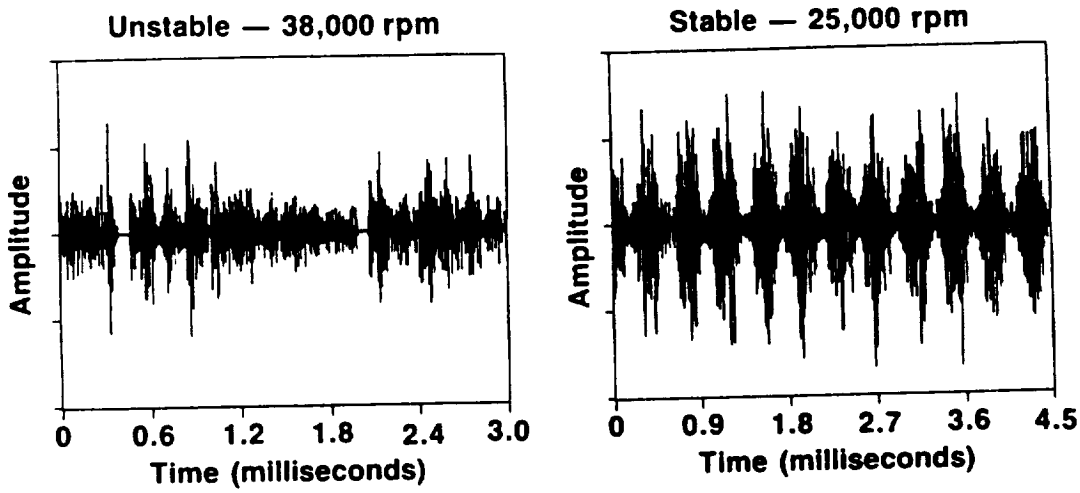

Fig. 3.37 AE MONITORING IDENTIFIES SUBTLE CHANGES IN THE ROLLER ELEMENT STABILITY

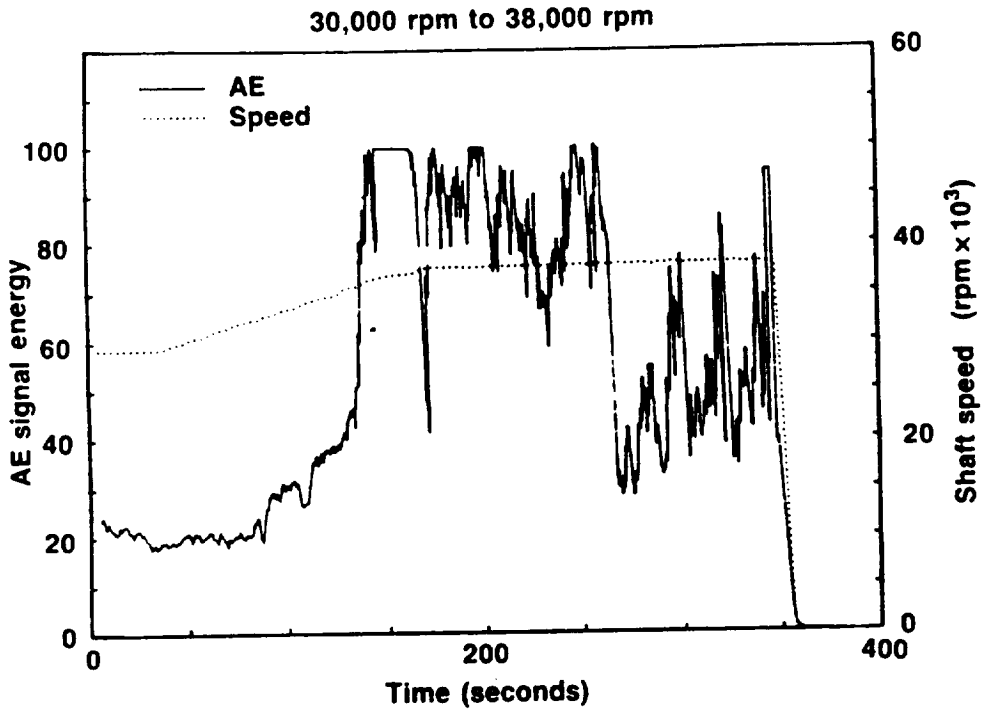

Fig. 3.38 AE MONITORING IDENTIFIED THE UNSTABLE OPERATION OF A ROLLER BEARING 3 MINUTES BEFORE FAILURE

during engine operation. Blade temperature is indicative of its condition: as a blade cracks, its ability to conduct heat away is reduced and consequently, the blade becomes hotter. This information about the operating conditions of the turbopump can be utilized in fault detection algorithms and provide specific diagnostic information about turbine health.

The likely use of this sensor for real-time monitoring will be to detect hot spots on the turbine blades. The high frequency bandwidth of the sensor signal (500 kHz) requires both analog and digital signal processing to obtain the temperature measurements. The detection of hot spots is computationally simple and would thus impose little additional burden on the HMS. The complexity of the processing increases as the amount of the information about the turbine blade temperature map increases.

3.2.2.4 Polyvinylidene Fluoride Sensor.—Polyvinylidene Fluoride (PVDF) is a synthetic polymer film which exhibits piezoelectric and pyroelectric properties. Its characteristic large and durable dipole polarization varies linearly with applied stresses such as electric fields, mechanical stress, and temperature changes.[5] This allows it to be used to provide electrical signals to monitor mechanical and thermal stresses.

PVDF film is being investigated as an advanced technology sensor for burn through detection applications in the ALS-RECMS program. A blanket of this material would either be affixed to the component of interest, or be attached or imbedded in thermal insulations or shields. A hot gas leak would burn through the film or create a localized hot spot. A voltage signal would be generated by the film which would be unique to the type and location of the burn through.

The PVDF sensor as a burn through leak detector would require minimal signal processing. Simple analog noise reduction techniques followed by thresholding would be used to detect an event. This sensor has been demonstrated on MX missile transport canisters as a means to detect canister penetration caused by various methods including projectiles, flames, and chemicals. A significant effort would be required to implement this technique on the SSME, since no rocket engine application programs for this sensor are underway.

3.2.2.5 Solid State Leak Sensors.—Gas sensitive semiconductors have been developed for some industrial applications and are now being evaluated for their utility in the rocket engine environment. The conductivity of these devices increases in the presence of combustible gases such as hydrogen, carbon monoxide, methane, and propane.[6] The small size of these devices makes them ideal for an array of sensors which monitors specific points on the SSME for hydrogen leaks.

Gas sensitive semiconductor sensors are n-type bulk devices mainly composed of metal oxides such as sintered tin dioxide (SnO_2). When the sensor is heated in the air, oxygen is dissociatively absorbed on the device surface, having a negative charge caused by the electron transfer from donor levels in the surface region. Consequently, an electron depletion region develops from the surface to the bulk substrate; this region is positively charged to balance the surface negative charge of the oxygen. This process forms potential barriers against bulk conduction electrons, and the sensor has very high resistance. When combustible gas is supplied to the sensor, it is absorbed by the surface and reacts with the absorbed oxygen, effectively decreasing the potential barriers in the device and reducing resistance. Sensor resistance decreases exponentially with gas concentration. Figure 3.39 depicts a typical gas sensitive semiconductor sensor and its associated sensitivity characteristics.

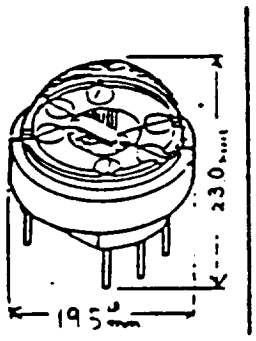

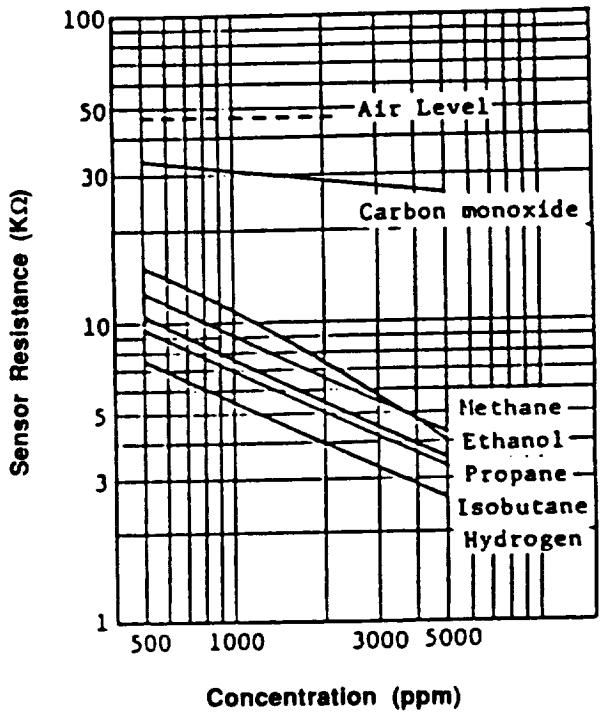

Fig. 3.39 GAS SENSITIVE SEMICONDUCTOR SENSOR
Figaro Gas Sensors (TGS 911) and its sensitivity characteristics

The signal processing requirements for this sensor are very simple. Following analog circuitry that measures the resistance change of the sensor, a thresholding would be used to identify gas concentrations above a preselected level. Readings from several sensors would be used for corroboration and location of the leak. Solid state leak sensors are still in their development stage for rocket engine applications. Major issues that need resolving are their sensitivity to temperature and other environmental conditions. Furthermore, existing sensors are not yet capable of detecting a single specific gas and therefore, may be confused by extraneous gases unrelated to the desired leaking gas type. However, it is expected that these sensors could be available for ground test within 5 years.

3.2.2.6 Plume Electrical Diagnostics.—The SSME exhaust plume has the potential of supporting various sensing technologies that exploit the presence of particles and species in the plume to provide specific diagnostic information about engine and component erosion and wear. Plume electrical diagnostics is a nonintrusive sensing technology which classifies engine events based upon electrostatic gas path signatures.

Distresses in the SSME, such as turbine blade rubs or combustor burns, will produce particles of debris which carry electrostatic charge. Plume electrical diagnostics involves monitoring electrostatic probes in the plume to detect these charged particles. As the exhaust gases will have a nominal level of electrostatic charge, a background signal will exist. The signal processing and diagnostics must detect changes above this background signal, extract features from the probe signals, and employ classification techniques to determine if a fault has occurred.

Electrostatic techniques have been successfully applied to the analysis of gas turbine engines by P&W, HS, Sikorsky, and UTRC Divisions of UTC. It was found that the electrostatic pulses had characteristic signatures that could be correlated with known engine events. Turbine blade erosion, for example, manifested itself in the electrostatic analysis as a negatively charged pocket in the gas path which, as it moved past the electrostatic sensor, produced a 25 ms wide time-varying voltage signature.

Measurement of plume electrical signatures is relatively simple to implement, but it is rather complex to understand the significance of the resulting signal. This technique will need to be tested extensively in the SSME environment in order to determine optimal probe placement, and to build a database of electrostatic signatures which correlate with engine events. The computational requirements for inclusion of plume electrical diagnostics into an HMS are expected to be significant, since they generally include various pattern recognition techniques. Some preliminary work on implementing this technique for rocket engines has been done by NASA-MSFC.

3.2.2.7 Fiber Optic Deflectometer.—Fiber optic deflectometers use light reflections to measure outer race deflections due to roller element passage in order to quantify bearing and race conditions in the SSME turbopumps. This is an intrusive device that requires a through-hole to the bearing outer race. It has been included for possible incorporation into the HMS, as it may be configured to fit in the same mounting fixture that is used by the acoustic emission sensor on the SSME-ATD turbopumps.

UTRC has developed deflectometers for various industrial applications to measure surface displacements. Rocketdyne has been evaluating a probe manufactured by MTI for potential SSME application[7]. The probe consists of a laser light source, fiber optic cables in close proximity to the bearing outer race, and a photodetector to receive the light reflected by the outer race. Light from the light source is transmitted through the optical fibers, is reflected off of the bearing race, and is transmitted through the

receiving optical fibers to the photodetector (see Figure 3.40a). The intensity measured is a function of the gap width between the cable tip and the bearing outer race.

Race deflections from normal bearing operation produce a distinctive half-sinusoidal signature at the ball pass frequency. Changes in the smooth sinusoid signal are indicative of potential faults in the bearing (see Figure 3.40b). Fault detection algorithms will require frequency analysis to extract bearing component fundamental frequencies and their harmonics. The computational requirements for this processing will be high due to the required spectral estimation techniques. Additionally, pattern recognition may also be appropriate for detection of signatures which correlate with unique subtle faults within the bearing.

3.2.2.8 Laser Vibration Sensor.—A Fiber Optic Laser Vibration Sensor (FOLVS) has been developed by UTRC for vibration measurements in locations where the size and mass of piezoelectric accelerometers preclude their use. The FOLVS technique utilizes the principles of a common path interferometer using a coherence multiplexing technique to measure vibration in either contacting or noncontacting modes (see Figure 3.41). As part of the SSME-ATD program, the FOLVS technique is being adapted to detect bearing faults in the HPFTP[4].

Using this technique, a fiber optic cable wrapped around the outer race of the bearing directly measures vibration. A fiber optic beam splitter splits the light beam from a solid state short coherence length laser diode into reference and sensor beams. The reference beam passes through a phase modulator, which changes its frequency by a known amount, and then through a fiber optic coil which delays the reference beam by a fixed amount. The optical beam coupler recombines the reference and sensor beams such that their difference exceeds the coherence length, so that interference will not occur.

This combined beam travels along a single optical fiber allowing external influences to affect both the reference and sensor signals. Part of the light is reflected at the partial reflector and returns along the transmitting fiber to form a reference beam, while the rest travels the full length of the optical fiber which is wrapped around the bearing outer race. This light is totally reflected and returned to the partial reflector. The round trip length from the partial reflector to the total reflector is equal to the path length difference introduced by the optical delay in the reference beam. Hence, reflected beam is now coherent with the portion from the partial reflector; changes in fiber length or strain in bearing outer race cause interference.

The interference signal is an FM signal with frequency of the phase modulator and sidebands indicative of the dynamic changes in fiber length. The demodulated signal, proportional to the fiber length change, is a measure of strain and vibration in the bearing race. The device has a uniform frequency response from DC to tens of megahertz, and is absolutely calibrated to the wavelength of the laser source.

The computational requirements for bearing fault detection algorithms using the laser vibration sensor will be high, and will potentially require both spectral estimation and pattern recognition techniques.

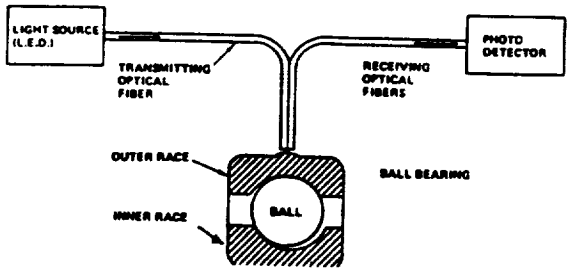

a) Probe functional diagram

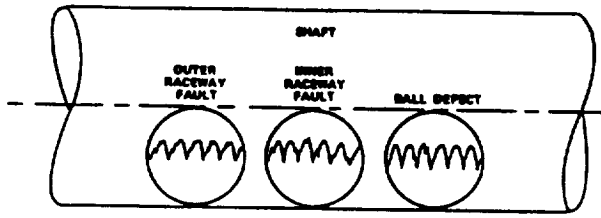

b) Bearing and raceway degradation signatures

Fig. 3.40 FIBER OPTIC DEFELECTOMETER

Outer race deflections due to ball passage are measured through light reflections.

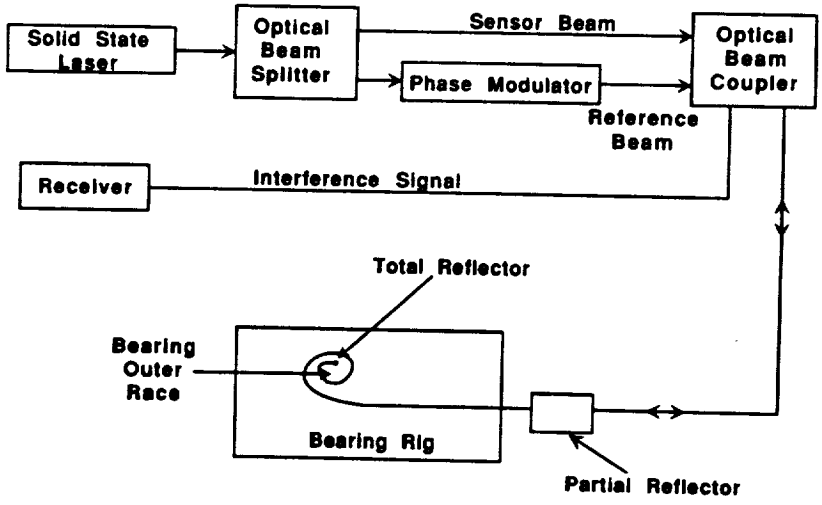

Fig. 3.41 FIBER OPTIC LASER VIBRATION SENSOR (FOLVS)

FOLVS for Bearing Diagnostics uses principles of a common path interferometer to measure bearing vibrations

SECTION 4.0
FRAMEWORK FOR THE HEALTH MANAGEMENT SYSTEM

The major purpose of formulating an architecture for the HMS was to demonstrate the interrelationships of its various functions and to provide an assessment of the hardware and software complexity required to implement the focused HMS. The formulation of the HMS framework architecture began with the establishment of the system requirements. The main requirements were: the real-time, simultaneous operation of various fault detection algorithms; the use of existing SSME instrumentation; the use of near-term technology hardware; the incorporation of nonintrusive, near-term advanced technology sensors; the phased implementation of the HMS on the SSME teststand; and a clear migration path from a Ground Test HMS to a Flight HMS. The initial step was to outline a functional architecture which served to identify the major system tasks, identify the interrelationships of these tasks, and to show the information flow between the tasks.

Once the functional architecture was formulated, an iterative design methodology was used to develop the hardware architecture that could support the functional requirements. The emphasis in this task was to identify and demonstrate an overall approach to the hardware design, and not just to determine how many processors, buses, or other hardware interfaces would be required to implement the HMS. The effort described in this report is the first pass through a detailed design study that would be performed prior to implementation of an HMS. The intent is to highlight the major issues that need to be addressed rather than provide final design answers for those issues. To aid in this design methodology, UTRC demonstrated a computer architecture simulation tool, originally developed to assist the designers of VHSIC architectures, to evaluate the various hardware/software configurations for the SSME HMS.

4.1 HMS Functional Architecture

The requirements for a ground test version of the HMS were used as the basis for the design of the HMS functional architecture. The Flight HMS will incorporate a suitable subset of the ground test functions. The major functions of the ground test system are shown in Figure 4.1. The system task manager function oversees the entire operation of the HMS: it provides the user I/O, system resource management, and task scheduling based on the current HMS configuration and status. The five major tasks supervised by the task manager are engine health monitoring, test data logging, off-line data analysis, database management, and system communications. The engine health monitoring task contains all of the functions for fault detection and decision making that must run in real time to provide engine shutdown capability, and is the most critical to the HMS framework. Consequently, the health monitoring task was studied in greater detail than the other major HMS tasks. It will be shown in the hardware architecture section (Section 4.2) that this task requires dedicated hardware to operate in real time. Engine test data logging is another time critical task, in that it must provide real-time storage of all desired sensor data during a test. Its purpose is to provide local data to the HMS in the proper format for use in off-line data analysis and algorithm development.

The remaining three major HMS tasks (off-line data analysis, database management, and system communications) are not time critical, but provide essential "housekeeping" capabilities to the HMS. It is anticipated that these functions will be provided by commercial off-the-shelf hardware that is part of many current scientific workstations. The off-line data analysis task will provide the ability to analyze data from SSME ground tests, verify existing algorithms, and develop new fault detection techniques which will be

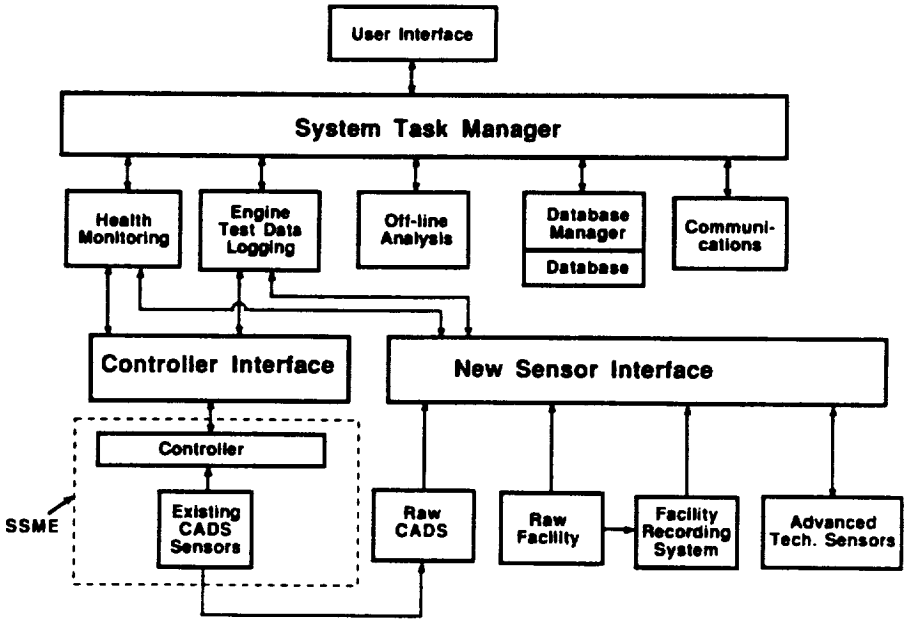

Fig. 4.1 HMS FUNCTIONAL ARCHITECTURE

essential in maintaining and updating the monitoring coverage of the system. The database manager will provide the utilities to allow all HMS system data to be organized and maintained in an orderly fashion. The database will also contain all of the parameters, models, and thresholds that will be downloaded to the real-time HMS health monitoring functions. The communication task will allow the operator to transmit and receive information, such as the HMS data, and provide remote access to the system.

4.1.1 Health Monitoring Task.—The purpose of this task is to provide the capability necessary to acquire sensor information, run fault detection algorithms, and provide a real-time assessment of the engine health. When an engine fault is detected, the system will transmit an engine shutdown signal to the controller through the CADS system. This function can be enabled or disabled as desired.

The engine health monitoring task implements a hierarchical process in which a decision to shut down the engine is reached after several levels of information processing. In this hierarchy, the bottom levels process the sensor signals, while the middle levels determine the nominal or off-nominal operation of various engine parameters. The middle levels also combine the outputs of multiple fault detection algorithms to assess health of specific engine components. The top level of hierarchy then combines the health assessments of the various engine components to determine the overall engine health, and outputs a yes/no decision to shut down the engine. The functional architecture for this task is presented in Figure 4.2.

The principle inputs to the health monitoring task are the sensors depicted in Figure 4.2, which include the existing CADS and facility sensors along with the near-term technology sensors selected for inclusion in the HMS. Separate interfaces will be required for each of the sensor information sources. Information from existing CADS sensors will be provided by the controller. The facility sensor information will be obtained through an interface to the existing facility recording system.

The first step in the health monitoring task is the sensor processing function. The sensor processing function conditions any analog sensor data input signals, performs the analog-to-digital conversion, and scales the sensor data. The processing function then verifies the integrity of all the data before it is used by the fault detection algorithms. Sensor channels that are determined to be faulty are disabled. Running the fault detection algorithms described in detail in Section 3.1.3 for the CADS sensors, and those qualitatively discussed in Section 3.2 for near-term technology sensors is the final step in the processing function.

The second step in the health monitoring task integrates the outputs of multiple fault detection algorithms to cross-check and confirm that a fault has occurred within an LRU. This process is contained within the component status modules shown in Figure 4.2. Each component status module would be responsible for determining the health of a specific LRU, or group of LRUs, by using information supplied by various fault detection algorithms. For example, the health of the HPFTP would be assessed based on the information provided by the clustering algorithm operating on a set of sensors which focused on the HPFTP, along with the output from the ARMA algorithms operating on single sensors related to the HPFTP. Additionally, the HPFTP status module would check the information provided by the acoustic emission bearing diagnostics algorithms in conjunction with the plume spectroscopy algorithms to confirm the existence of a bearing degradation fault such as a cage deterioration. Further information about the HPFTP hot gas power transfer would be obtained from the optical pyrometer algorithms which would indicate a turbine blade hot spot. In this manner, many sources of information are used to compile a scenario of the potential fault. The cross-checking of multiple information sources reduces the potential for a false alarm caused by the spurious output of a single fault detection algorithm. Furthermore, the high degree of

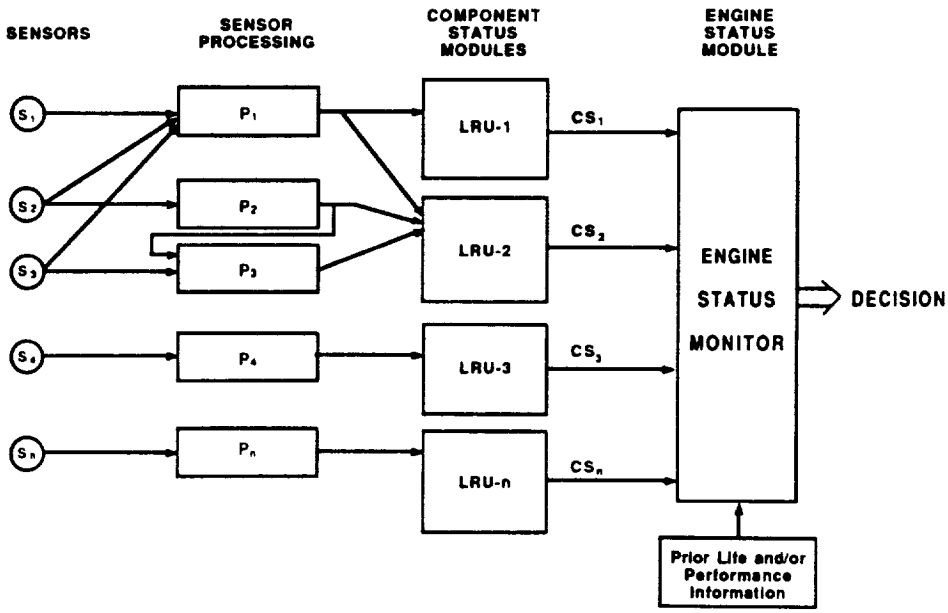

Fig. 4.2 FAULT DETECTION FUNCTIONAL ARCHITECTURE

interrelatedness in the operation of the LRUs enhances the ability of the component status module to confirm the fault in a specific LRU by using information from the operation of other LRUs. The correlation of the multiple information sources is one of the steps required for identification, rather than just detection, of the fault. Thus, the ability to detect and identify a fault could be included in the functions of the component status module.

The next logical step beyond the component status modules is the engine status module shown in Figure 4.2. The function of this step in the hierarchical process is to make a decision as to whether the engine should be shut down or continue to operate. Just as the component status modules are responsible for individual components, the engine status module is responsible for utilizing several sources of information to assess the overall health of the engine. The primary information would come from the output of the component status modules as a confirmation that a fault existed within the engine and possibly an identification and localization of the fault. The engine status module may also use prior knowledge about the performance or useful life of a specific component in assessing whether it should act on a fault indication. For example, knowing that the main injector of the engine under operation has already achieved 95% of its predicted useful life and would thus have a higher probability of failure, the engine status module would take this into account when acting on the indication of a potential main injector related problem. At this decision making level, knowledge about prior performance degradation that has been confirmed to exist in the engine can be utilized to make the shutdown decision process more or less sensitive to the indication of a particular fault.

The component status and engine status modules are implemented using an expert systems approach, with a set of rules which correlate a certain set of circumstances with a certain conclusion or action. For example, given certain outputs from the cluster analysis, the optical pyrometer, and the plume spectrometer, a turbine blade fault may be concluded to exist. Next, given that a turbine blade fault does exist, given that the fault appears to be growing rapidly, and given that the turbine blades in the turbopump on the engine under test are made from a new material that erodes quickly, the action to shut the engine down will be taken. The number of such rules will be kept small so as to enable the real-time implementation of this strategy. The rules will be developed from a combination of studies of teststand data and the experience of SSME test and operation personnel. Flexibility in the expert system modules required will be so that improvements in the decision making process can be incorporated as the understanding of the fault detection and identification processess increases. The development of these expert systems will be included as a technology development program in the HMS implementation.

4.2 HMS Breadboard Hardware Architecture

The HMS hardware architecture was developed through a preliminary design process such that it supported the system functional requirements while conforming to the constraints imposed by the overall program goals. Both the Ground Test HMS and the Flight HMS were studied to identify the major issues that would need to be addressed in a detailed design to be performed as part of the implementation program. Although these systems operate in different environments, they both evolve from the same functional requirements. The flight system evolves from the ground test system through the incorporation of the unique constraints and requirements presented by the flight regime. Consequently, a smooth transition from ground operation to in-flight health monitoring can be achieved. The goal of this effort was to demonstrate a design methodology and present a strawman hardware architecture design, and in doing so, address issues such as the real-time implementation of diagnostic algorithms, the maximum limits of HMS functionality, and the identification of concerns unique to a Flight HMS. The final system design would be based on a more

comprehensive study of each of the critical issues and a rigorous cost versus benefits analysis of the flexible Health Management System.

The preliminary design methodology used in this study includes the following major steps:

1. Definition of functional requirements;
2. Generation of throughput estimates;
3. Generation of HMS Hardware block diagrams including the System Block Diagram (SBD) and the Detailed Block Diagram (DBD)
4. Parametric studies on weight, and power
5. Assessment of reliability

The purpose of this multistep effort was to demonstrate the design process rather than produce a detailed design. The results of each of the steps listed above are presented in the following sections. The program to implement the HMS will begin with an effort to re-examine each of these steps to refine the results.

4.2.1 Hardware Functionality.—The primary drivers of the HMS hardware design are the number and complexity of the functions that the HMS must support. The engine health assessment decision methodology presented in the discussion of the functional architecture is sufficiently robust and flexible to incorporate virtually any number of sensors and algorithms operating in parallel. The sensors and algorithms discussed in this report range from those studied in detail as part of the Phase I program effort, to those whose specific functional requirements will not be known until further development on the sensors and/or algorithms is completed. One goal of the preliminary hardware design process is to determine the extent to which both the known and the unknown functions can be incorporated with state-of-the-art hardware, within the general program guidelines.

Another key goal to be achieved in the design of the HMS hardware is the flexibility for the system to evolve as the results from technology development programs become available. The intent is to design a system which contains the functions that have been sufficiently proven for immediate implementation, and to provide the flexibility to incorporate additional functions as they become proven enhancements.

4.2.1.1 Ground HMS Hardware Functionality.—A comprehensive set of functions for health management using current and future sensors was selected as the basis for the HMS hardware design. The ARMA, clustering, and RESID algorithms demonstrated on the CADS sensor data form the proven core functions of the HMS. Enhanced system performance will be achieved through the addition of functional modules (groups of algorithms directed at a single sensor or sensor type). A simple and logical addition of HMS functionality is the ability to implement the proven CADS algorithms on similar low frequency facility data measurements. Provisions have been made in the hardware design to incorporate the advanced spectral analysis techniques required for processing the raw, unfiltered data from selected CADS sensors, Facility sensors, and accelerometers. Furthermore, the HMS hardware design provides the processing capability to incorporate a selected set of advanced technology sensors. The advanced technology sensors include plume spectroscopy, acoustic emission bearing diagnostics, optical deflectometer, and the optical pyrometer. Finally, the processing required to implement the rule-based hierarchical decision making process has been included. It will be shown that, through appropriate design considerations, each of these enhancements to the system can be added at the appropriate time without detrimental effects on HMS performance.

4.2.1.2 Flight HMS Hardware Functionality.—There is no aspect of the HMS hardware design that would initially preclude any of the functions from the Ground Test HMS to be used in the flight system. Practical considerations, such as the ability to fly the advanced technology sensors and the impact of the extra weight penalties and power requirements of the HMS, will certainly limit the number of the HMS functions which are transferred from the Ground Test HMS to the Flight HMS. Additionally, all of the Ground Test HMS functions associated with the facility sensors would be eliminated, since the facility sensors are not available for use in flight.

4.2.2 HMS Hardware Requirements.—There are several general design requirements for both the Ground Test HMS and the Flight HMS: flexibility, cost, and a clear migration path from ground test to a flight system. As previously discussed, the hardware must be flexible in order to add new sensor interfaces, functionality, and/or computational capability. This is especially important for technology programs that have changing requirements. Also, the costs to procure, operate, and maintain the hardware must be minimized. Reliability rates for the HMS hardware, defined here as the Missed Detection of Fault (MDF) rate and the False Alarm (FA) rate, should not significantly impact the total reliability of the HMS. Finally, the Ground Test HMS must have the capability to smoothly evolve into the Flight HMS by maintaining as much commonality as is practical between the two systems.

An additional requirement which results from the need for flexibility, high performance, and low cost is that of a modular architecture approach for packaging the hardware. In a modular architecture, the increasing processor and I/O requirements can be easily accommodated through the simple of addition of circuit cards called Line Replaceable Modules (LRM). A further requirement to use off-the-shelf modular components provides additional cost and maintainability benefits: off-the-shelf commercial modules are less expensive than custom circuit boards and are readily available if the need for replacement arises. Some development cost savings can also be realized with commercially available modules since design costs have been amortized by the LRM manufacturer across many LRM sales.

In addition to these general system requirements, there are further requirements which are specific to either the ground system or the flight system. This issue is briefly addressed in the next two sections.

4.2.2.1 Unique Requirements for the Ground Test HMS.—The primary goal of the Ground Test HMS is to prevent engine failures, and thereby, reduce operational and maintenance costs. This is accomplished by shutting down an engine that has an impending failure. The size, weight, and power requirements for the Ground Test System, as opposed to those for the Flight System, are not major concerns since the Ground Test HMS is intended for operation in the control room.

4.2.2.2 Unique Requirements for the Flight HMS.—The Flight System has the same general requirements as the Ground Test System, because it will evolve from the Ground Test HMS. Operationally, the Flight HMS differs from the Ground HMS in that the primary goal of the Flight HMS is to prevent loss of life, and hence, unique issues must be addressed. The MDF and FA rates must be lower for a Flight System. False alarms are critical because of the extremely limited engine-out capability of the shuttle and the potential safety risk to the crew if takeoffs are aborted due to engine shutdown. The Flight HMS hardware must be flight worthy in a very harsh environment. This includes immunity to severe shock, vibration, and temperature. Reliability (Mean Time Between Failure [MTBF] and Pre-Liftoff Abort Rate) is of greater concern for the Flight System, as are the size, weight, and power requirements.

4.2.3 Throughput Analysis.—Throughput analysis assesses the processing and I/O requirements for the selected functions. It provides the initial insight into the complexity of the hardware required to support the functional architecture. On the basis of throughput alone, there is no distinction required between the Flight HMS and the Ground Test HMS, since the computation load for a specific algorithm is independent of the application location. The number of functions, and hence the total system throughput, for the Flight HMS will differ from the Ground Test HMS simply because the flight system will likely support fewer functions.

For the purposes of the throughput study, the functional architecture for the real-time health monitoring function was subdivided into three parts:

1. Reading the signal,
2. Implementing the fault detection algorithms
3. Performing the expert system engine shutdown decision.

The throughput for the first part is the amount of processing required to read the signal and validate it. This includes the operations to manipulate the A/D conversion and the multiplexers, perform range checking, filter, and convert the signal to engineering units. If the signal conversion has failed hard (many times in a row), the signal is declared to be failed, and a flag is set. The higher level processing must reconfigure around that fault.

The second part of the throughput calculation considers the single processing required for the implementation of the fault detection algorithms. Algorithms for the sensors discussed in Section 3.1.3 were considered in this study. As a general rule, twice the number of facility sensors as CADS sensors were assumed for the processing algorithms that operate on the low and high frequency facility data. The Fast Fourier Transform (FFT) was assumed to be the spectral estimation technique used for the raw facility and raw CADS sensor processing, the advanced vibration processing, the acoustic emission processing, and the deflectometer processing. All FFTs were assumed to have 1024 points.

The third part of the calculation quantifies the throughput required to perform the hierarchical decision making. This includes the processing for algorithms to combine outputs of the various fault detection algorithms as well as the computations for the rule based expert systems which will make the fault/no-fault decisions.

The results of the throughput study are summarized in Table 4.1 which provides the results in units of million instructions per second (MIPS). Several conclusions can be drawn from Table 4.1:

1. The CADS Serial Link Processing (ARMA, clustering, and RESID) is a very small part of the total throughput required.
2. An extensive amount of processing is required for the advanced vibration monitoring and the unfiltered raw CADS and facility sensors. This is due to the uncertainty in the algorithms that will be required for this processing and the likely reliance on computationally intensive FFT processing to provide spectral information.
3. Processing requirements for the advanced technology sensors are generally very small. The exception is acoustic emission bearing diagnostics, because the maturity of the technique to date still requires high frequency digital signal processing. This computational load is expected to be dramatically reduced in the near future as analog signal processing circuits are developed.

Table 4.1 THROUGHPUT REQUIREMENTS FOR HMS FUNCTIONS

Function	I/O	FFT	Algs.	Total
CADS Serial Link Data Processing	0.1	0.0	13.8	13.9
Low Frequency Facility	0.2	0.0	27.6	27.8
Raw CADS Data Proc.	0.6	23.4	8.5	32.5
Raw Facility Data Proc.	1.1	46.8	44.5	92.4
Advanced Vibration	0.1	10.2	28.1	38.4
Adv. Tech. Sensors:				
Plume Spectroscopy	0.1	0.1	-	0.2
Acoustic Emissions	6.1	9.9	3.7	19.7
Optical Deflectometer	0.9	5.5	1.1	7.5
Optical Pyrometer	0.1	-	0.1	0.2
Engine, Component Status Modules	0.1	-	0.1	0.2
Total	9.4	95.9	127.5	232.8

Note: The above data is based on the number of instructions that an Intel 80960CA processor would take to the given function. Based on an analysis of the Intel data sheets, the processor was conservatively assumed to operate at an effective throughput of 12 Million Instructions Per Second (MIPS). Further, it is assumed that all software is coded in Ada. Current Ada compilers generate code that takes estimated two to five times longer than manually generated assembly code to execute.

4. The raw facility data processing represents nearly half the total system processing load, and hence, it is logical to separate this function and place it on a single subsystem. In this manner, calculations are not fragmented and the migration to a Flight HMS is simplified since the facility sensor processing will not be required in flight.

5. The FFT processing is a very large portion of the computations and is an excellent candidate for implementation by special purpose processors such as a UTMC (United Technology Microelectronics Center) chip that can perform a 1024 point FFT calculation in 700 microseconds.

6. 200 MIPS is an extremely large throughput requirement for an embedded system. (Typical gas turbine fuel controls are on the order of 1 to 10 MIPS.) The processing requirements for the implemented HMS will be significantly less, since it is not likely that all of the functions will be incorporated into the system.

4.2.4 HMS Hardware Block Diagrams.—Discussions of the hardware block diagrams for the Ground Test HMS and the Flight HMS are presented in this section. A subset of the Ground Test HMS will serve as a prototype for the Flight HMS.

4.2.4.1 Ground Test HMS.—The HMS must be integrated into the SSME environment with minimum impact. The interfaces should be as simple as possible in order to minimize the design errors associated with integration and also teststand downtime. Above all, HMS reliability is critical: it is essential that the probability of fault propagation from the HMS to the SSME controller is extremely low.

Figure 4.3 represents a concept for integrating the Ground Test HMS with the SSME. The existing Ground Test System is composed of the SSME, CADS and Facility Sensors, the Block II SSME Controller, actuators, and the teststand facility itself. The CADS sensor suite is dual redundant and provides signals to the dual channel controller. The controller, in turn, transmits commands that control the fuel and oxidizer valves. The controller also has a serial link (CADS Serial Link) which transmits 128 parameters (conditioned sensor values and status words) every 40 ms.

New HMS equipment will consist of a Ground Test HM Subsystem, Facility Data HM subsystem, and Advanced Technology Sensors. The Ground Test Health Monitoring Subsystem will be a rack of cards that will serve as the prototype for the Flight HMS electronics. The Facility Data HM Subsystem represents the electronics dedicated to collecting data unique to the facility, and will only be used for ground test. Based upon the throughput study previously described, this partitioning of the Ground Test HMS is logical because the computational loads are approximately equal, and the capability to migrate to a flight system is maintained.

The Advanced Technology Sensors block represents near-term sensors which provide additional diagnostic information to the HMS. These include a plume spectroscopy system, acoustic emission sensors, optical pyrometers, and fiber optic deflectometers. Each advanced technology sensor will require a separate interface to the Ground Test HM Subsystem. The final interface between the existing test system and the Ground Test HM Subsystem will be receiving raw CADS sensor data. It is essential that the HMS raw CADS sensor signals without adversely impacting the controller reliability. Rocketdyne suggested in the final report for SAFD-Phase III[1], that no electronic components be placed in the path of the CADS serial link and that the signal be tapped using a high impedance transformer. The same design philosophy can be extended to tapping into the controller-sensor cable. Only those sensors which are not critical to engine control are

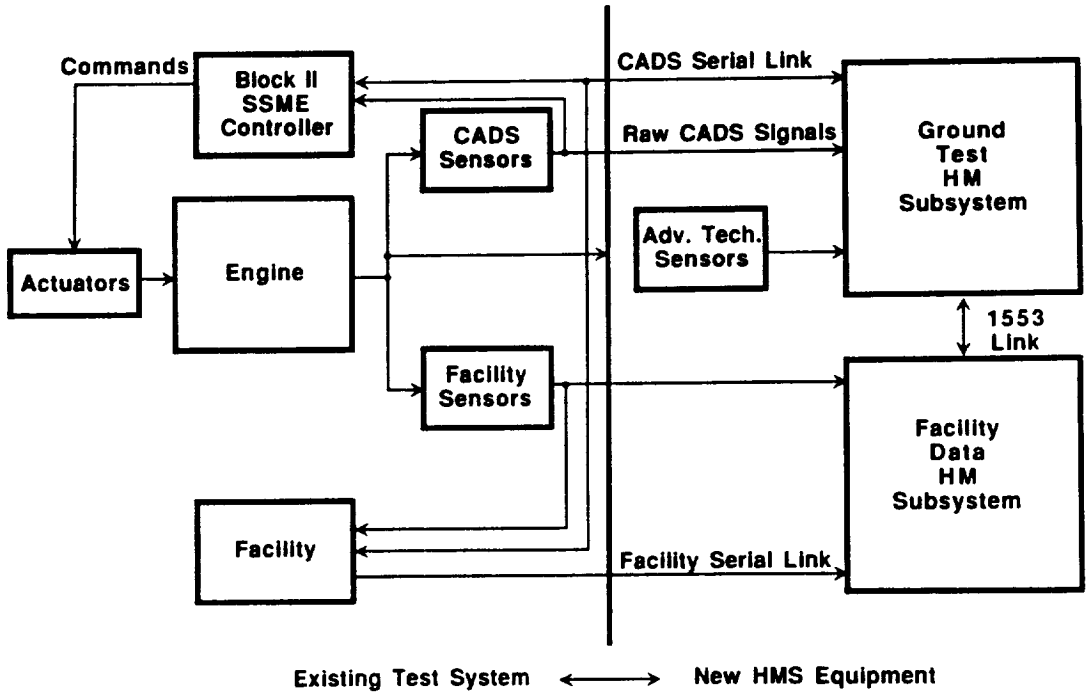

Fig. 4.3 GROUND TEST SYSTEM LEVEL BLOCK DIAGRAM

candidates for this approach. Careful study and a trade off analysis is required to assess reliability costs versus benefits.

4.2.4.1.1 Ground Test HMS Block Diagram.—A detailed hardware block diagram for the Ground Test HM Subsystem is shown in Figure 4.4. The system is composed of industry standard VME cards and buses. In order to keep cost of development low, a limited number of cards will be used in multiple applications within the HMS.

Sensor measurements are processed by a group of cards referred to as a Data Processing Functional Group (DPFG). The Ground Test HM subsystem consists of DPFGs to process data from the CADS Serial Link, Raw CADS Sensors, Vibration Sensors, and the Advanced Technology Sensors. One of the CPU cards shown on the right side of the diagram is used for the Component Status Modules and the Engine Status Module. The Mass Storage System, depicted as a single card and controlled by the second CPU card shown in the upper right half of the figure, collects the data generated by the DPFGs in real time. There are two serial links in the system: one is used to collect data from the Facility Data Processing Subsystem, while the other card, the High Speed Data Bus (HSDB), is used to transmit data to the Facility. Finally, an option has been included for a redundancy management card.

The serial links to the Facility, and the Facility Data Processing Subsystem are the only parts of the Ground Test HM Subsystem that would not migrate into the flight system. Hence, they could be purchased off-the-shelf without being concerned about flight system issues. The result is that these cards will be inexpensive to procure and integrate into the system. The card selected for transmitting data to the Facility, the HSDB card, utilizes a fiber optic based protocol and yields very high data transfer rates. There are many other viable options which include 1553, conventional RS-232, or the existing CADS Serial Link protocol. The choice would most likely be made by consulting with the facility test staff to minimize cost of retrofitting the facility.

To save on non-recurring hardware and software development costs, the Facility Data Processing Subsystem, Figure 4.5, uses the same card types as the Ground Test HM Subsystem.

4.2.4.1.1.1 Data Processing Functional Groups (DPFGs).—The DPFGs, shown in Figure 4.6, are configured using a minimum number of card types. A DPFG may consist of one, two, or three cards; the most common cards are the CPU and DSP cards.

There are two very important DPFG attributes. First, a private bus between the CPU card and the interface card allows the designer to avoid the data transfer bottlenecks common in systems with only one data bus. Second, the DPFG forms a type of "Fault Containment Region (FCR)." In a system, faults do not propagate from one region to another. In this case, the DPFG forms a containment region that deters fault propagation out of the DPFG. The isolation is not 100%, as faults can propagate over power supply lines and the DPFG's interface to the HMS, but many faults within a DPFG (i.e. DSP failure, private bus failure, etc.) will not propagate. Thus, the distributed architecture of the HMS Subsystem increases the system dispatchability (in comparison to a conventional, single bus system) despite localized failures.

4.2.4.1.1.2 Interface.—Expanded views of the Ground Test HM Subsystem (Figure 4.7) depict the various interface boards and VME cards required. The interface boards for the DPFGs can be procured from commercial vendors. Note, however, that sometimes commercial products are not applicable to aerospace

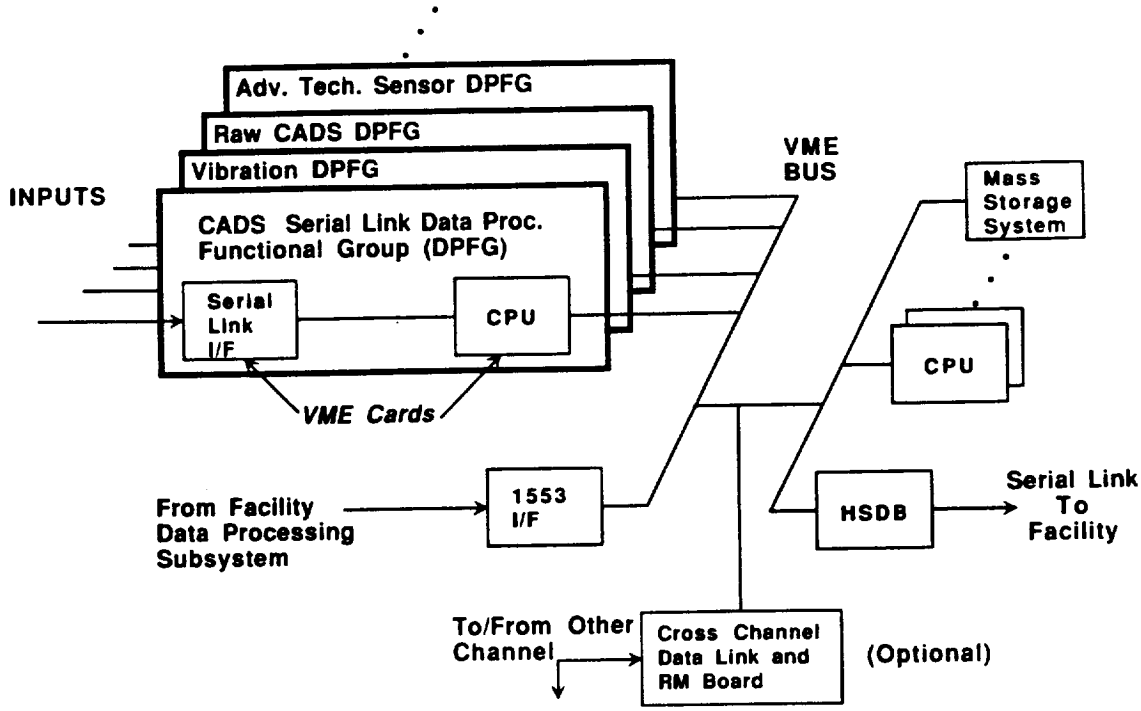

Fig. 4.4 GROUND TEST SUBSYSTEM DETAILED BLOCK DIAGRAM

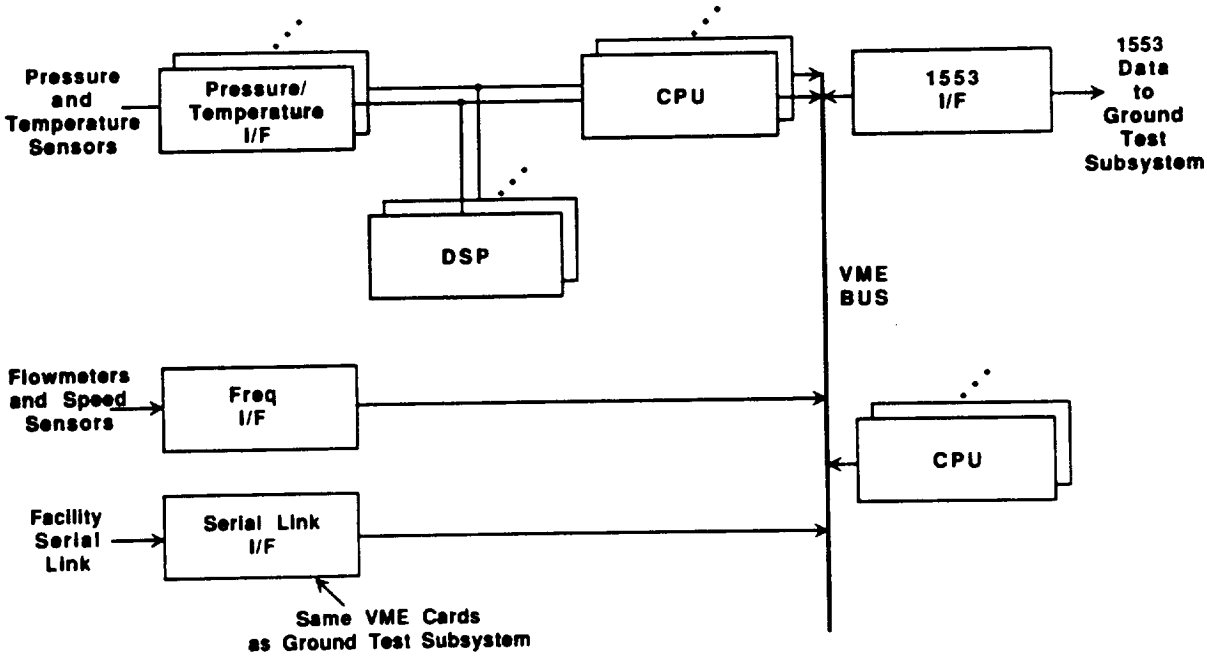

FIG. 4.5 FACILITY DATA PROCESSING SUBSYSTEM DETAILED BLOCK DIAGRAM

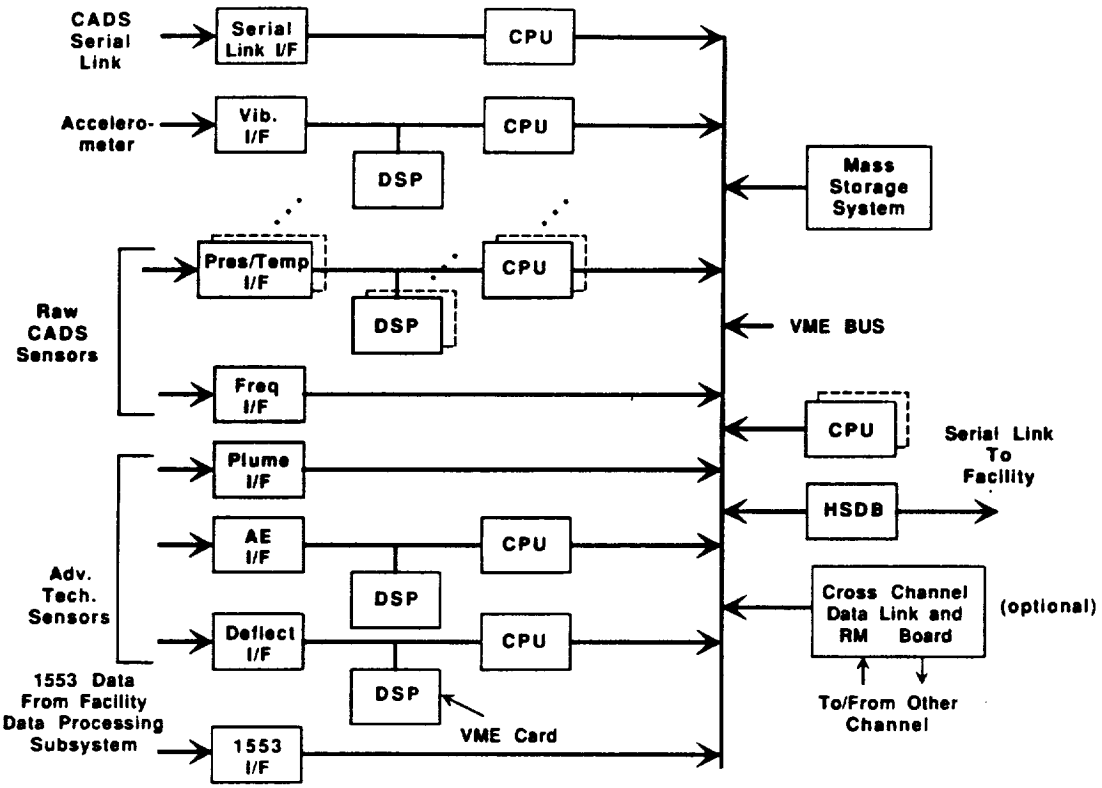

FIG. 4.7 EXPANDED VIEW OF GROUND TEST SUBSYSTEM DETAILED BLOCK DIAGRAM

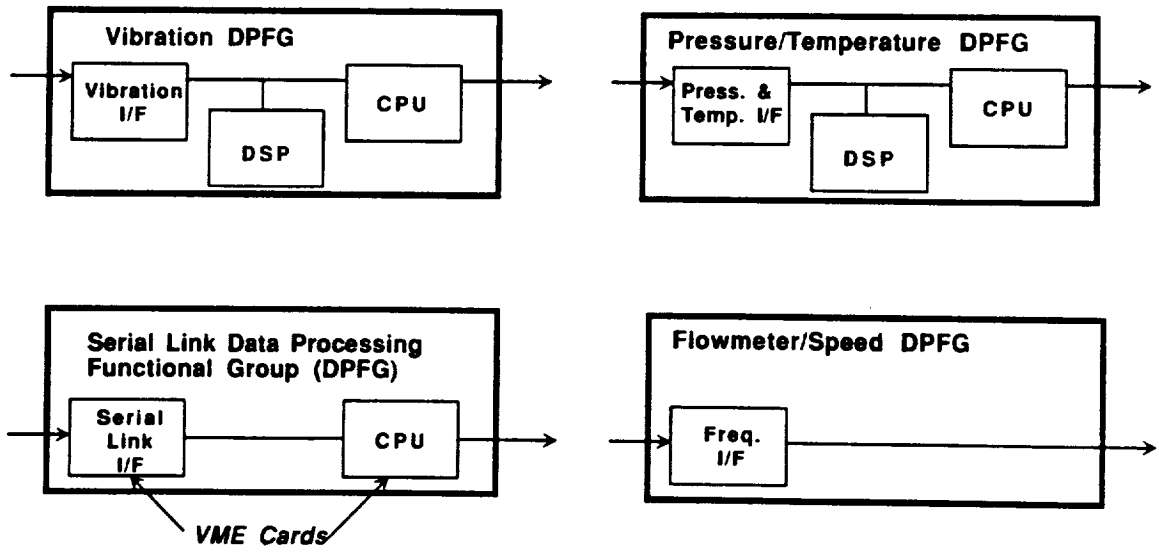

Fig. 4.6 LIBRARY OF DPFGs

embedded systems: real world problems include data latencies, lack of verified interface software, and inability to adequately detect cable opens and shorts. The alternatives are to modify existing commercially available boards or to custom design boards. Careful selection of custom designed cards and commercially available cards can help to optimize the system configuration. (Note that optimum is defined here as the trade-offs between the risks involved in migration to a flight system and the development costs).

United Technologies Hamilton Standard, for example, has developed VME interface boards such as the frequency board, the pressure/temperature board, LVDT board, and analog input boards under the National Aero-Space Plane (NASP) Program. In some cases, notably the LVDT card, there is no commercially available card that meets the requirements of the sensor. Another reason to design a card is to utilize components with the power, weight, reliability and performance that a flight system may require. The use of similar components minimizes risk in developing the Flight System.

4.2.4.1.1.3 Processor.—The processor card is the most important card in the system because of its widespread application through the system. The processor selected for the HMS is the Intel 80960CA, which is synchronized using a master 10 ms interrupt. There is a serial link for downloading programs and uploading data. The CPU would contain a small boot program (approximately 2 K) that would provide the instructions for reading and writing the program/data, as well as initiating the start of the program. Most importantly, the card will be capable of interfacing both to the main VME bus and a local/private bus. Depending on cost and criticality, this card might have Built-In-Test (BIT) hardware such as Loss-of-Clock detectors, memory parity check circuitry, and watchdog timers that force a system reset if the card fails.

4.2.4.1.1.4 Mass Storage System. —The Mass Storage System will consist of a bulk RAM card (Random Access Memory, a form of volatile memory). At a user defined time during the ground test, or at the completion of the ground test, the HMS will write the data from this card to the hard disk. Typically, the data cannot be written in real time, as the data transfer rates on hard disks are not fast enough.

4.2.4.1.2 Redundancy Management. —The system could include a Cross Channel Data Link and Redundancy Management Board. It is envisioned that most SSME testing will only require simplex (single channel) redundancy. However, when development of a flight system is initiated, the redundancy management will be incorporated with minimal impact to the existing Ground Test Subsystem. The major components of such a redundancy management board are currently being developed by United Technologies Hamilton Standard Division under IRD program #89DA4.3.13. The algorithms that this concept utilizes have been proven under the NASA sponsored contract for the X-Wing aircraft.

4.2.4.1.3 Software.—The software development methodology will be in accordance with DoD-STD-2167A, the DoD Standard for developing software, or in accordance with a NASA equivalent standard. The methodology is shown in Figure 4.8. The first step is to specify the system (both hardware and software) in a document known as System Software Specification (SSS). Next, the functional requirements for the software are specified in a Software Requirements Specification (SRS). A top level design is generated and is followed by the corresponding detailed design. Both of these steps are documented in the Software Design Document (SDD). Only after these steps are performed, can the actual coding begin. The code is read and then module checked. The software is tested on the hardware in a step known as CSC Integration Testing. Finally, the software is formally tested against the SRS in a verification step known as CSCI (Computer Software Configuration Item) Testing. The result is a well disciplined software development process that performs to cost and schedule requirements with a minimum of errors.

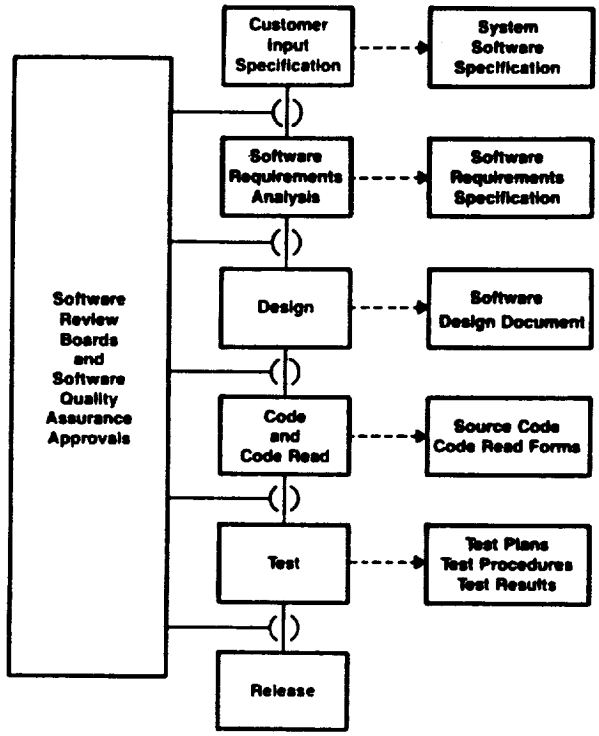

Fig. 4.8 DOD-STD-2167A SOFTWARE DEVELOPMENT PROCESS

4.2.4.1.4 Physical Packaging.—The triple height VME boards for the Ground Test Subsystem fit into one VME rack, while those for the Facility Data Processing Subsystem fit into another. Both VME racks will be housed in a standard 19 inch cabinet with a service door on one side and electrical connectors on the other. The cabinet is six feet tall, and the power supplies will be mounted in the bottom. Such a system is easy to configure and maintain.

If cable runs are extremely long, with potentially heavy electro-magnetic interference (EMI), the system could be outfitted with fiber optic interfaces that convert electrical signals to light-based signals. Note that long runs are typical of rocket test installations.

4.2.4.1.5 Support Equipment.—The principle piece of support equipment for the HMS is the Development Test System (DTS). This is a VME based system housed in the same type of cabinet as the application hardware. The VME cards in the DTS simulate rocket engine sensor signals. The DTS has a desk top computer that allows the operator to download program and to upload data via a serial link to the processor cards, and a hard disk for program and data storage. Current versions of the DTS use RS-422 or MIL-STD-1553B asynchronous data formats for the serial link. The operator can command the DTS to simulate engines in real time automatically using data from a prepared database. Additionaly, the DTS can be used to verify the integrity of the hardware as part of acceptance testing.

The DTS is linked with a VAX based host computer, via either a RS-232 data link or a conventional modem, for remote operation. The HMS software will be developed on the host computer. In addition, the VAX communicates with the workstation where the fault detection algorithms are developed, so that algorithm designers can generate test cases, evaluate their results, and verify real-time system implementation. The host computer would also be capable of converting the data from 9-track computer tapes of actual rocket engine tests for real-time simulation by the DTS.

Finally, the entire DTS, complete with signal simulation capability, can be taken to the teststand to aid in isolating faults during integration. Very often, only the desktop computer is required in the field. The benefit of this reduced system will be the cost savings.

4.2.4.2 FLIGHT HMS.—Figure 4.9 shows the relationship of the Flight HMS to the existing SSME controller. This installation is dual channel both in the control and the HMS, and represents the optimal redundancy. In contrast, a simplex system would have an unacceptably high False Alarm rate, since HMS faults could not be distinguished from engine faults. Unlike the ground test system, false alarms significantly impact the mission success rate. A triplex system, on the other hand, is excessive and represents an unacceptable cost, weight, reliability, and power penalty.

4.2.4.2.1 Flight HMS Block Diagram.—The architecture of the Flight HMS is virtually identical to that of the ground test unit with several functional exceptions (Figure 4.10). First, there is no serial link required for the Facility Data Processing. Second, the Mass Storage System is not required for flight. Third, the Line Replaceable Modules (circuit boards) would be repackaged for the rigors of a flight environment. These changes to the ground test hardware are fairly minor, and thus result in a low risk, synergistic design.

4.2.4.2.1.1 Data Processing Functional Groups.—It is desired to retain the same DPFGs in the Flight HMS as in the Ground Test HMS. There will be one, two or three cards in a group that will perform signal processing. In the case of the three card DPFG, there will be an interface card, a DSP (Digital Signal Processing) Card and CPU card.

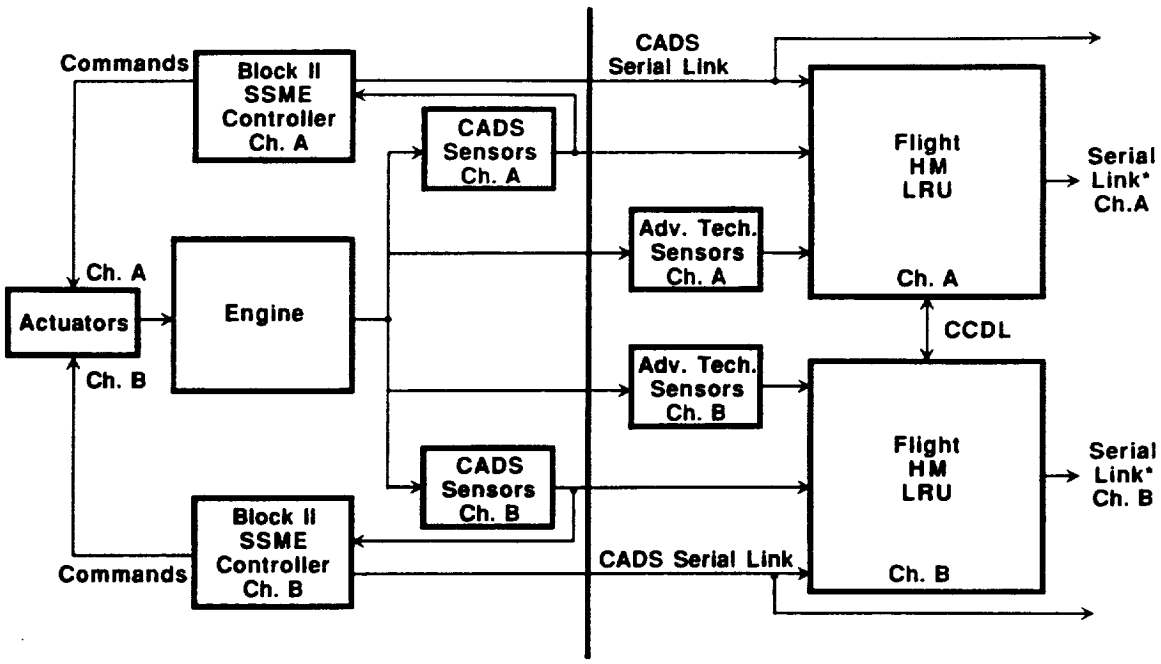

Fig. 4.9 FLIGHT SYSTEM LEVEL BLOCK DIAGRAM

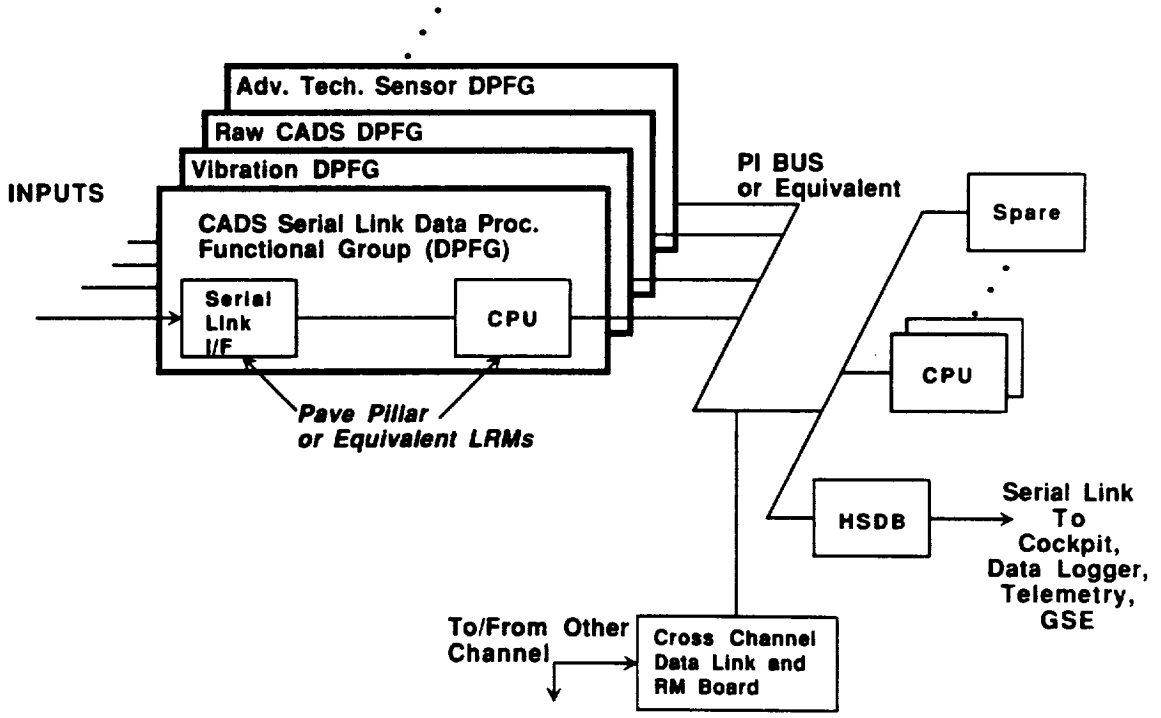

Fig. 4.10 FLIGHT SUBSYSTEM DETAILED BLOCK DIAGRAM

The use of DPFGs will maintain the design concept developed for the Ground Test HMS and assure a smooth migration between the two systems.

4.2.4.2.1.2 Interface.—It is desired to re-use the electronic design that was developed in the Ground Test HMS. The only change is that the card will be repackaged to withstand the flight environment. The use of common designs minimizes risk to the hardware design. Furthermore, software costs and schedule impacts are minimized in transition to the Flight HMS.

4.2.4.2.1.3 Processor.—A very important commonality between the Ground Test HMS and the Flight HMS is the CPU card. If the same CPU card is used in both systems, substantial software costs and schedule savings will be realized. Furthermore, the design risks typically associated with a change in the CPU card are greatly reduced.

Note that the discussion is not limited to the microprocessor on the CPU card; it can extend to commonality of the entire board. Manipulation of timers, interrupts, fault logic, etc. by the software would remain identical between the two versions of the HMS. In summary, if design changes are truly limited to repackaging of the card, then cost, schedule, and risk can be substantially reduced.

4.2.4.2.2 Redundancy Management.—The same electronic design of the Redundancy Management Card from the Ground Test HMS will be used in the Flight HMS.

4.2.4.2.3 Software.—As mentioned above, the use of common hardware designs between the Ground Test HMS and Flight HMS results in substantial cost savings in software development. Furthermore, schedule and risk are minimized.

The software methodology will follow DoD-STD-2167A. The flight system, however, will have a more stringent development procedure which will include module code read, module test, and more formalized system level tests. By delaying these steps until the Flight HMS program, there is substantial cost savings realized during the ground test development.

4.2.4.2.4 Physical Packaging.—Some standard LRMs may not be able to withstand the harsh environment of engine mounting and flight systems. Of particular concern are requirements for vibration, weight, size, power consumption, reliability, and cost.

A typical LRM is shown in Figure 4.11. In this example, the board size is specified by SEM-E format. This format has been specified in the past by DoD. The most recent version of the SEM-E specification can be found in the Joint Avionics Working Group (JIAWG) document number J88-G2B. JIAWG is responsible for setting up a common avionics baseline for the Advanced Tactical fighter (ATF), the Light Helicopter Program (LHX) and the A-12 Navy Aircraft. Typically, a board generates 20 to 30 watts of power and weights 1.5 to 2.5 pounds. The dimensions are 5.88 in. by 6.68 in. The thermal wedge lock clamps have a dual purpose: they provide a high thermal conductivity path to dissipate heat from the board to the rack and secure the card in the rack.

This board would have components mounted on both sides of the board using surface mount technology (SMT). SMT offers four times the packaging density of conventional dual in-line packages. The challenge with SMT is to ensure that solder stresses are minimized. A common source of stress is due to the component and

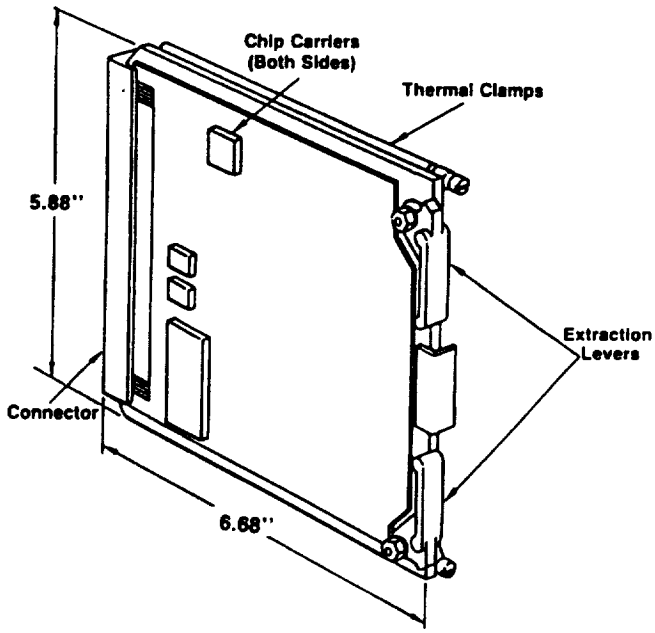

Fig. 4.11 TYPICAL LINE REPLACEABLE MODULE

circuit board's different thermal rates of expansion. The solution is to mount the circuit board on a material that has a similar rate of expansion as the board. A typical approach is to sandwich a copper–invar–copper core between the circuit boards; the copper acts as a good heat sink, while the invar controls the rate of thermal expansion of the boards.

The question of what standard LRM format to be used is a trade–off issue that must be addressed prior to detailed design. The goal of any LRM standard is to reduce the Life Cycle Costs by eliminating the need for custom designs and being able to mass produce hardware. Another concern is the cost of implementing a function using standard LRMs. If, for example, it takes two cards to implement a function using one custom design card, the standard evokes a weight, size, power and reliability penalty. The end result is that the trade must consider the design costs, schedule, procurement and maintenance costs as well as potential size, weight, power and reliability impacts.

4.2.5 Power and Weight Parametric Studies.—The weight, power consumed, and failure rate of the hardware described in the previous sections can be calculated. The results, given in Table 4.2, yield the upper bound for a possible Flight HMS with a very high degree of functionality.

The parameters for the HMS with varying functionality were also computed. The results, shown in Table 4.3, demonstrate that there is a trade–off between functionality and weight. If the system with full functionality is not feasible in terms of weight, power and reliability, then a subset of the HMS might be. The assumptions made in the parametric studies are summarized in Table 4.4.

4.2.6 Markov Modeling Analysis of the HMS.—Markov modeling analysis was used to assess the reliabilities of the Ground Test HMS and the Flight HMS. The results of this analysis are discussed below.

4.2.6.1 Ground Test Reliability.—The Ground Test HMS pre–firing abort rate, missed detection of faults (MDF) rate, and false alarm (FA) rate (components of the HMS reliability) are calculated in this subsection.

4.2.6.1.1 Pre–Firing Abort Rate.—It is assumed that the only time a ground test would be halted prior to firing would be if there were a gross failure of the HMS, i.e. any failure that completely fails the entire single channel HMS. The statistically significant causes include:

Pps	=	Probability of Power Supply Failure per Firing
Pcpu	=	Probability of CPU Failure per Firing (Note this is the Engine/Component Status Module CPU)
Phsdb	=	Probability of HSDB Card Failure per Firing
Pbus	=	Probability of a Internal Bus Failure per Firing

Assuming that the HMS is powered for one hour prior to firing, the probabilities are estimated to be:

Pps	=	80 failures per million firings
Pcpu	=	80 failures per million firings
Phsdb	=	80 failures per million firings
Pbus	=	40 failures per million firings

The probability of a ground test pre–firing abort for a simplex system is the arithmetic sum of these four rates: 0.000280 failures per firing. If the engine failure rate is on the order of 0.01 failures per firing, then the HMS has a negligible contribution to the engine failure rate.

Table 4.2 MAXIMUM WEIGHT, POWER AND RELIABILITY OF HMS

Equipment	Weight (lb)	Power (Watts)	Failure Per Million Hours
HM LRU	36.0	600	1480
Rack	21.5	0	200
Cables	19.9	0	124
Sensors	13.6	0	340
Total for 1 Channel	91.0	600	2144
Multiply by 2			
Total for 2 Channels	182.0	1200	4288

Table 4.3 RESULTS OF PARAMETRIC STUDIES OF OTHER SYSTEMS WITH VARYING FUNCTIONALITY

	Option			
FUNCTION	1	2	3	Strawman
CADS Serial Link DP	x	x	x	x
Vibration DP		x	x	x
CADS Sensor DP			x	x
Adv. Tech. Sensors DP				x
Weight (lb)	37.4	66.3	101.5	182.0
Power (Watts)	336	528	768	1200
MTBF (hours)	1030	586	409	233

Table 4.4 ASSUMPTIONS USED IN PARAMETRIC STUDIES

Equipment	Weight (lb)	Power (Watts)	FPMH*
Digital LRMs	1.50	30.0	80
PS LRM	2.50	40.0	80
Other LRMs	1.50	20.0	40
Rack (54 slots)	43.00	43.0	200
Cable (per sensor)	0.32	0.0	2
Sensor	0.40	0.0	10

* FPMH: Failures per Million Hours

4.2.6.1.2 MDF and FA Rates.—The results of this modeling are summarized in Table 4.5; a ground test HMS with algorithm coverage, Ca, of .90 will result in a order of magnitude reduction in the loss of engines. Similarly, the probability of false alarm per firing, Pfa, must be less than 0.06 false alarms per test. A discussion of the analysis follows.

The Markov Model for the ground test system is shown in Figure 4.12. The symbols are defined as follows:

Pe	=	Probability per Flight of Engine Failure
Ph	=	Probability per Flight of Massive HMS Failure
Ph*	=	Probability, given an engine failure, that the HMS has a gross failure prior to engine fault detection (a one second window during which a power supply or Engine/Component Status Module or CPU within one channel fails)
Pspurius	=	Probability per flight that the HMS fails due to lighting, EMI or power transient
Ch	=	Coverage of the HMS expressed as a Probability, given a massive HMS Failure, that the failure is detected by either the failed channel or the remaining healthy channel
Pfa	=	Probability per Flight of False Alarm due to the HMS
Ca	=	Coverage of algorithm, expressed as a probability, given that the engine failed, that the algorithm will correctly identify the engine as being failed

For all tests it was assumed that an engine is fired for 10 minutes and that Pspurius is negligible. Based on the HMS having a 95 % Built-In Test (BIT) coverage, the value of Ch for a single channel system is typically 0.95.

Normally, coverage refers to the ability of a controller to detect and isolate a failure, and then reconfigure around it. In the case of a single channel HMS, there is no need to isolate the failure any further than the HMS. Also, having the HMS deactivate itself is an acceptable form of reconfiguration; engine tests can continue without the HMS even though it represents a statistical risk. This risk is small because the chance of both an HMS failure and an engine failure is relatively remote.

To assess the impact of the hardware on the MDF and FA rates, it was assumed that the algorithm was perfect, that is, the Ca parameter was 1.000 and Pfa was 0.0000. The resulting MDF and FA rates were, respectively, 6.6E-6 and 1.6E-5 events per test. Note that the critical path for MDF is the path through states A, C, G, K and I. The FA rate is dominated by the path through states A, C, H, and L.

The goal of the hardware implementation was for the hardware contribution to the MDF and FA rates to be an insignificant (approximately 10% or less) portion of the total MDF and FA rates. However, these rates are not known since the Ca and Pfa parameters for the real world, imperfect algorithms are not known. But, they can be derived from the propulsion system failure rate which consists of the failure rate for the engine and the fuel storage and delivery system (tanks, pipes, shutoff valves, etc.). The MDF rate should be at least an order of magnitude lower than the propulsion failure rate. If one assumes that the propulsion failure rate is

Table 4.5 MISSED DETECTION OF FAULTS (MDF) AND FALSE ALARM RATE (FA) FOR GROUND TEST SYSTEM

Assumption	HMS with Perfect Alg.	HMS with Real World Algorithm	No HMS
Coverage of Alg. (Ca)	1.000	0.900	N/A
Probe of False Alarm Rate (PFA)	0.000	0.060	N/A
Source of Failure	Hardware	Hardware & Software Algorithm	N/A
Resulting Rates			
MDF	6.6 E-6	0.002	0.020
FA	1.6 E-5	0.060	0.000

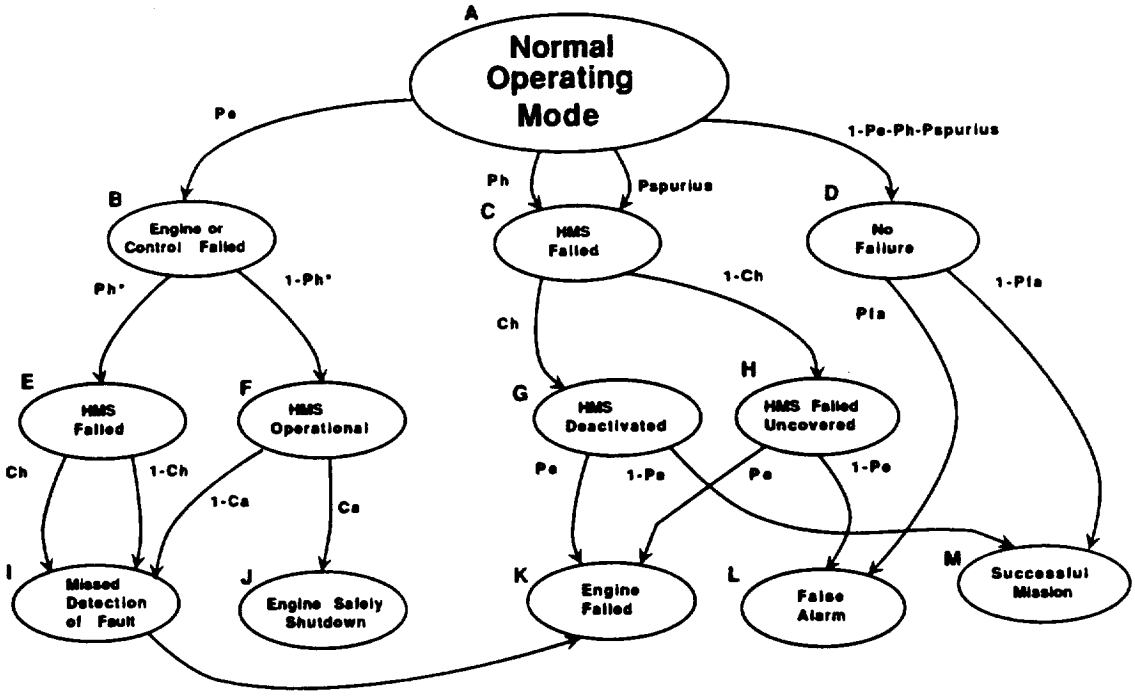

Fig. 4.12 MARKOV MODEL USED TO CALCULATE MDF AND FA RATES FOR GROUND TEST

0.02, then the resulting sum of the MDF rates for an HMS equipped engine is 0.002, an insignificant contribution.

Also, the MDF rate figure can useful in determining requirements for Ca. If MDF is equal to 0.002, then Ca must be 0.90 based on the Markov Model of Figure 4.12. The requirement for Pfa can also be determined. Suppose one required that the false alarm rate to be no greater than three times the rate of propulsion failures, or 0.06. The corresponding Pfa for the Ground Test HMS would be 0.06 false alarms per engine test.

4.2.6.2 Flight System Reliability.—The Flight HMS pre-liftoff abort rate, MDF rate, and FA rate (components of Flight System realiability) are calculated in this subsection.

4.2.6.2.1 Pre-Liftoff Abort Rate.—The calculation of the Flight HMS pre-liftoff abort rate is similar to that of the ground test. The difference is due to additional the Redundancy Management Card and the dual channel redundancy of the flight system. Defining Prm (the probability of a redundancy management card failure per flight) equal to that of Pcpu, the resulting pre-liftoff abort rate is estimated to be 0.000720 failures per flight. It is assumed that if either channel fails grossly prior to liftoff, the flight will be aborted. Again, the HMS will have a negligible contribution to the overall abort rate.

4.2.6.2.2 MDF and FA Rates.—The main difference between the Ground Test System and the Flight System is that the latter is dual redundant. Ph is then double that for a single channel HMS system, approximately 0.004 failures per million hours. Based on each channel having a 95% BIT coverage on itself and a coverage of 95% on the other channel's uncovered faults, the value of Ch for a dual channel system is typically 0.9975.

The coverage parameter, Ch, has a somewhat different meaning for the Flight HMS. Coverage is formally defined as the ability to detect and isolate the fault and then reconfigure around it. The Flight HMS need only fail safe, as the Space Shuttle can fly without the HMS, although it represents a statistical risk. That risk is small because the chance of both an HMS failure and a engine failure is relatively remote. Hence, for fail safe operation, the ability to isolate the fault is restricted to the HMS as a whole, not any particular channel. Furthermore, fail safe is a very simple form of reconfiguration.

To assess the impact of the hardware on the total MDF and FA rates, it was assumed that the algorithm was perfect, that is, the Ca parameter was 1.000 and Pfa was 0.0000. The resulting MDF and FA rates are 1.3E-5 and 1.7E-6 events per test.

The goal of the hardware implementation was for the hardware contribution to the MDF and FA rates to be an insignificant (approximately 10% or less) portion of the total MDF and FA rates. Unfortunately, these rates are determined by a vehicle level Markov Model. In the vehicle level model, the end state probabilities (loss of vehicle, loss of crew, etc) are defined by NASA. The MDF and FA rates are dependent variables in this case and become the requirements of the HMS. Correspondingly, they will dictate the Ca and Pfa parameters.

The Markov Model in Figure 4.13 is very complex to analyze since there are three engines and there are several windows for mission abort and crew escape. It is apparent that Ca and Pfa are inversely related and must be traded in terms of vehicle reliability goals. Nevertheless, Figure 4.13 does demonstrate the relationship between the HMS MDF/FA rates (including both hardware and software/algorithm reliability effects) and the vehicle safety goals.

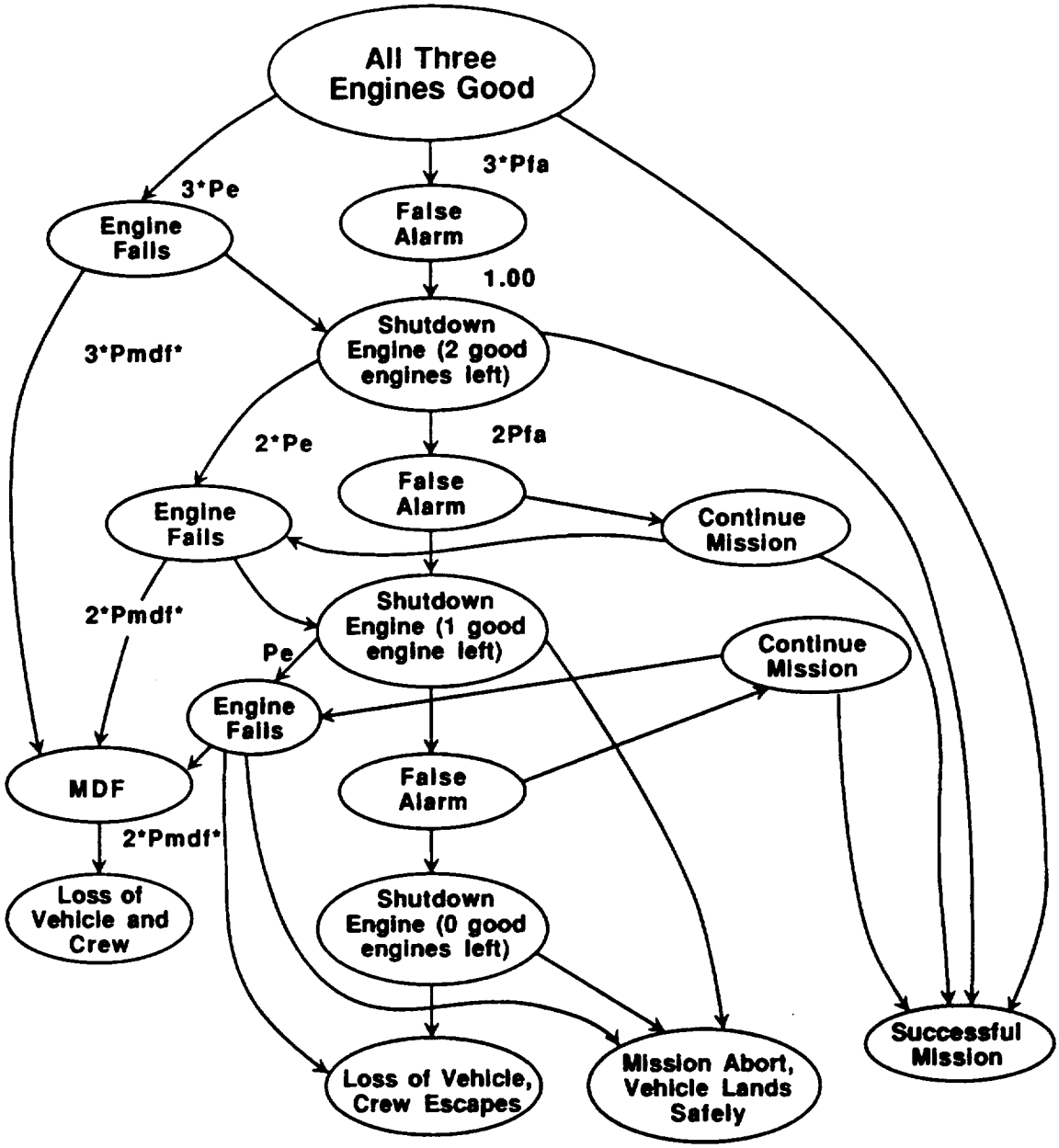

Fig. 4.13 TYPICAL VEHICLE LEVEL MARKOV MODEL FOR THREE ENGINE/MANNED VEHICLE (Show complex relationship between customer defined end states and probability of missed detection of fault, and false alarm)

4.3 Optimization Tool for Hardware/Software Integration

UTRC has a variety of tools to assist in the design and evaluation of hardware and software architectures. One tool, ADAS (Architectural Design and Simulation), was used to demonstrate the optimization procedure during the design of HMS hardware architecture.

4.3.1 Architectural Design And Simulation (ADAS) Description.—Based on petri nets, ADAS enables a designer to map the data flow of an electronic system to its block diagram and simulate system execution. The designer can then examine the results of simulation for hot spots and bottlenecks. With this tool set, the designer can iterate to a balanced architecture with hardware resources allocated to achieve uniform utilization.

Developed by the Center for Digital Systems Research at Research Triangle Institute, ADAS was aimed at the design of large scale integrated circuits. Such circuits have outgrown the traditional breadboard, and more efficient design methods were essential.

Rather than fabricating a breadboard, an ADAS user constructs the data flow diagram and may also construct a hardware block diagram with a graphical editor, EDIGRAF. The mapping of hardware to the data flow diagram may be performed by ASH, the hardware to software mapping utility. Alternatively, the mapping may be directly assigned or overridden by the user. This mapping is illustrated in Figure 4.14.

In this Figure, Tasks 1 and 2 are mapped to separate CPUs and therefore can operate in parallel. Since Task 3 requires results from both Tasks 1 and 2, the beginning of Task 3 is postponed until those results are available. Because Task 3 is executed on the same CPU as Task 2, the Task 2 results are available immediately upon conclusion of Task 2. The Task 1 results however suffer an additional delay for communication. This is accounted for in the DATA XFER block of the software data flow graph which is mapped to the BUS block of the hardware connectivity graph. To the left of this figure, the method of accounting for utilization is illustrated. Each block in the data flow graph is allocated a delay time consistent with the amount of time required to process its work on the hardware available to it. Each connecting line (arc) in this graph is able to hold tokens up to a user defined maximum number. When all input arcs to a block contain at least a threshold number of tokens, then the block may prime. On priming, the block consumes a user defined number of tokens from each separately defined input arc. After the appropriate delay for this block, the block fires and produces a user definable number of tokens on its output arcs.

Once mapped, the software or data flow graph is exercised. GIPSIM determines hardware utilization and latency by simulation, while XPETRI provides the user with the same information by petri net analysis. A consistency checker CONCH helps the user validate the model and a report generator DBPRINT assists with documentation. Hardware description languages HELIX, and ISPS may be used and functionality of the nodes may be defined by ADA or C program code.

4.3.2 ADAS Model.—During the HMS architecture definition process, a candidate architecture was extracted, simplified, and modeled in ADAS as an example of how the tool set could benefit the system design. The first iteration results, shown in Figure 4.15, demonstrate an unbalanced architecture with inadequate computational resources. This first iteration is unable to keep up with the required system input rate as illustrated by the less than 100% utilization of the input data block. With the addition of more computational hardware as illustrated in Figure 4.16, the architectural balance is improved and the system becomes able to

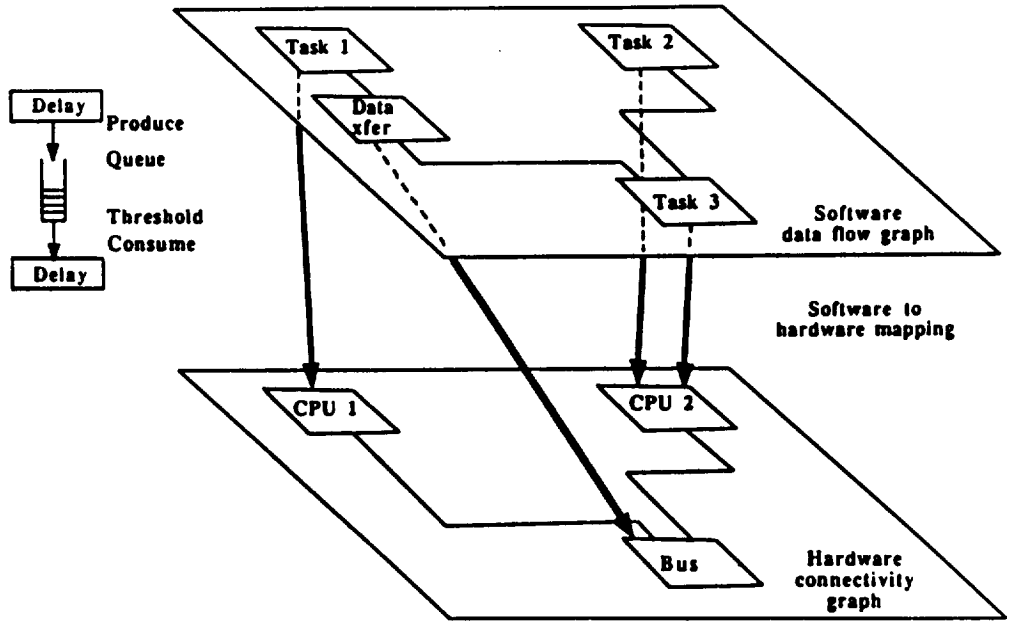

Fig. 4.14 ADAS TOOL UTILIZED IN HMS HARDWARE ARCHITECTURE STUDY.
ADAS System Modeling maps software data flow onto hardware connectivity.

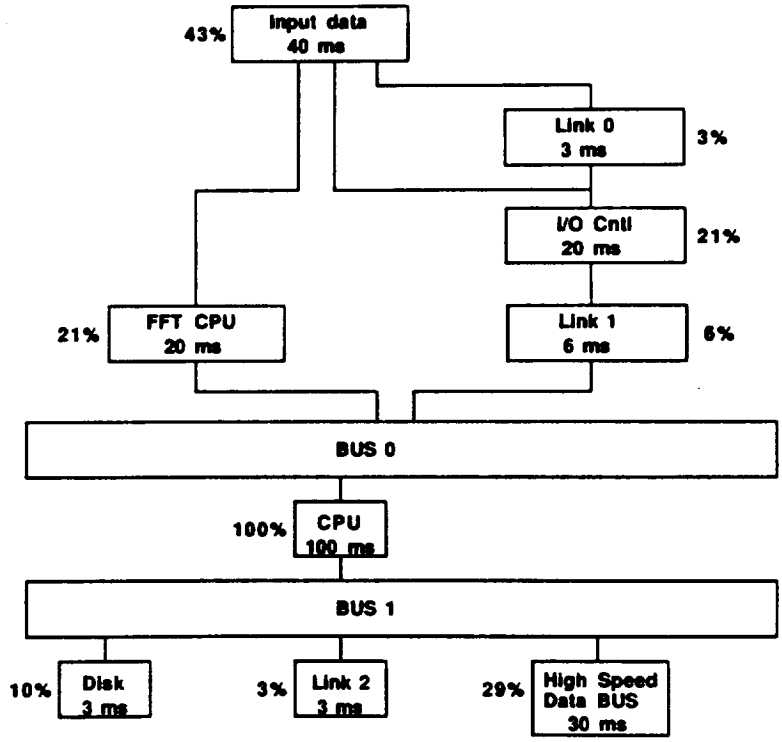

Fig. 4.15 ADAS RESULTS SHOW LOADS FOR SIMPLE ARCHITECTURE
The 43% utilization of the input data block indicates the simple architecture is CPU limited.

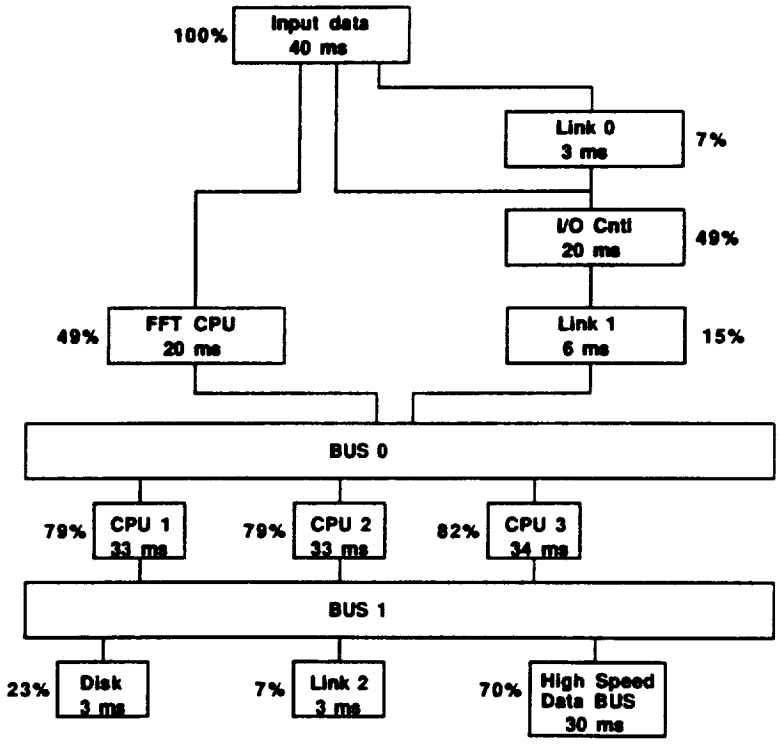

Fig. 4.16 ADAS RESULTS SHOW LOADS FOR COMPLEX ARCHITECTURE

100% utilization of the input data block indicates that a triple processor architecture supports the full workload.

meet the HMS requirements. It must be noted that adding more processing power is not always beneficial. In fact, when the system is communication limited, adding more processing hardware can actually slow the output because more time is wasted fighting for access to the overtaxed data buses. This scenario is analogous to the traffic arteries of a city at rush hour when adding more vehicles to move people results in a slowdown. In the case of the HMS, however, even with the tripling of processing power, the buses and links are lightly loaded. Such an observation presents the designer with an opportunity to explore the possibility of replacing those buses and links with slower, less expensive implementations.

Other factors can override the desire to balance the architecture. For instance, the links are modeled after the 1553B which was designed to provide the reliability required for military aircraft. Because the design of the 1553B is already paid for, and because of its wide ranging compatibility, substitution of a lower performance bus in this case would probably increase the cost rather than decrease it. Although ADAS helps the designer to assess the relative performance of design alternatives, the decisions are still the purview of the designer.

4.4 Summary

An HMS strawman hardware architecture with a high degree of functionality has been presented. The actual hardware will be a subset of this system. Many requirements were discussed which in turn necessitated a modular HMS approach. A throughput study was performed along with an assessment of power, weight, and reliability requirements.

The Ground Test HMS was envisioned as a VME based system. The notable feature of the architecture was the use of DPFGs. A typical DPFG consists of a private bus to transfer data from the I/F card to the DSP, card and finally to the CPU card. The DSP board will be based on a special purpose floating point FFT processor such as one manufactured by UTMC. The CPU card will be based on the Intel 80960, with the Motorola 68030 as an alternate choice. The software will be written in accordance with Ada per MIL-STD-1815 and developed per DoD-STD-2167A. The hardware will be housed in a six foot 19 inch rack for operation in the control room. Support equipment will include a VME based development test system for simulating the rocket engine and testing the HMS electronics.

The Flight System will be a logical adaptation of the Ground Test HMS, and will be dual redundant both in control and the HMS. The differences in hardware will be the dual redundant HM channels, and the elimination of facility sensor hardware and Mass Storage hardware. The maximum weight of the Flight HMS, including sensors and cables will be 182 pounds. The maximum power consumed will be 1200 watts, and the minimum MTBF will be 4200 hours. The desired goal is that the Ground Test and Flight HMS share identical electronic design. The main difference between the two is that the Flight HMS will be dual redundant and repackaged to withstand the harsh flight environment. The benefits of this approach include the re-usability of the software code resulting in cost, schedule, and risk reduction. Also, the hardware design will have been adequately debugged prior to the Flight HMS repackaging phase, further minimizing the risk of Flight HMS implementation.

Two design techniques were demonstrated during this task. Markov modeling was used to determine abort, False Alarm and Missed Detection of Faults rates. The second technique, ADAS, was used to optimize the hardware/software configuration for the Ground Test and Flight HMS. ADAS is one of many tools that are available for design and verification of an HMS.

SECTION 5.0
IMPLEMENTATION PLAN FOR THE HEALTH MANAGEMENT SYSTEM

This implementation plan reflects the UTRC design methodology for the development of a breadboard HMS. A systematic approach for the definition of system requirements, hardware and software development, system validation and verification, and teststand integration was taken. The purpose of this implementation plan is to provide a vehicle from which the actual and detailed implementation program plan can be derived. The intent is to show a variety of cost, capability, and complexity options that can be tailored to match the eventual scope of the implementation program.

Two health management systems will be developed (one will remain at UTRC, the other at the SSME teststand). The modular HMS provides for a phased implementation in which the total HMS is designed as a baseline system which is expanded by a number of subsystem options. The baseline system provides a near-term, low risk implementation of the algorithms developed as part of Phase I, Task 2. Subsystems centered around a particular sensor or sensing technology, which will increase the diagnostic capabilities of the HMS, are presented as optional additions to the baseline system. A technology program is included to fill the near-term technology voids.

The Baseline HMS consists of a Data Logging System, CADS Serial Data Link and a Health Monitoring Function. A general purpose workstation/minicomputer will provide the following non time-critical functions: user interface; system task manager; off line analysis; database; database manager; and a communications link. The critical real-time health monitoring and data logging functions will be implemented in a system to be added onto the workstation. The baseline system itself will be implemented in stages to allow for a smooth integration of the baseline and subsystems into the teststand environment.

The CADS Serial Data Link and Data Logging System will be ready for teststand integration and operation 10 months after the start of the program. This will provide data for algorithm verification and support, as well as feedback regarding issues encountered during the integration phase that can impact the implementation of the algorithms in the Health Management portion of the baseline system. Teststand integration and operation of the complete Baseline HMS will begin 24 months after program start.

The verification process is a substantial and integral portion of the implementation plan. It is extremely important to verify that the HMS can detect and accommodate faults in a timely fashion to minimize component degradation and prevent the development of catastrophic situations. An ideal scenario for complete performance validation and verification would involve installing the HMS on an engine and conducting a number of full scale engine tests run intentionally with component abnormalities. Clearly, this is unrealistic in terms of the costs and schedules involved. Instead, a significant amount of resources and effort have been allocated to the development of verification tools such that hardware, software, and algorithms for the Baseline HMS and subsystems will be verified prior to system integration at the teststand.

A systematic method of validation and verification will integrate component and subcomponent bench testing with simulations for algorithm testing. The hardware and software will be tested in both non real-time and real-time environments. The HMS will be tested in real-time simulation to assess the impact of computer cycle times, memory requirements, and data transfer rates on its ability to successfully perform safety related functions.

There are inherent limitations on the systems which will be used to determine the reliability of the HMS. These include issues of how well the test conditions resemble the real SSME environment; how accurate the engine models are; how responsive and reliable the algorithms are. These questions will be answered during the implementation and testing phase of the program.

The phased implementation plan for the modular HMS is divided into seven tasks. The HMS consists of the Baseline HMS and Data Logging system, and six separate subsystems which can be integrated into the HMS. These subsystems are options to be selected individually or in combination to provide additional functionality and capability to the baseline HMS. Some subsystems require support from a Near Term Technology Development Program.

The following paragraphs describe the work to be accomplished in these tasks, and discuss how program goals are to be met. The 48 month program schedule is summarized in Figure 5.1. A Work Breakdown Structure (WBS) (Figure 5.2) and a summary of man months and other direct costs (Table 5.1) are included as supplements to this implementation plan.

5.1 Baseline System Discussion:

5.1.1 Task 1- Baseline System Implementation: CADS Serial Link.

Task 1.1 Preliminary Design - The system requirements defined in HMS Phase I, Task III, will be reviewed to determine if they are consistent and complete. Customer requirements, program management requirements, HMS statement of work, and technical specification documents will be revisited. If the requirements are found to be insufficient, further requirements will be allocated to the HMS functions, and design modifications incorporated as required. A system segment specification (SSS) detailing the hardware and software modules will be produced.

Task 1.2 Algorithm Verification and Support.—ARMA models, nonlinear regression, and the clustering detection algorithms identified and developed in HMS Phase I, Task 2 will be verified and refined for optimal performance. Nonlinear regression techniques will be used during SSME startup and shutdown phases, while the ARMA models and clustering detection algorithms will be used for fault detection during mainstage operation. As the actual numerical constants and detection thresholds used in the algorithms were only preliminary, this task will encompass algorithm constant/threshold selection and algorithm verification.

The verification process will include running the algorithms on CADS data from a number of SSME nominal and failure tests to establish algorithm performance with respect to correct fault detection rates, detection times, and robustness. Algorithm constants, confidence intervals, and thresholds will be established to minimize false alarm rates and detection times. False alarm rates will be assessed and quantified.

This task will support algorithm development during the period that the hardware is in its implementation phase. Once the system reaches the teststand, algorithm changes and tweaking will be supported by the teststand integration and operation effort.

Task 1.3 Hardware Development Process. —Hardware will be developed to support two health management systems (one to remain at UTRC, the other at the teststand). A modular design will be implemented for the HMS, as it allows for a flexible implementation and room for growth. A general purpose

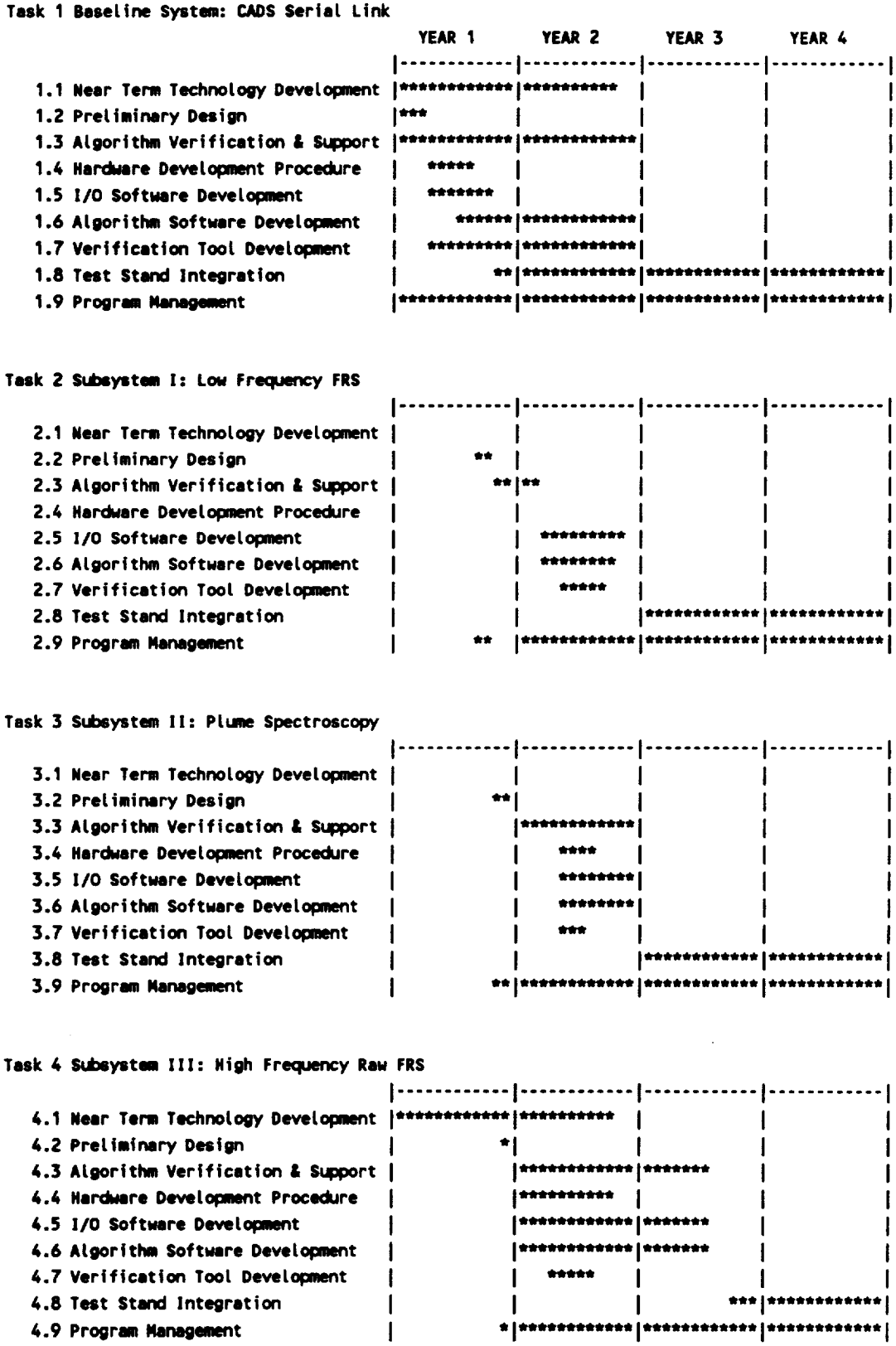

FIG. 5.1 HMS IMPLEMENTATION PLAN SCHEDULE

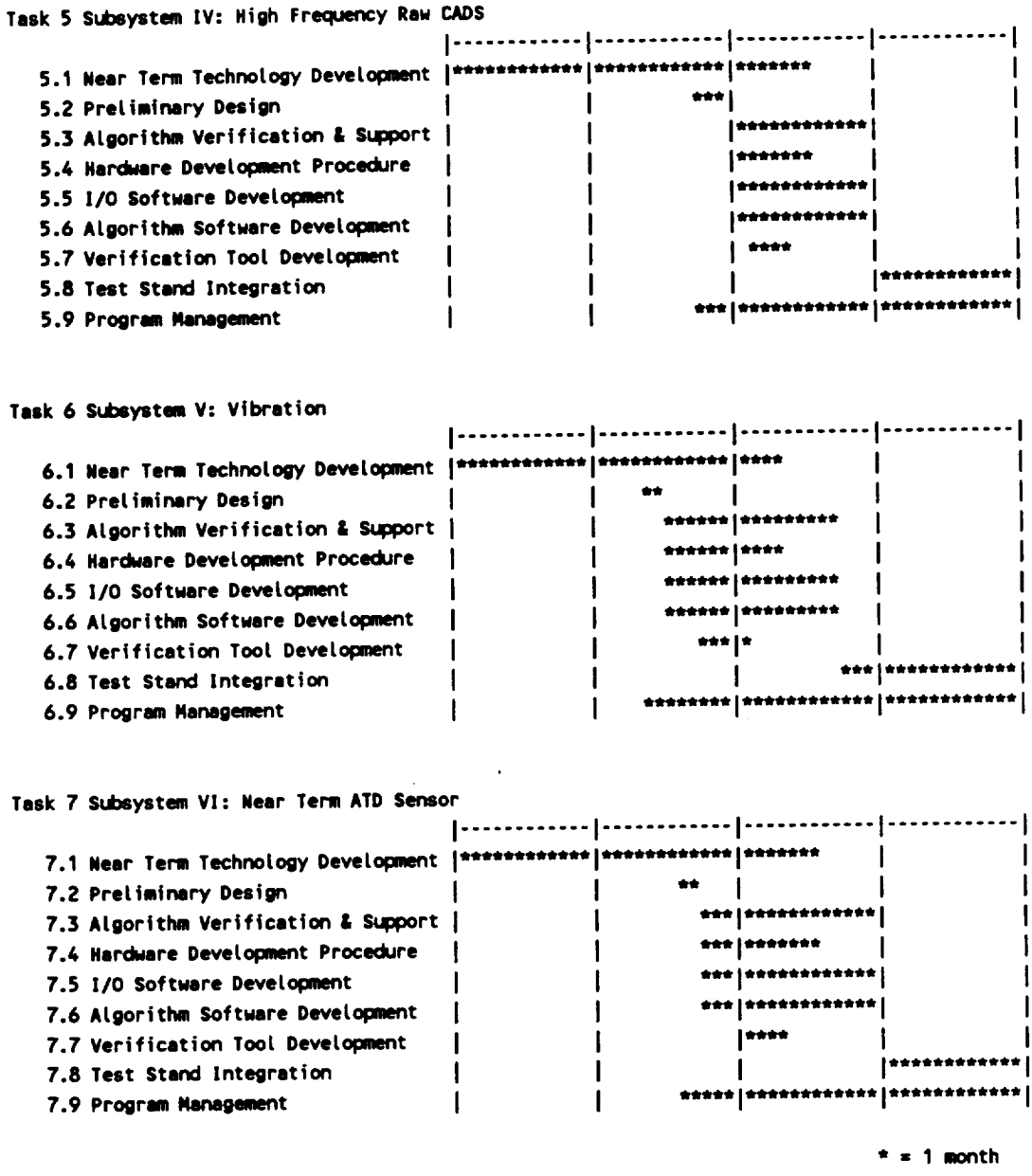

FIG. 5.1 HMS IMPLEMENTATION PLAN SCHEDULE (continued)

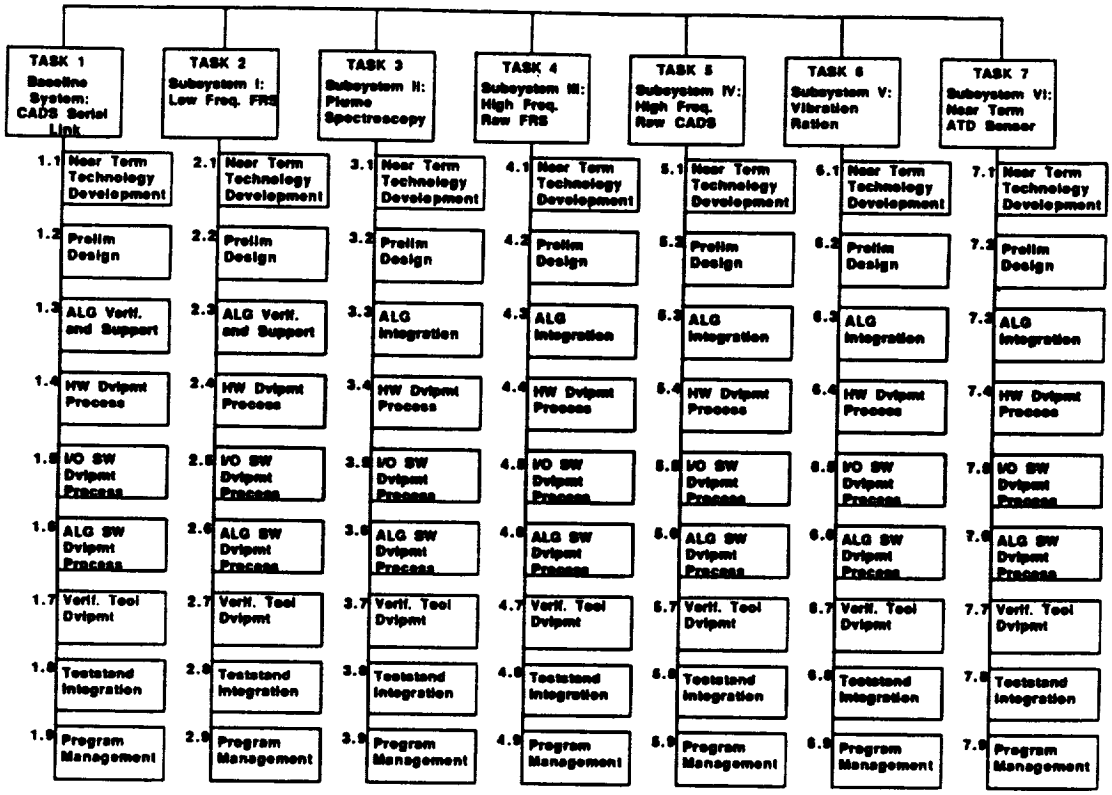

Fig. 5.2 HMS WORK BREAKDOWN STRUCTURE

Table 5.1 LABOR AND HARDWARE REQUIREMENTS

	Base (HMS)	Sys I	Sys II	Sys III	Sys IV	Sys V	Sys VI	Total
LABOR FOR TASK:	1.x	2.x	3.x	4.x	5.x	6.x	7.x	
x.1 Near Term Technology Development	20.0	0.0	0.0	33.0	22.0	33.0	11.0	119.0
x.2 Preliminary Design	7.0	1.0	1.0	5.0	1.0	1.0	1.0	17.0
x.3 Algorithm Verification & Support	30.0	5.0	6.0	6.0	6.0	6.0	6.0	65.0
x.4 Hardware Development Procedure	21.5	0.0	4.0	15.9	0.0	8.0	8.0	57.4
x.5 I/O Software Development	36.0	7.2	5.4	50.4	14.4	14.4	14.4	142.2
x.6 Algorithm Software Development	32.0	9.7	4.8	58.0	19.3	14.5	14.5	152.8
x.7 Verification Tool Development	16.0	4.0	4.0	4.0	4.0	4.0	4.0	40.0
x.8 Test Stand Integration & Operation	72.0	6.0	12.0	13.5	13.5	13.5	13.5	144.0
x.9 Program Management	26.1	3.7	4.1	20.6	8.9	10.5	8.0	81.9
TOTAL (man-months)	260.6	36.6	41.3	206.4	89.1	104.9	80.4	819.3
HARDWARE COSTS:								
Breadboard	225.0	50.0	25.0	300.0	100.0	75.0	75.0	850.0
Development Test System	157.5	35.0	17.5	210.0	0.0	52.5	52.5	525.0

FUNCTION:							
CADS Serial Link Logging	x						
CADS Serial Link Diagnostics	x						
Facility Data Link		x					
Plume Spectroscopy			x				
Raw CADS, High Frequency				x			
Raw Facility, High Frequency					x		
Vibration						x	
Near Term ATD Sensor							x

workstation/minicomputer will provide the following non time-critical functions:

-user interface
-system task manager
-off line analysis
-database
-database manager
-communications link

The critical real-time health monitoring and data logging functions will be implemented in a baseline HM System on a commercial bus architecture to be integrated with the workstation. The baseline system will consist of the workstation and VME cards for the following: CADS serial link interface and CPU; a main system CPU; mass storage system; VME busses.

A Development Test System (DTS) will be acquired and modified for use as an HMS verification tool.

Task 1.4 I/O Software Development Process.—An I/O interface requirement specification (IRS) and a software requirement specification (SRS) will be generated. Following these, detailed software will be designed, coded in ADA, and downloaded into the system. Hardware/Software integration and testing will be performed using the DTS. A system test plan will be developed and test procedures written for the complete system verification and test prior to teststand integration.

Task 1.5 Algorithm Software Development.—The algorithmic techniques of Task 1.2 will be implemented within the software structure of the HMS. Software for the fault detection algorithms will be developed and coded in ADA per an algorithm IRS and SRS.

Task 1.6 Verification Tool Development.—The verification process is an integral portion of the HMS Implementation Plan. It is not appropriate to simply validate system operation at the teststand. Once the teststand integration phase is reached, any problems incurred will have a substantial impact upon the program in terms of cost and scheduling. Therefore, a significant amount of resources and effort have been allocated to the development of verification tools so that hardware, software, and algorithms for the baseline HMS and subsystems will be verified prior to system integration at the teststand.

Appropriate hardware and software integration tools will be selected for development. The HMS verification tools will include such tools as ADAS, the DTS, and the COMDISCO system, described below.

ADAS will be employed to analyze the databus and CPU loadings and provide an optimal architecture for the HMS and Data Logging System. ADAS maps software data flow graphs onto the hardware set and produces a hardware connectivity graph which optimizes the design.

The Development Test System (DTS) is a stand alone system to be used for component/subcomponent bench testing and system integration testing of the complete hardware and software packages. The DTS will simulate the inputs to the HMS. Software enhancements to the DTS will be supported under this task. These enhancements might include, for example, the capability to simulate sensor loss/failure in order to validate teststand integration, as well as to test algorithm robustness.

COMDISCO will be used in the development, testing, and verification of the fault detection algorithms. The COMDISCO system is a workstation based design environment which allows one to model signal

processing systems and to simulate and fine tune DSP algorithms. The fault detection algorithms will be simulated on the COMDISCO system, and deficiencies will be highlighted and corrected.

Task 1.7 Test Stand Integration and Operation.—Teststand integration and support of the Baseline CADS Serial Link HMS will be provided for at both the teststand and at UTRC. UTRC will train one person in the operation of the HMS.

Integration and operation of the baseline hardware at the teststand will begin 10 months after program start. The workstation and Baseline CADS Serial Link hardware and Data Logging system will be integrated on the teststand and perform data logging functions while the HMS algorithms are still in their verification/implementation phase. Not only will this provide for a smoother integration of the baseline HMS and Subsystems and algorithm support via the data logging, but it will also provide essential feedback which can impact the development process. Teststand integration and operation of the complete Baseline HMS will begin 24 months after program start.

Task 1.8 Program Management.—This task includes the effort to plan and direct the project as well as the preparation and attendance at various levels of reviews. The task also includes the preparation of documentation and reports. The traditional management tasks of high visibility, rapid problem solving, and accurate program control will be followed rigorously. Special emphasis will be placed upon interaction with NASA personnel between program tasks.

Task 1.9 Near Term Technology Development.—Expert Systems techniques will be developed and incorporated to manage the diagnostic information from the baseline HMS and subsystems. A high level automatic decision making process will utilize a priori knowledge about SSME and LRU operation, as well as incorporate the diagnostic information from the subsystems. The a priori knowledge could include, for example, information such as turbopump efficiencies, component wear, engine test history, and teststand conditions. The decision making scheme will use expert system rules to determine engine health.

5.2 Subsystem Description

A modular HMS has been proposed for its capability of phased implementation and its flexibility. With this in mind, six subsystems have been defined as HMS options which can be added onto the baseline system. These subsystems may be selected individually, or in combination, to provide additional HMS functionality and capability. It is stressed that these subsystems are not to be implemented as stand-alone systems, but rather as additions onto the baseline HMS. Some subsystems require development efforts covered by the Near Term Technology Program to enable their implementation. Each subsystem selected will be developed according to each of the subtasks described under the baseline system.

5.2.1 Task 2. Subsystem I: Low Frequency Facility Data Link.—The Low Frequency Facility Data Link will interface to the Facility Recording System (FRS) as it currently exists and provide the HMS with the conditioned facility sensor data. This subsystem will employ the fault detection algorithms utilized in the baseline CADS Serial Data Link, and therefore require minimal technology development. An optimal subset of FRS sensors will be selected for the implementation. The algorithms will be run on data from a number of SSME nominal and failure tests to verify their operation and performance, as well as to tweak algorithm constants, confidence intervals, and thresholds. False alarm rates will be assessed and quantified. The hardware required for this subsystem will include VME cards for the FRS data interface and the subsystem CPU.

Teststand integration of the Low Frequency Facility Data Link will begin 24 months after program start.

5.2.2 Task 3. Subsystem II: Plume Spectroscopy.—A plume spectroscopy system and its associated processing algorithms are assumed to be developed outside of the scope of this program. A plume spectrometer detects infrared emission and absorption of ionized species within the SSME plume. The spectral lines of these species can be correlated to internal engine erosion and wear. The output of a 'sensor' will be the intensity of preselected spectral lines which correspond to the species of interest.

The Optical Plume Anomaly Detector System, OPADS, will exist at the teststand and interface with the HMS via a VME card. Extensive testing will be required to develop a database with sufficient detail to identify intensity patterns which correlate with faults. Expert Systems techniques, developed under the Near Term Technology Development task, will be used to integrate the additional diagnostic capabilities into the HMS.

Teststand Integration of the Plume Spectroscopy Subsystem will begin 24 months after program start.

5.2.3 Task 4. Subsystem III: High Frequency Raw Facilities Data Link.—The HMS will interface directly to a specified set of Facility data lines before the signals are conditioned by the Facility Recording System. This will provide the HMS with high frequency, unconditioned data which will contain more diagnostic information than that which is conditioned and recorded by the FRS. The HMS interface will be isolated such that the integrity of the Facility data will be maintained. A subset of the FRS data lines will be selected for implementation in the HMS failure detection algorithms.

The hardware required for this subsystem will include VME cards for the interface, A/D and signal processing, and CPU(s). The number of signal processing cards and CPUs required will depend upon the number of facility sensors selected. Signal processing and fault detection algorithms will be developed under the Near Term Technology Development task. Hardware and Software modules will be implemented, tested, and verified using the DTS, ADAS, and COMDISCO prior to teststand integration and testing.

Teststand integration of the High Frequency Raw Facilities Data Link Subsystem will begin 30 months after program start.

5.2.4 Task 5. Subsystem IV: High Frequency Raw CADS Data Link.—The High Frequency Raw CADS Data Link HMS Subsystem will follow the high frequency Facility effort, and will be similar in function to the Raw Facilities Data Link, and therefore cannot be implemented without its predecessor. The HMS will interface directly to a specified subset of the CADS data lines, before the signals are conditioned by the SSME controller. This will provide the HMS with high frequency, unconditioned data which will contain more diagnostic information than that which is conditioned by the controller. The HMS interface will be isolated such that the integrity of the CADS data entering the controller is maintained.

The hardware required for this subsystem will include VME cards for the interface, A/D and Signal Processing, and CPU(s). The fault detection algorithms developed for Subsystem III, the High Frequency Raw Facilities Data Link, will be utilized in this subsystem's implementation and therefore will require minimal technology development effort. Hardware and Software modules will be implemented, tested, and verified using the DTS, ADAS, and COMDISCO prior to teststand integration and testing.

Teststand integration of the High Frequency Raw CADS Data Link Subsystem will begin 36 months after program start.

5.2.5 Task 6. Subsystem V: Advanced Vibration Analysis.—The Advanced Vibration Subsystem for the HMS will interface to the existing accelerometer suite to obtain vibration data. The algorithms for the Vibration Subsystem of the HMS will not duplicate the efforts of FASCOS, but will involve more advanced vibration signature analysis.

The hardware required for this subsystem will include VME cards for the interface, A/D and signal processing, and CPU. Signal processing and fault detection algorithms will be developed under the Near Term Technology Development task. Hardware and Software modules will be implemented, tested, and verified using the DTS, ADAS, and COMDISCO prior to teststand integration and testing.

Teststand integration of the Vibration Subsystem will begin 33 months after program start.

5.2.6 Task 7. Subsystem VI: ATD Sensor.—A number of advanced sensing technologies which provide additional diagnostic information about SSME health are being developed under the Alternate Turbopump Development (ATD) Program. The technologies being considered for the HMS subsystem are:

-Acoustic Emission
-Fiber Optic Deflectometer
-Optical Pyrometer

Acoustic Emission sensors monitor high frequency stress waves which result from the interaction of bearing components. Features extracted from time and frequency domains are analyzed by correlation and neural network techniques to identify the state of operation of the bearing. As both time and frequency analysis are required for the AE techniques, a dedicated signal processing group must be developed.

Fiber optic deflectometers use light reflections to measure outer race deflections due to bearing passage in order to quantify bearing and race condition. Frequency analysis is required to extract bearing component harmonics. These highly computational algorithms must be developed on dedicated hardware to provide real-time diagnostic information.

Fiber optic probes with indium-gallium-arsenide detectors measure radiant energy from turbine blades during engine operation to provide a linear map of blade temperature. As computational requirements are high, special dedicated processing will be developed.

Note that the signal processing and fault detection algorithms associated with each sensor will be developed outside of the scope of the HMS Program, most likely as part of the ATD Program.

Development of this subsystem requires that the production ATD pumps incorporate one or more of the above mentioned sensors. As the ATD Program continues, these sensors will be evaluated for their implementation feasibility. The Near Term Technology Development task will support the modifications to fault detection and signal processing algorithms which will be required to include the sensor(s) as part of the HMS.

The hardware required for this subsystem, though somewhat dependent upon the sensing technologies selected, will include VME cards for the sensor interface(s), A/D and signal processing, and CPU(s). Hardware and Software modules will be implemented, tested, and verified using the DTS, ADAS, and COMDISCO prior to teststand integration and testing.

Teststand integration for the Near Term ATD Sensor Subsystem will begin 36 months after program start.

SECTION 6.0
CONCLUSIONS

UTRC has developed a focused HMS framework design for the SSME. The UTRC HMS framework integrates fault detection algorithms with proven sensor technologies to provide monitoring during all phases of the SSME operation. Three fault detection algorithms, ARMA, RESID, and clustering, form the proven core of a hierarchial decision process that was mapped onto a state-of-the-art, off-the-shelf hardware architecture capable of real-time operation. Key elements of the UTRC HMS framework are:

- All phases of SSME operation covered;
- Three algorithmic approaches used to cover faults with different manifestations;
- Algorithms demonstrated 100% detection of faults for the test database using only CADS sensor information;
- Low preliminary false alarm rate;
- Robust to sensor loss;
- Minimal algorithm complexity;
- Modular hardware architecture provides flexibility, reliability, and maintainability while allowing realtime operation of the fault detection algorithms;
- Phased implementation provides near term benefits;
- Clear migration path to a Flight HMS established in the hardware design.

UTRC has demonstrated the feasibility of a focused HMS that can provide immediate benefits on the SSME teststand. A low-risk, phased implementation plan will provide near term enhancements to safety while allowing the incorporation of advances in algorithm and sensor technologies as they become available. The successful demonstration by UTRC of the essential fault detection strategies along with a viable hardware design provides the necessary framework from which the SSME HMS can can be implemented.

APPENDIX A
FAILURE DETECTION ALGORITHM RESULTS

This appendix contains a description of each of the sixteen SSME tests from which data were available for analysis, and also a description of the results of the HMS failure detection algorithms. Descriptions of the failure incidences were taken directly from the Rocketdyne SAFD Phase II Report [1]; no efforts to further explain the causes and propagation of the failures were taken. A plot of the MCC_PC for each test is included, as the Main Combustion Chamber Pressure is proportional to the engine power level, and thus indicative of the test thrust profile. (Note: an MCC_PC of 3006 psia = 100% RPL).

A discussion of the failure detection algorithm results follows the failure incidence summary. Depending upon the failure and the PIDs available in the test dataset, one, two, or all three of the failure detection algorithms may have been applied. For each test, the results and supporting figures of data and output are presented for each appropriate algorithm.

Regression analysis was appropriate during startup and shutdown sequences. A plot of the error between the predicted and actual MCC_PC is shown. Time series analysis failure detection techniques were appropriate during mainstage operation at a steady power level. Data for suspect parameters, as well as their corresponding ARMA error signal correlation functions, are shown.

The Cluster algorithm was appropriate during mainstage operation. Table A-1 lists the missing PIDs for each test. A plot of the results (correlation coefficient) of running the cluster algorithm, with a template for the reduced sensor set, on nominal SSME test data is presented. This is to show that no false alarms occurred for a nominal engine test with the selected sensor set and detection thresholds. Finally, a plot of the Cluster algorithm results for the failure data is shown, along with the fault detection threshold.

1. Test 901-110: HPOTP LOX Seal Burn

According to Rocketdyne SAFD Phase II report[1], during stable operation at 75% of rated power level, the engine controller issued a cutoff command when a fire occurred in the HPOTP. The fire started in the LOX primary seal drain cavity. The exact cause of the fire could not be positively determined, however, nine sources were determined to have the potential of causing the ignition. These are listed below:

1) Loss of hydrodynamic lift resulting in rubbing of the primary oxidizer seal against the mating ring, creating enough heat to initiate burning; 2) Primary oxidizer seal bellows weld failure allowing oxygen leakage; 3) Ignition at the interface of the bellows and its vibration damped as a result of friction; 4) Contamination in the primary oxidizer seal area; 5) Rubbing of the primary oxidizer seal due to changing phase (liquid to gas); 6) Effects of hot gas leakage past the intermediate seal into the primary oxidizer seal cavity; 7) Rubbing of the primary oxidizer seal against the mating ring due to mating ring vibration; 8) Leakage of hot gas containing hydrogen past the intermediate seal into the primary oxidizer seal cavity, creating a combustible mixture; and 9) Other leak paths allowing communication between the drain systems. (Test conducted on 24 March 1977, cutoff time: t = 74.1 seconds.)

CADS Data: A plot of the MCC_PC, shown in Figure A-1.1, depicts the engine power profile for the test.

TABLE A-1 CLUSTER ALGORITHM FAULT DETECTION RESULTS

TEST	MISSING PIDS	EVENT DETECTION THRESHOLD	FAULT DETECTION THRESHOLD	TIME OF DETECTION
901-110	PC CMD MISSING	---	---	---
901-436	NONE	.89	5/5	302.4
901-364	18	.89	5/5	42.7
901-307	18, 225, 226	.89	5/5	8.6
SF10-01	231,232,59,260,261, 52,225,226,32	.68	5/5	*
902-198	NONE	.90	5/5	5.8
902-249	58	.89	5/5	5.2
901-225	231,232	.92	5/5	255.6
750-168	58	.89	5/5	300.2
901-284	232,59,18,261,266	.74	5/5	5.2
750-259	52	.89	5/5	101.5
901-173	58,231,232,18,52,53	.93	5/5	102.1
901-331	58,231,232,59	.67	5/5	50.2
901-222	MAINSTAGE NOT ACHIEVED, FAILURE DURING STARTUP			---
901-340	58,231,232,59	.94	5/5	405.5
SF6-01	---------- CORRUPTED DATA ----------			---

*See section A-5

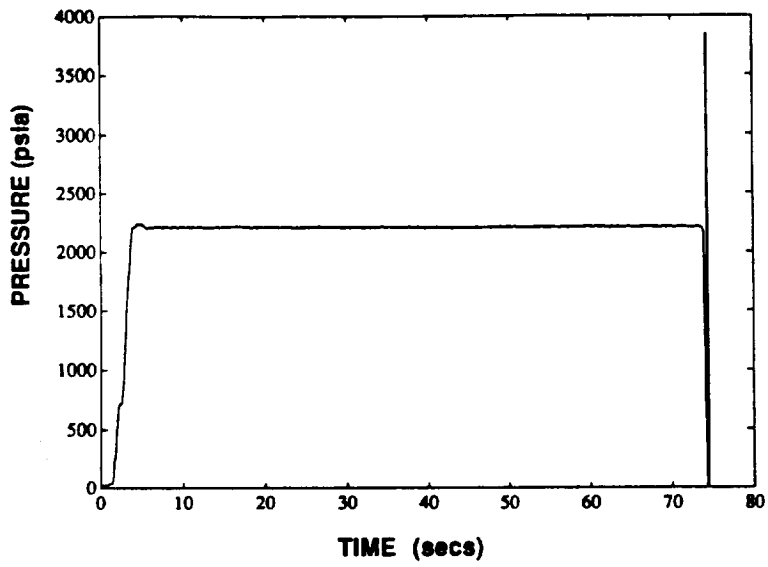

Fig. A-1.1 MCC PRESSURE (PID NO. 130) FOR TEST 901-110

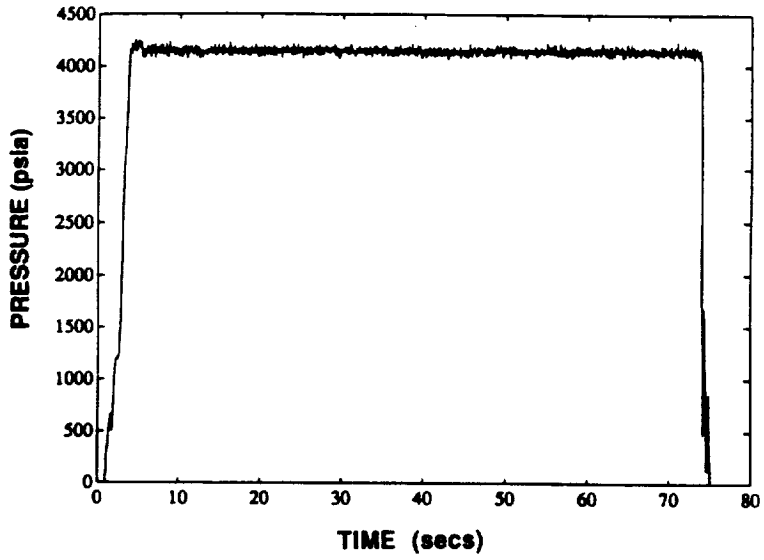

Fig. A-1.2 LPFT DISCHARGE PRESSURE (PID NO. 86) FOR TEST 901-110

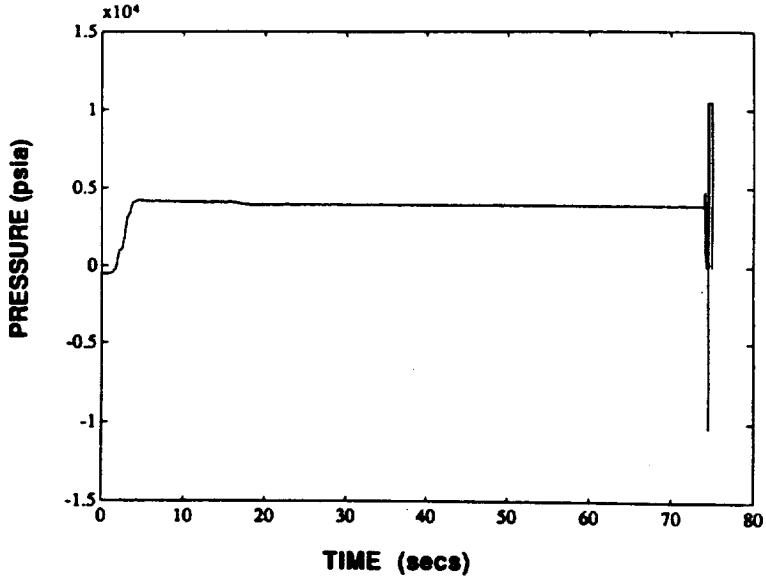

Fig. A-1.3 HPFT DISCHARGE PRESSURE (PID NO. 52) FOR TEST 901-110

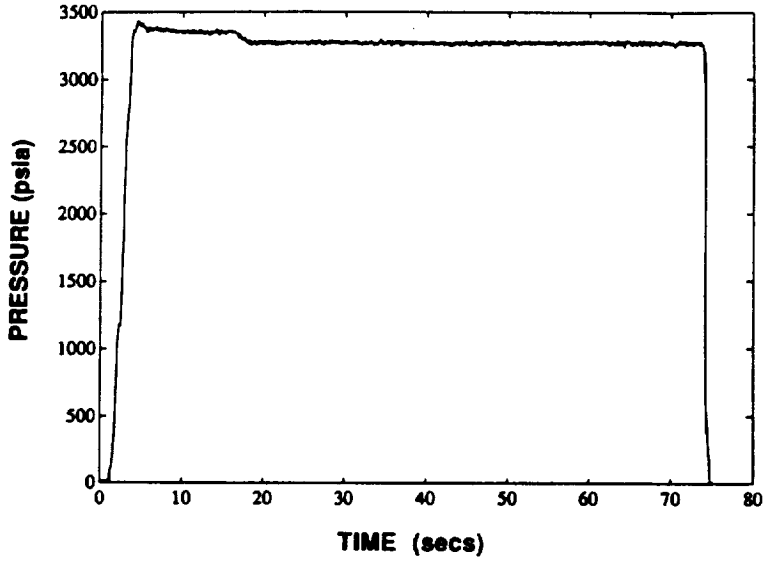

Fig. A-1.4 MCC COOLANT PRESSURE (PID NO. 17) FOR TEST 901-110

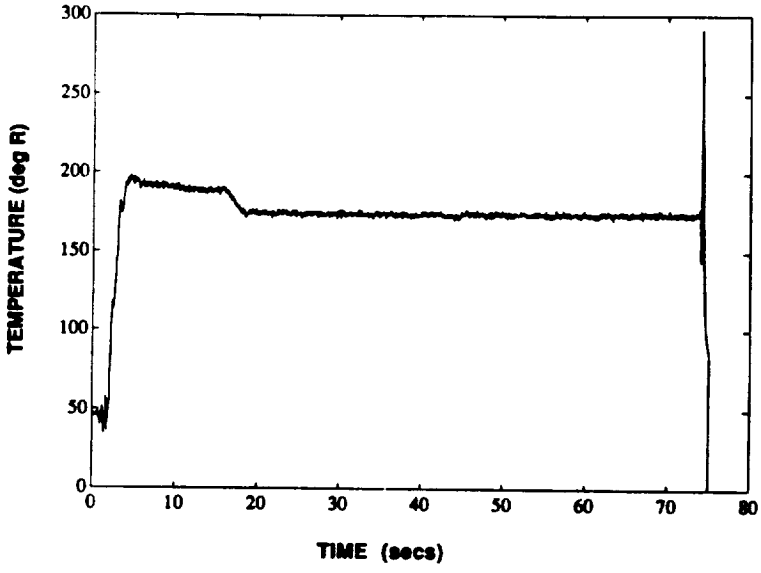

Fig. A-1.5 LPFT DISCHARGE TEMPERATURE (PID NO. 15) FOR TEST 901-110

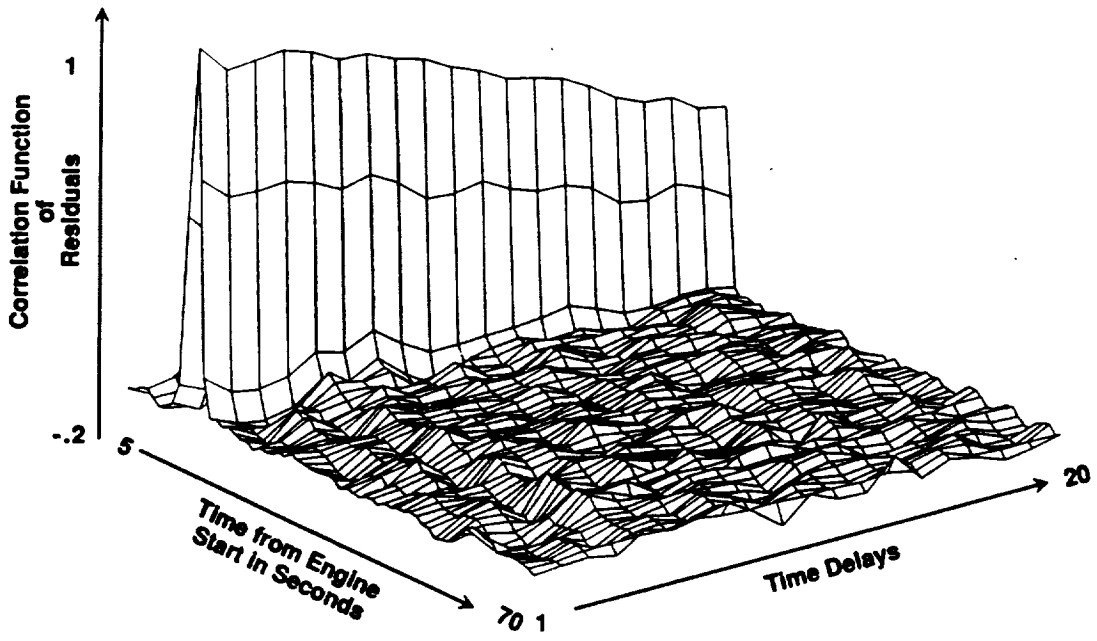

Fig. A-1.6 FAILURE DETECTION USING ARMA MODELS FOR PARAMETER LPFT DISCHARGE PRESSURE FOR TEST 901-110.

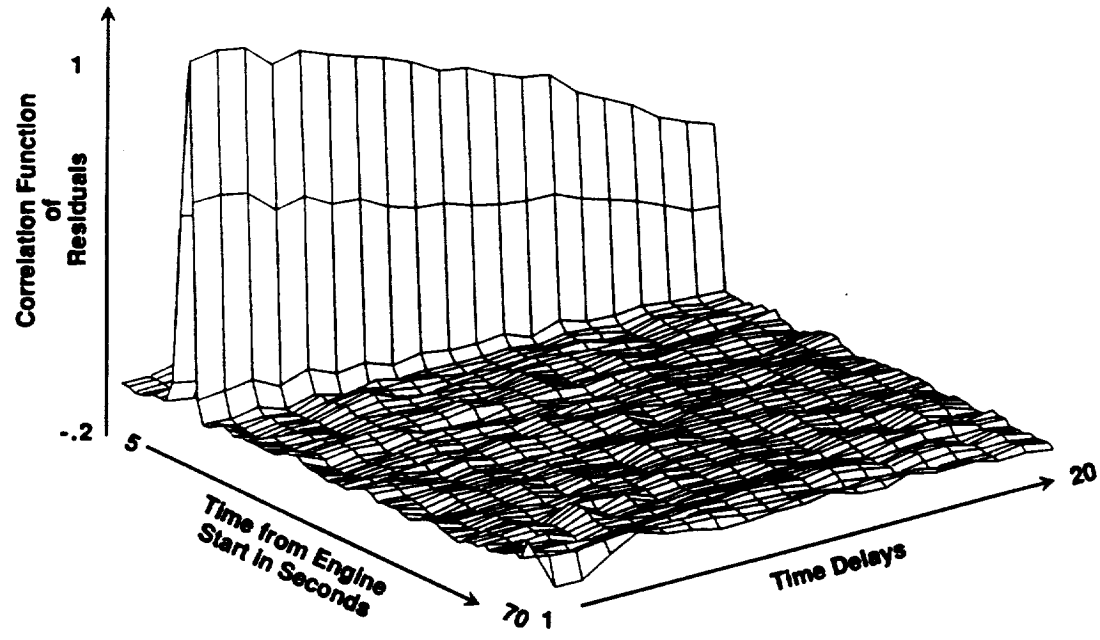

Fig. A-1.7 FAILURE DETECTION USING ARMA MODELS FOR PARAMETER HPFT DISCHARGE PRESSURE FOR TEST 901-110.

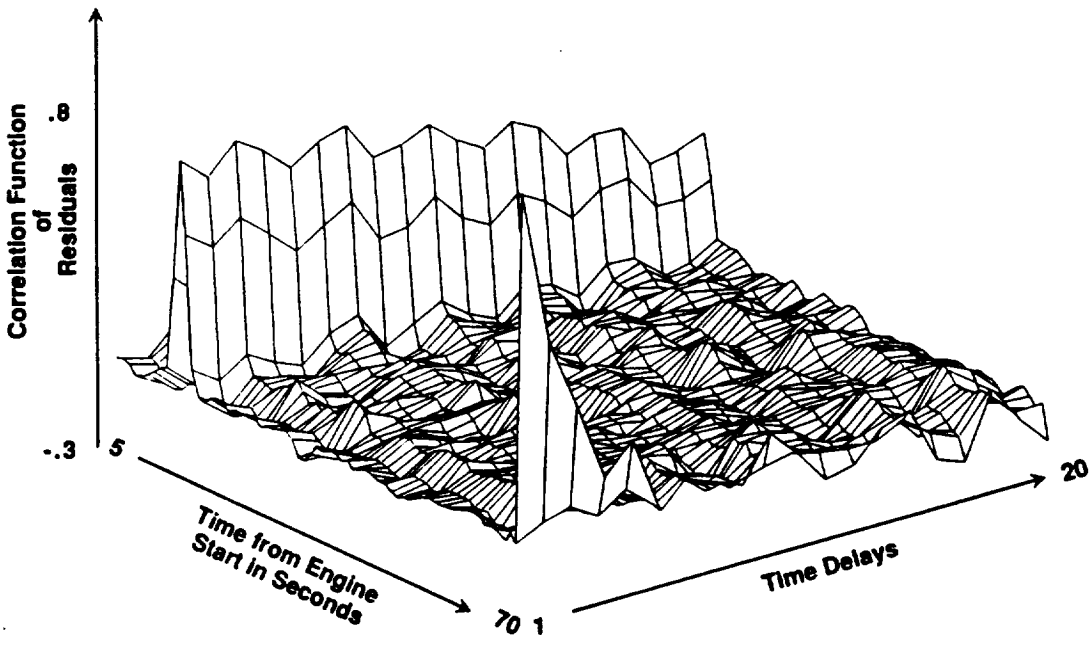

Fig. A-1.8 FAILURE DETECTION USING ARMA MODELS FOR PARAMETER MCC COOLANT DISCHARGE PRESSURE FOR TEST 901-110.

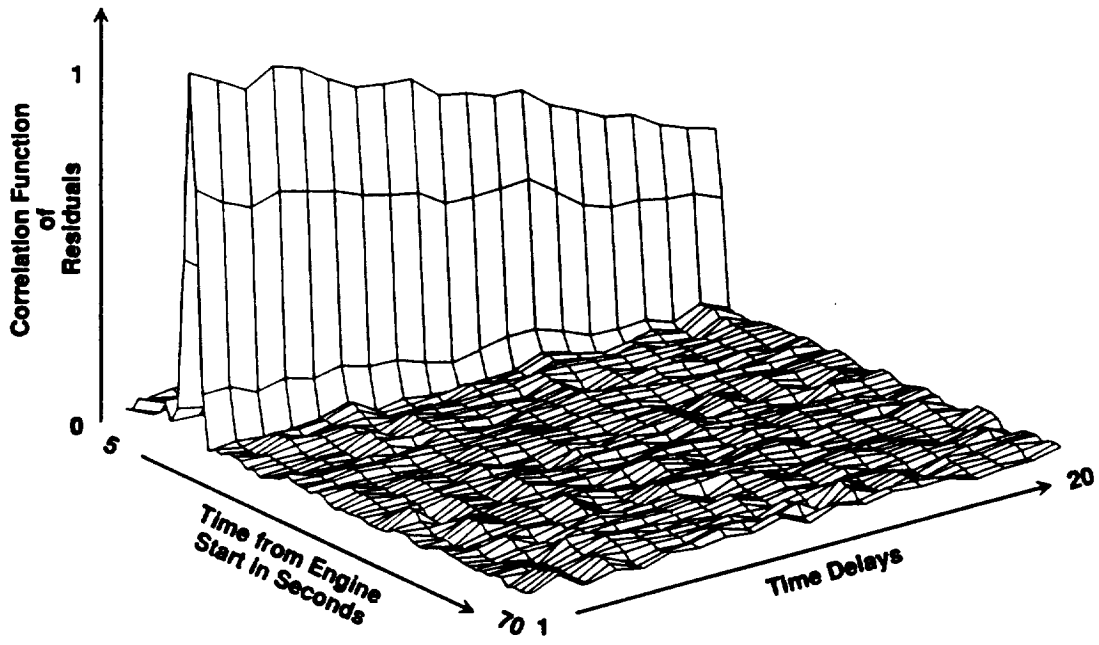

Fig. A-1.9 FAILURE DETECTION USING ARMA MODELS FOR PARAMETER LPFT DISCHARGE TEMPERATURE FOR TEST 901-110.

Time Series Analysis: During the mainstage operation at 75% RPL, abnormal behavior was detected around 16 seconds from the start for a number of parameters. Figures A-1.2 through A-1.9 show the data and corresponding ARMA error signal correlation function plots.

Cluster Analysis: The clustering algorithm was not run on this data because the PC command data was not included in the CADS data set. This CADS parameter is required for all sensor data normalization.

2. Test 901-436: HPFTP Coolant Liner Buckle

According to the Rocketdyne SAFD Phase II report, during stable operation at 109% of rated power level, the following series of events occurred within the HPFTP : (1) pieces from the interstage seal pass through the 2nd stage platform gap, decreasing the 2nd disc cavity pressure and increasing the seal stack leakage into the coolant liner at approximately t = 598.5 seconds from start; (2) an interstage seal piece lodges in the 2nd stage shank, increasing the 2nd platform seal gap and exciting 12 stiffener vanes per revolution at t = 607 seconds; (3) the coolant liner begins to buckle at t = 610.35 seconds, and, (4) the T/A (turn around) sheet metal begins movement, reducing the flow area at t = 610.44 seconds. At t = 611.06 seconds, the test was shutdown due to a High Pressure Fuel Turbine (HPFT) discharge temperature redline. (Test conducted on 14 February 1984, cutoff time: t = 611.06 seconds.)

CADS Data: A plot of the MCC_PC is shown in Figure A-2.1. During the mainstage operation, fuel venting and propellant transfer occurred at 10 seconds from the start. Figure A-2.2 shows the effect of fuel venting on the HPFP_IN_PR.

Time Series Analysis: For this test, the nominal ARMA models for parameters such as FPB_PC, HPFP_IN_PR, or MCC_CLNT_DS_PR over a 4 second window (100 data points) did not indicate any failures till the redline cutoff. However, nominal ARMA models over a longer time of 40 seconds (1000 data points) were effective in detecting deviations from the nominal, beginning around 30 seconds from the start, due to gradual drifting in parameter values. Because of the 1000 point window, failure detection was indicated at 70 seconds. Figures A-2.3 through A-2.7 show the data and corresponding ARMA error signal correlation function plots.

Cluster Algorithm: Input to the clustering algorithm consisted of the thirteen selected sensors (see Table 3.2a) minus those missing sensors listed in Table A-1. The event threshold was 0.89 and the fault detector was set for a five out of five event threshold.

The performance of the algorithm on the nominal data set 902-463 is shown in Figure A-2.8. Deviations from the correlation coefficient, R, value of 1 occur when the engine power drops to 65% RPL; when the engine is transitioning from 104% to 109% RPL; and when the engine is transitioning from 65% to 100% RPL prior to shutdown. All R values remain above .89, and thus no false alarms occur during the test.

The correlation values for 901-436 and the detection threshold are shown in Figure 2.9. At the start of mainstage operation, the R values are above the threshold. While maintaining a constant power of 109% RPL, the R values decrease until fault detection at 302.4 seconds.

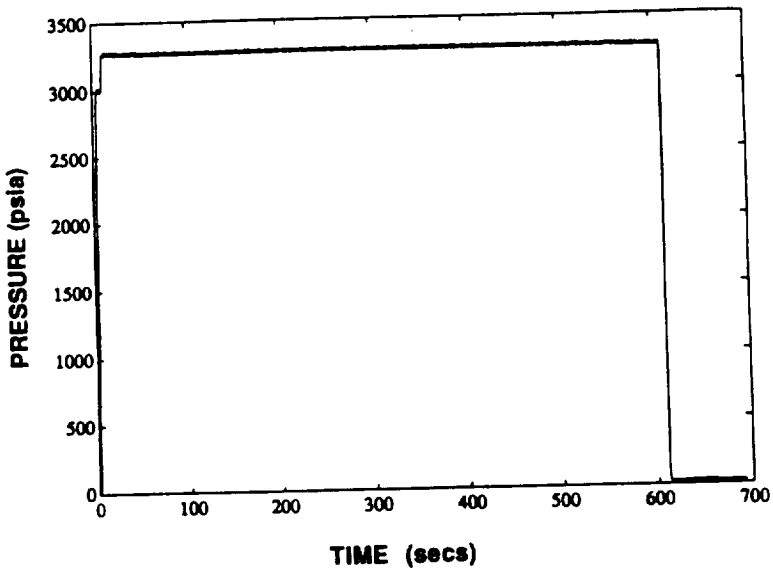

Fig. A-2.1 MCC PRESSURE (PID NO. 130) FOR TEST 901-436

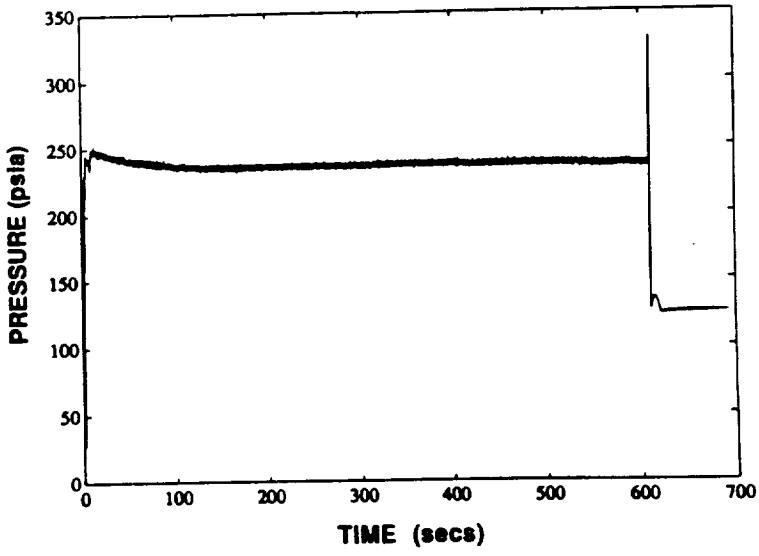

Fig. A-2.2 EFFECT OF VENTING ON HPFP INLET PRESSURE (PID NO. 86) AT 10 SECS FOR TEST 901-436

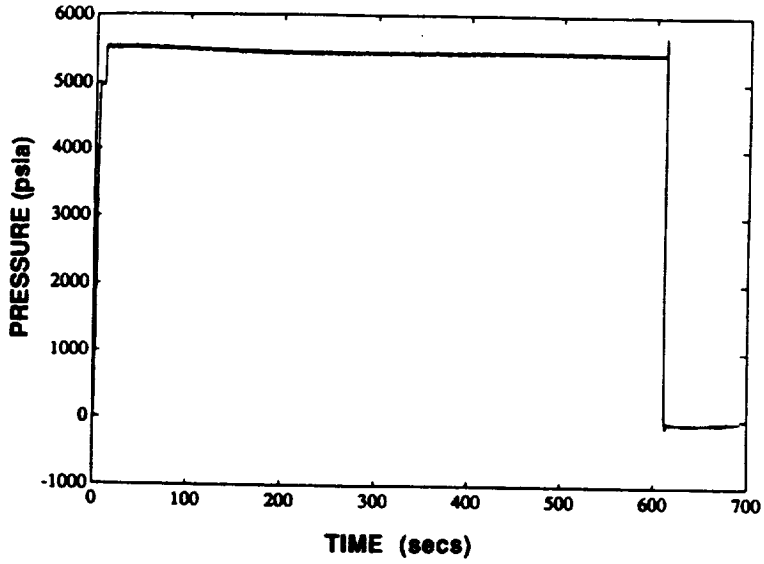

Fig. A-2.3 FPB CHAMBER PRESSURE (PID NO. 158) FOR TEST 901-436

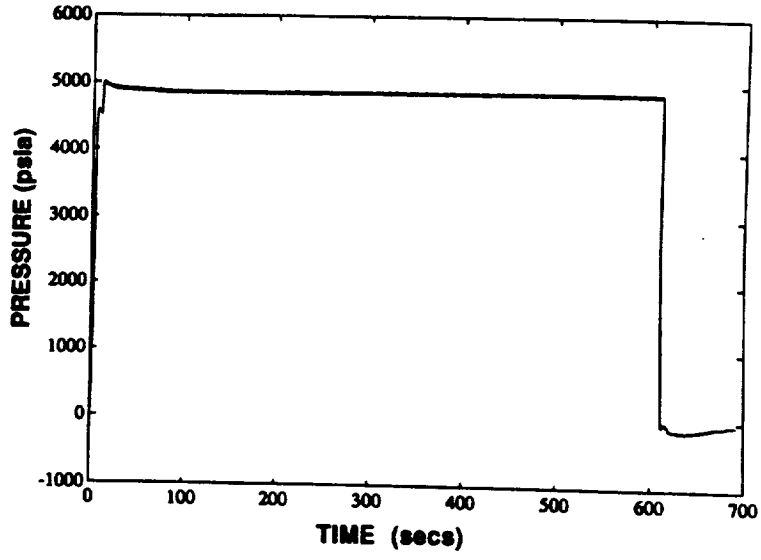

Fig. A-2.4 MCC COOLANT DISCHARGE PRESSURE (PID NO. 17) FOR TEST 901-436

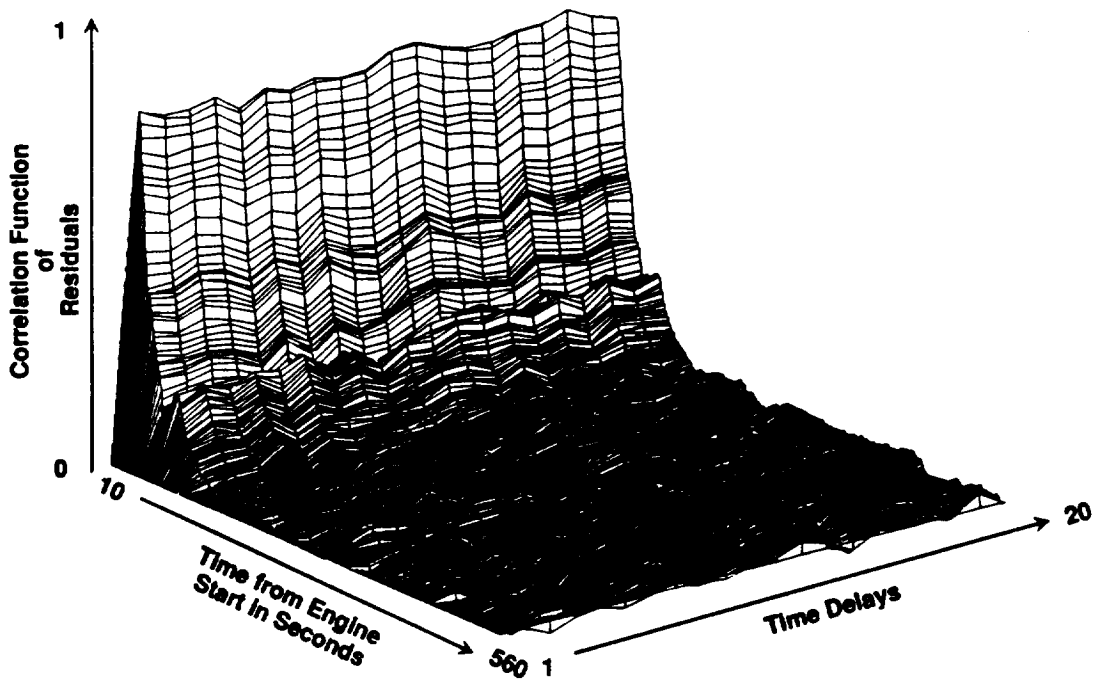

Fig. A-2.5 FAILURE DETECTION USING ARMA MODELS FOR PARAMETER HPFP INLET PRESSURE FOR TEST 901-436.

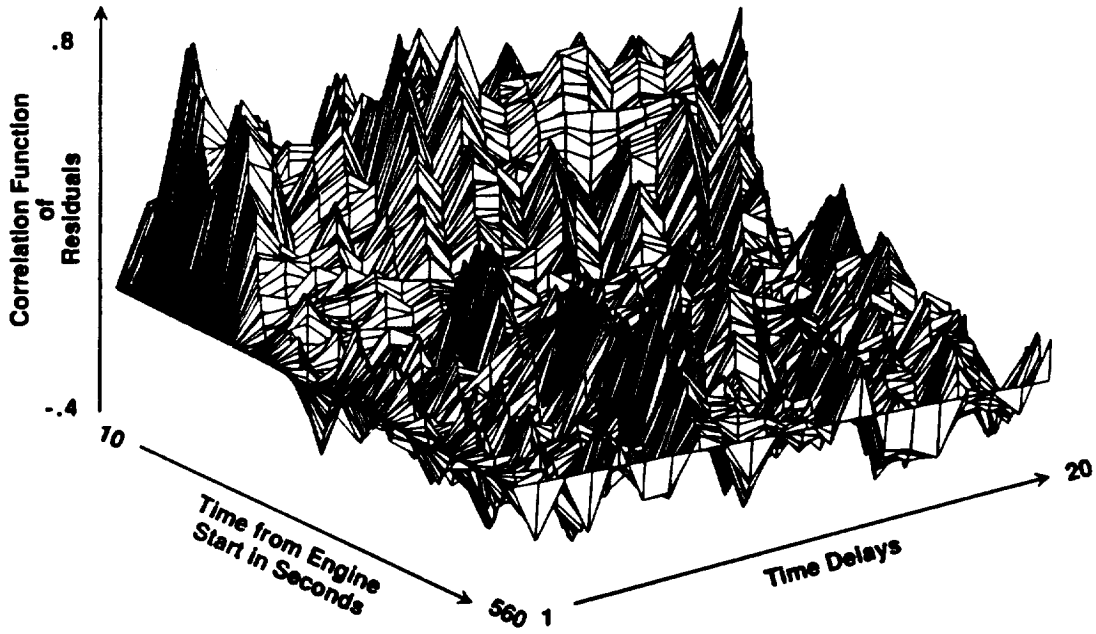

Fig. A-2.6 FAILURE DETECTION USING ARMA MODELS FOR PARAMETER FPB CHAMBER PRESSURE FOR TEST 901-436.

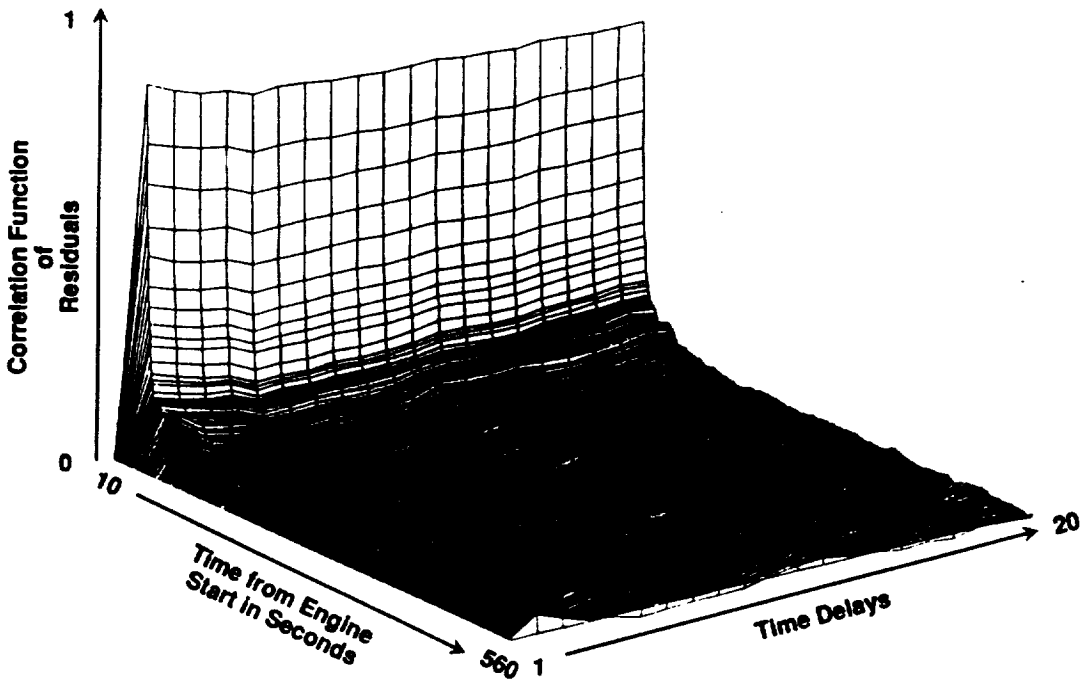

Fig. A-2.7 FAILURE DETECTION USING ARMA MODELS FOR PARAMETER MCC COOLANT DISCHARGE PRESSURE FOR TEST 901-436.

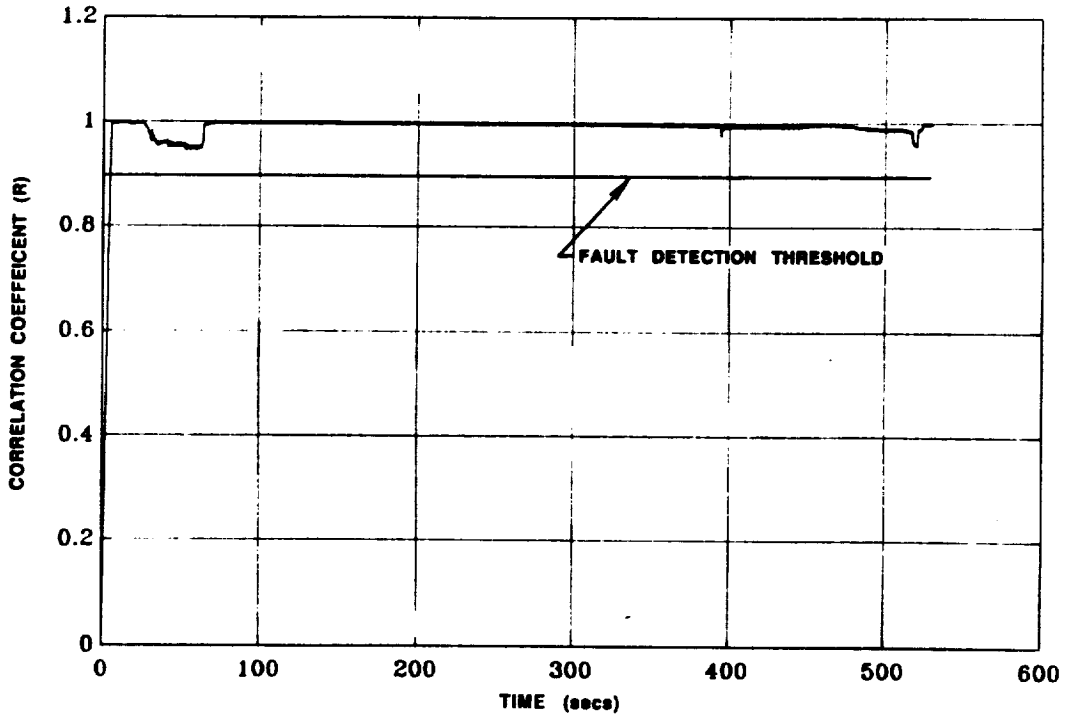

Fig. A-2.8 THE CLUSTERING ALGORITHM RESULTS SHOW NO FALSE ALARMS FOR THE 902-463 NOMINAL DATA USING THE 901-436 SENSOR SUBSET.

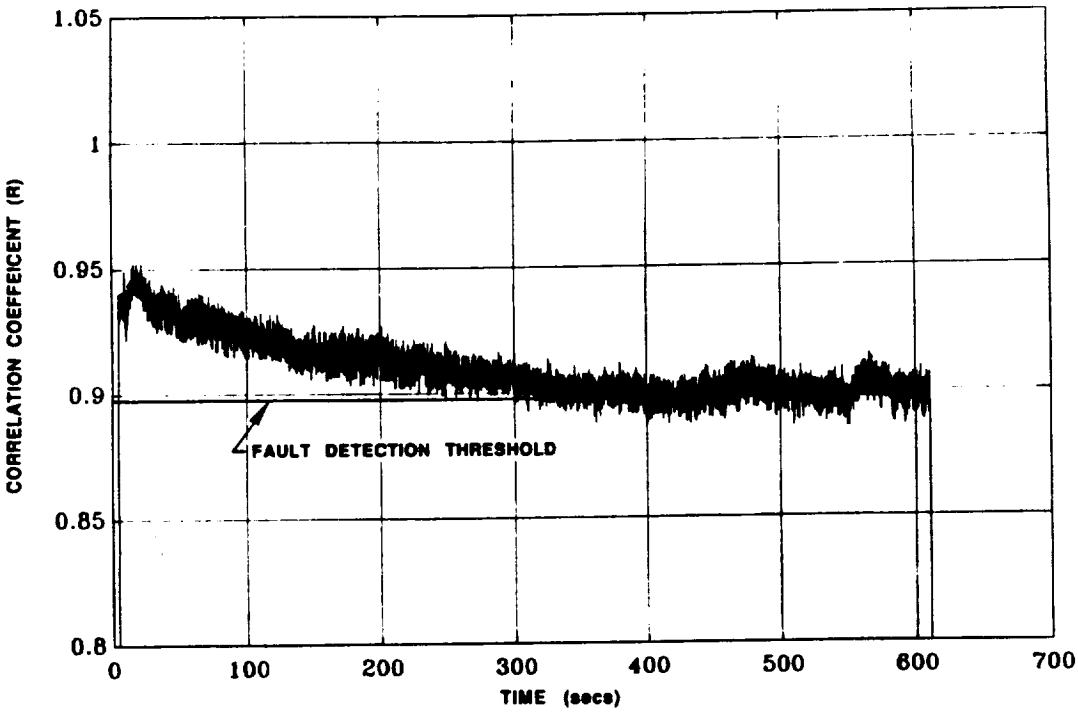

Fig. A-2.9 THE CLUSTERING ALGORITHM RESULTS FOR TEST 901-436. FAULT DETECTION OCCURED AT 302.4 SECONDS.

3. Test 901-364: HPFTP Kaiser Nut Failure

According to the Rocketdyne SAFD Phase II report, during stable operation at 109% of rated power level, the test shutdown prematurely due to a LOX preburner pump radial accelerometer redline. The probable cause of the failure was a new HPFTP thermal shield retainer nut assembly, used for the first time on this test. The geometry of the nut allowed a direct leak path through the heat shield for the high temperature ASI gas, producing two jets which impinged directly upon the turbine end cap (Kaiser helmet) and reduced material properties in the impingement zone. The sequence of failure follows: 1) A breach in the Kaiser helmet occurs from a combination of heat shield vibration-induced loads, pressure differential across the thickness of the Kaiser helmet, and material degradation and fatigue; 2) The hot gas interrupts coolant flow and heats the turbine and bearings; 3) Heating produces an increase in bearing stiffness, which causes increasing synchronous vibrations; and 4) Synchronous vibration continues to build up until bearing failure occurs, followed by large rotor displacement, severe blade rubbing, and eventual blade breakage, turbine seizing, fuel flow stoppage, rupture of the pump inlet volute, and finally a severe fire caused by the resulting LOX-rich shutdown. (Test conducted on 7 April 1982, cutoff time: t = 392.15 seconds.)

CADS Data: A plot of the MCC_PC is shown in Figure A-3.1. During the mainstage operation, fuel venting occurred at 100 seconds from the start, and LOX tank pressurization occurred at 200 seconds. Figure A-3.2 shows the effect of fuel venting on the HPFP_IN_PR.

Time Series Analysis: During the mainstage operation at 109% RPL, abnormal behavior is detected around 210 seconds from the start for a number of parameters. Figures A-3.3 through A-3.8 show the data and corresponding ARMA error signal correlation function plots.

Cluster Algorithm: Input to the clustering algorithm consisted of the thirteen selected sensors (see Table 3.2a) minus those missing sensors listed in Table A-1. The event threshold was 0.89 and the fault detector was set for a five out of five event threshold.

The algorithm performance for the nominal data set 902-463 is shown in Figure A-3.9. As shown in the plot, deviations in the correlation coefficient, R, values occur when the engine power drops to 65% RPL; when the engine is transitioning from 104% to 109% RPL; and when the engine is transitioning from 65% to 100% RPL prior to shutdown. No false alarms occurred for the given threshold.

The correlation values for 901-364 and the detection threshold are shown in Figure A-3.10. At the start of mainstage operation, the R values are above the threshold. When the engine transitions from 109% to 90% RPL, the R values descend below the detection threshold, causing a fault detection at 42.7 seconds. The R values increase again when the engine accelerated to 109 % RPL, but while at a steady power level, the R values decrease until the detection threshold is crossed again at 130 seconds.

4. Test 901-307: FPB LOX Post Fracture

According to the Rocketdyne SAFD Phase II report, this test was one of several designed to determine the minimum LOX level upstream of the LPOP (i.e., minimum NPSH) with which the pump could operate

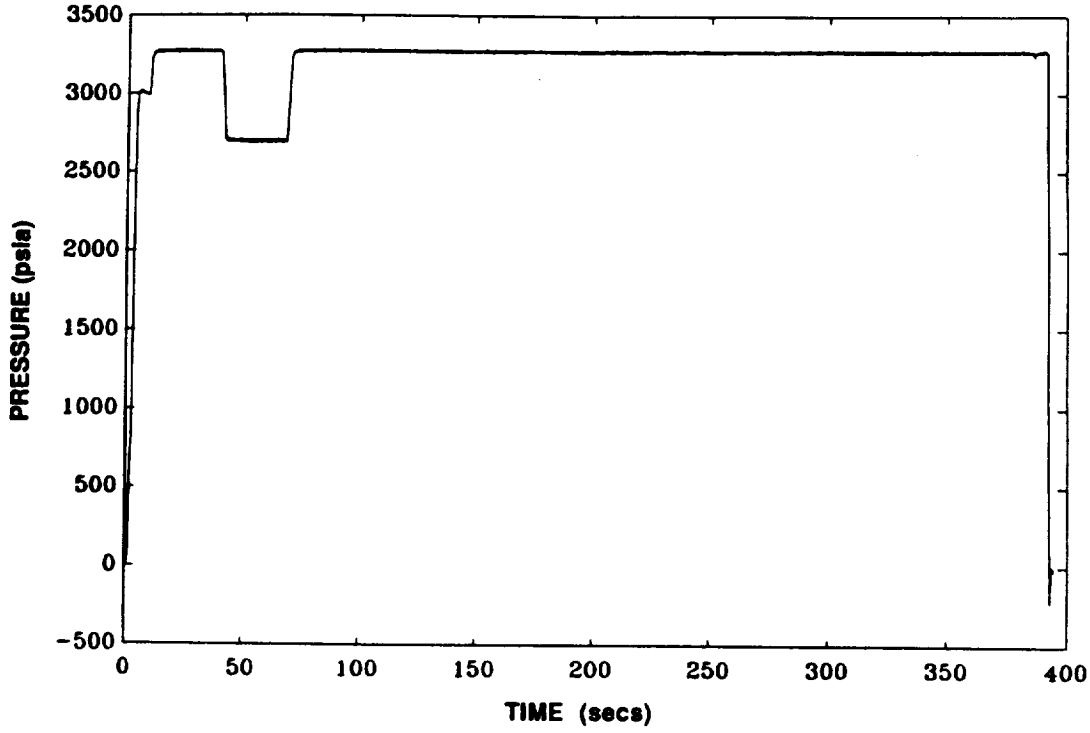

Fig. A-3.1 MCC PRESSURE (PID NO. 130) FOR TEST 901-364

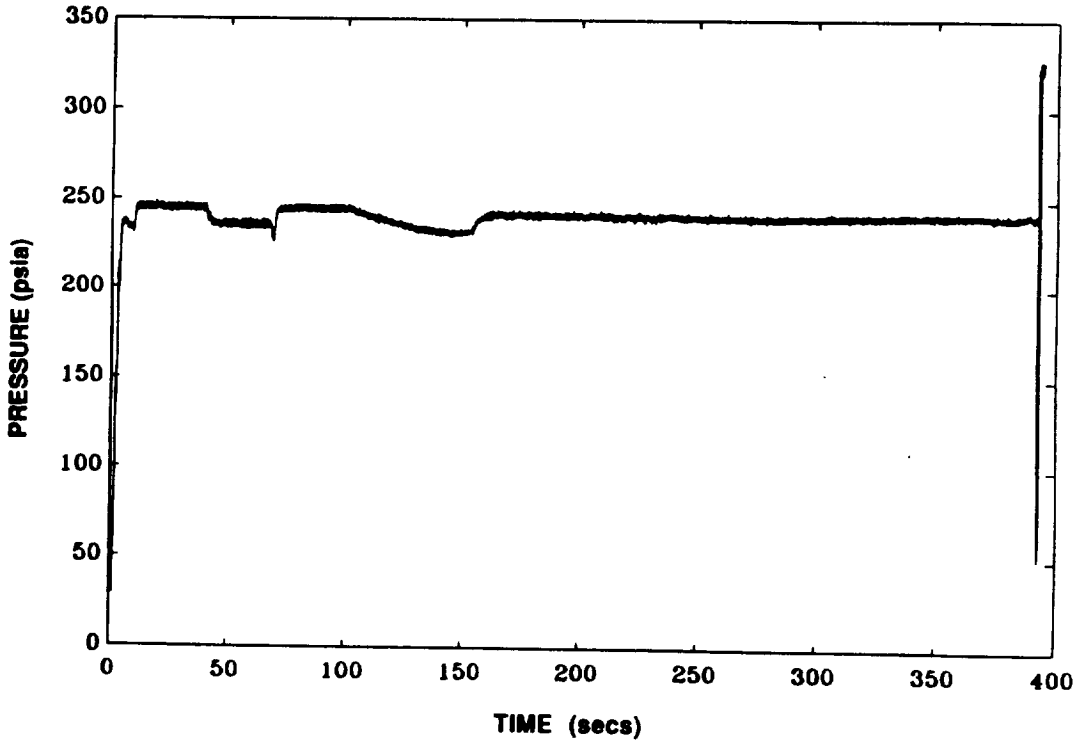

Fig. A-3.2 HPFP INLET PRESSURE (PID NO. 86) FOR TEST 901-364

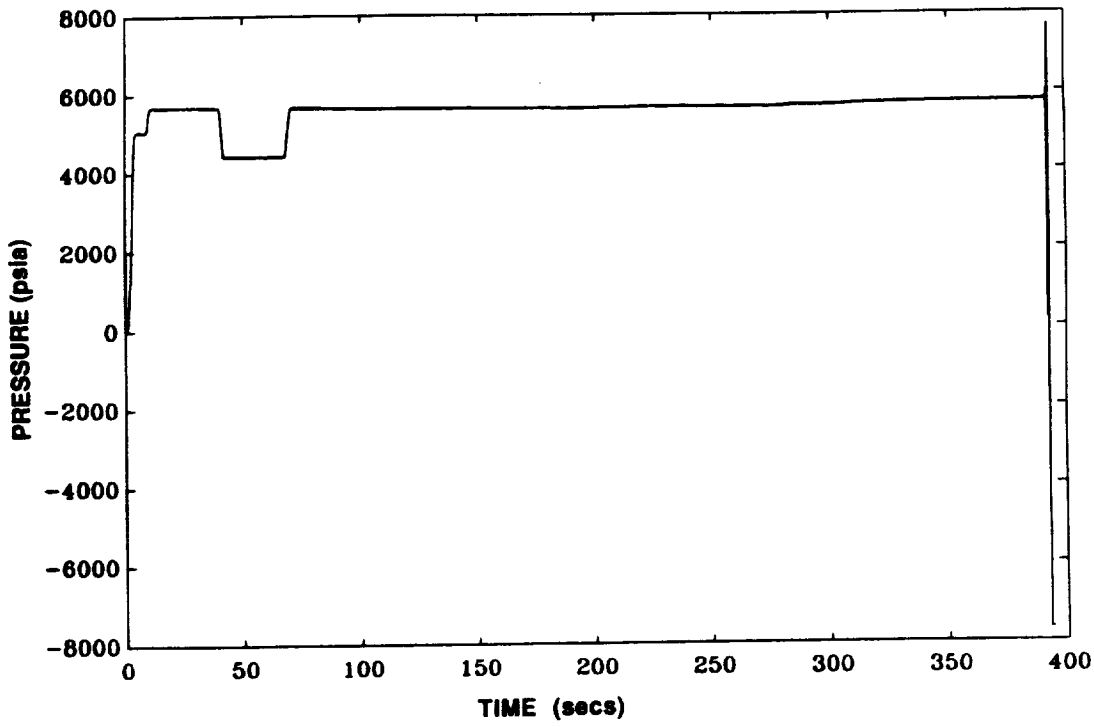

Fig. A-3.3 FPB CHAMBER PRESSURE (PID NO. 58) FOR TEST 901-364

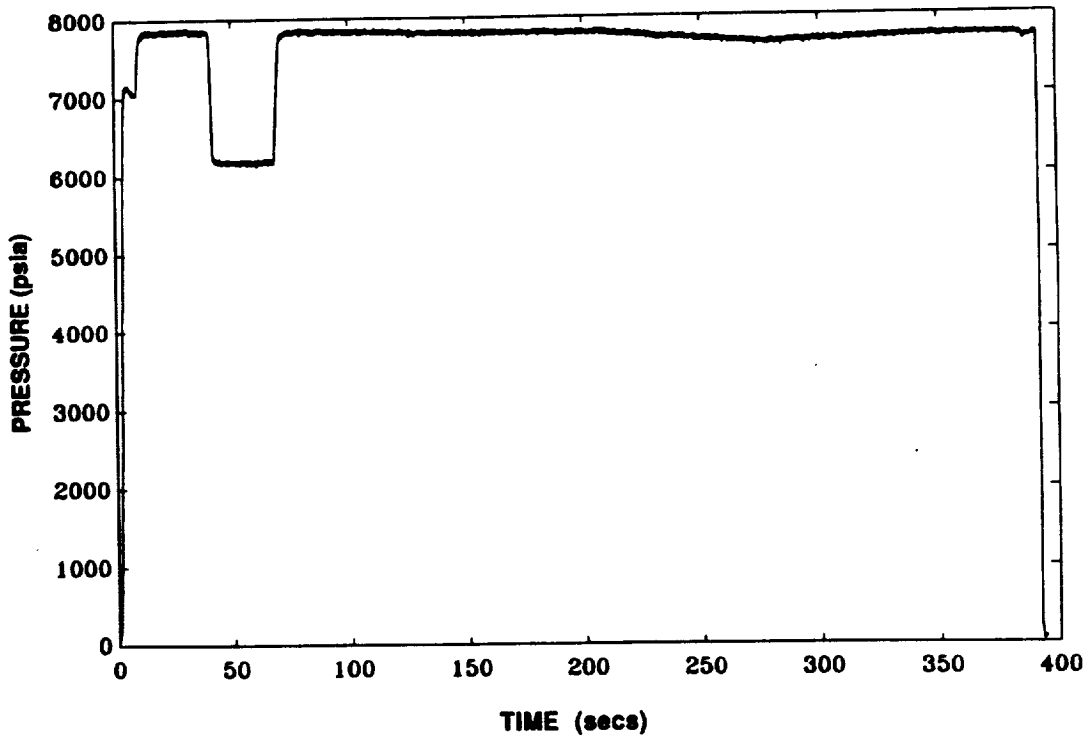

Fig. A-3.4 PBP DISCHARGE PRESSURE (PID NO. 59) FOR TEST 901-364

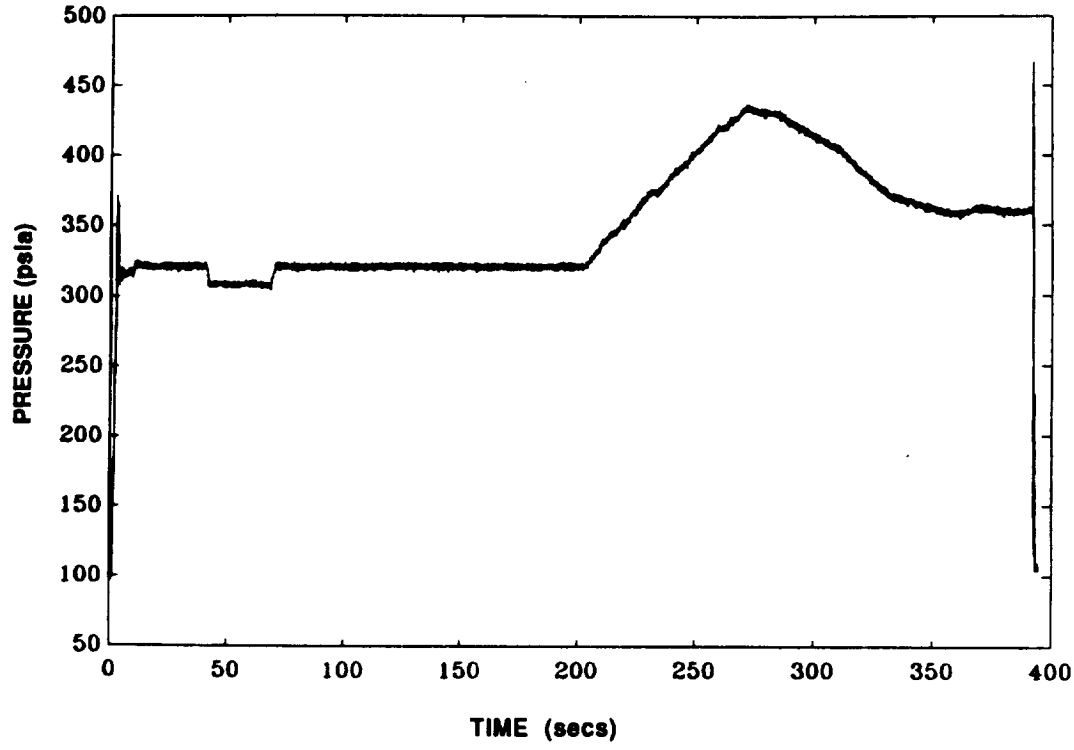

Fig. A-3.5 HPOP INLET PRESSURE (PID NO. 209) FOR TEST 901-364

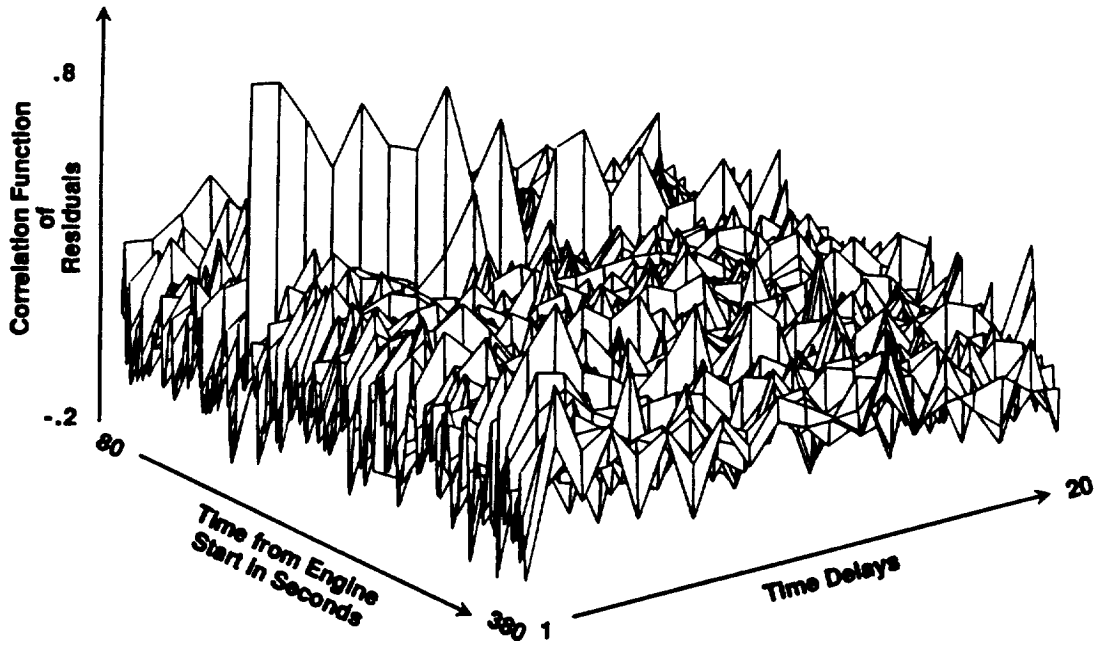

Fig. A-3.6 FAILURE DETECTION USING ARMA MODELS FOR PARAMETER FPB CHAMBER PRESSURE FOR TEST 901-364.

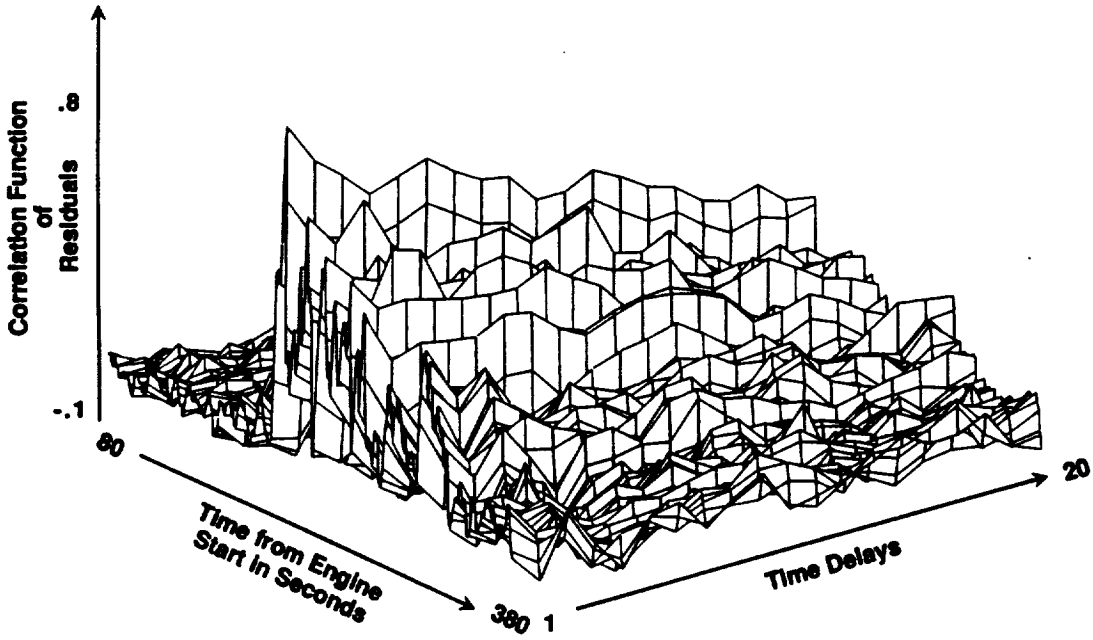

Fig. A-3.7 FAILURE DETECTION USING ARMA MODELS FOR PARAMETER HPOP INLET PRESSURE FOR TEST 901-364.

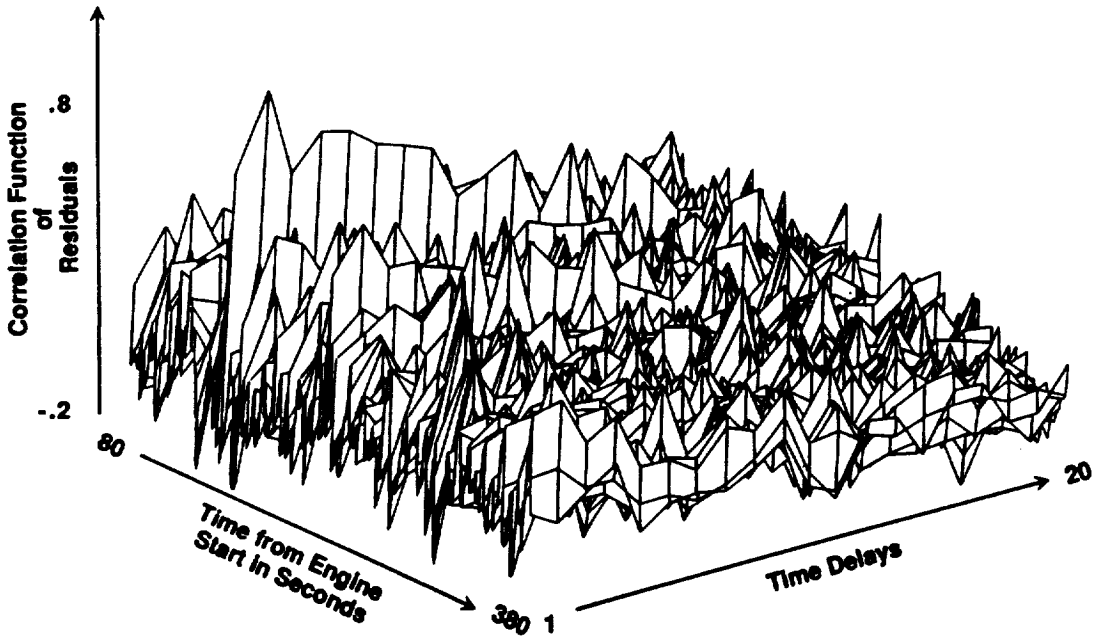

Fig. A-3.8 FAILURE DETECTION USING ARMA MODELS FOR PARAMETER PBP DICHARGE PRESSURE FOR TEST 901-364.

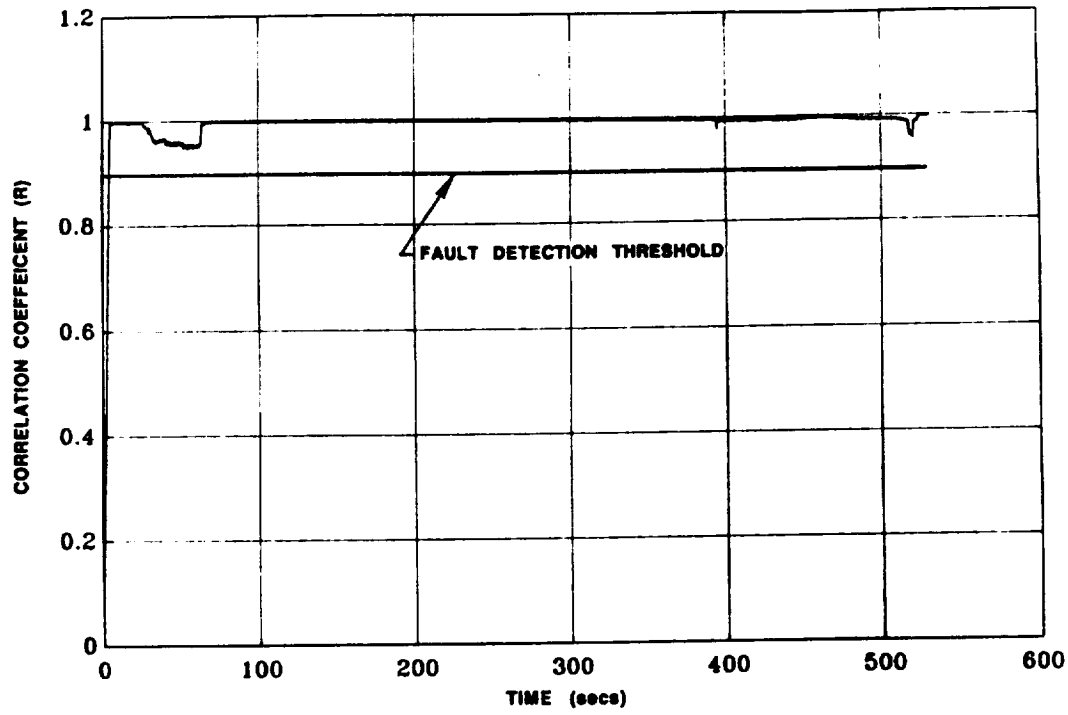

Fig. A-3.9 THE CLUSTERING ALGORITHM RESULTS SHOW NO FALSE ALARMS FOR THE 902-463 NOMINAL DATA USING THE 901-364 SENSOR SUBSET.

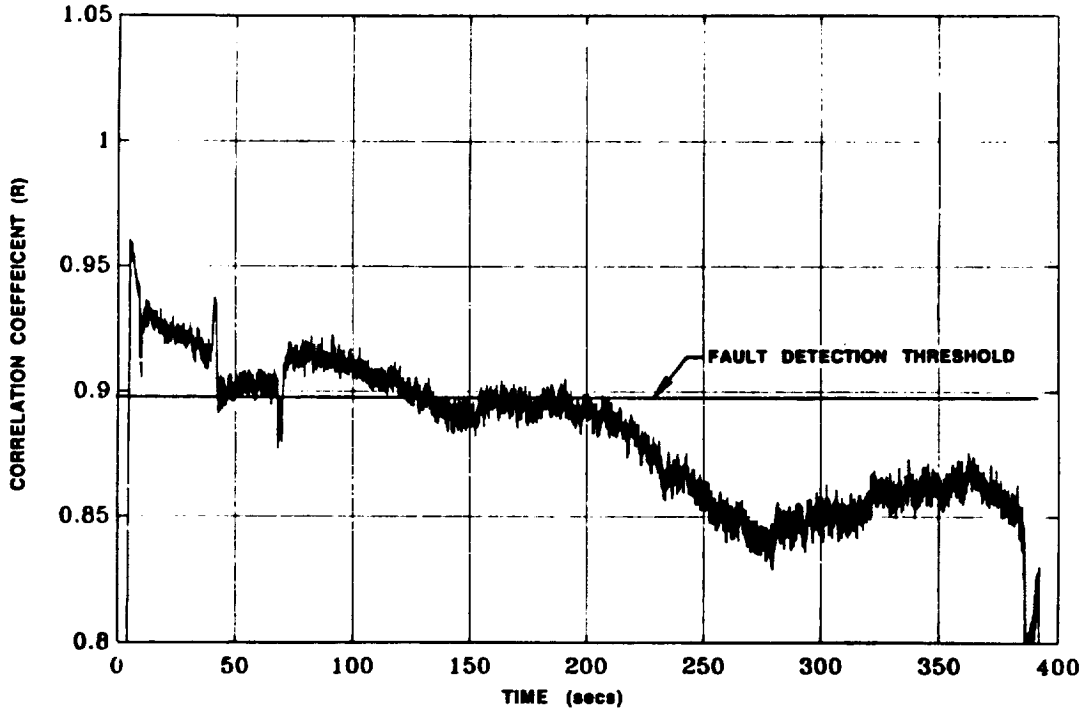

Fig. A-3.10 THE CLUSTERING ALGORITHM RESULTS FOR TEST 901-364. FAULT DETECTION OCCURED AT 42.7 SECONDS.

without overspeed. The test terminated as designed with a redline cutoff at the elevation-level of the LPOP inlet duct. During operation at 109% rated power level, a High Cycle Fatigue (HCF) through crack developed at the fuel preburner's injector LOX post/element A-8. The fuel mixed with the LOX through this crack, ignited, and burned the LOX post tip. Additional damage to the fuel sleeve and faceplate followed. After cutoff initiation, the GH2 backflowed and ignited the residual LOX within the dome, causing the remaining damage. (Test conducted on 28 January 1981, cutoff time: t = 75.0 seconds.)

CADS Data: A plot of the MCC_PC is shown in Figure A-4.1. The CADS data do not show operation at 109% power level as stated by the SAFD report. According to MCC_PC plot, the mainstage begins at 100% power level and then drops down to 65% power level until the redline cutoff around 75 seconds from the start.

Time Series Analysis: During the mainstage operation at 100% RPL, abnormal behavior is detected around 7.5 seconds from the start for a number of parameters. Figures A-4.2 and A-4.3 show the data and corresponding ARMA error signal correlation function plots.

Cluster Algorithm: Input to the clustering algorithm consisted of the sensors (see Table 3.2a) minus those missing sensors listed in Table A-1. The event threshold was 0.89 and the fault detector was set for a five out of five event threshold.

The performance of the algorithm on the nominal data set 902-463 is shown in Figure A-4.4. As shown in the plot the significant deviations in the correlation coefficient, R, values occur when the engine power drops to 65% RPL; when the engine is transitioning from 104% to 109% RPL; when the engine is transitioning from 65% to 100% RPL, prior to shutdown. No false alarms occurred for the given threshold.

The correlation values for 901-307 and the detection threshold are shown in Figure A-4.5. The engine is initially at 100% RPL, and transitions to 65% RPL ten seconds from start. The R values are initially well above the detection threshold, but rapidly begin to decrease. At 8.6 seconds, the R values have crossed the threshold, 1.4 seconds before the power transition starts, causing a fault detection to be declared. Following the power transition to 65% RPL, the R values continue to gradually decrease until engine shutdown.

5. Test SF10-01: FPB Injector Erosion

According to the Rocketdyne SAFD Phase II report, during 102% of rated power level operation, this test was terminated when fire detectors and hazardous gas detectors triggered in the aft fuselage. Based on a review of the movie films, the digital data, pre-test and post-test hardware inspections, and on previous experience, the most probable cause of the failure was an erosion of the fuel preburner injector element H-13 during the start transient followed by slag deposits in the fuel annulus in the sector adjacent to the liner wall. The resultant higher mixture ratio in the outer zone in combination with the large (.042 to .045 inches) liner end cap gap for this preburner (allowing hot combustion gas to flow behind the liner, diluting the coolant gas), then caused the burnthrough of the liner and, subsequently, the preburner body. Whether or not contamination played a role in the initiation of the erosion is conjecture. However, the deflection of the faceplate created a fuel annulus gap which was smaller than the fuel element orifices (.018 in.) designed to protect the annulus from contamination. (Test conducted on 12 July 1980, cutoff time: t = 104.8 seconds.)

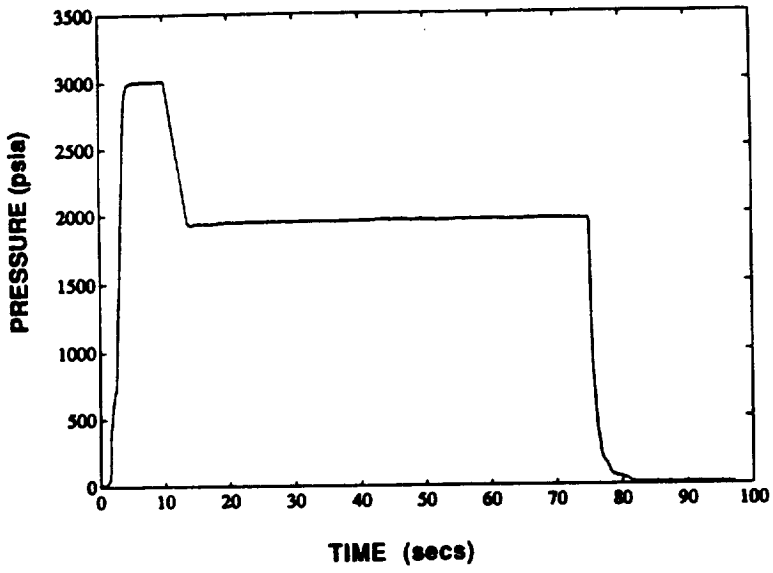

Fig. A-4.1 MCC PRESSURE (PID NO. 130) FOR TEST 901-307

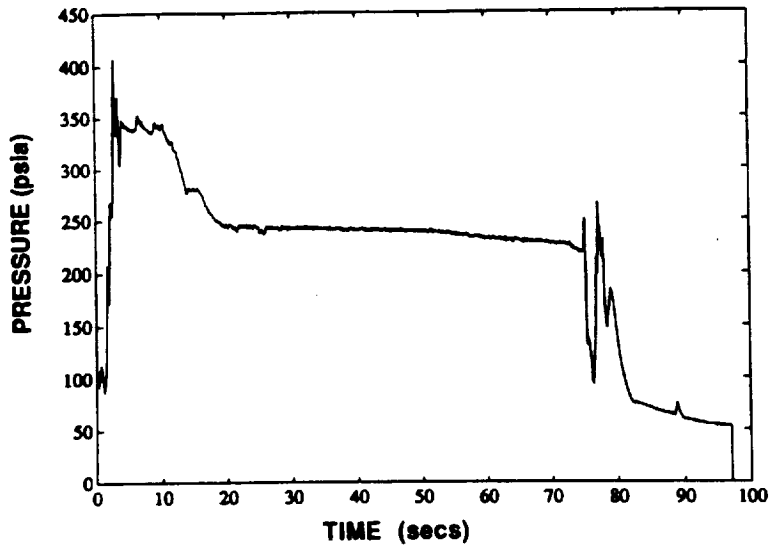

Fig. A-4.2 LPOP DISCHARGE PRESSURE (PID NO. 209) FOR TEST 901-307

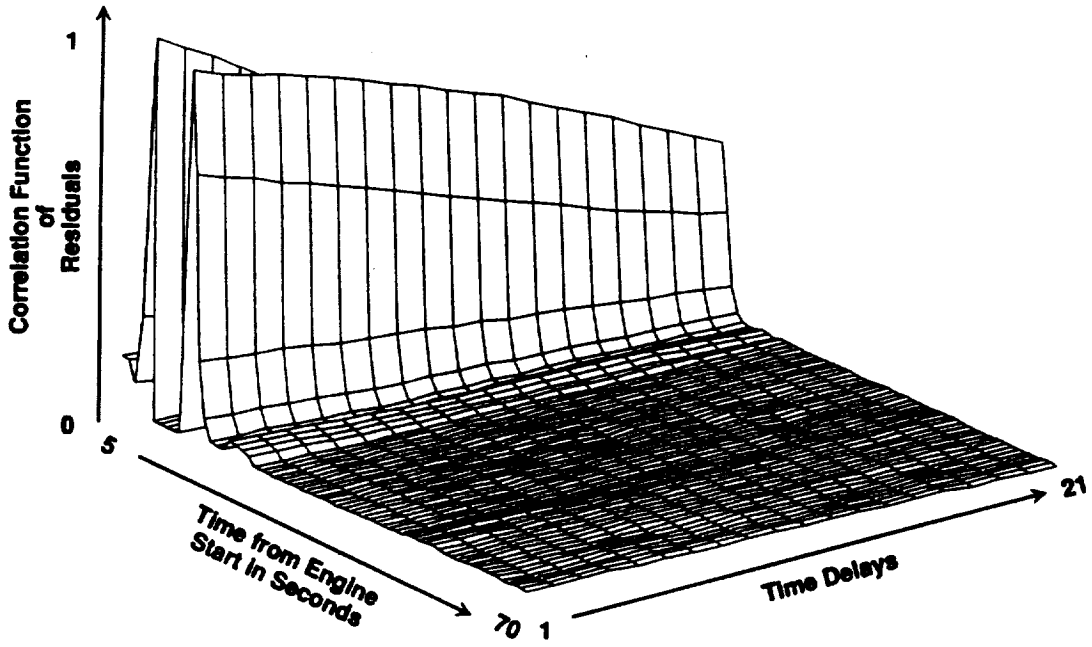

Fig. A-4.3 FAILURE DETECTION USING ARMA MODELS FOR PARAMETER LPOP DISCHARGE PRESSURE FOR TEST 901-307.

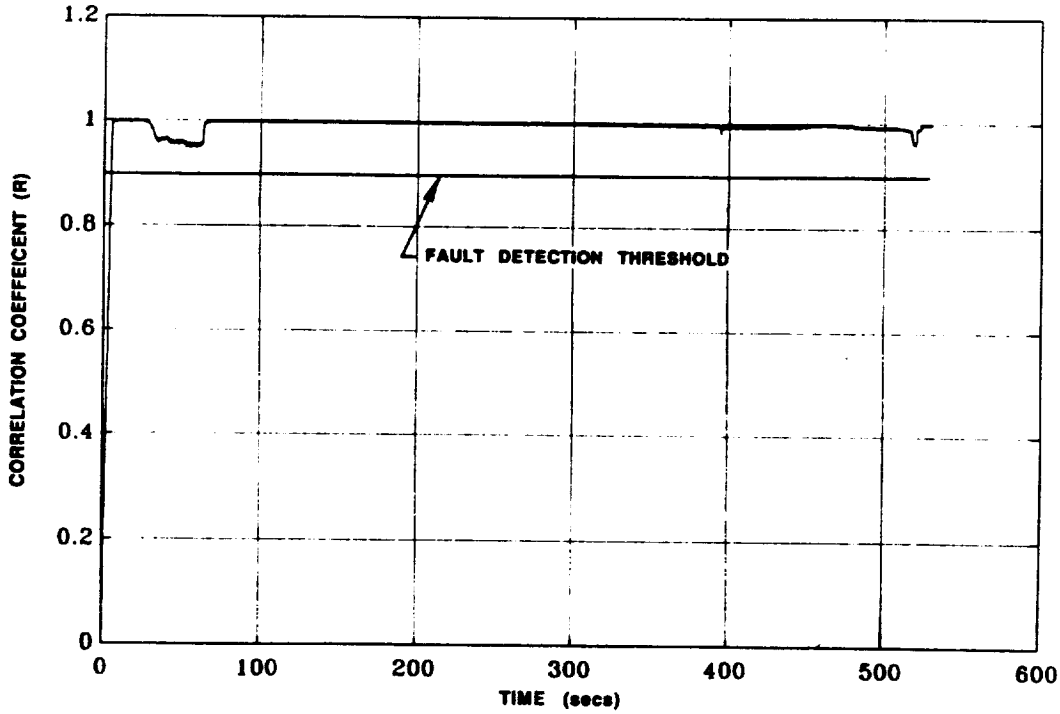

Fig. A-4.4 THE CLUSTERING ALGORITHM RESULTS SHOW NO FALSE ALARMS FOR THE 902-463 NOMINAL DATA USING THE 901-307 SENSOR SUBSET.

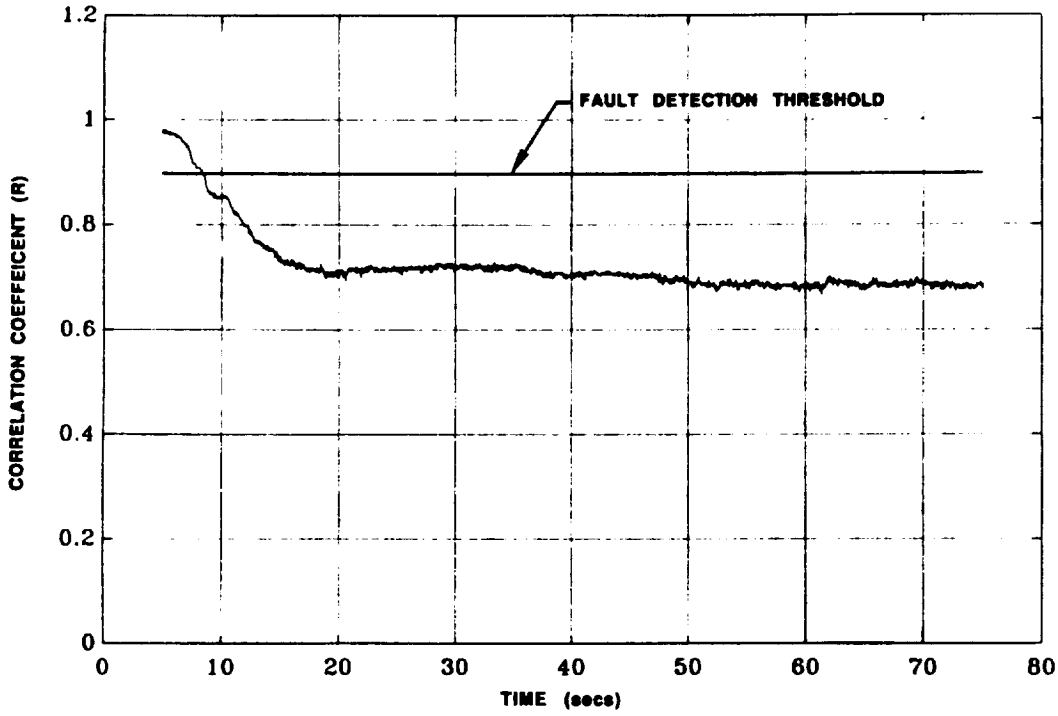

Fig. A-4.5 THE CLUSTERING ALGORITHM RESULTS FOR TEST 901-307. FAULT DETECTION OCCURED AT 8.6 SECONDS.

CADS Data: A plot of the MCC_PC, shown in Figure A-5.1, shows the engine power profile for this test. Several CADS sensors for this data set were bad or missing.

Time Series Analysis: The CADS Data do not have sensor measurements during the redline cutoff time period. The ARMA models did not indicate failure during the mainstage operation, nor could they detect the failure at redline cutoff because of lack of data.

Cluster Algorithm: Input to the clustering algorithm consisted of the thirteen selected sensors (see Table 3.2a) minus those missing sensors listed in Table A-1. The event threshold was 0.68 and the fault detector was set for a five out of five event threshold.

The performance of the algorithm on the nominal data set 902-463 is shown in Figure A-5.2. Unlike the previous tests, SF10-1 had only four sensors available for input. The other sensors were either not in the data set, corrupted or removed due to venting effects. The results of using a small input set is apparent in the plot of the correlation coefficient, R, values. Transitions in power now cause significant deviations in the R values, leading to false alarms at 28 seconds, 52 seconds, and 517 seconds.

The correlation values for SF10-1 and the detection threshold 0.68 are shown in Figure A-5.3. The engine performs several power transitions, and the R values are below the threshold at 5.1 seconds, 20 seconds, 41 seconds, and 48 seconds. Detections were declared for each these crossings. Because the reduced sensor set grossly affected the performance of the algorithm during power transitions, the detections resulting from transitions were removed as possible detections times and the detection at 48 seconds was listed as the detection time.

6. Test 902-198: Main Injector LOX Post Fracture

According to the Rocketdyne SAFD Phase II report, during stable operation at 102% of rated power level, LOX post 61, row 12 cracked through between the primary and secondary faceplate. Test data analysis revealed that the LOX post failure occurred first, and subsequently did major damage to the injector. The loss of fuel through the primary faceplate and from the ruptured nozzle tubes resulted in a oxidizer rich condition in the oxidizer preburner, and led to a HPOT discharge temperature redline cutoff at t = 8.5 seconds. (Test conducted on 23 July 1980, cutoff time: t = 8.5 seconds.)

CADS Data: A plot of the MCC_PC, shown in Figure A-6.1, displays the engine power profile for the test.

Time Series Analysis: During this test, the mainstage phase lasted for less than 4 seconds before the redline cutoff was initiated. Since the ARMA models require a window of 4 seconds, the redline cutoff coincided with the ARMA model failure indications.

Cluster Algorithm: Input to the clustering algorithm consisted of the thirteen selected sensors (see Table 3.2a) minus those missing sensors listed in Table A-1. The event threshold was 0.89 and the fault detector was set for a five out of five event threshold.

The performance of the algorithm on the nominal data set 902-463 is shown in Figure A-6.2 As shown in the plot, deviations in the correlation coefficient, R, value occur when the engine

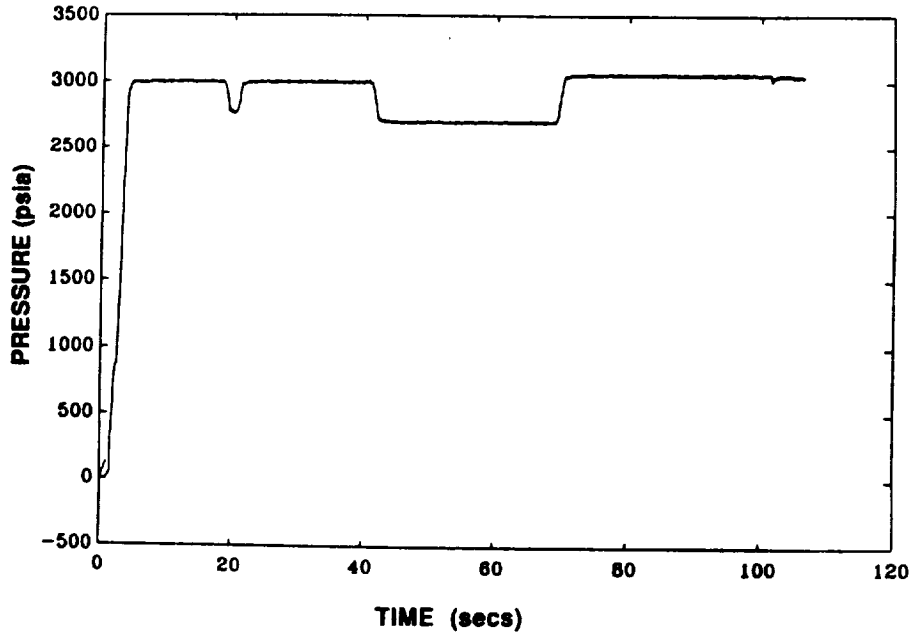

Fig. A-5.1 MCC PRESSURE (PID NO. 130) FOR TEST SF10-01

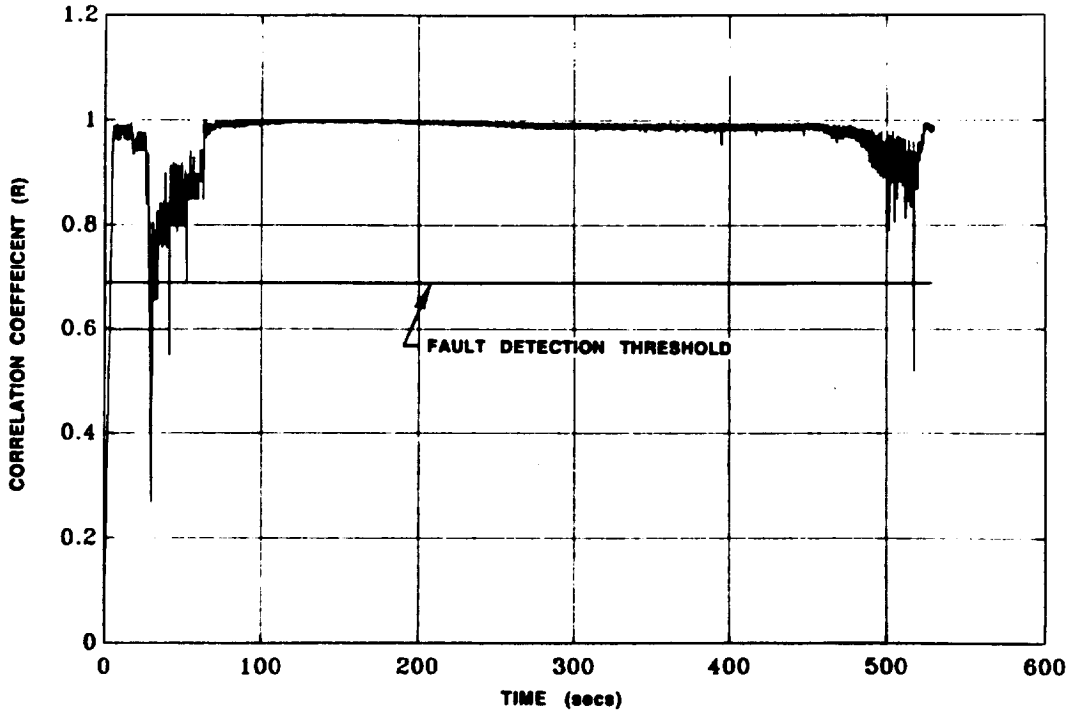

Fig. A-5.2 THE CLUSTERING ALGORITHM RESULTS SHOW FALSE ALARMS OCCURING AT 28, 52 AND 517 SECONDS FOR THE 902-463 NOMINAL DATA USING THE SF10-01 SENSOR SUBSET.

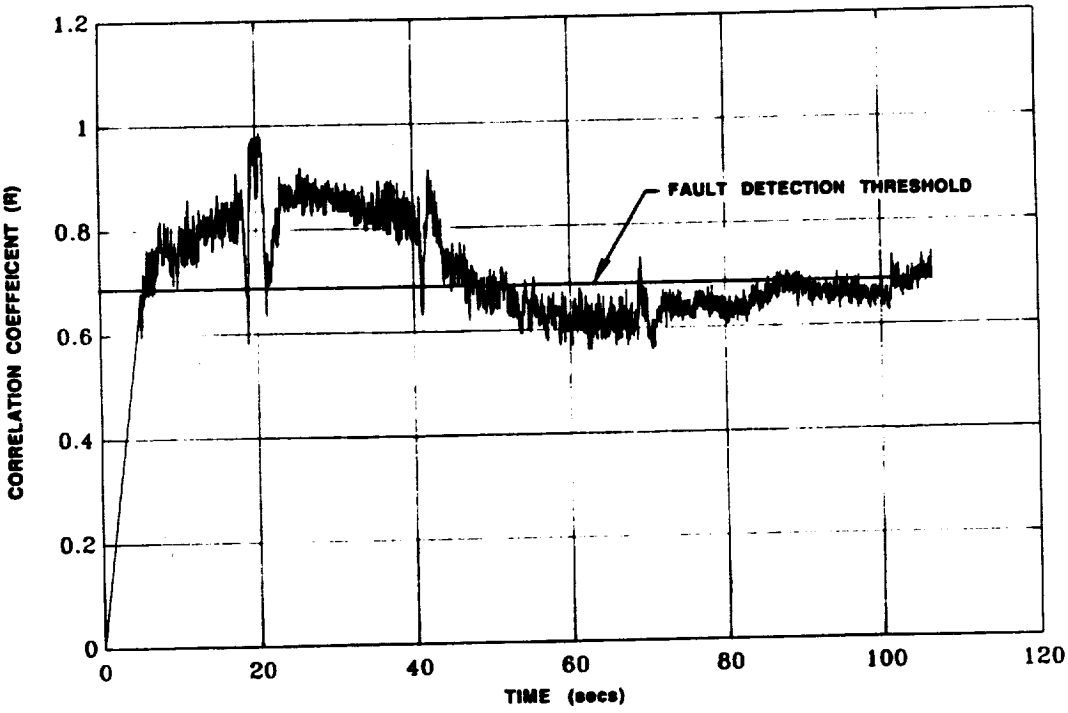

Fig. A-5.3 THE CLUSTERING ALGORITHM RESULTS FOR TEST SF10-01. FAULT DETECTION OCCURED AT 48 SECONDS.

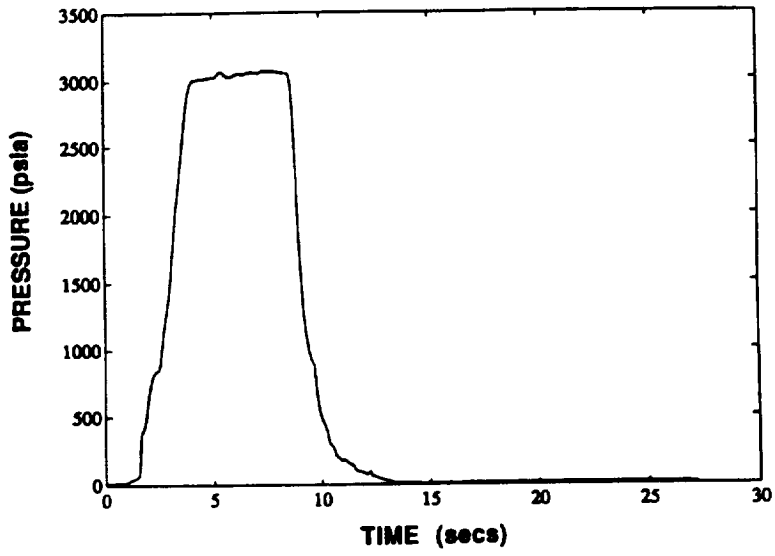

Fig. A-6.1 MCC PRESSURE (PID NO. 130) FOR TEST 902-198

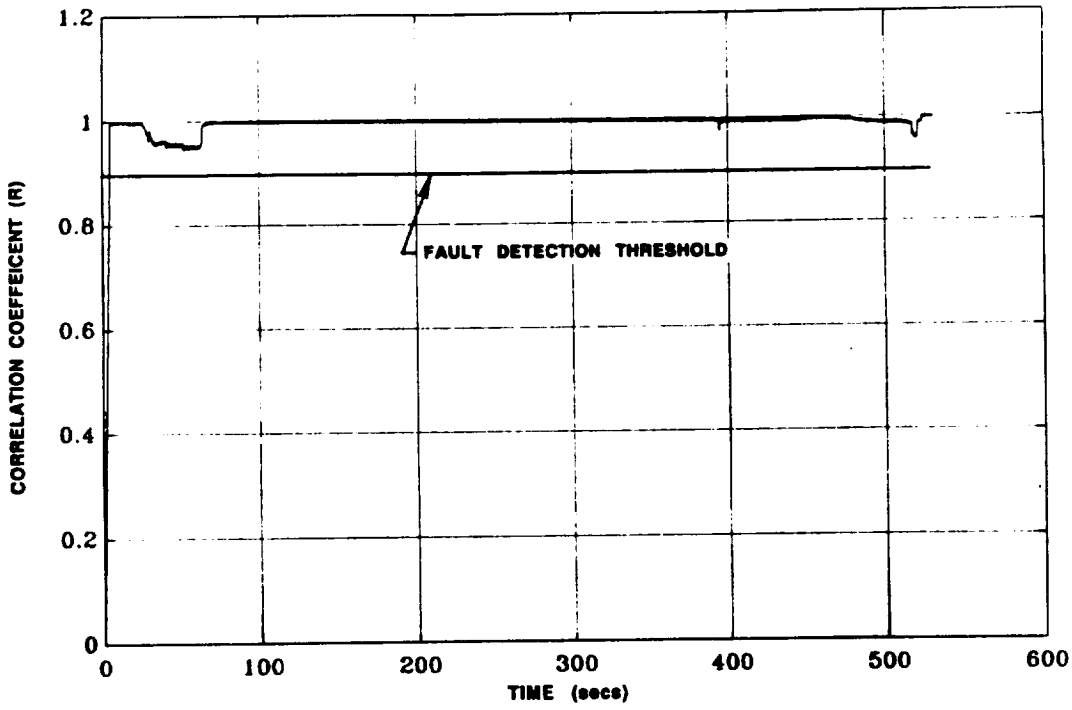

Fig. A-6.2 THE CLUSTERING ALGORITHM RESULTS SHOW NO FALSE ALARMS FOR THE 902-463 NOMINAL DATA USING THE 902-198 SENSOR SUBSET.

power drops to 65% RPL; when the engine is transitioning from 104% to 109% RPL; and when the engine is transitioning from 65% to 100% RPL prior to shutdown. No false alarms occurred for the given thresholds.

The correlation values, R, for 902-198 and the detection threshold are shown in Figure A-6.3. Initially the R values are above the detection threshold but rapidly begin to decrease and cross the threshold at 5.6 seconds causing a fault detection. The R values remain below the threshold until 6.2 seconds, and return to their previous levels. Unlike the previous failures, the detection for this test results from a transient event in the system.

7. Test 902-249: HPFTP Turbine Blade Failure

According to the Rocketdyne SAFD Phase II report, during stable operation at 109% of rated power level, the test shutdown prematurely due to a HPFTP accelerometer redline, and the associated massive failure of the HPFT first stage turbine blade. The sequence of events leading to the blade failure follows:

1. Initial turbine damage at t = 3.0 seconds. The FPB injector nonuniform flow condition experienced in at least two previous test may have persisted (despite rework) and worsened.

2. Engine fuel inlet temperature increases and the high pressure fuel pump begins to cavitate at t = 108.0 seconds. The temperature increase was brought about by propellant transfer. The increase lowers the fuel density causing an increase in HPFP volumetric flowrate, speed, and power necessary to hold thrust constant. As the flow and speed increase, the HPFP approaches the conditions at which the suction capability of the hardware is exceeded, and cavitation starts. Once cavitation is initiated the efficiency of the pump degrades, causing an increase in the pump speed required to maintain pump output and hold thrust constant, causing worsening cavitation conditions and an increase in HPFT inlet temperature.

3. Kel-F rub ring flexes and melts at t = 374 seconds. The released Kel-F particles plug nozzle tubes causing them to rupture, contributing to the HPFT inlet temperature increase.

4. The first stage turbine blade failures at t = 450.52 seconds. (Test conducted on 21 September 1981, cutoff time: t = 450.58 seconds.)

CADS Data: A plot of the MCC_PC is shown in Figure A-7.1. During this test, LOX side venting occurred at 20 seconds from the start, and propellant transfer occurred at 100 seconds from the start. Figure A-7.2 shows the LPOP_DS_PR with possible effects due to LOX venting. Figures A-7.3 and A-7.4 show the HPFP speed and the HPFP inlet temperature respectively.

Time Series Analysis: During the mainstage operation at 109% RPL, abnormal behavior was detected at approximately 160 seconds from the start for some parameters. Figures A-7.5 through A-7.7 show the ARMA error signal correlation function plots.

Cluster Algorithm: Input to the clustering algorithm consisted of the thirteen selected sensors (see Table 3.2a) minus those missing sensors listed in Table A-1. The event threshold was 0.89 and the fault detector was set for a five out of five event threshold.

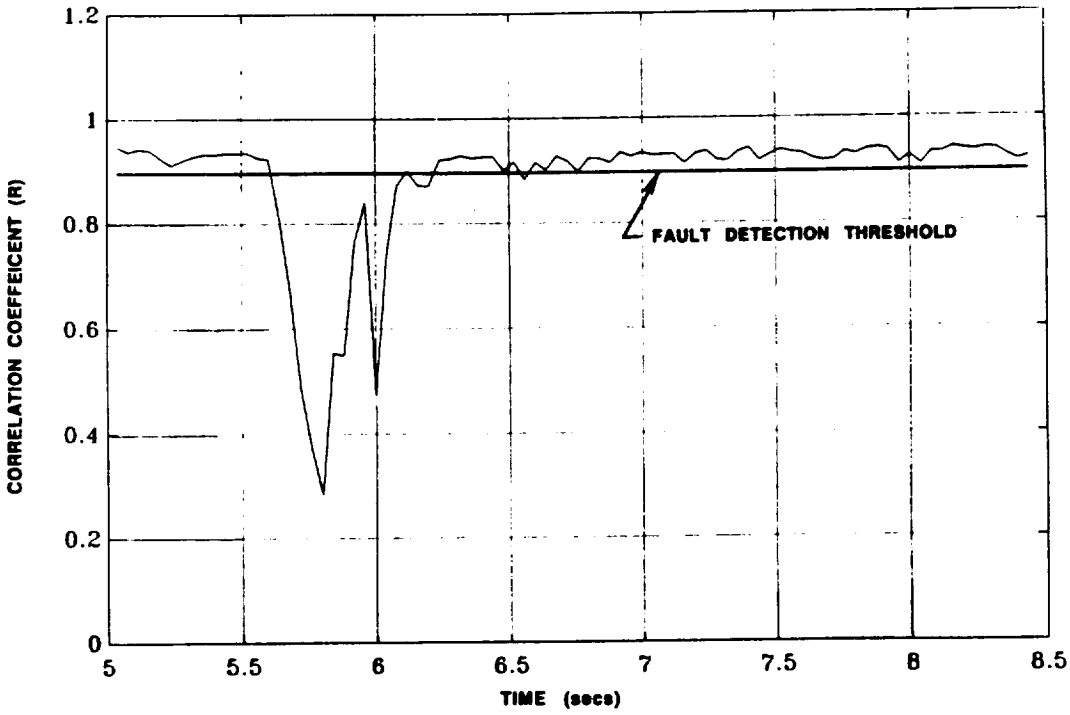

Fig. A-6.3 THE CLUSTERING ALGORITHM RESULTS FOR TEST 902-198. FAULT DETECTION OCCURED AT 5.8 SECONDS.

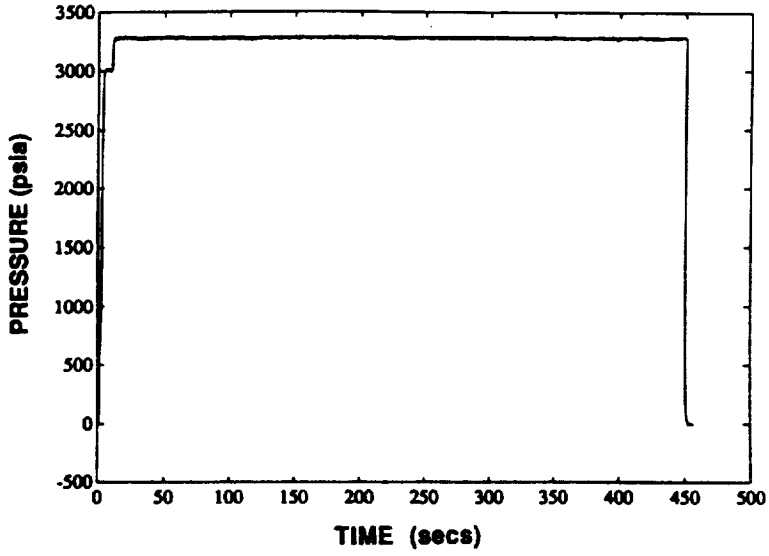

Fig. A-7.1 MCC PRESSURE (PID NO. 130) FOR TEST 902-249

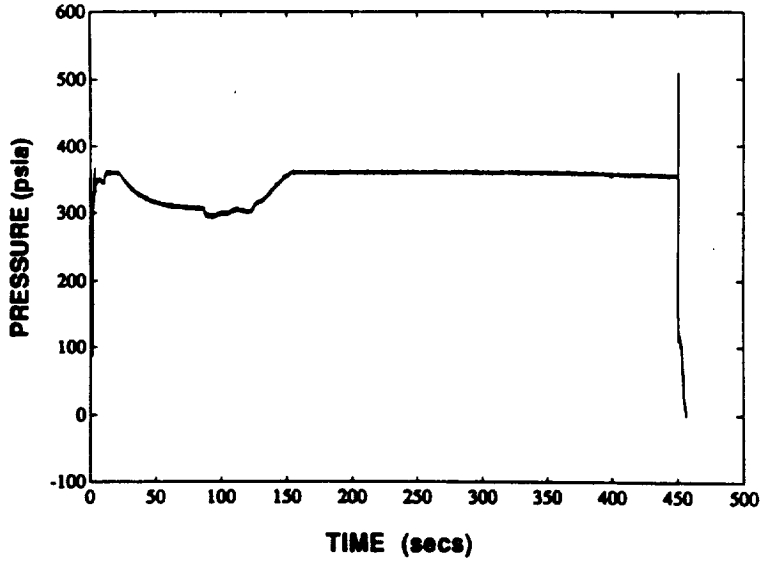

Fig. A-7.2 LPOP DISCHARGE PRESSURE (PID NO. 209) FOR TEST 902-249

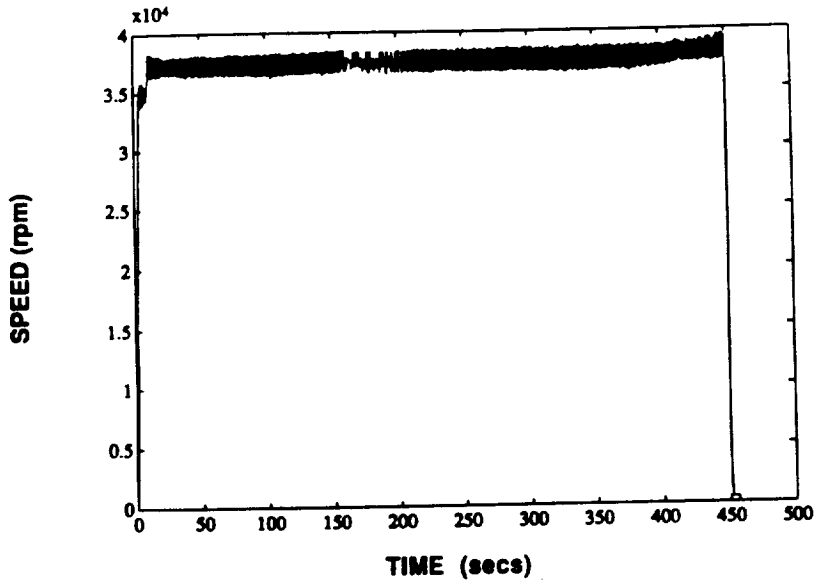

Fig. A-7.3 HPFP SPEED (PID NO. 260) FOR TEST 902-249

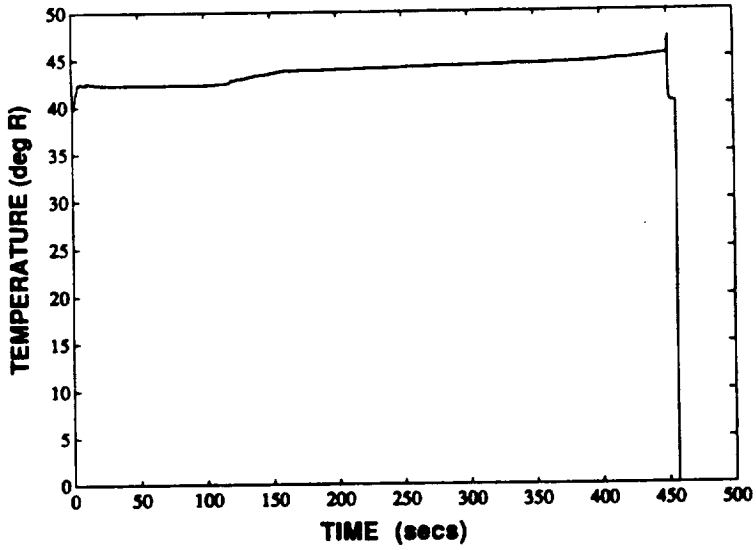

Fig. A-7.4 HPFP INLET TEMPERATURE (PID NO. 226) FOR TEST 902-249

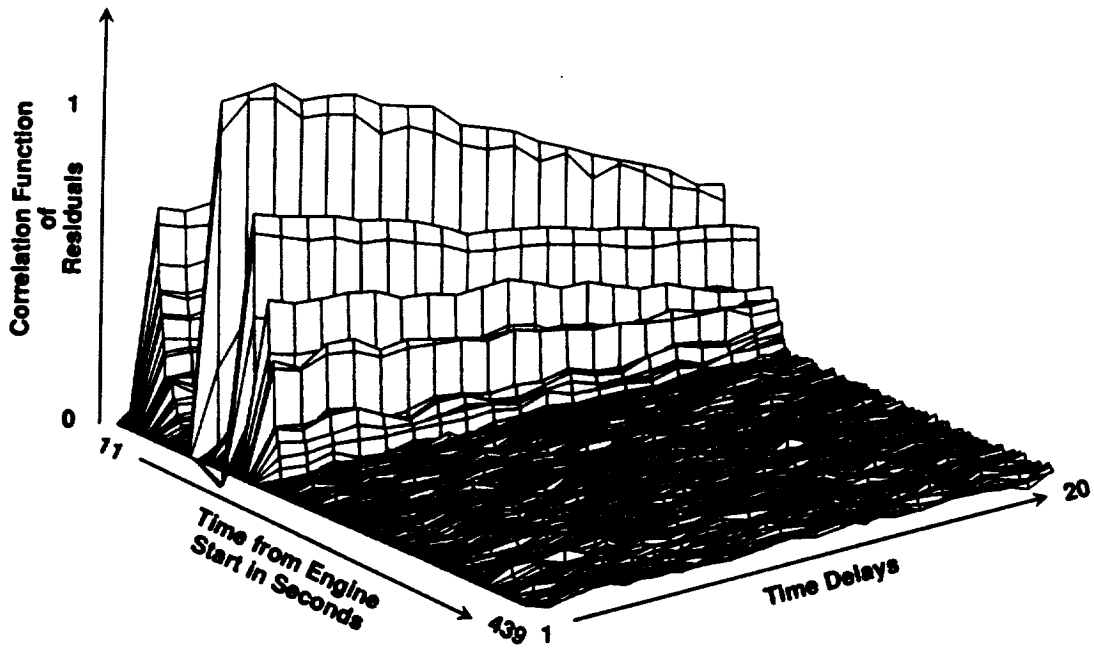

Fig. A-7.5 FAILURE DETECTION USING ARMA MODELS FOR PARAMETER LPOP DISCHARGE PRESSURE FOR TEST 902-249.

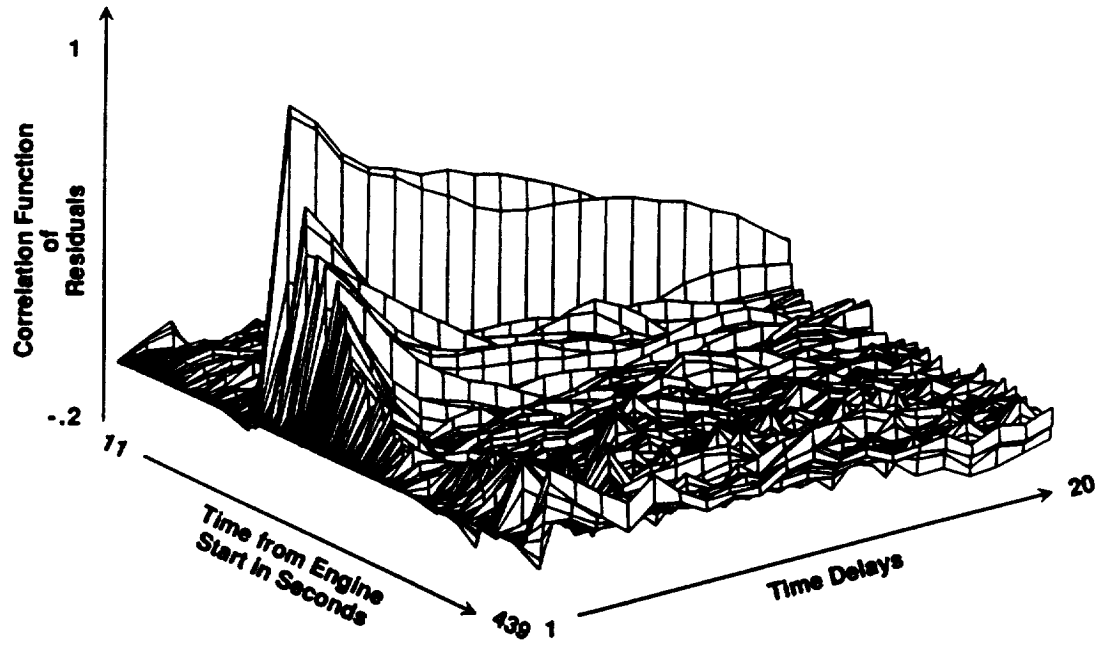

Fig. A-7.6 FAILURE DETECTION USING ARMA MODELS FOR PARAMETER HPFP SPEED FOR TEST 902-249.

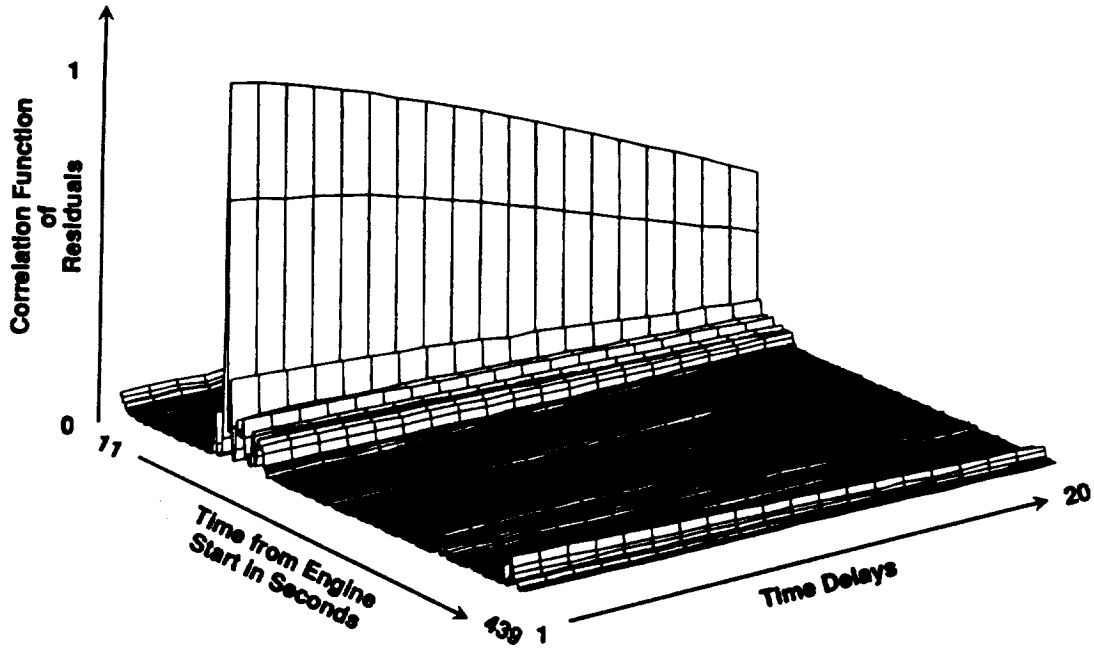

Fig. A-7.7 FAILURE DETECTION USING ARMA MODELS FOR PARAMETER HPFP INLET TEMPERATURE FOR TEST 902-249.

The performance of the algorithm on the nominal data set 902-463 is shown in Figure A-7.8. Deviations in the correlation coefficient, R, values occur when the engine power drops to 65% RPL; when the engine is transitioning from 104% to 109% RPL; and when the engine is transitioning from 65% to 100% RPL prior to shutdown. No false alarms resulted from the deviations.

The correlation values for 902-249 and the detection threshold are shown in Figure A-7.9. The R values start below the detection threshold causing a detection to occur at 5.2 seconds. The low R values concur with the engine failure scenario which indicated flow problems within the pump and turbine blade failure at 3.0 seconds.

8. Test 901-225: MOV Fretting

According to the Rocketdyne SAFD Phase II report, during stable operation at 100% of rated power level, the Voting Logic Cutoff Device initiated a shutdown when the HPFT discharge temperature redline was exceeded. Failure analysis indicates the incident was caused by fretting at the main oxidizer valve inlet sleeve-to-bellows flanged joint, which resulted in the initiation of a fire within the MOV. Flow oscillations at four times the high pressure oxidizer turbopump speed caused sufficient excitation of the MOV sleeve to overcome the retention screw preload, and allowed fretting between the bellows mating surfaces and shims. The heat generated by fretting produced ignition of the LOX environment. Metal combustion of the MOV caused an over pressure at the valve which increased the initial LOX flow to the main injector and raised the back pressure to the high Pressure oxidizer turbopump (HPOTP). The back pressure increase uprated the HPOTP turbine power and resulted in an increase of LOX to the fuel preburner causing the HPFT discharge temperature to exceed its redline. (Test conducted on 27 December 1978, cutoff time t = 255.61 seconds.)

CADS Data: A plot of the MCC_PC is shown in Figure A-8.1. During this test at 100% RPL operation, one fuel flowrate PID, out of a total of 4 fuel flowrate PIDs, showed presence of high levels of noise, which affected the MCC_PC. Figures A-8.2 through A-8.5 show the fuel flowrate PIDs, while Figure A-8.6 shows the fuel flowrate average PID.

Time Series Analysis: During the mainstage operation at 100% power level, abnormal behavior was detected approximately 16 seconds from the start for the MCC_PC and the PBP_DS_PR. Figure A-8.7 shows the ARMA error signal correlation function plot for the MCC_PC.

Cluster Algorithm: Input to the clustering algorithm consisted of the thirteen selected sensors (see Table 3.2a) minus those missing sensors listed in Table A-1. The event threshold was 0.93 and the fault detector was set for a five out of five event threshold.

The performance of the algorithm on the 902-463 nominal data set is shown in Figure A-8.8. Principle decreases in the correlation coefficient, R, values occur at 65% RPL and during power transitions. No false alarms resulted from these deviations.

The correlation coefficients, R, for 901-225 and the detection threshold are shown in Figure A-8.9. Throughout the test the R values remain above the threshold until engine shutdown.

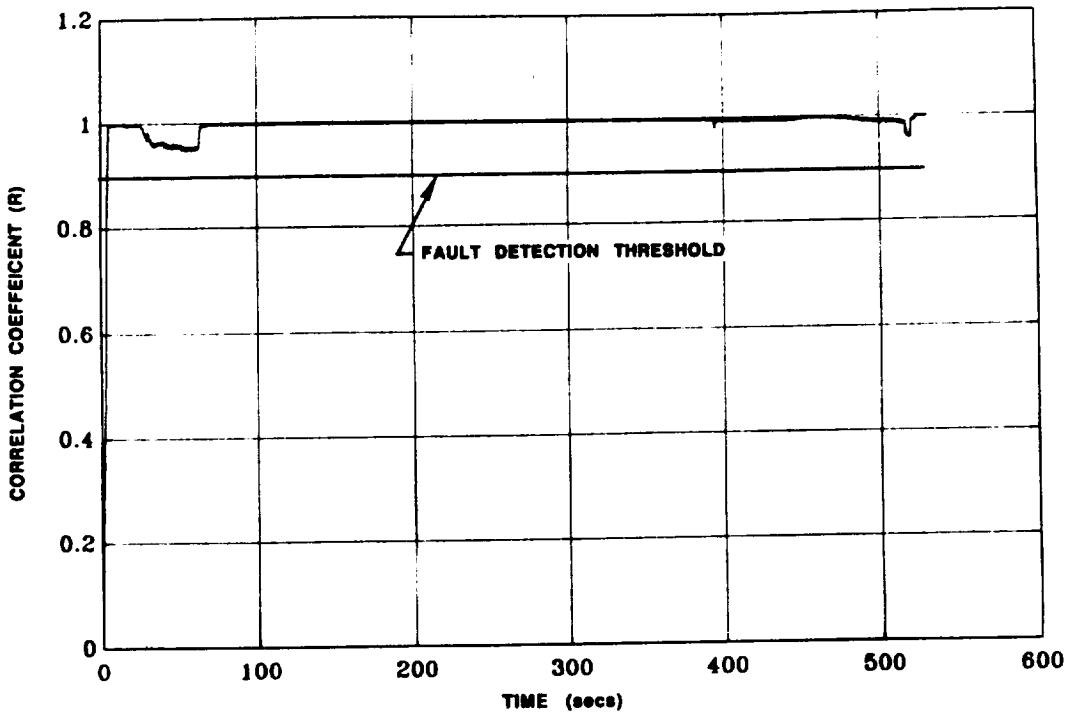

Fig. A-7.8 THE CLUSTERING ALGORITHM RESULTS SHOW NO FALSE ALARMS FOR THE 902-463 NOMINAL DATA USING THE 902-249 SENSOR SUBSET.

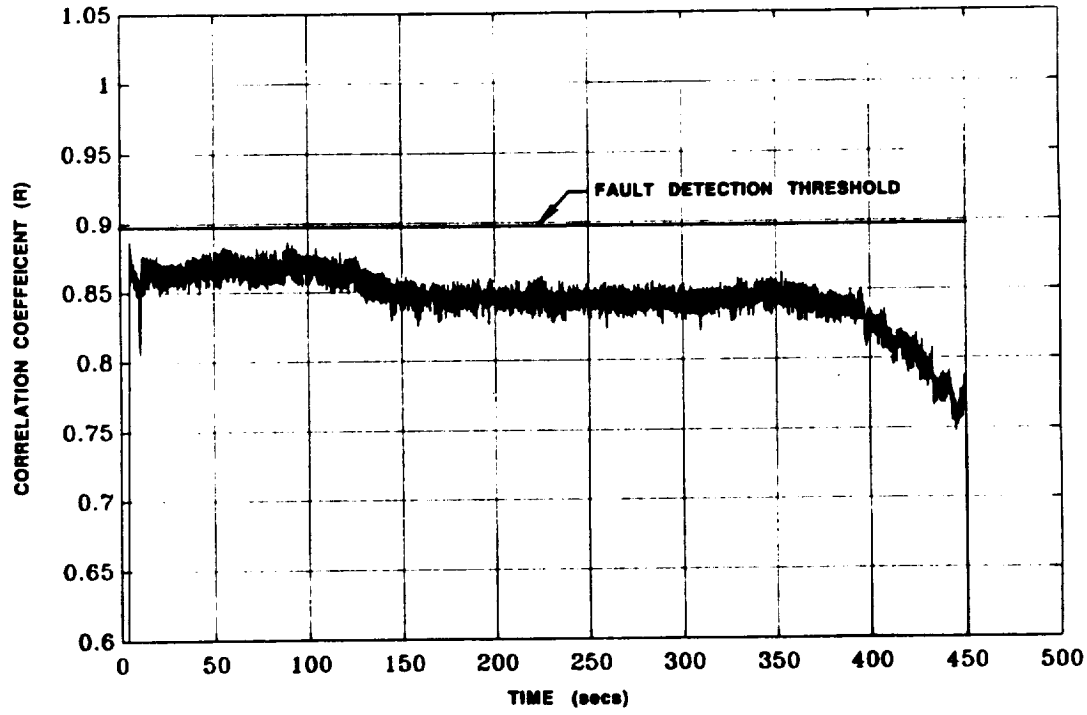

Fig. A-7.9 THE CLUSTERING ALGORITHM RESULTS FOR TEST 902-249. THE CORRELATION COEFFICIENTS START BELOW THE THRESHOLD CAUSING A DETECTION TO OCCUR AT 5.2 SECONDS.

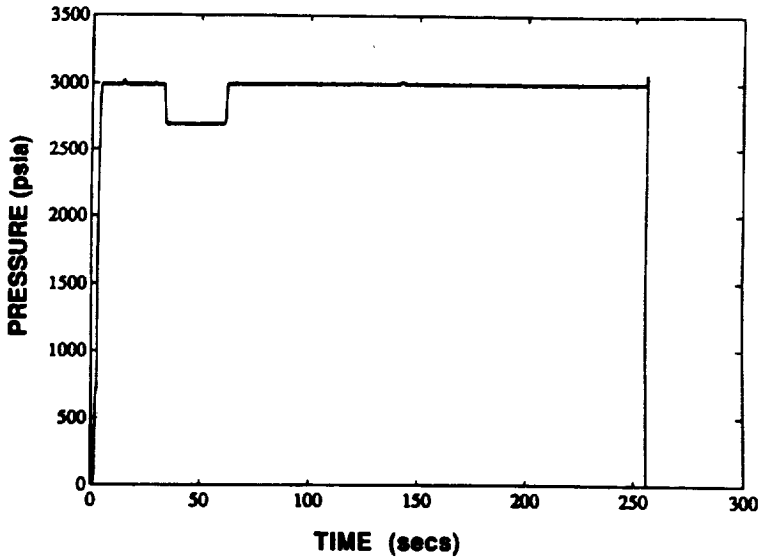

Fig. A-8.1 MCC PRESSURE (PID NO. 163) FOR TEST 901-225

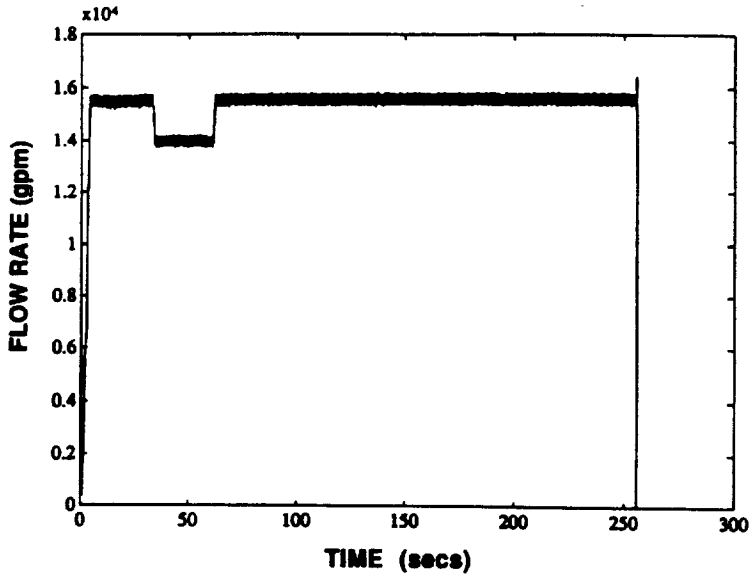

Fig. A-8.2 FUEL FLOW (PID NO. 250) FOR TEST 901-225

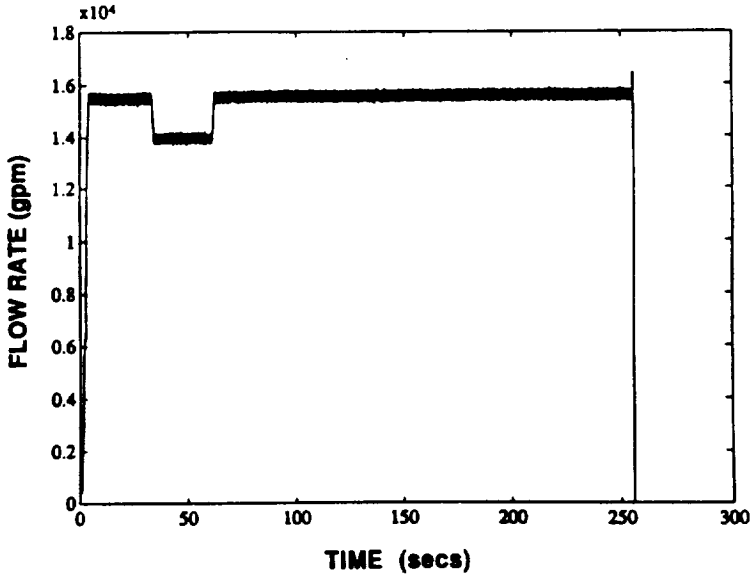

Fig. A-8.3 FUEL FLOW (PID NO. 251) FOR TEST 901-225

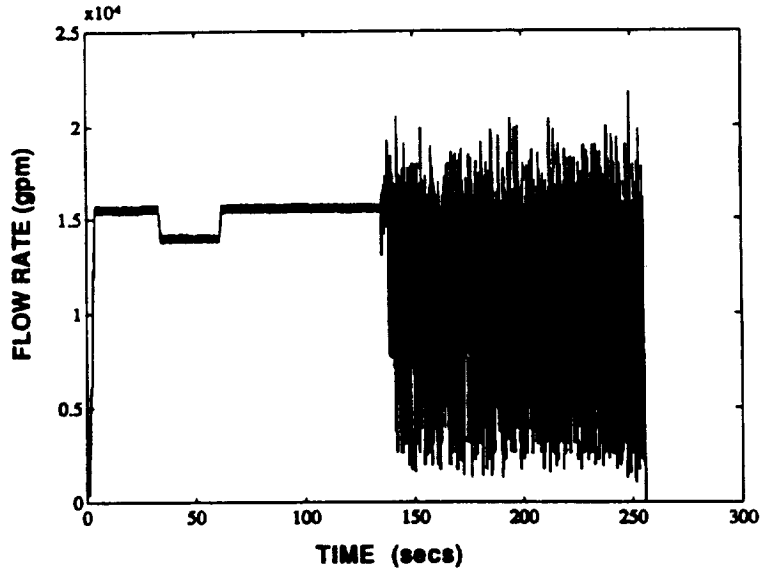

Fig. A-8.4 FUEL FLOW (PID NO. 252) FOR TEST 901-225

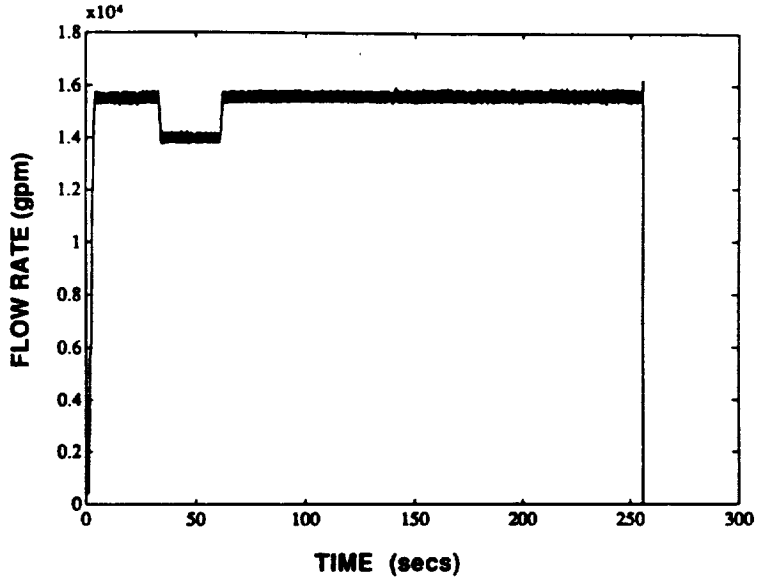

Fig. A-8.5 FUEL FLOW (PID NO. 253) FOR TEST 901-225

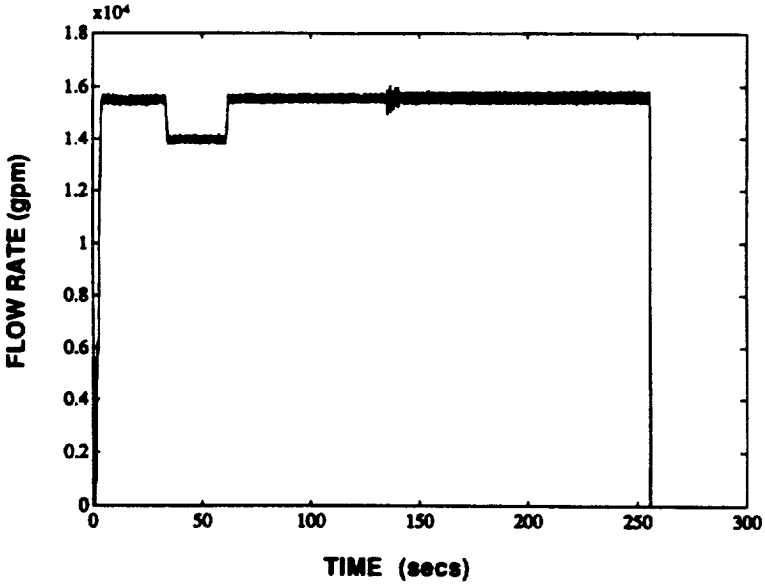

Fig. A-8.6 AVERAGE FUEL FLOW (PID NO. 131) FOR TEST 901-225

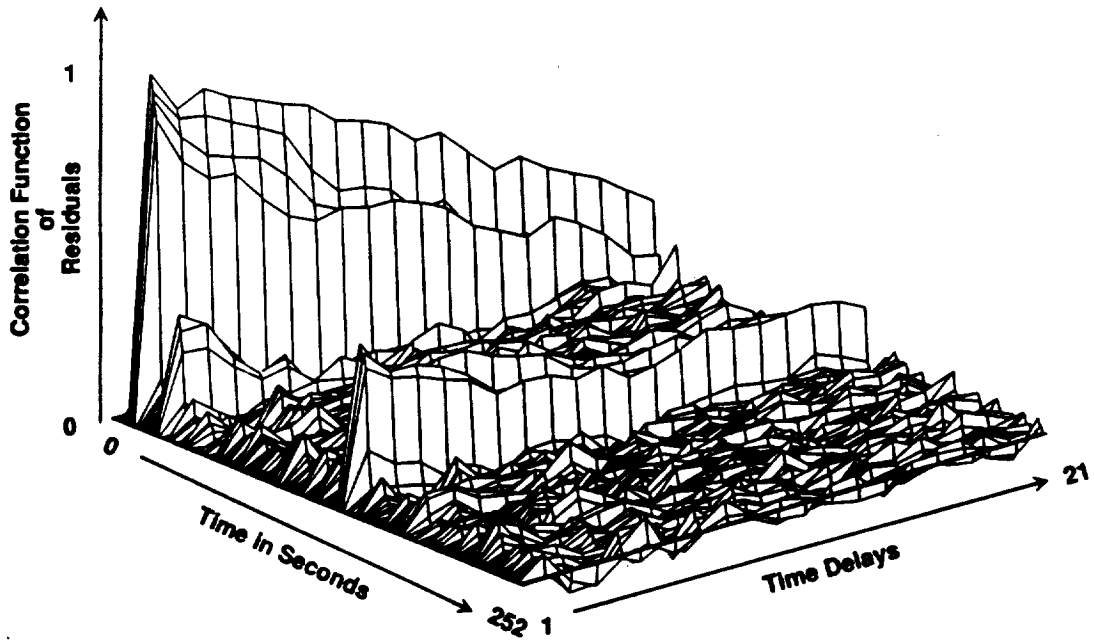

Fig. A-8.7 FAILURE DETECTION USING ARMA MODELS FOR PARAMETER MCC PRESSURE FOR TEST 901-225.

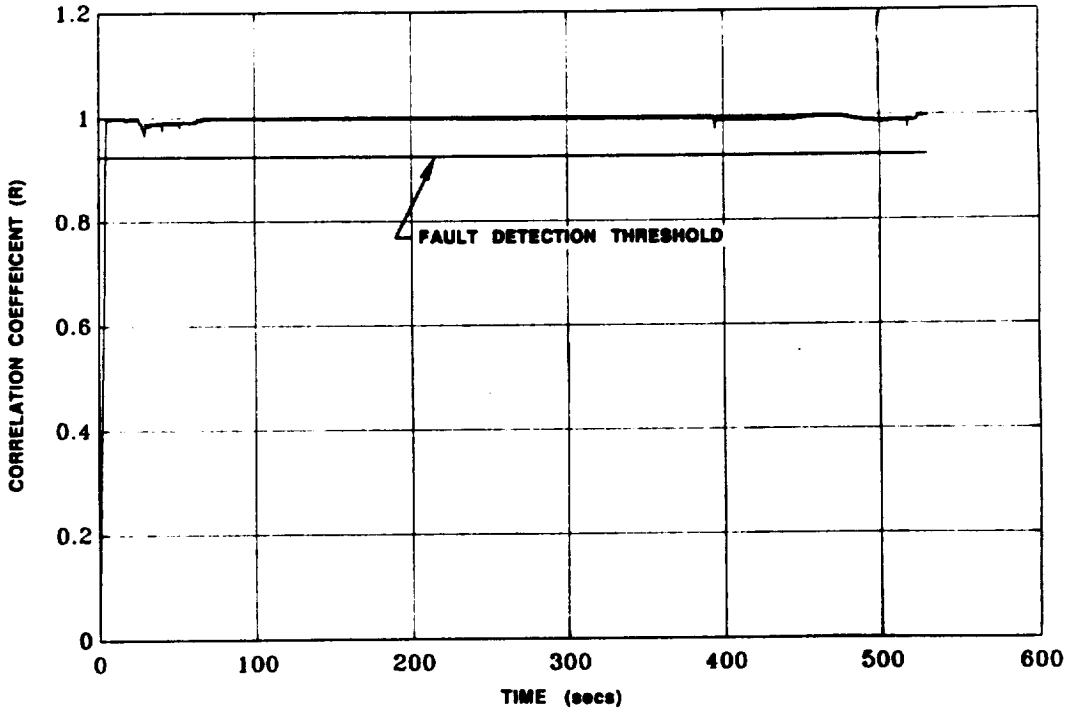

Fig. A-8.8 THE CLUSTERING ALGORITHM RESULTS SHOW NO FALSE ALARMS FOR THE 902-463 NOMINAL DATA USING THE 901-225 SENSOR SUBSET.

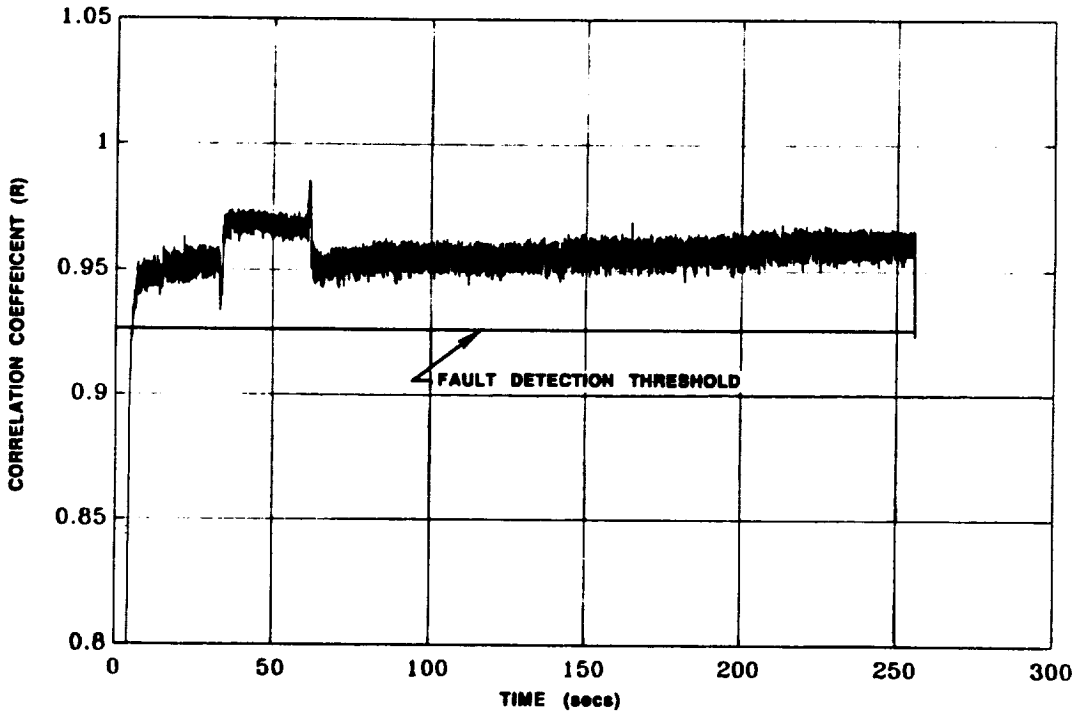

Fig. A-8.9 THE CLUSTERING ALGORITHM RESULTS FOR TEST 901-225. THE CORRELATION COEFFICIENTS REMAINED ABOVE THE DETECTION THRESHOLD UNTIL ENGINE SHUTDOWN.

9. Test 750-168: Valve Seal Failure

According to Cikanek [ ], the failure was caused by anomalous augmented spark ignitor operation which caused cumulative damage to the OPOV downstream seal and resulted in high HPOT temperatures. (Cutoff time t = 300.2 seconds.)

CADS Data: A plot of the MCC_PC, shown in Figure A-9.1, displays the engine power profile for the test.

Regression Analysis: This failure occurred during the shutdown sequence. A model to predict the MCC_PC as a function of fuel and LOX flow rates is used to detect the failure as shown in Figure A-9.2.

Cluster Algorithm: Input to the clustering algorithm consisted of the thirteen selected sensors (see Table 3.2a) minus those missing sensors listed in Table A-1. The event threshold was 0.89 and the fault detector was set for a five out of five event threshold.

The performance of the algorithm for the nominal data set 902-463 is shown in Figure A-9.3. The principle deviations in the correlation coefficient, R, values occur at 65% RPL and during power transitions. No false alarms occurred on this data set.

The correlation values for 750-168 and the detection threshold are shown in Figure A-9.4. The R values are above the detection threshold throughout the test.

10. Test 901-284: Sensor Failure

According to the Rocketdyne SAFD Phase II report, near the close of a nominal start, the following major events occurred:

1. Channel B of the Controller cut itself off at t = 3.25 seconds (under launch conditions, this would have resulted in engine shutdown) due to a failure of electronic components in the facility power supply.

2. At approximately t = 3.9 seconds, the Lee Jet orifice (used to purge the Channel A PC transducer passage) became dislodged and caused the PC transducer to sense the MCC coolant flow pressure instead of chamber pressure. This erroneous reading (3800 psi) caused the Controller to close the OPOV to reduce PC to the desired 3012 psi level. A few milliseconds later, the Controller calculated a mixture ratio of 9.0 and commanded the FPOV full open in an attempt to reduce the mixture ratio to 6.0.

a. The immediate result of the Controller's actions (based on an erroneous PC) was operation in an abnormal mode, characterized by high fuel flow and low turbine inlet temperatures of the oxidizer and fuel preburner. In fact, the oxidizer preburner turbine inlet temperature fell quickly to about 440 deg-R, which assured freezing of the water which makes up about 10% of the total flowrate of 40 lbs/sec.

b. The ultimate result of the Controller's actions was a fire in the HPOTP at about 9.7 seconds due to rubbing in the area of the LOX primary seal slinger. The rubbing was caused by a high axial

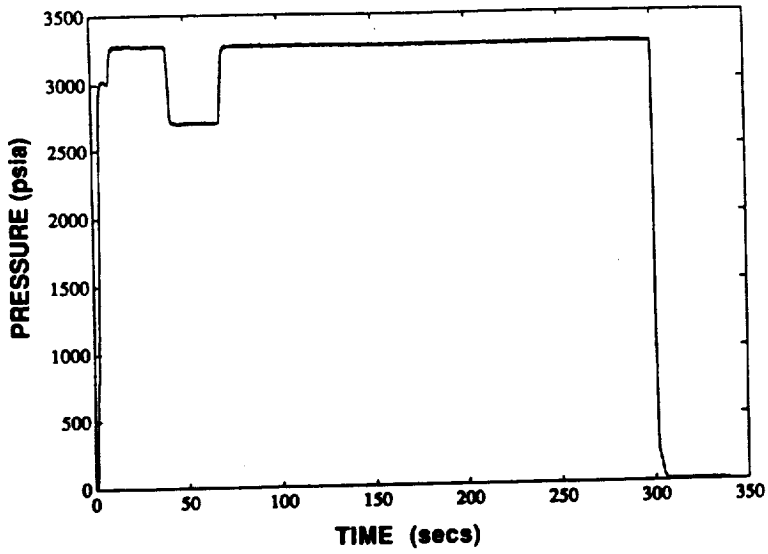

Fig. A-9.1 MCC PRESSURE (PID NO. 130) FOR TEST 750-168

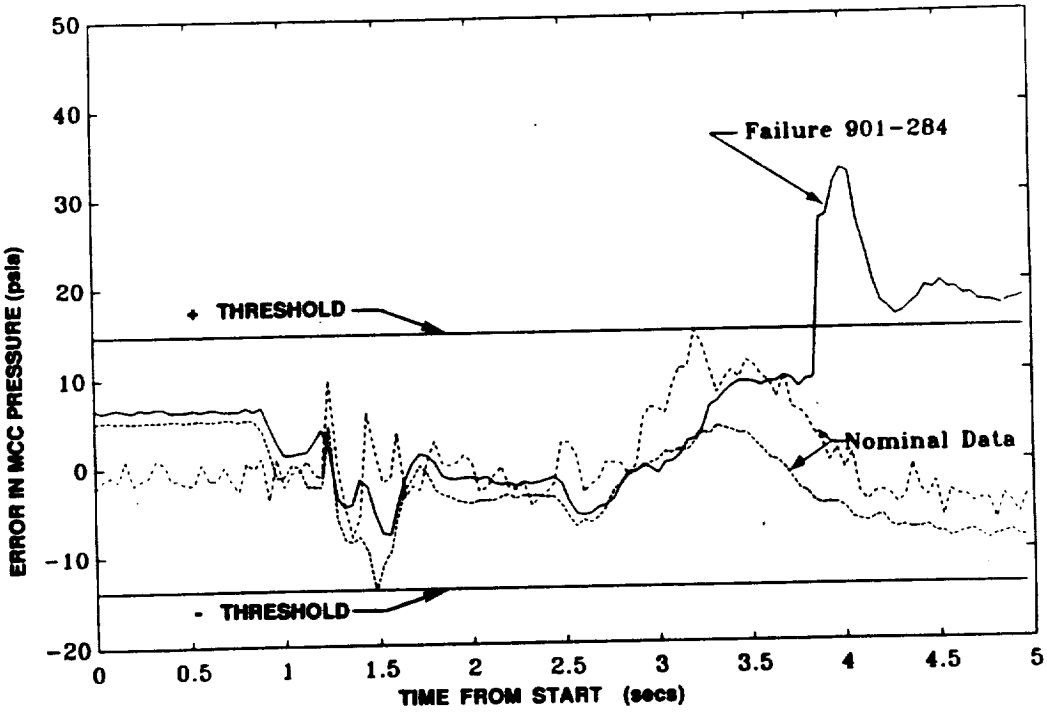

Fig. A-9.2 NONLINEAR REGRESSION METHOD: DETECTION OF FAILURE DURING STARTUP

Error in predicted MCC pressure crossing threshold indicates failure.

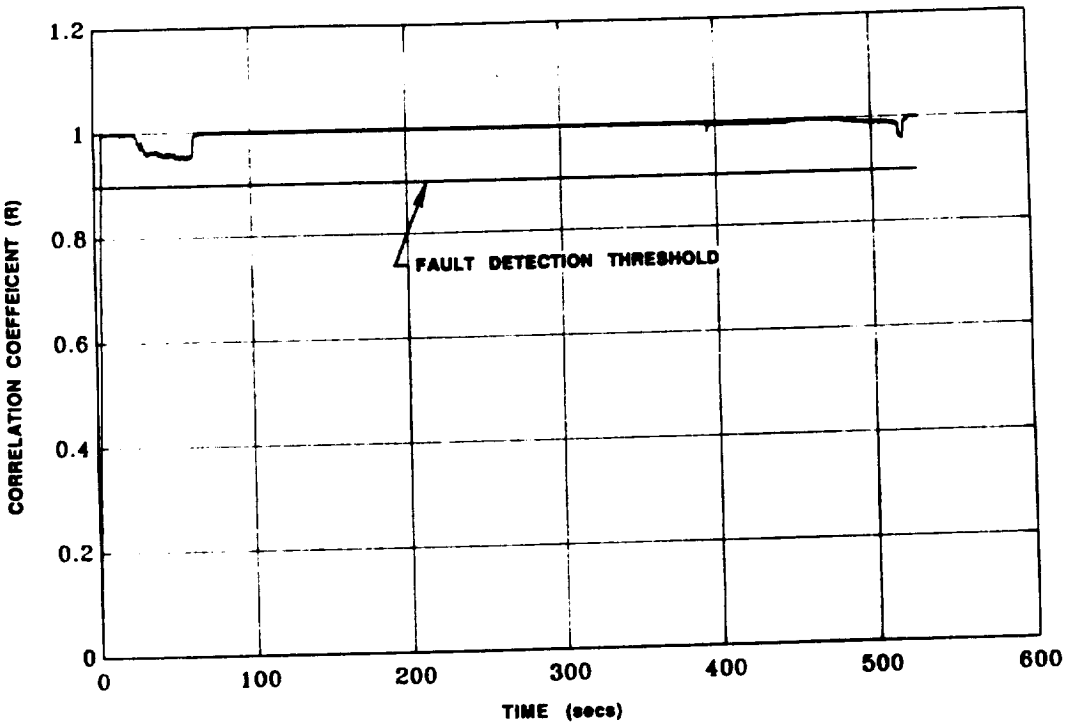

Fig. A-9.3 THE CLUSTERING ALGORITHM RESULTS SHOW NO FALSE ALARMS FOR THE 902-463 NOMINAL DATA USING THE 750-168 SENSOR SUBSET.

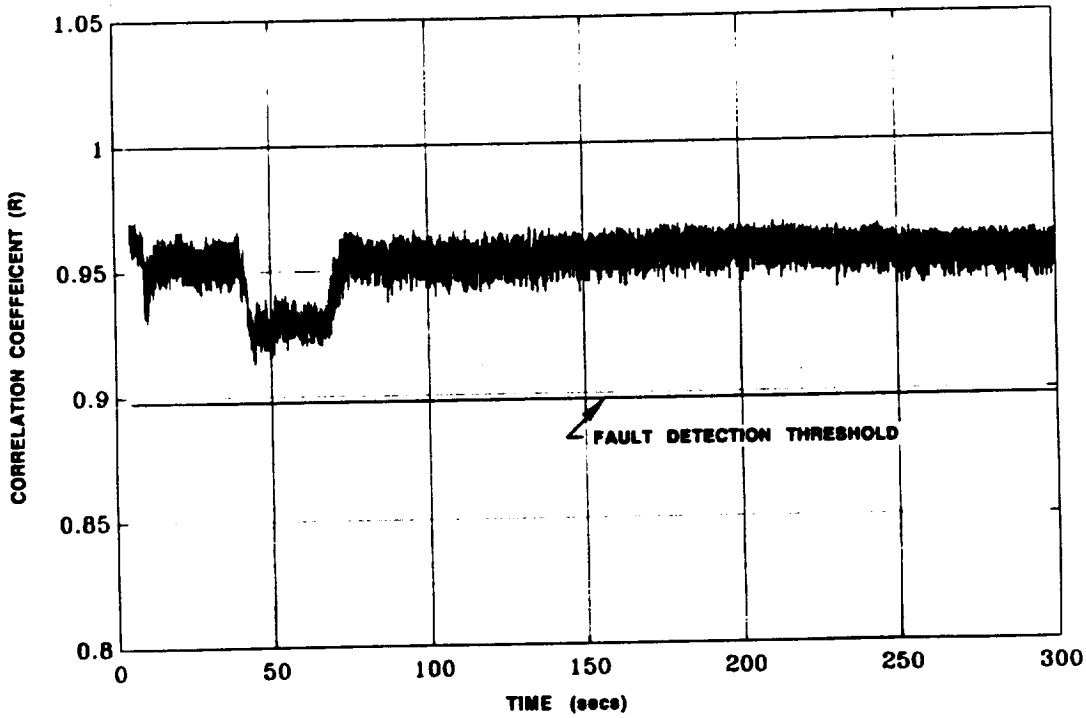

Fig. A-9.4 THE CLUSTERING ALGORITHM RESULTS FOR TEST 750-168. THE CORRELATION COEFFICIENTS REMAINED ABOVE THE DETECTION THRESHOLD UNTIL ENGINE SHUTDOWN.

load which displaced the rotor assembly toward the pump end of the HPOTP housing. This high axial load was caused by ice formation in the cavity between the housing and the second stage turbine wheel which resulted in reduction in the cavity pressure from about 2500 psi to near ambient. This reduced pressure on one side of the turbine wheel caused an estimated increase in rotor axial force of about 31,000 lbs, which far exceeded the control capability of the balance pistons to control the position of the rotor.

3. At 9.88 seconds, the test was terminated when the high pressure oxidizer preburner pump radial accelerometer exceeded the 10g redline. (Test conducted on 30 July 1980, cutoff time: t = 9.88 seconds.)

CADS Data: A plot of the MCC_PC, shown in Figure A-10.1, displays the engine power profile for the test.

Regression Analysis: This failure occurred during the startup sequence. A model to predict the MCC_PC as a function of fuel and LOX flow rates is used to detect the failure as shown in Figure A-10.2.

Cluster Algorithm: Input to the clustering algorithm consisted of the thirteen selected sensors (see Table 3.2a) minus those missing sensors listed in Table A-1. The event threshold was 0.744 and the fault detector was set for a five out of five event threshold.

The performance of the algorithm on the nominal data 902-463 is shown in Figure A-10.3. As shown in the plot, the correlation coefficient, R, values which drop below the threshold occur during three of the power transitions. Of these events, the crossings at 30 and 41 seconds led to false alarms. A preliminary analysis has identified the likely cause of the false alarms to be the absence of PID 59, the Preburner Pump Discharge Pressure. As discussed in Section 3.1.3.3.2, PID 59 is an example of a parameter whose magnitude was poorly modelled by the PBM estimator and thus given a larger weighting in the clustering algorithm. The loss of a highly weighted parameter decreases the algorithm stability during power level changes, and therefore, produces false alarms during those transitions.

The correlation values for 901-284 and the detection threshold are shown in Figure A-10.4. The R values are below the threshold throughout the test. This concurs with the fact that the failure occurred during startup and forced the engine into an abnormal operational state prior to entering mainstage.

11. Test 750-259: MCC Duct Fracture

According to the Rocketdyne SAFD Phase II report, during stable operation at 109% of rated power level, a small fuel leak developed in the MCC outlet neck (determined by film review). The leak caused less than .25% change in nominal values for the LPFP speed, discharge pressure and OPOV position. The fuel leak remained essentially constant until approximately 200 milliseconds prior to cutoff, at which time a major fuel leak occurred at apparently the same location based on both data and film review. In response to the rupture, the LPFP rapidly decayed in speed. This speed drop reduced the pump's discharge pressure and the high pressure fuel pump (HPFTP) went into deep cavitation. As a consequence, the HPFTP speed (PID-261) exceeded its nominal speed by approximately 10,000 rpm. The off-nominal condition led the pump to exceed

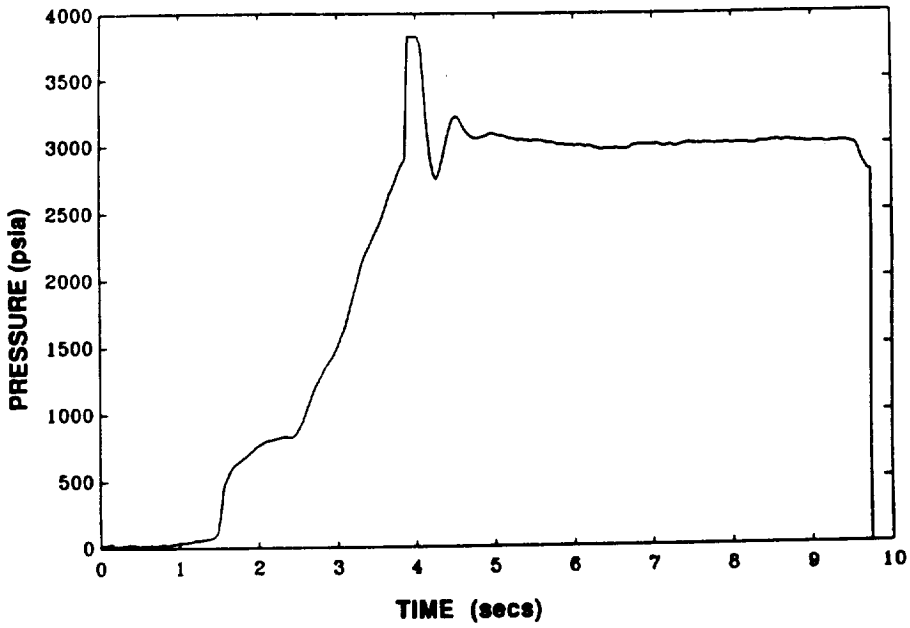

Fig. A-10.1 MCC PRESSURE (PID NO. 130) FOR TEST 901-284

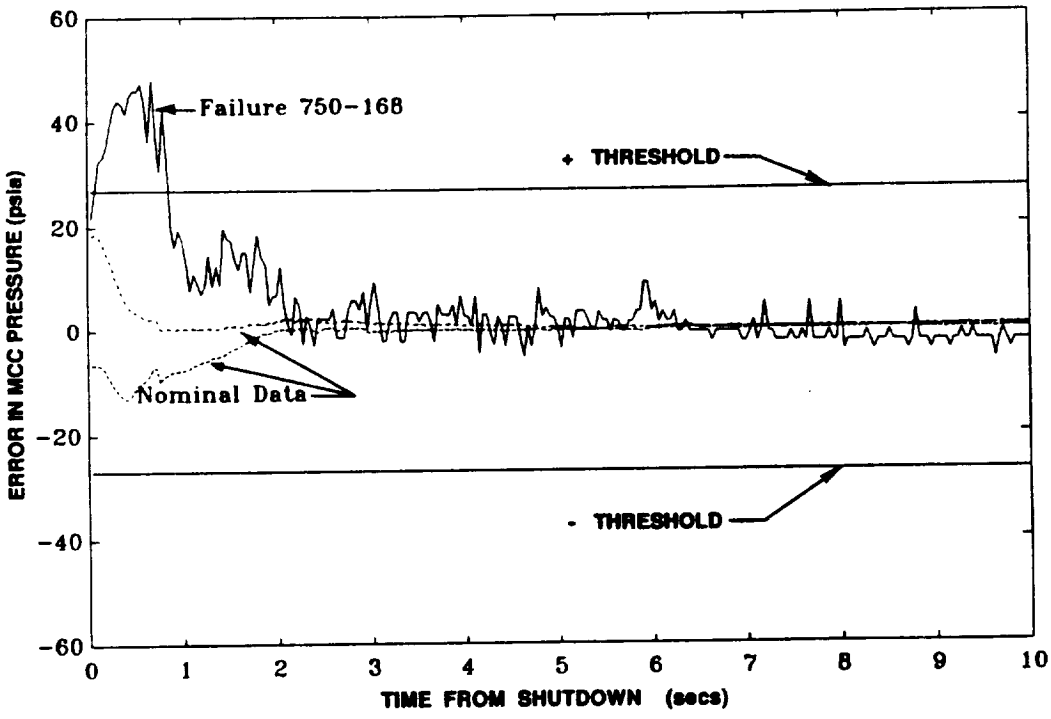

Fig. A-10.2 NONLINEAR REGRESSION METHOD DETECTION OF FAILURE DURING SHUTDOWN

Error in MCC pressure crossing threshold indicates failure.

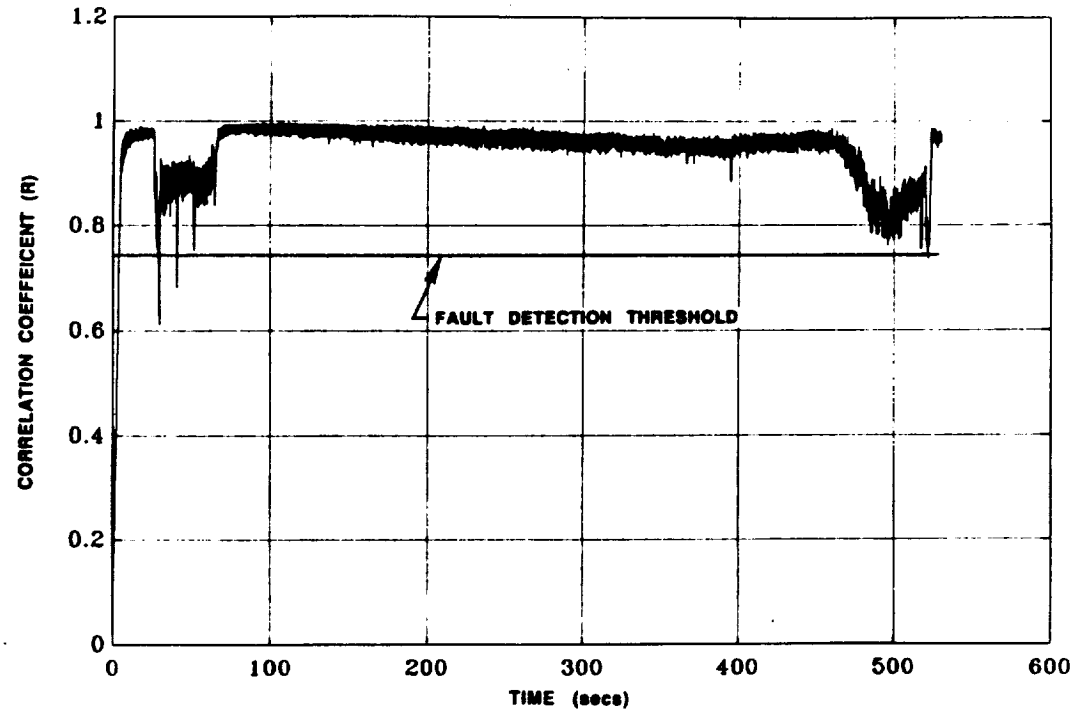

Fig. A-10.3 THE CLUSTERING ALGORITHM RESULTS SHOW FALSE ALARMS OCCURING AT 30 AND 41 SECONDS FOR THE 902-463 NOMINAL DATA USING THE 901-284 SENSOR SUBSET.

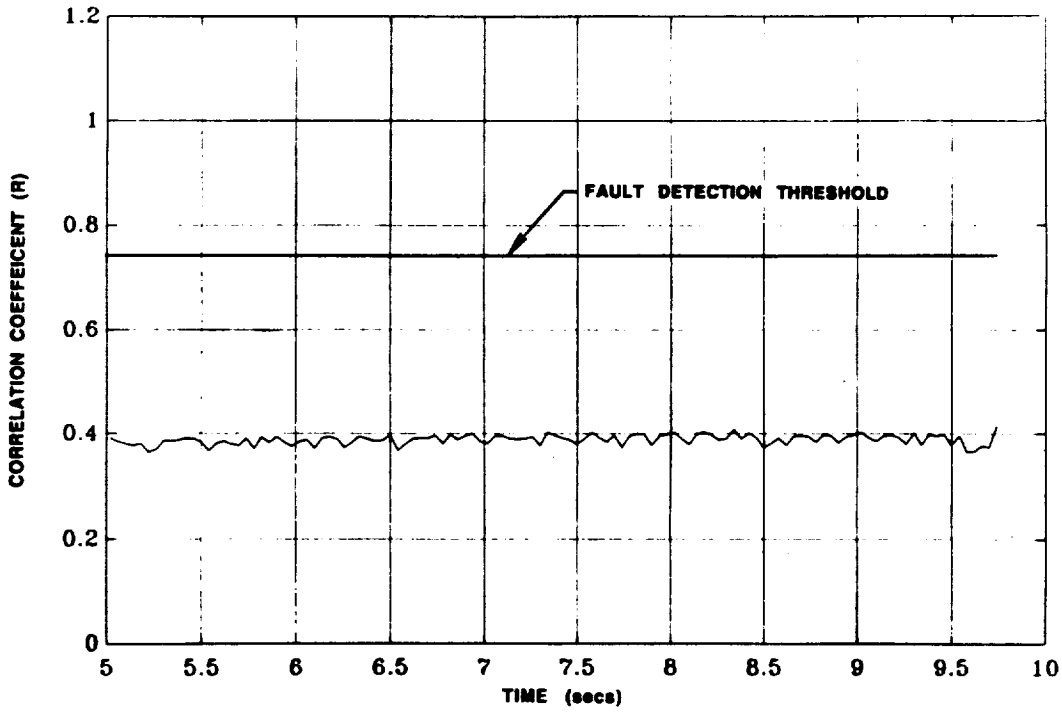

Fig. A-10.4 THE CLUSTERING ALGORITHM RESULTS FOR TEST 901-284. THE CORRELATION COEFFICIENTS ARE BELOW THE DETECTION THRESHOLD THROUGHOUT THE TEST.

its vibration redline and led to a cutoff command. Following cutoff, the fuel caviation condition resulted in: reduced engine fuel flow, a severe oxygen-rich condition, burnout of the turbines, burn-through of the hotgas manifold, severe erosion of the gimbal bearing, and eventual separation of the engine below the low pressure pumps. (Test conducted on 27 March 1985, cutoff time: t = 101.5 seconds.)

CADS Data: A plot of the MCC_PC is shown in Figure A-11.1.

Time Series Analysis: For this test, the nominal ARMA model for a parameter such as LPFT_DS_PR, over a 4 second window (100 data points) did not indicate any failures until the redline cutoff as shown in Figure A-11.2. However, nominal models over a longer time of 40 seconds (1000 data points) were effective in detecting deviations from the nominal beginning around 12 seconds from the start for LPFT_DS_P, and 27 seconds from the start for the HPFP_DS_PR in Figure A-11.3. Because of the 1000 point window, the earliest possible failure indication occurred at 52 seconds from the start. Figures A-11.4 through A-11.6 show the ARMA error signal correlation function plots for LPFT_DS_PR and HPFP_DS_PR.

Cluster Algorithm: Input to the clustering algorithm consisted of the thirteen selected sensors (see Table 3.2a) minus those missing sensors listed in Table A-1. The event threshold was 0.89 and the fault detector was set for a five out of five event threshold.

The performance of the algorithm on the nominal data set 902-463 is shown in Figure A-11.7. The decreases in the correlation coefficient, R, values are associated with the engine operating at 65% RPL and the transitions in engine power. No false alarms occurred for the given threshold.

The correlation values for 750-259 and the detection threshold are shown in Figure A-11.8. Throughout the test, the R values remained well above the detection threshold until engine shutdown. This is expected, since the major sensor changes did not occur until 200 milliseconds (5 data samples) prior to normal engine shutdown.

12. Test 901-173: Main Injector Fracture

According to the Rocketdyne SAFD Phase II report, during stable operation at 92% of rated power level, LOX post 10, row 13 cracked through at the tip radius between the primary and secondary faceplates. Hot gas flow into the LOX post ignited and burned out the post. LOX pouring into the face coolant manifold caused burn through of the primary and secondary faceplates, dumping face coolant into the hot gas manifold. Ejection of burner debris caused severe nozzle tube rupture (46 tubes). Fuel loss to the preburners coupled with engine control reactions to maintain MCC_PC caused the HPFT discharge temperature to exceed its redline, producing a premature cutoff at t = 201.17 seconds. (Test conducted on 4 April 1978, cutoff time: t = 201.17 seconds.)

CADS Data: A plot of the MCC_PC is shown in Figure A-12.1. A significant number of PIDS such as the HPFT_DS_T, HPOT_DS_T_B, FPB_PC, and OPB_PC were missing from CADS data.

Time Series Analysis: For the first 100 seconds of operation at 70% RPL, the ARMA models indicate nominal operation. After the power level change to 92% RPL, a number of

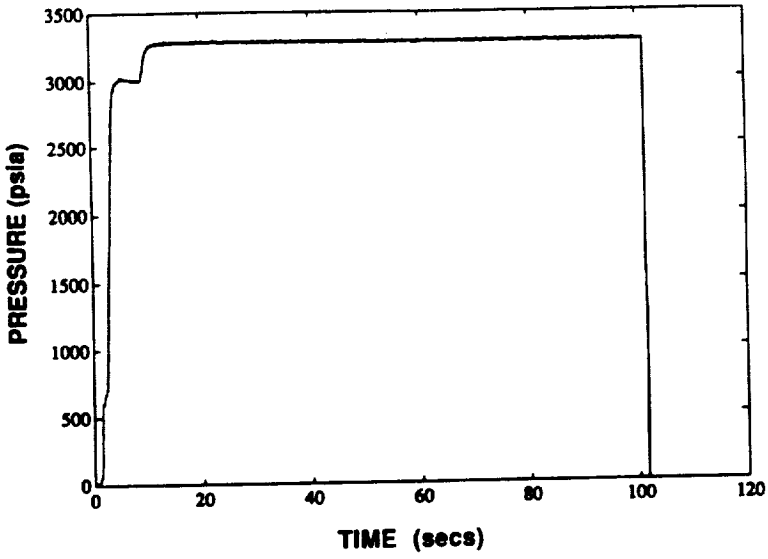

Fig. A-11.1 MCC PRESSURE (PID NO. 130) FOR TEST 750-259

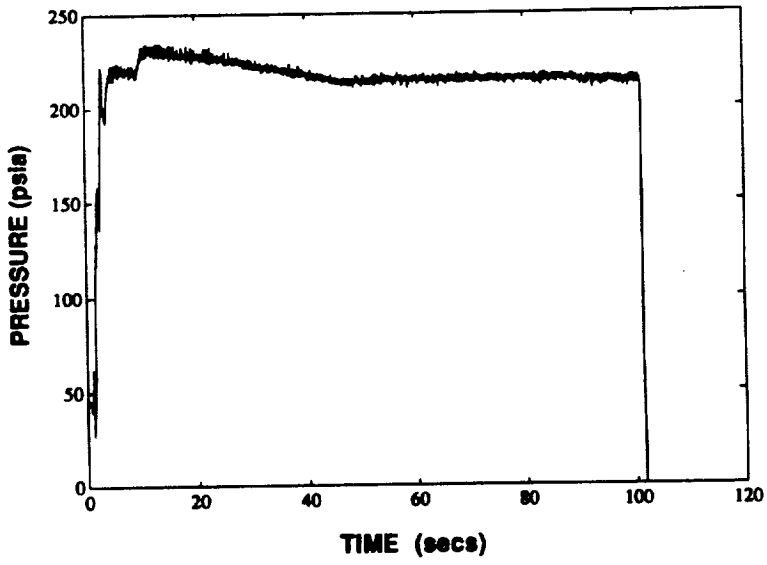

Fig. A-11.2 LPFT DISCHARGE PRESSURE (PID NO. 203) FOR TEST 750-259

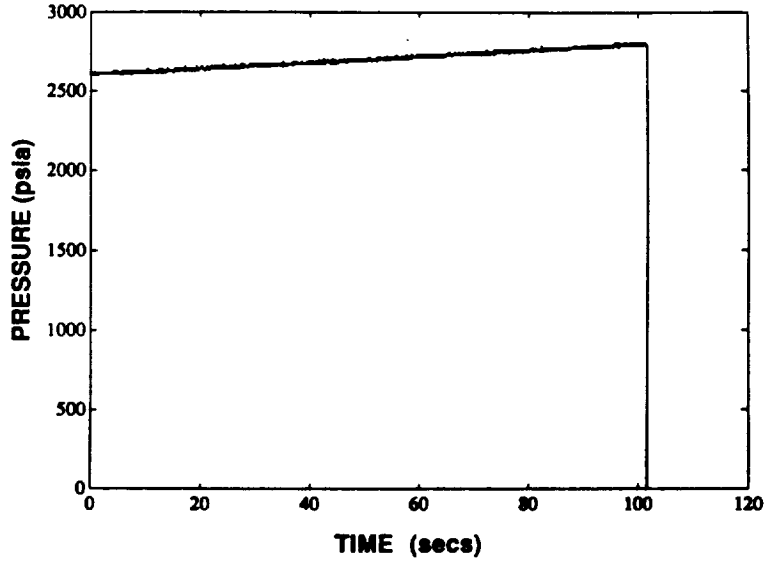

Fig. A-11.3 HPFT DISCHARGE PRESSURE (PID NO. 52) FOR TEST 750-259

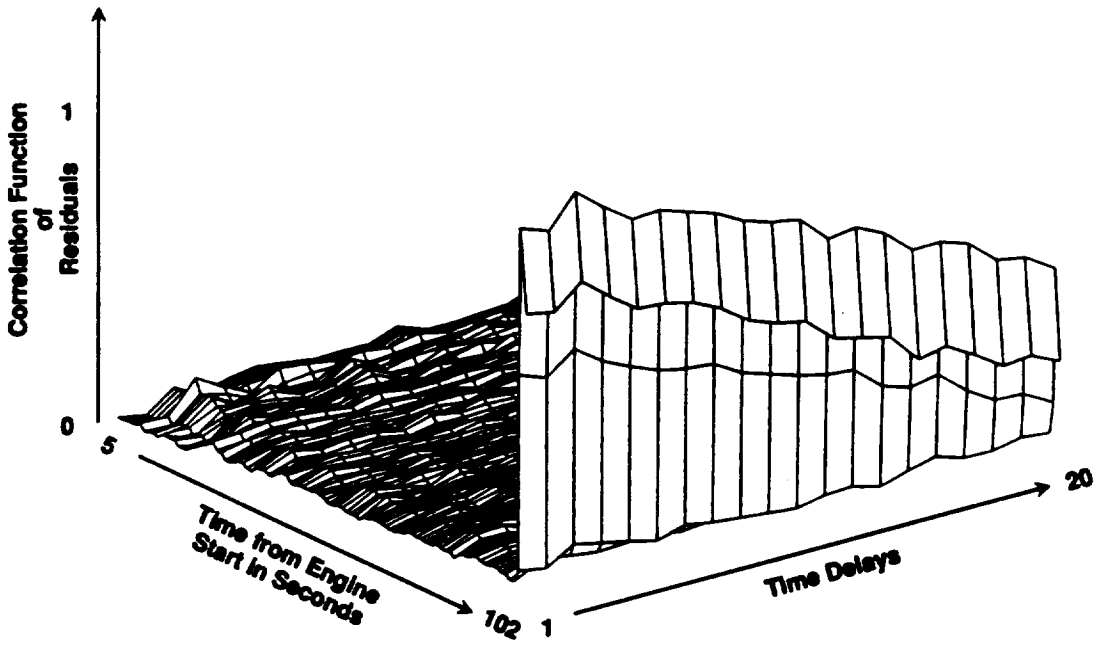

Fig. A-11.4 FAILURE DETECTION USING ARMA MODELS FOR PARAMETER LPFT DISCHARGE PRESSURE FOR TEST 750-259.

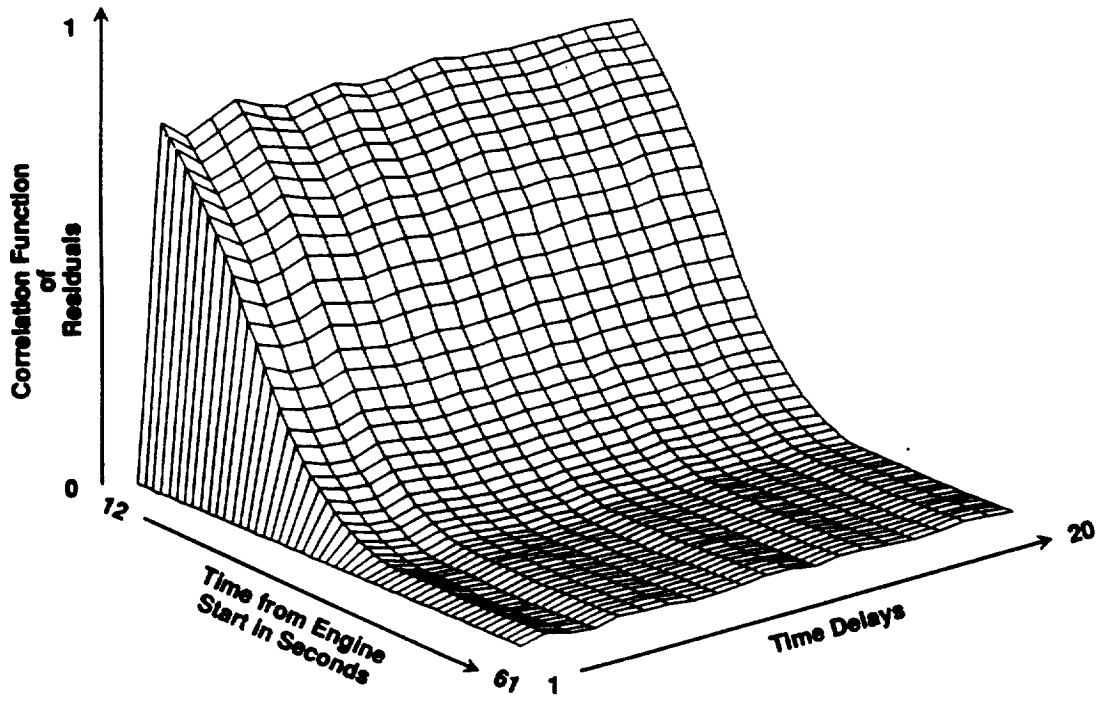

Fig. A-11.5 FAILURE DETECTION USING ARMA MODELS FOR PARAMETER LPFT DISCHARGE PRESSURE FOR TEST 750-259 (40 sec window).

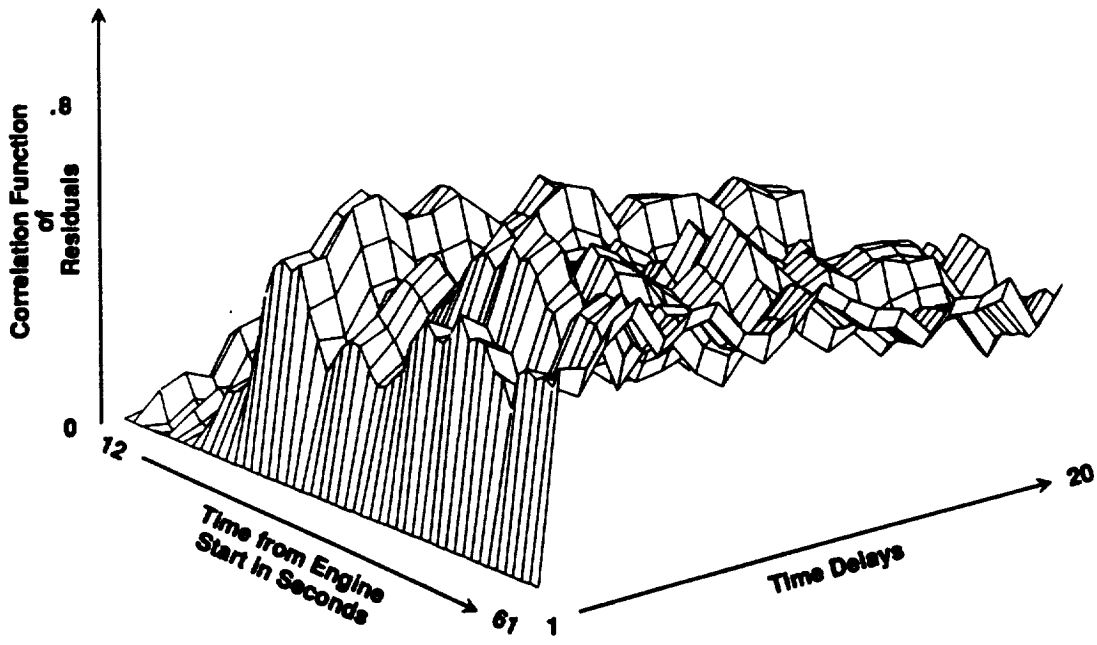

Fig. A-11.6 FAILURE DETECTION USING ARMA MODELS FOR PARAMETER HPFT DISCHARGE PRESSURE FOR TEST 750-259 (40 sec window).

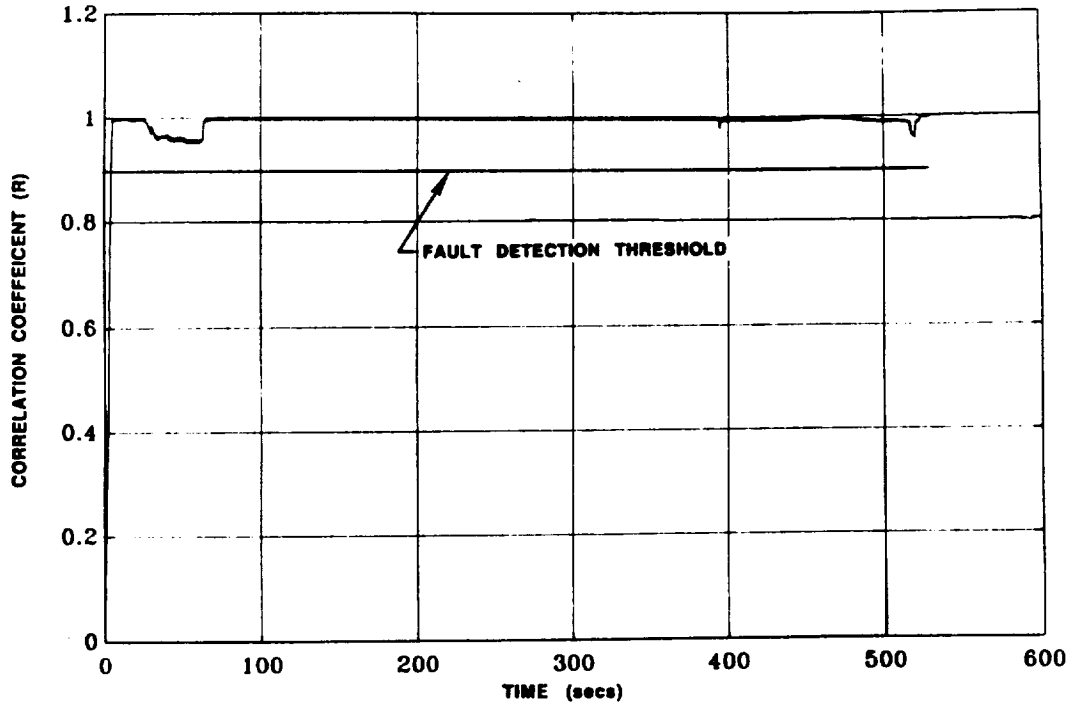

Fig. A-11.7 THE CLUSTERING ALGORITHM RESULTS SHOW NO FALSE ALARMS FOR THE 902-463 NOMINAL DATA USING THE 750-259 SENSOR SUBSET.

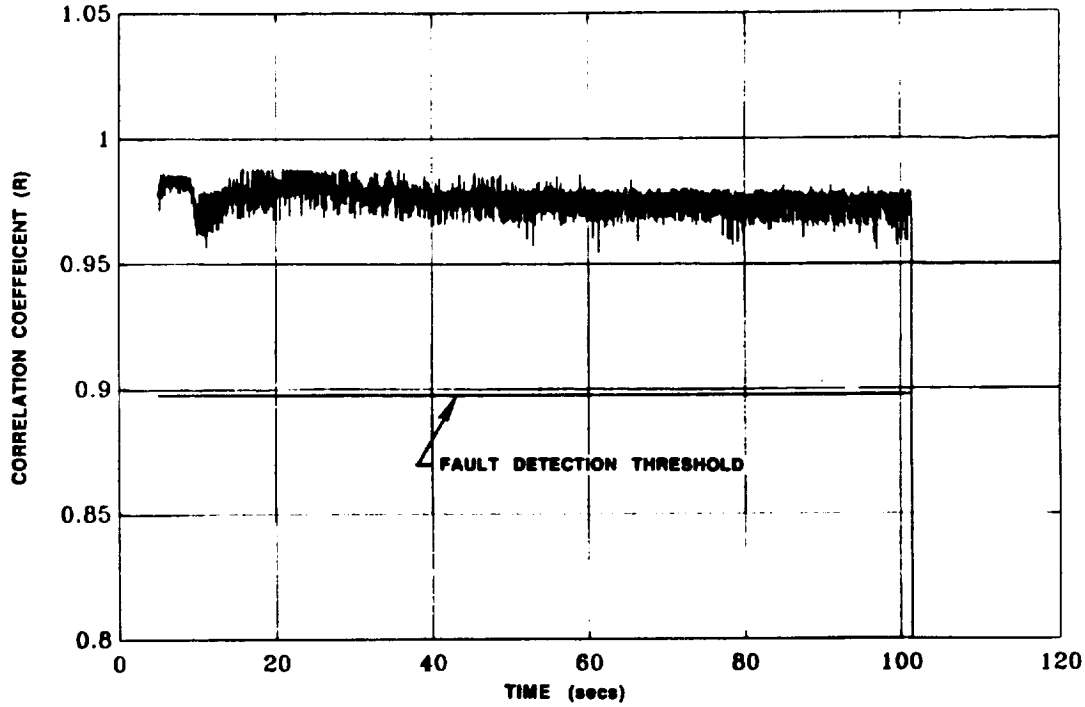

Fig. A-11.8 THE CLUSTERING ALGORITHM RESULTS FOR TEST 750-259. THE CORRELATION COEFFICIENTS REMAINED ABOVE THE DETECTION THRESHOLD UNTIL ENGINE SHUTDOWN.

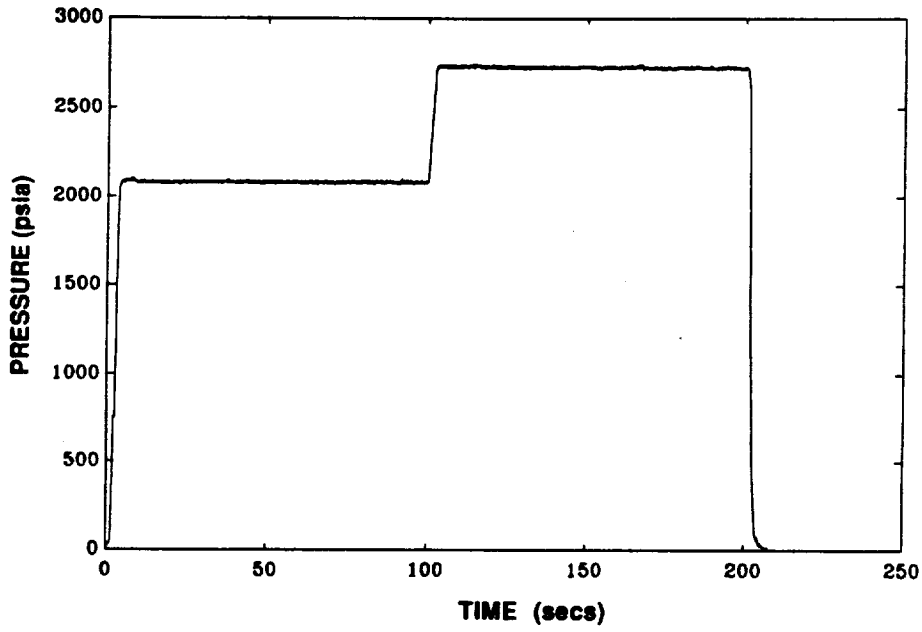

Fig. A-12.1 MCC PRESSURE (PID NO. 130) FOR TEST 901-173

parameters including OPOV_ACT_POS, LPFP_SPD, HPFP_SPD, and HPOP_SPD start to show deviations from the nominal. OPOV_ACT_POS shows deviations from as early as 160 seconds from the start. Figures A-12.2 through A-12.9 show the plots of data and the correlation functions of the residuals.

Cluster Algorithm: Input to the clustering algorithm consisted of the thirteen selected sensors (see Table 3.2a) minus those missing sensors listed in Table A-1. The event threshold was 0.94 and the fault detector was set for a five out of five event threshold.

The performance of the algorithm for nominal data is shown in Figure A-12.10. No false alarms occurred for the given threshold.

The correlation values, R, for 901-173 and the detection threshold are shown in Figure A-12.11. The R values remain above the detection threshold when the engine is operating at 69% RPL. While the engine transitions to 90% RPL (at 100 seconds), the R values drop below the threshold at 102.1 seconds, and continue decreasing even though the engine maintains a constant power.

13. Test 901-331: Main Injector Fracture

According to the Rocketdyne SAFD Phase II report, during stable operation at 100% of rated power level, LOX post 79, row 13 failed in the 316L material at the inertial weld (which joins a 316L post to an INCO718 interpropellant plate stub). Test data analysis reveals that the LOX post failure occurred first, and subsequently, did major damage to the injector. Once the injector was damaged, a loss in C-star efficiency resulted and caused a reduction in MCC_PC. The engine control system responded by increasing the OPOV (Oxidizer Preburner Oxidizer Valve) open position. The increased LOX flowrate necessary to maintain the 100% rated power level caused the HPOT discharge temperature to exceed its redline (1760 deg-R). The test was thus cutoff prematurely at t = 233.14 seconds. (Test conducted on 15 July 1981, cutoff time: t = 233.14 seconds.)

CADS Data: A plot of the MCC_PC, shown in Figure A-13.1, displays the engine power profile. A plot of the LPOP discharge pressure, used for the ARMA fault detection is shown in figure A-13.2.

Time Series Analysis: During mainstage operation at 100% RPL, failure detection by the ARMA models occurred at the time of the redline cutoff, as shown in Figure A-13.3.

Cluster Algorithm: Input to the clustering algorithm consisted of the thirteen selected sensors (see Table 3.2a) minus those missing sensors listed in Table A-1. The event threshold was 0.669 and the fault detector was set for a five out of five event threshold.

The performance of the algorithm for nominal data is shown in Figure A-13.4. As shown in the plot, the threshold is exceeded during power transitions at 28 seconds, 41 seconds, 52 seconds, and 517 seconds. Each detection resulted in a false alarm. Similar to test 901-284 described in Section A-11, these false alarms are attributed to the absence of PID 59, the Preburner Pump Discharge Pressure.

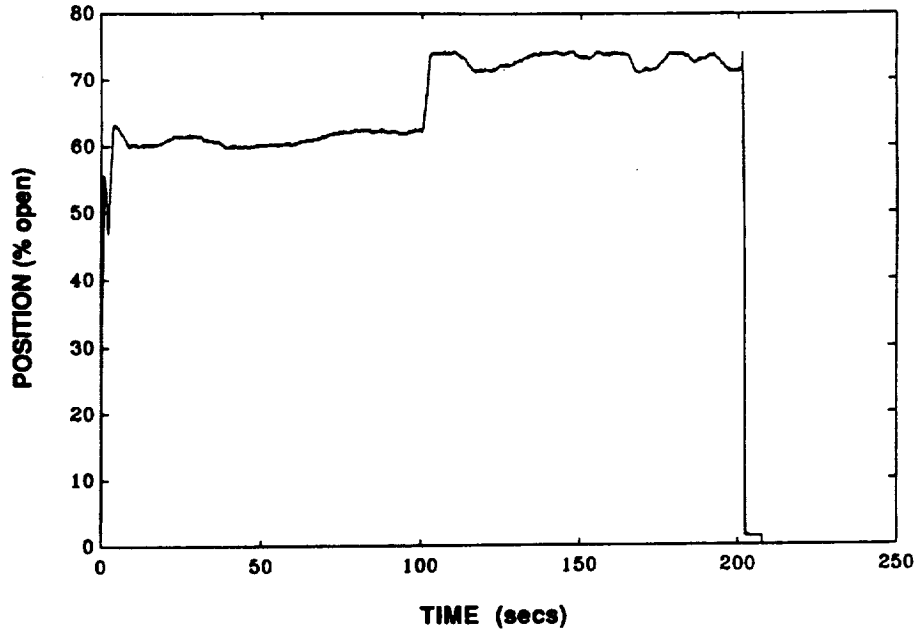

Fig. A-12.2 OPOV ACTUATOR POSITION (PID NO. 140) FOR TEST 901-173

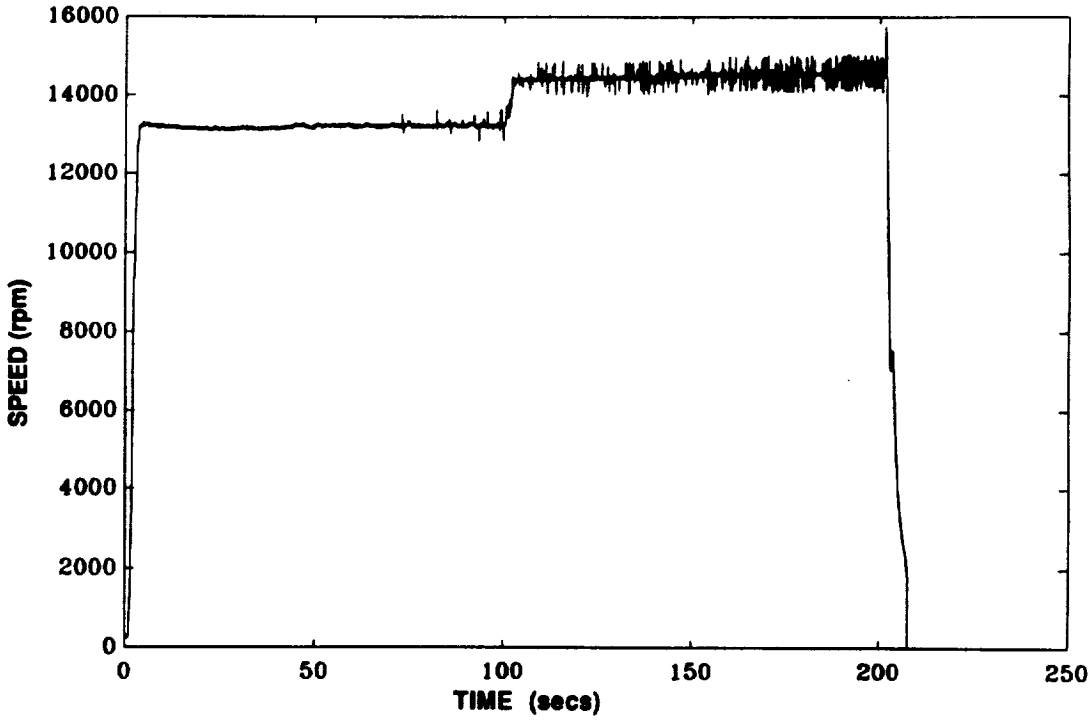

Fig. A-12.3 LPFP SPEED (PID NO. 32) FOR TEST 901-173

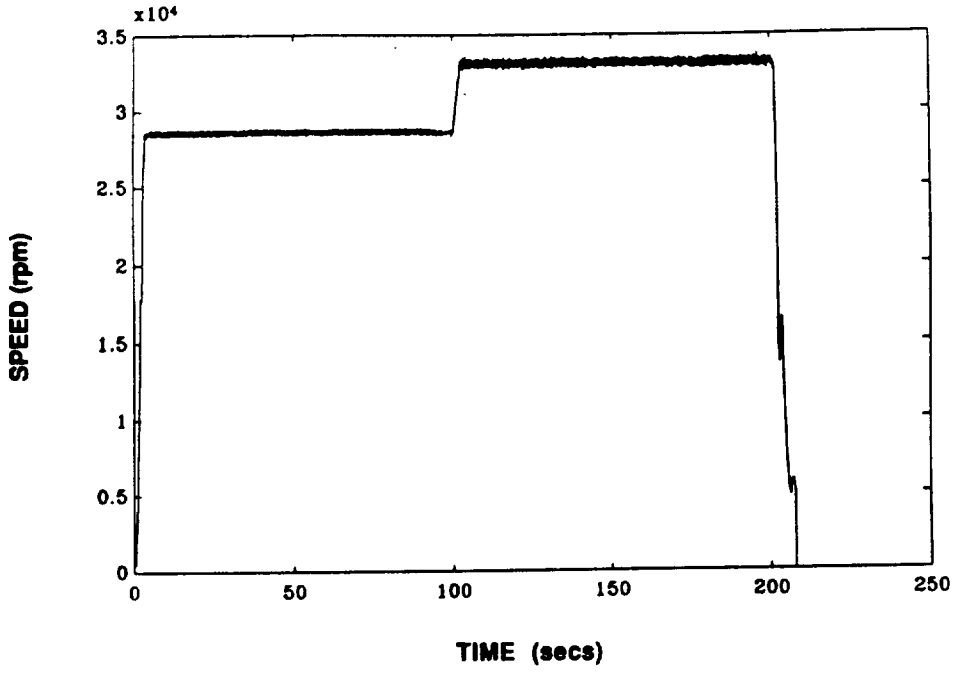

Fig. A-12.4 HPFP SPEED (PID NO. 261) FOR TEST 901-173

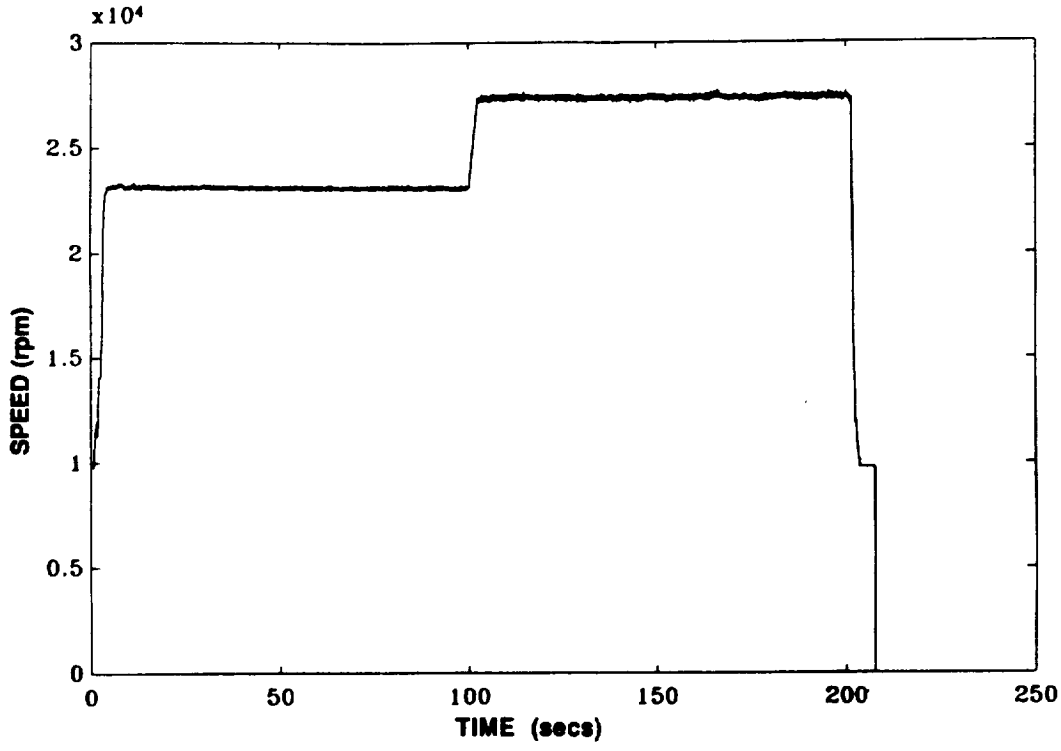

Fig. A-12.5 HPOT SPEED (PID NO. 128) FOR TEST 901-173

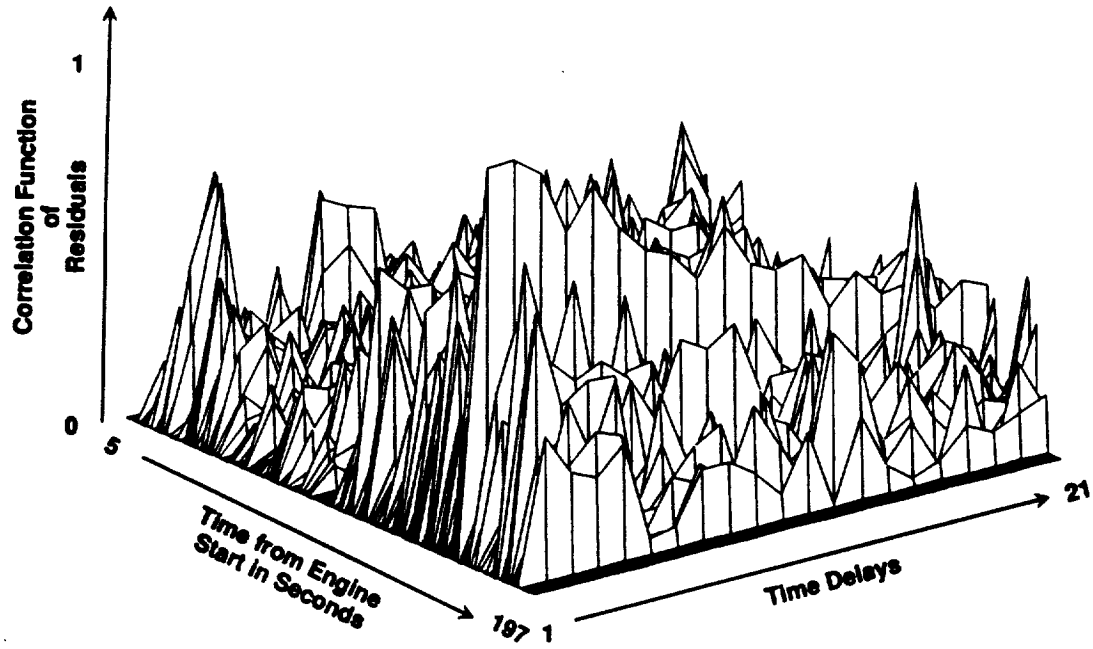

Fig. A-12.6 FAILURE DETECTION USING ARMA MODEL FOR PARAMETER OPOV ACTUATOR POSITION FOR TEST 901-173.

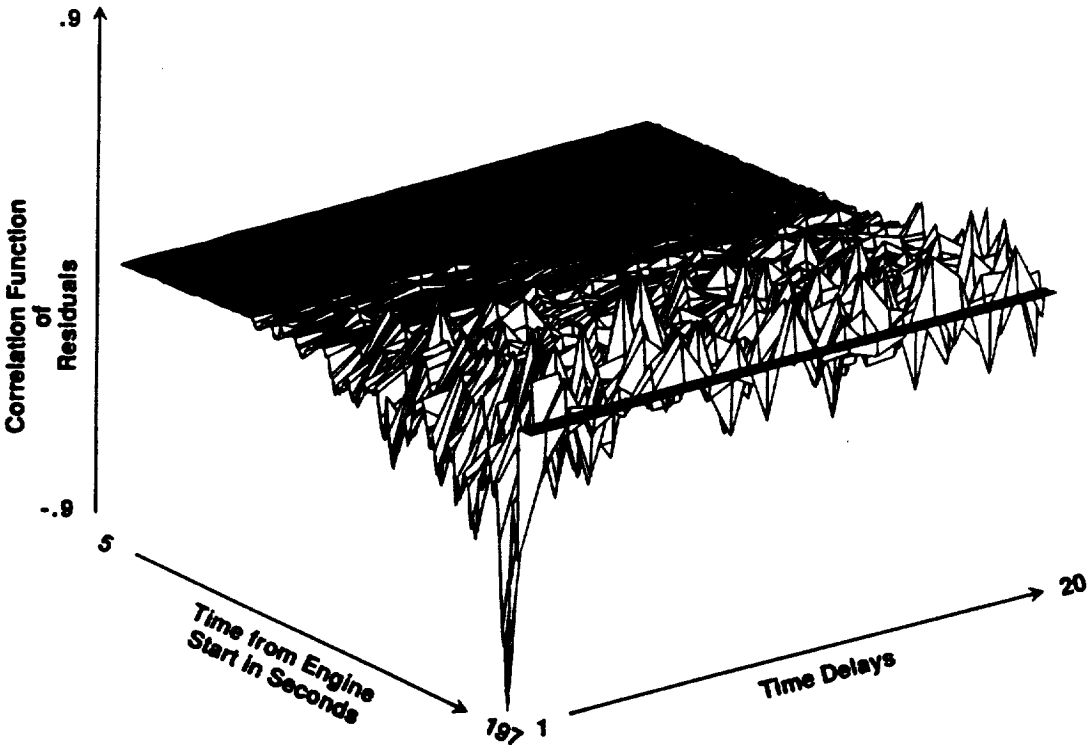

Fig. A-12.7 FAILURE DETECTION USING ARMA MODELS FOR PARAMETER LPFP SPEED FOR TEST 901-173.

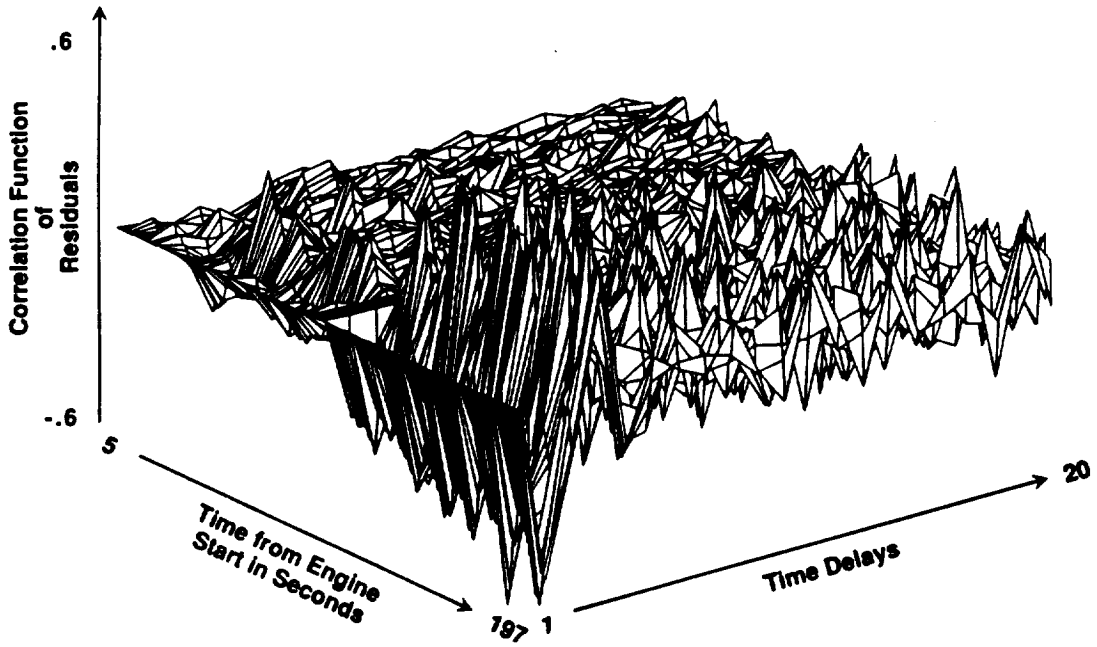

Fig. A-12.8 FAILURE DETECTION USING ARMA MODELS FOR PARAMETER HPFP SPEED FOR TEST 901-173.

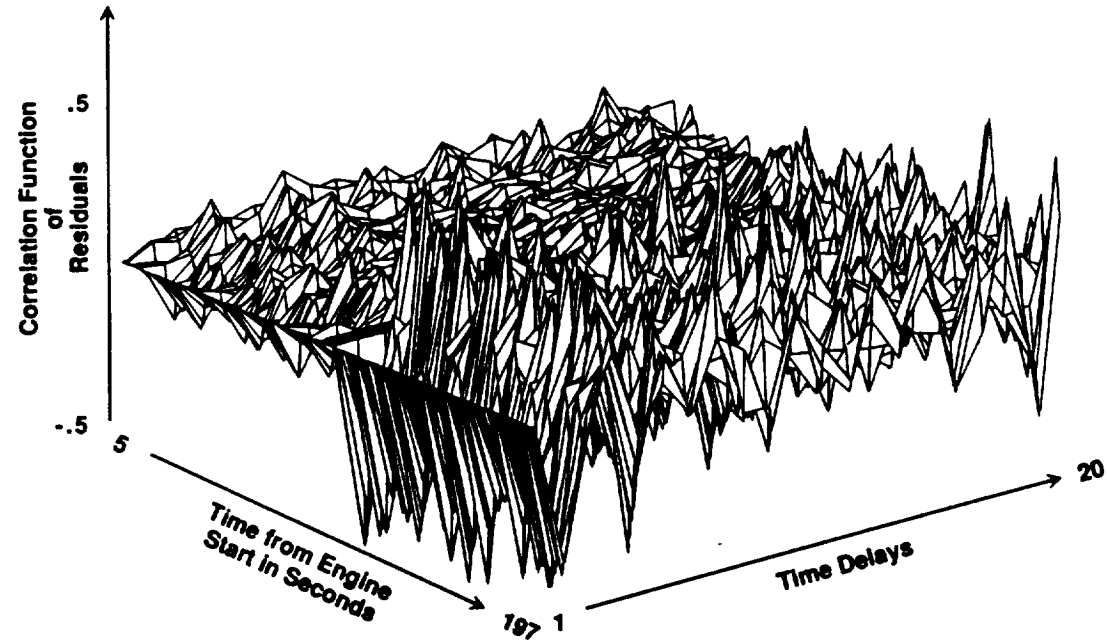

Fig. A-12.9 FAILURE DETECTION USING ARMA MODELS FOR PARAMETER HPOT SPEED FOR TEST 901-173.

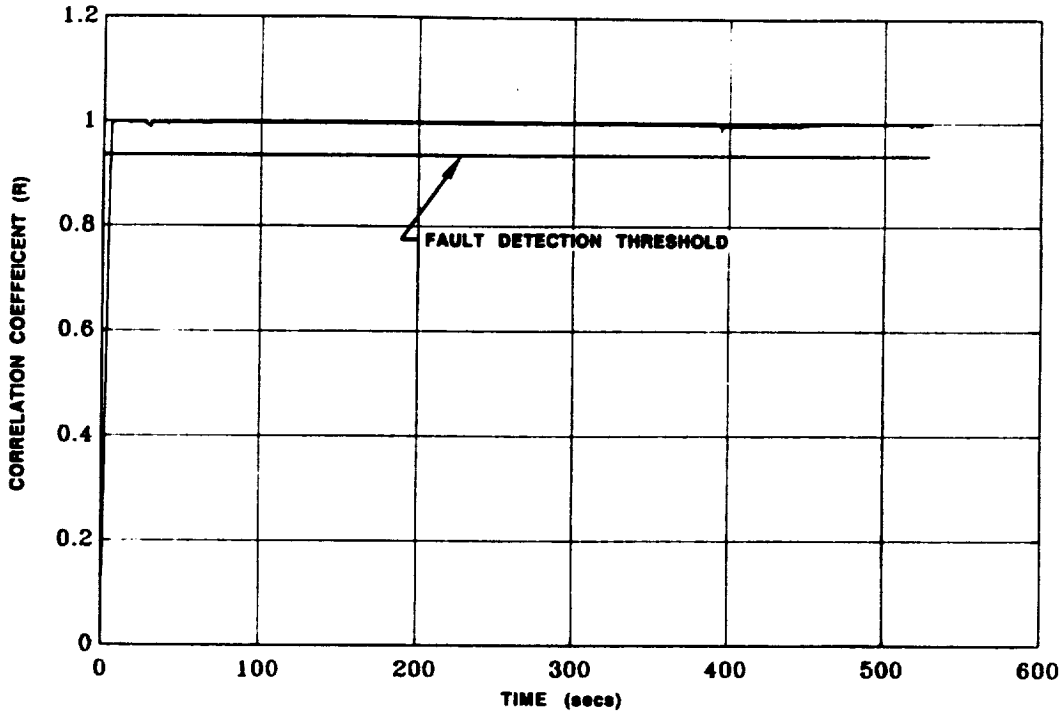

Fig. A-12.10 THE CLUSTERING ALGORITHM RESULTS SHOW NO FALSE ALARMS FOR THE 902-463 NOMINAL DATA USING THE 901-173 SENSOR SUBSET.

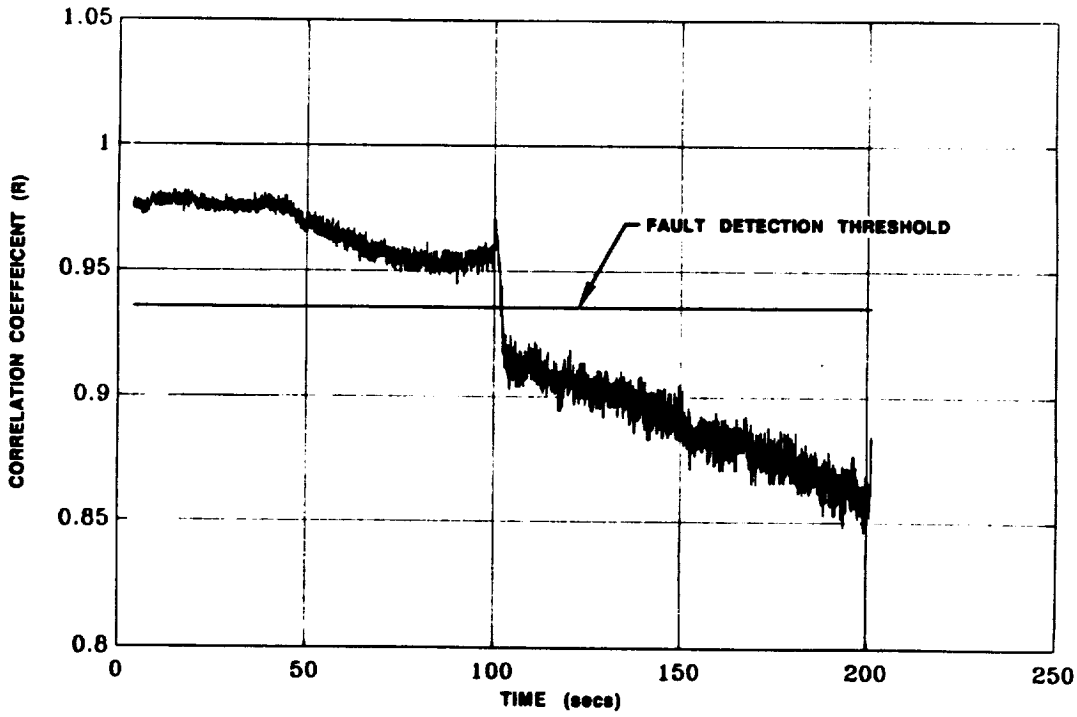

Fig. A-12.11 THE CLUSTERING ALGORITHM RESULTS FOR TEST 901-173. FAULT DETECTION OCCURED AT 102.1 SECONDS.

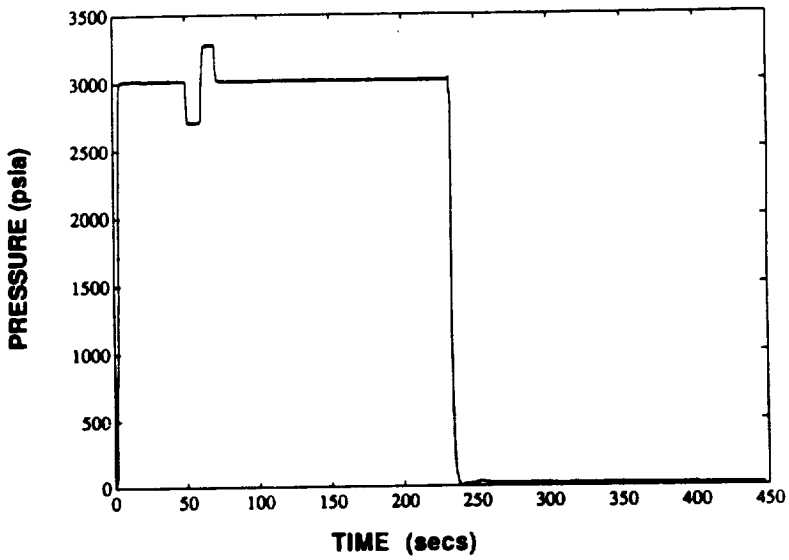

Fig. A-13.1 MCC PRESSURE (PID NO. 63) FOR TEST 901-331

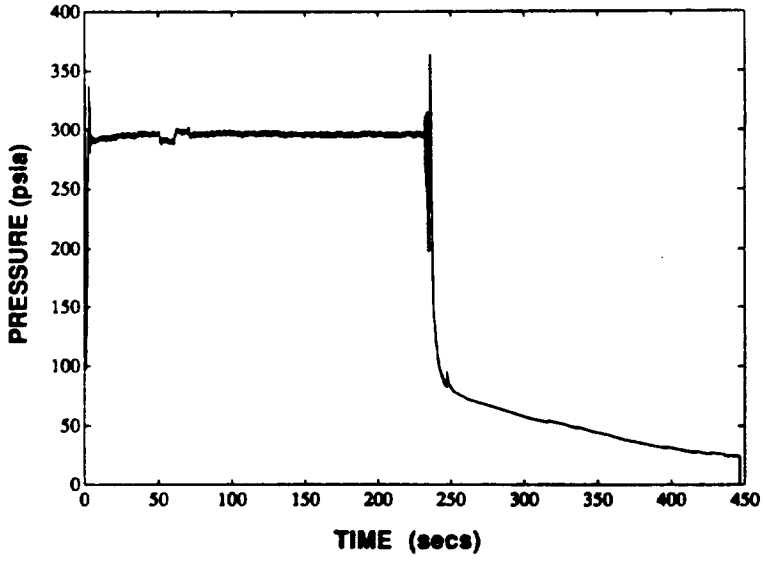

Fig. A-13.2 LPOP DISCHARGE PRESSURE (PID NO. 209) FOR TEST 901-331

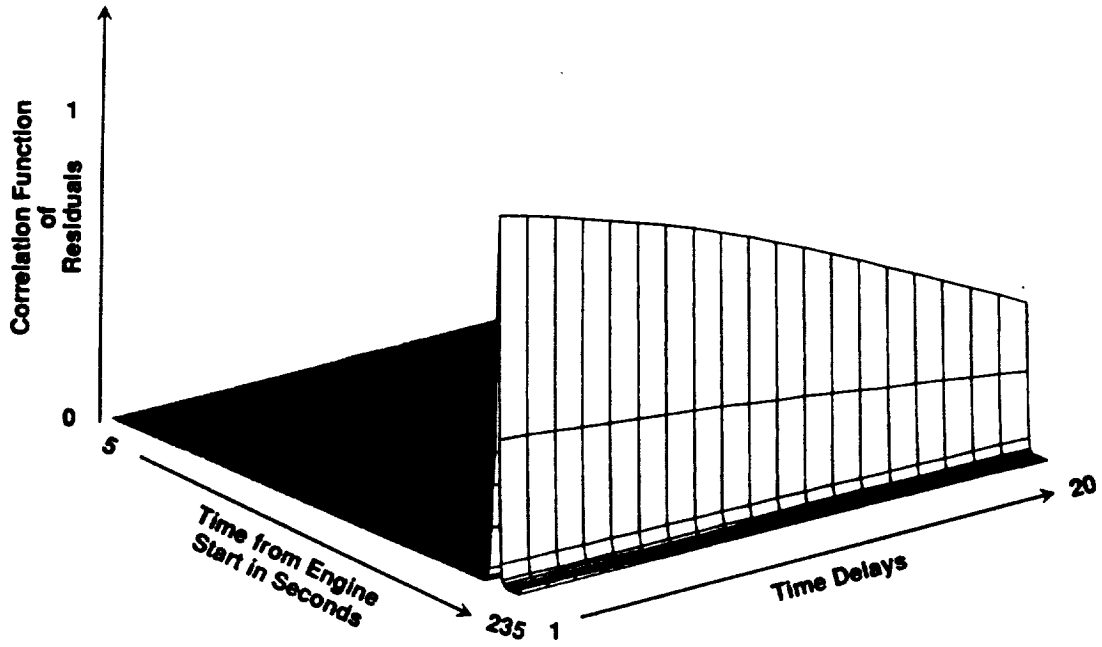

Fig. A-13.3 FAILURE DETECTION USING ARMA MODELS FOR PARAMETER LPOP DISCHARGE PRESSURE FOR TEST 901-331.

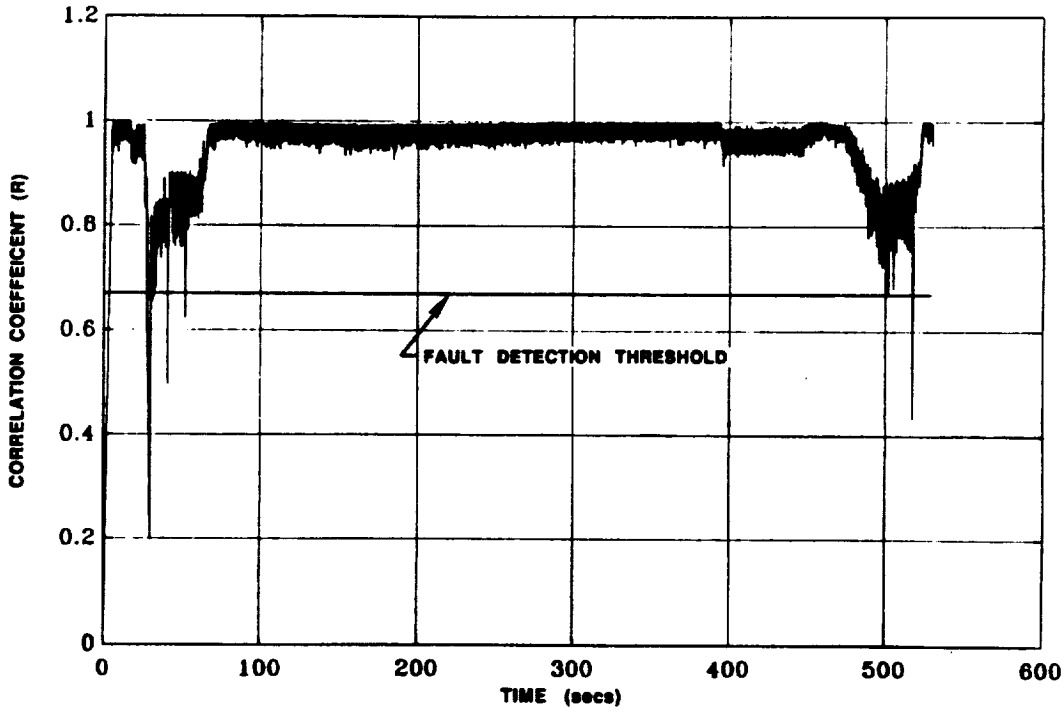

Fig. A-13.4 THE CLUSTERING ALGORITHM RESULTS SHOW FALSE ALARMS OCCURING AT 28, 41, 52 AND 517 SECONDS FOR THE 902-463 NOMINAL DATA USING THE 901-331 SENSOR SUBSET.

The correlation coefficients, R, for 901-331 and the detection threshold are shown in Figure A-13.5. The R values are above the detection threshold at the during most of the test. At 50 seconds from start, when the engine transitions from 100% RPL to 90% RPL, the R values drop below the threshold and cause a fault detection at 50.2 seconds. Since the engine was maintaining a steady power of 90% RPL, the detection at 50.2 seconds is considered valid and not a false alarm due to a transition.

14. Test 901-222: Heat Exchanger Tube Leak

According to the Rocketdyne SAFD Phase II report, at the close of engine start, the test was terminated by the heat exchanger outlet pressure minimum redline. It was concluded from the test data that the incident was caused by a leak in the heat exchanger coil. The leak occurred prior to, or during the early part of the start, as evidenced by the excessive coil pressure drop. The high pressure drop indicates increased mass flow. The coil failure was located near the heat exchanger inlet and discharge area, as shown by the hardware damage. Oxygen from the leak became entrained in the fuel-rich preburner combustion gas. The mixed gases were ignited when the turbine discharge gas reached a high enough temperature during the thrust build-up ramp. The radial accelerometer spike at 3.4 seconds indicates that ignition occurred as a detonation, and was near the heat exchanger inlet/outlet area. The continued combustion of the hydrogen-rich preburner combustion products and leaking oxygen caused burning of the coil; the change in nozzle flame pattern at 3.58 seconds shows evidence of metal burning. The heat exchanger coil pressure decayed to below the hot gas manifold pressure at 3.71 seconds, indicating that the heat exchanger coils were completely severed, with extensive communication occurring between the coil and hot gas. Hot gas flowing into the discharge end of the severed coil combusted in the discharge line, with oxygen from the bypass system. The discharge line burned through (4.185 seconds in the motion pictures) causing a rapid decay in discharge pressure at 4.212 seconds. (Test conducted on 6 December 1978, cutoff time: t = 4.33 seconds.)

CADS Data: A plot of the MCC_PC, shown in Figure A-14.1, depicts the engine power profile.

Regression Analysis: This failure occurred during the startup sequence. A model to predict the MCC_PC as a function of fuel and LOX flow rates is used to detect the failure, as shown in Figure A-14.2.

Cluster Analysis: The engine did not achieve mainstage, therefore the cluster algorithm was not applicable.

15. Test 901-340: T/A Duct Rupture

According to the Rocketdyne SAFD Phase II report, during stable operation at 109% of rated power level, the following series of events occurred within the HPFTP : (1) the 2nd rotor platform seal and the T/A (Turn Around) duct inner wall fractures at t = 20.6 seconds from start; (2) the nut erodes, the 2nd rotor exit straightening vane breaks out, and the T/A duct inner wall fractures propagate at t = 277 seconds; (3) the washer lodges on the nozzle vane, and T/A duct sheet metal deflects at t = +280 seconds; (4) major ruptures occur in the T/A duct at t = 290 seconds; (5) the T/A duct sheet metal flap breaks loose at t = 357 seconds. At t = 405.5 seconds the test was shutdown due to a High Pressure Fuel Turbine (HPFT) discharge temperature redline. (Test conducted on 15 October 1981, cutoff time: t = 405.50 seconds.)

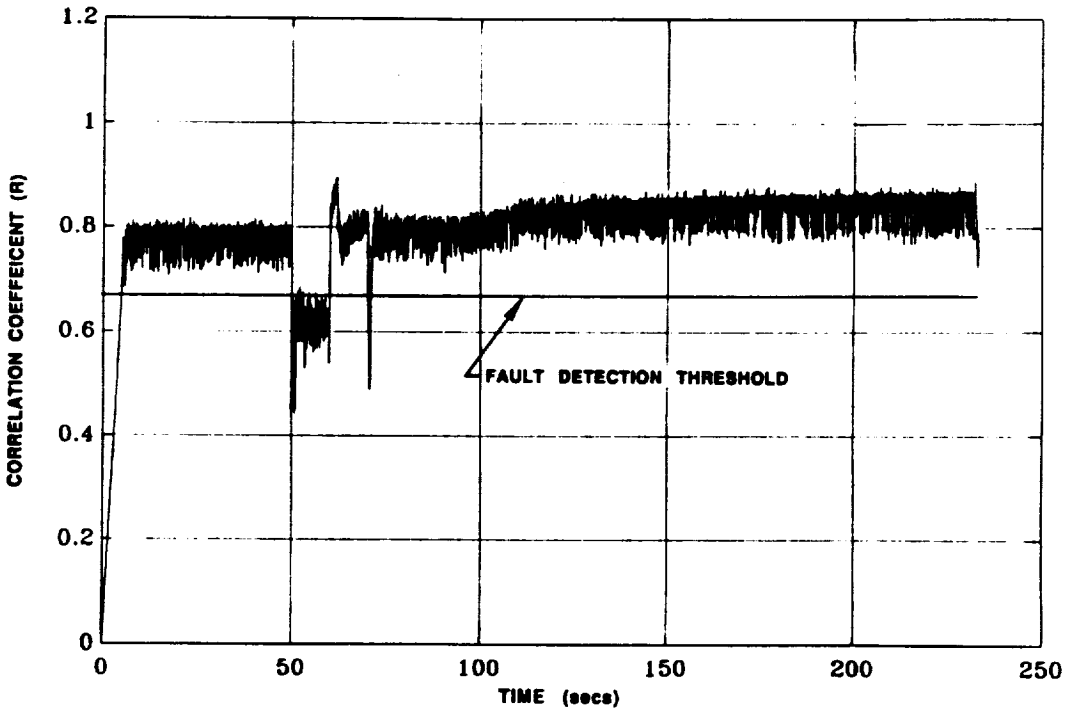

Fig. A-13.5 THE CLUSTERING ALGORITHM RESULTS FOR TEST 901-331. FAULT DETECTION OCCURED AT 50.2 SECONDS.

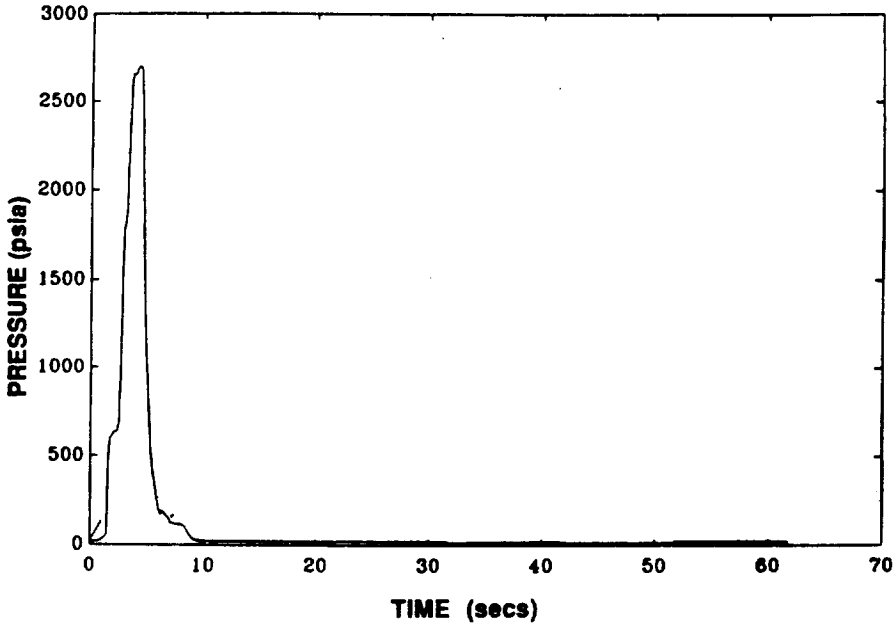

Fig. A-14.1 MCC PRESSURE (PID NO. 130) FOR TEST 901-222

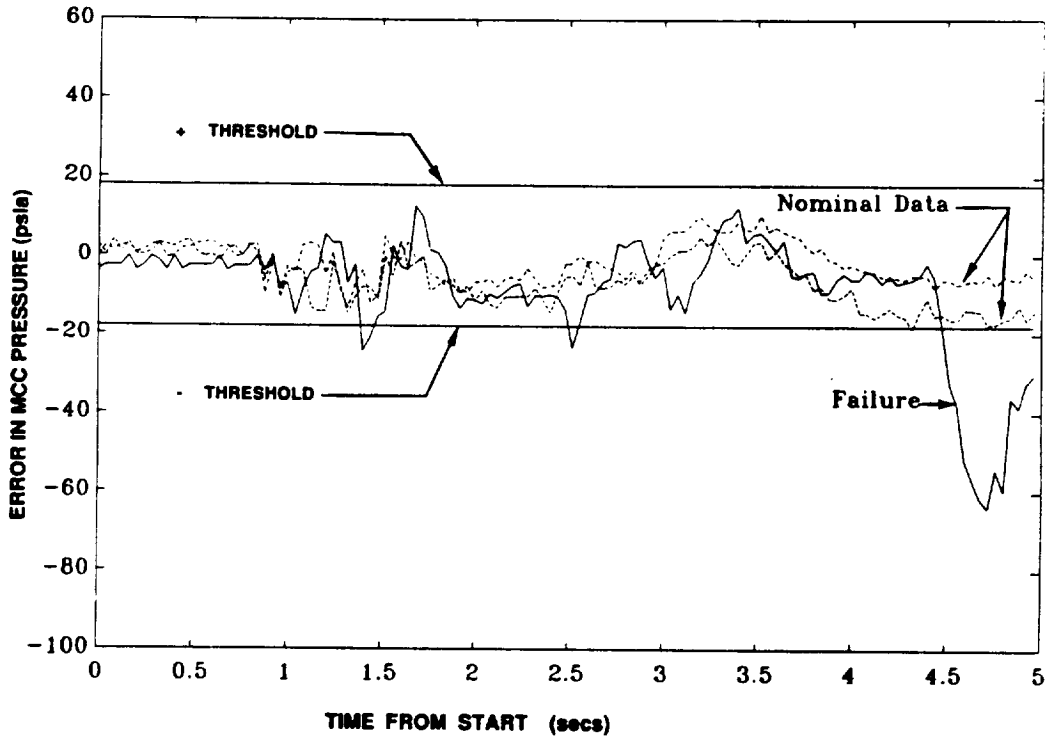

Fig. A-14.2 DETECTION OF FAILURE DURING STARTUP FOR TEST 901-222

CADS Data: A plot of the MCC_PC, Figure A-15.1, depicts the engine power profile.

Time Series Analysis: During the mainstage operation at 109% RPL, abnormal behavior was detected approximately 16 seconds from the start for a number of parameters. Figures A-15.2 through A-15.6 show the data and corresponding ARMA error signal correlation function plots.

Cluster Algorithm: Input to the clustering algorithm consisted of the thirteen selected sensors (see Table 3.2a) minus those missing sensors listed in Table A-1. The event threshold was 0.94 and the fault detector was set for a five out of five event threshold.

The performance of the algorithm on the nominal data set 902-463 is shown in Figure A-15.7. There are no significant deviations in the plot and the correlation coefficient, R, values are all above the .936 threshold. No false alarms occurred on this data set.

The correlation values for 901-340 and the detection threshold are shown in Figure A-15.8. The R values are above the detection threshold throughout the test until shutdown.

16. Test SF6-01: MFV Crack

According to the Rocketdyne SAFD Phase II report, during stable operation at 100% of rated power level, the Main Fuel Valve (MFV) on Main Engine-1 (ME-1), engine 2002, developed a cracked housing allowing hydrogen to leak into the boattail area. The loss of hydrogen caused the high pressure fuel turbine discharge temperature to rise above its redline and a shutdown was initiated. The failure occurred due to fatigue, initiated at small surface defects caused by either salt stress corrosion, surface oxidation, or hydrogen embrittlement. (Test conducted on 2 July 1979, cutoff time: t = 18.58 seconds.)

CADS Data: No analysis could be performed because of corrupted data.

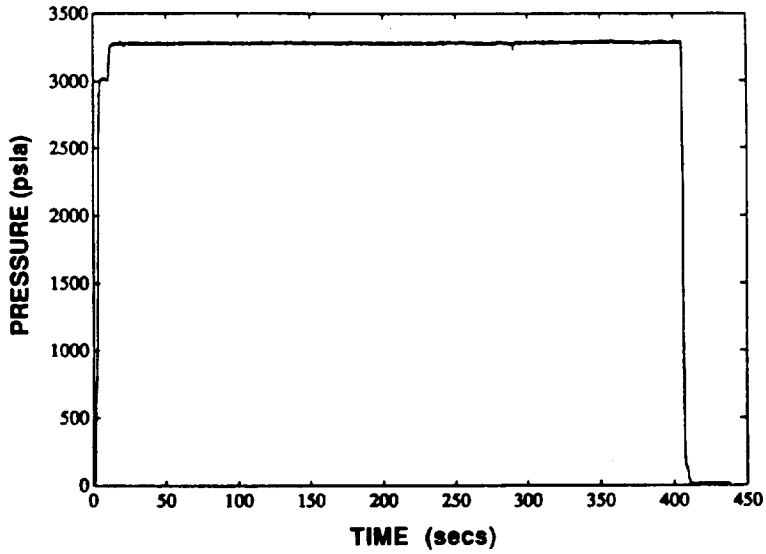

Fig. A-15.1 MCC PRESSURE (PID NO. 130) FOR TEST 901-340

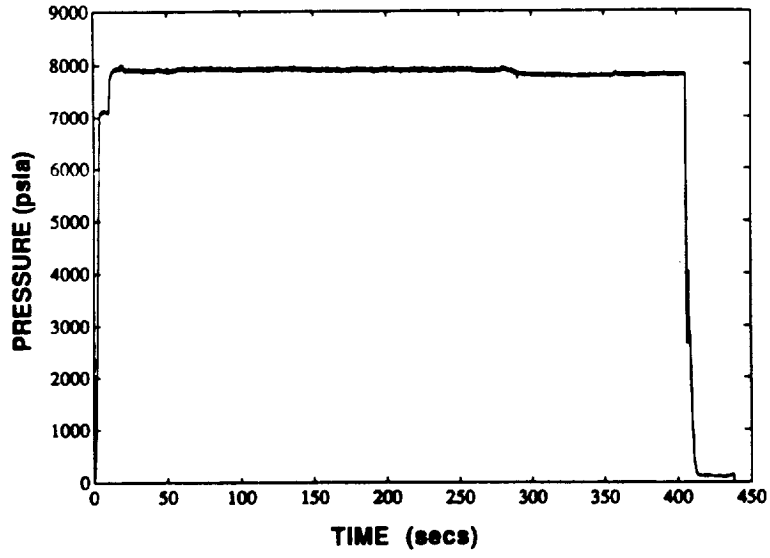

Fig. A-15.2 PBP DISCHARGE PRESSURE (PID NO. 59) FOR TEST 901-340

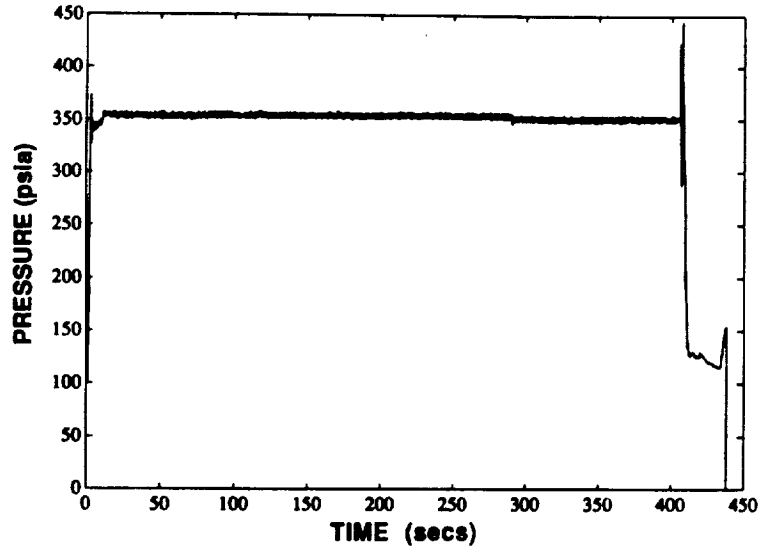

Fig. A-15.3 LPOP DISCHARGE PRESSURE (PID NO. 209) FOR TEST 901-340

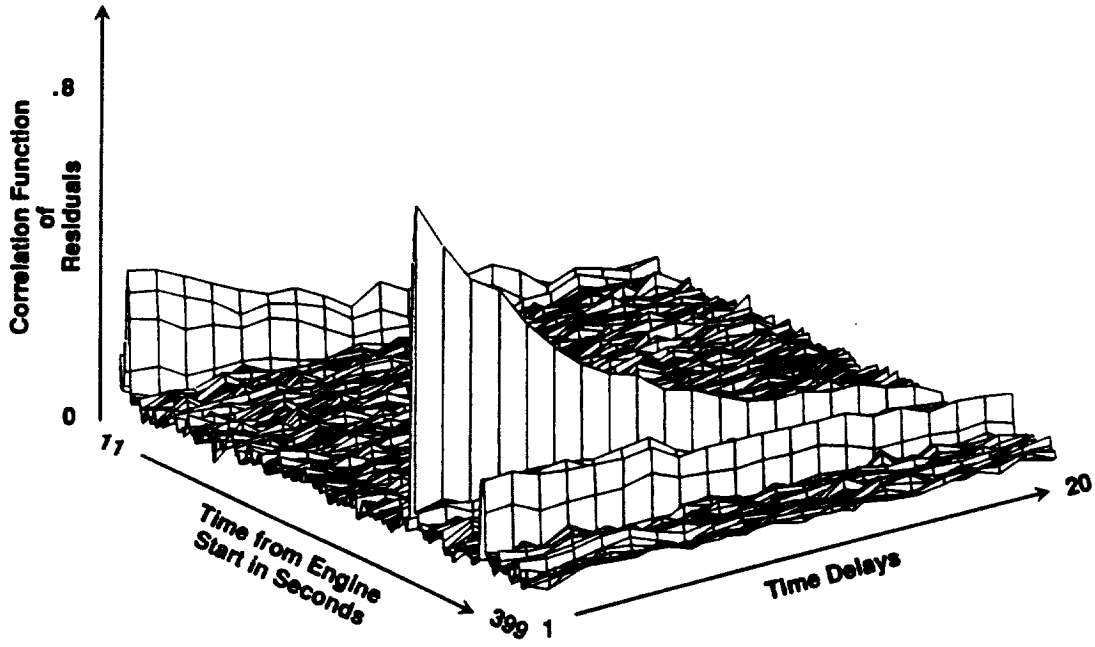

Fig. A-15.4 FAILURE DETECTION USING ARMA MODELS FOR PARAMETER MCC PRESSURE FOR TEST 901-340.

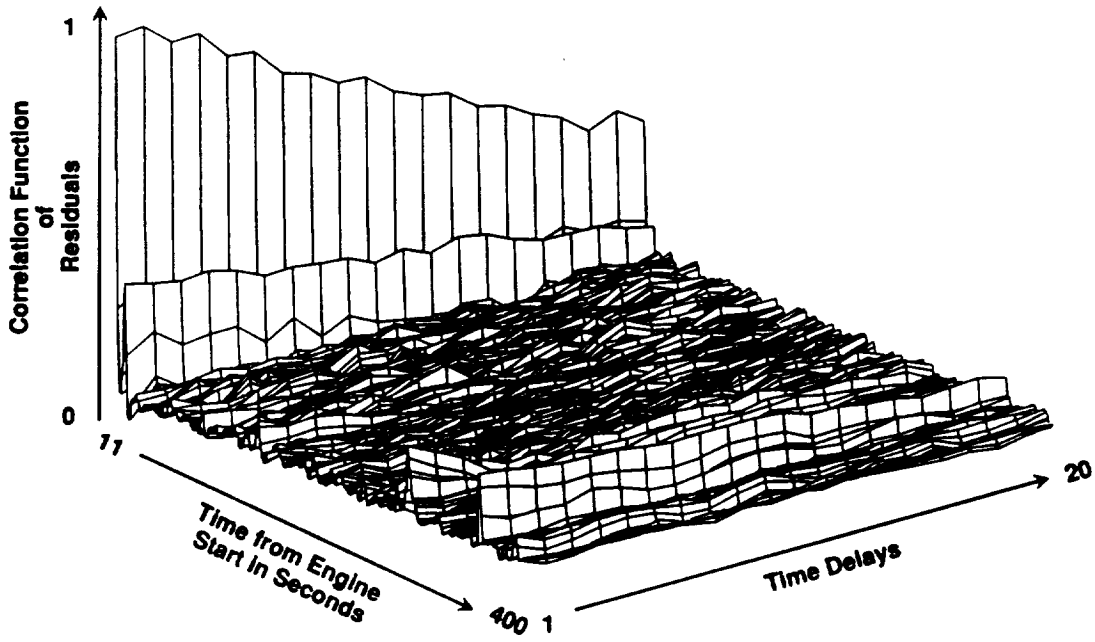

Fig. A-15.5 FAILURE DETECTION USING ARMA MODELS FOR PARAMETER PBP DISCHARGE PRESSURE FOR TEST 901-340.

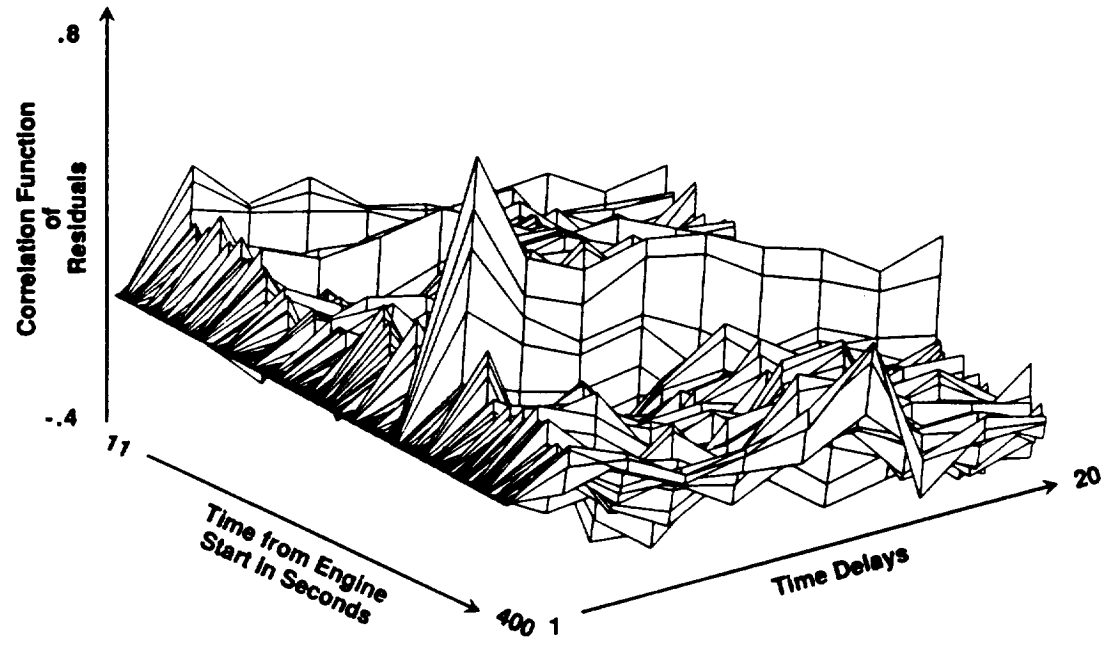

Fig. A-15.6 FAILURE DETECTION USING ARMA MODELS FOR PARAMETER LPOP DISCHARGE PRESSURE FOR TEST 901-340.

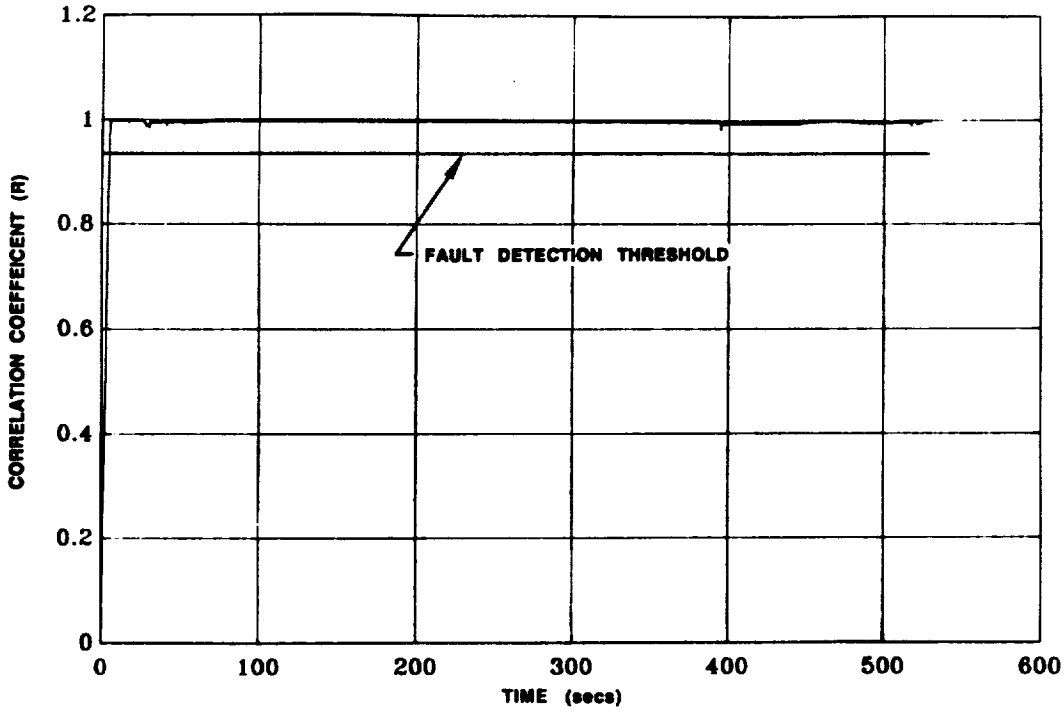

Fig. A-15.7 THE CLUSTERING ALGORITHM RESULTS SHOW NO FALSE ALARMS FOR THE 902-463 NOMINAL DATA USING THE 901-340 SENSOR SUBSET.

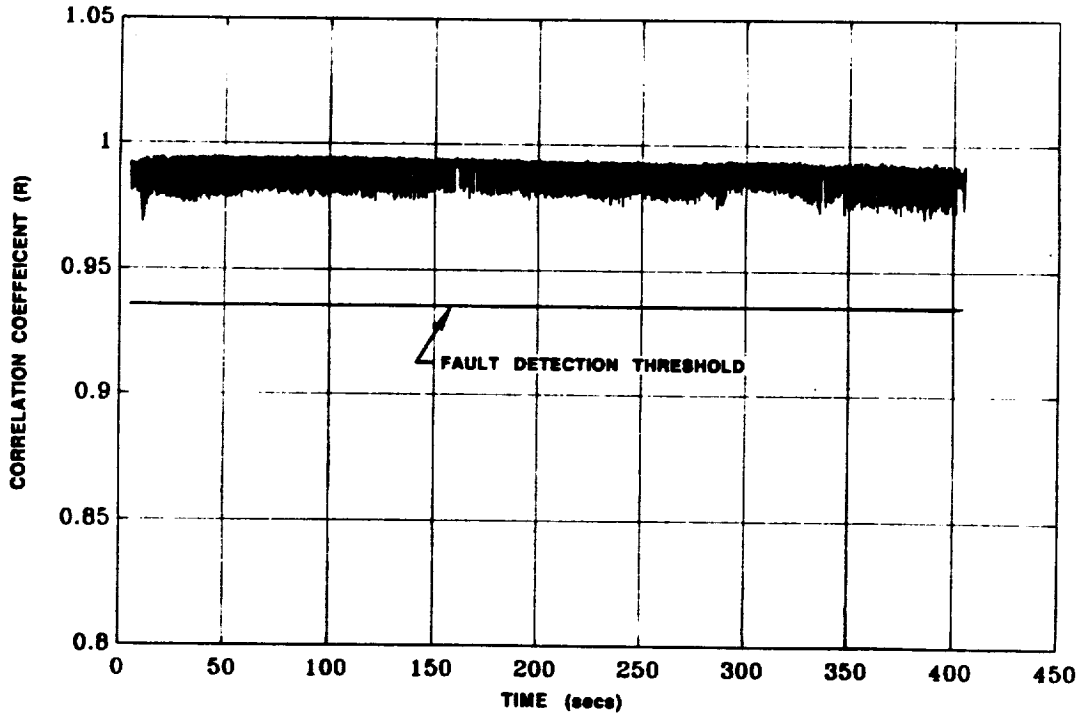

Fig. A-15.8 THE CLUSTERING ALGORITHM RESULTS FOR TEST 901-340. THE CORRELATION COEFFICIENTS REMAINED ABOVE THE DETECTION THRESHOLD UNTIL ENGINE SHUTDOWN.

REFERENCES

1. Taniguchi, M. H., et. al.: Failure Control Techniques for the SSME, Phase I, II & III, NASA MSFC/Rocketdyne NAS8-36305.

2. Proceedings of the 1st Annual Health Monitoring Conference for Space Propulsion Systems, Cincinnati, Ohio, November, 1989.

3. Hawman, M., and Galinaitis, W.: Acoustic Emission Monitoring of SSME-ATD Roller Bearings, AIAA/ASME 25th Joint Propulsion Conference, Monterey, CA, July 1989.

4. Gass, F. D., and Alcock, J., F.: Space Shuttle Main Engine- Alternate Turbopump Development (SSME-ATD) Health Monitoring Program, AIAA 24th Joint Propulsion Conference, Boston, MA, July 1988.

5. Chatigny, J. V., and Robb, L. E.: Sensors: Making the Most of Piezo Film. Sensor Review 7 (1), 15-20, IFS Publishing, 1986.

6. Madzsar, G. C.: Leak Detection Techniques for Hydrogen-Oxygen Rocket Engines, JANNAF Propulsin Meeting, Cleveland, OH, May 1989.

7. Hampson, M. E., and Collins, J. J.: SSME Bearing Health Monitoring using a Fiberoptic Deflectometer, Advanced Earth-to-Orbit Prop. Tech., Vol II, Huntsville, AL, May 1986.

NASA
National Aeronautics and Space Administration

Report Documentation Page

1. Report No.	2. Government Accession No.	3. Recipient's Catalog No.
NASA CR-185224		

4. Title and Subtitle
Framework for a Space Shuttle Main Engine Health Monitoring System

5. Report Date
May 1990

6. Performing Organization Code

7. Author(s)
Michael W. Hawman, William S. Galinaitis, Sharayu Tulpule, Anita K. Mattedi, and Jeffrey Kamenetz

8. Performing Organization Report No.
NRTC R90-997978

10. Work Unit No.
553-13-00

9. Performing Organization Name and Address
United Technologies Research Center
Silver Lane
East Hartford, Connecticut 06108

11. Contract or Grant No.
NAS3-25626

13. Type of Report and Period Covered
Contractor Report
Final

12. Sponsoring Agency Name and Address
National Aeronautics and Space Administration
Lewis Research Center
Cleveland, Ohio 44135-3191

14. Sponsoring Agency Code

15. Supplementary Notes
Project Manager, James Gauntner, Space Propulsion Technology Division, NASA Lewis Research Center.

16. Abstract

This report summarizes a six month program to develop a framework for a health management system (HMS) which is directed at improving the safety of operation of the Space Shuttle Main Engine (SSME). An emphasis was placed on near term technology through requirements to use existing SSME instrumentation and to demonstrate the HMS during SSME ground tests within five years. The HMS framework was developed through an analysis of SSME failure modes, fault detection algorithms, sensor technologies, and hardware architectures. A key feature of the HMS framework design is that a clear path from the ground test system to a flight HMS has been maintained. Fault detection techniques based on time series, nonlinear regression, and clustering algorithms were developed and demonstrated on data from SSME ground test failures. The fault detection algorithms exhibited 100% detection of faults, had an extremely low false alarm rate, and were robust to sensor loss. These algorithms were incorporated into a hierarchical decision making strategy for overall assessment of SSME health. A preliminary design for a hardware architecture capable of supporting real-time operation of the HMS functions was developed. Utilizing modular, commercial off-the-shelf components produced a reliable low cost design with the flexibility to incorporate advances in algorithm and sensor technology as they become available.

17. Key Words (Suggested by Author(s))	18. Distribution Statement
Health monitoring; Rocket engine diagnostics; Rocket engine fault detection; Health monitoring system hardware architecture	Unclassified – Unlimited Subject Category 20

19. Security Classif. (of this report)	20. Security Classif. (of this page)	21. No. of pages	22. Price*
Unclassified	Unclassified	189	A09

NASA FORM 1626 OCT 86

*For sale by the National Technical Information Service, Springfield, Virginia 22161

National Aeronautics and
Space Administration

Lewis Research Center
Cleveland, Ohio 44135

Official Business
Penalty for Private Use $300

FOURTH CLASS MAIL

ADDRESS CORRECTION REQUESTED

U.S.MAIL

Postage and Fees Paid
National Aeronautics and
Space Administration
NASA 451

NASA